UCL

Effect of molecular structure of liquid and gaseous fuels on the formation and emission of PAHs and soot

Hamisu Adamu Dandajeh

Submitted in partial fulfilment of the requirements

for the degree of Doctor of Philosophy

at University College London,

University of London.

February 2018

I, Hamisu Adamu Dandajeh confirm that the work presented in this thesis is my own. Where information has been derived from other sources, I confirm that this has been indicated in the thesis.

Dated: 12/02/2018

Abstract

This thesis reports an investigation into the effects of fuel molecular structure on the emission of exhaust PAHs from a tube reactor and from a diesel engine. The study was underpinned by the results of experiments conducted in the pyrolysis tube reactor aimed at understanding the formation processes of PAHs. The PAHs found in the diesel engine exhaust, both in gaseous state and on the soot particles, were also measured and analysed. The thesis focuses on the US EPA 16 priority PAHs formed from fossil diesel, C_1 to C_7 model hydrocarbon fuels, and blends of C_7 binary and tertiary fuels. Particular attention was paid to the B2 subgroup of PAHs which are possible human carcinogens. Particulate and gas phase PAHs were generated and sampled from the exit of the reactor and the exhaust of the diesel engine. The PAHs from the particulate and gas phase samples were then extracted using an accelerated solvent extraction (ASE) system. The PAHs were analysed qualitatively and quantitatively using gas chromatography coupled with mass spectrometry (GC-MS).

The experimental results obtained in the laminar flow, oxygen-free conditions of the reactor showed that, depending on the temperature at which a fuel is pyrolysed, the degree of unsaturation, isomerisation, aliphaticity, aromaticity and carbon number of the hydrocarbon fuels played an important role on the identity and concentration of PAHs formed. The identity of PAHs produced, and their concentration influenced the overall carcinogenic potential of the gaseous and particulate effluent. In the diesel engine, the total PAH concentrations of the fuels decreased with increase in ignition delay and proportions of premixed burn fractions while the influence of fuel composition on the exhaust PAHs was greater than the influence of the combustion characteristics such as ignition delay, heat release rate and premixed burnt fraction.

Acknowledgements

First, my profound gratitude goes to my PhD supervisor, Prof. Nicos Ladommatos, for his tireless contribution, support, guidance and prompt feedback throughout the course of this project. Special thanks go to my subsidiary supervisor, Dr. Paul Hellier, for his guidance and for being available in the laboratory whenever his attention was needed.

Many thanks to Dr. Aaron Eveleigh for his technical guidance during the tube reactor experiments and Dr. Midhat Talibi for his assistance in running the engine tests.

I wish to gratefully acknowledge the Petroleum Technology Development Fund (PTDF) for sponsoring my research studies at UCL and Ahmadu Bello University Zaria for granting me study fellowship.

I'm especially indebted to my wife and daughter for their enduring support and patience while I was away for my research studies. Thanks are due to my parents and siblings for their support and encouragement throughout this project.

Finally, I'm grateful to my friends within and outside UCL, particularly my colleagues in the thermodynamics laboratory of UCL Mechanical Engineering Department.

Contents

List of Figures

List of Tables

Nomenclature

2-EHN	2 ethylhexyl nitrate
ACN	acenaphthene
ACY	acenaphthylene
ALS	automatic liquid sampler
ATR	anthracene
ASE	accelerated solvent extraction
B(a)A	benzo(a)anthracene
B(a)P	benzo(a)pyrene
B(b)F	benzo(b)fluoranthene
B(ghi)P	benzo(g,h,i)perylene
B(k)F	benzo(k)fluoranthene
BTDC	before top dead centre
CAD	crank angle degree
CAS	chemical abstract service
CEF	compound extraction file
CI	compression ignition
CRY	chrysene
D(ah)A	dibenz(a,h)anthracene
DCM	dichloromethane
DMS	differential mobility spectrometer
EPA	environmental protection agency
EIC	extracted ion chromatograph
FLU	fluorene
FLT	fluoranthene
GCMS	gas chromatography, mass spectrometry
GP	gas Phase

H	heptane
HACA	hydrogen abstraction acetylene addition
HPLC	high purity liquid chromatography
HMW	high molecular weight
ICE	internal combustion engine
I(123cd)P	indeno(123-cd)pyrene
IMEP	indicated mean effective pressure
LMW	low molecular weight
MD	methyl decanoate
MMW	medium molecular weight
MSD	mass selective detector
NPH	naphthalene
PAH	poly-cyclic aromatic hydrocarbon
PHN	phenanthrene
PM	particulate matter
PP	particulate phase
PPM	part per million
PUF	polyurethane foam
PYR	pyrene
RRF	relative response factor
SIM	selected ion monitoring
SOC	start of combustion
SOI	start of fuel injection
STP	standard temperature and pressure
TEF	toxicity equivalence factor
T	toluene
TIC	total ion chromatograph
WC	weighted carcinogenicity

Greek Symbols

Φ	equivalent ratio
δ	standard deviation

Chapter 1

1. Introduction

The central goal of this thesis was to carry out systematic investigation on the effect of molecular structures of fuel molecules on the formation of polycyclic aromatic hydrocarbons (PAHs) which are probable human carcinogens and mutagens. A novel methodology was developed for generating particulate and gas phase PAH samples and for the extraction, identification and quantification of the PAHs from these samples. A homologous series of hydrocarbon fuels has been studied under pyrolysis (tube reactor) and combustion (diesel engine) conditions. This has led to insights, such as influence of unsaturation and carbon number on PAH emissions, that could inform the processing of fuels so that they produce fewer toxic PAH emissions.

1.1 Motivation

Atmospheric air quality is continually being degraded by particulate emissions from combustion sources, and stringent global particulate legislation has been enacted to reduce the adverse health effects that particulate cause. Understanding particulate production requires detailed knowledge of the formation and growth of particulate molecular precursors. Such understanding can aid the design of particulate controls in practical combustion systems including, for example, diesel engines for transport applications (Walter, 2008).

Particulates are produced from various stationary and mobile combustion sources, including domestic heating and industrial power generation systems using biomass and fossil fuels (coal, oil and natural gas). The most significant contributor to the mobile sources of particulates in most cities of the World is road transport, accounting, for example, in the London boroughs for about 80 % of the total airborne particles of diameters (D_p) below 10 μm (PM_{10}) (Raquel and

Mesquita, 2016). Diesel vehicles are the most prolific contributors to road traffic particulate mass emissions, mostly 10 – 100 times higher than gasoline powered vehicles (Kittelson, 1998). Among the criteria pollutants stipulated by the United State Environmental Protection Agency (US EPA), particulates arguably have the broadest environmental impacts including obscuring visibility, soiling of buildings, ecological effects, climate change and health effects (Matti, 2007).

PAHs, which are not directly regulated by diesel emissions regulations, are probable human carcinogens and mutagens (Franken *et al.*, 2017) and are abundant in atmospheric aerosols. Inhalable atmospheric coarse particles (Dp < 10 µm) emitted from diesel and gasoline vehicles could be accumulated into the superior respiratory airways, while ultrafine particles at sub-micron levels (Dp < 1 µm) and bearing carcinogenic-PAHs could be deposited into the human lung pulmonary alveoli (air sacs) of an individual (see Figure 1.1), causing lung cancer, cardiovascular diseases and ultimately premature death (Dockery and Pope, 1994).

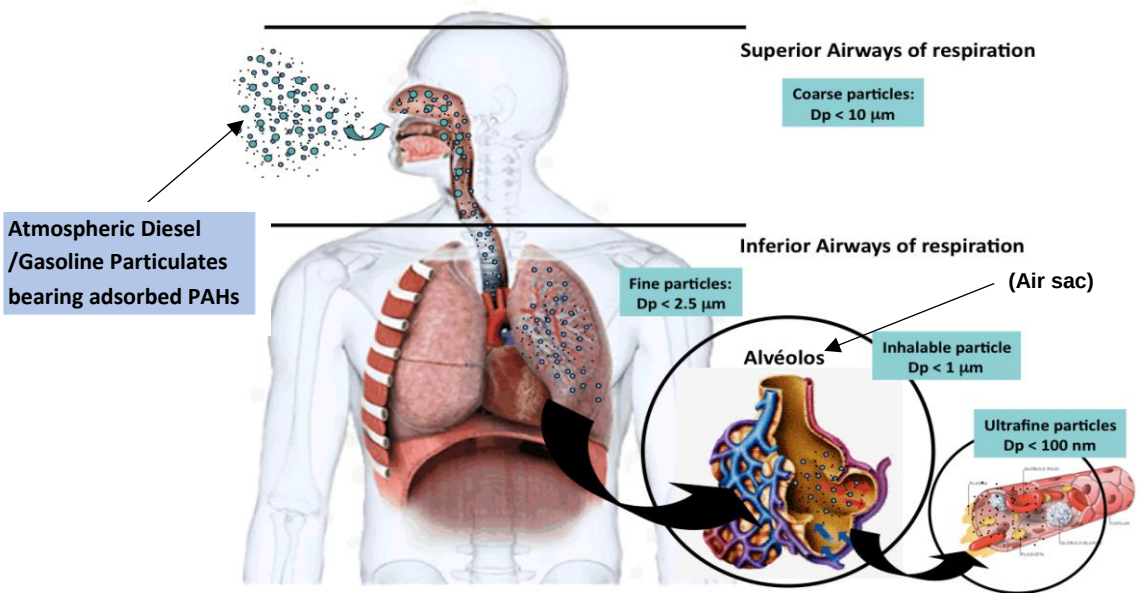

Figure 1.1: Typical human exposure to diesel and gasoline atmospheric aerosols bearing adsorbed PAHs (http://www.cleanairegypt.org/air-pollution-and-aerosols/: retrieved 04-06-2017).

Human mortality cases associated with air-bone particulates bearing adsorbed PAHs have been reported in some cities in the United Kingdom (Gowers *et al*., 2014) and the United States (Richter *et al*., 1999). For example, studies

conducted by the Public Health England (PHE) have estimated that in the London Borough of Camden, which has a population of 165,500 with an average age over 25 years, about 1126 people die annually (Gowers et al., 2014). Among the 1126 annual deaths, 87 deaths (7.7% of the total deaths) are associated with particulates which statistically shortened the average life expectancy for the 87 individuals by 13.3 years.

Polycyclic Aromatic Hydrocarbons (PAHs) are fused aromatic ring compounds consisting of carbon and hydrogen. Presently, there are several hundreds of PAHs in nature, but only 16 PAHs have been classified as potentially toxic by the US EPA and European Union (EU). Among the 16 priority PAHs, 6 PAHs having 4 - 6 aromatic rings were classified by the US EPA as group B2 (*possibly carcinogenic to humans*), while 7 PAHs out of the remaining 9 PAHs having 2 - 4 aromatic rings were categorised as Group D (*unclassifiable as to carcinogenicity)* (US EPA, 1993). PAHs are known for some time to be the main particulate precursors. They play an important role in the formation of particulates in two principal ways. Firstly, PAHs assemble themselves into larger structures which are the soot particles themselves. Secondly, they are mostly found, adsorbed on the surfaces of particulates and form their toxic components.

Toxicity of particulates bearing adsorbed PAHs is influenced by the molecular structure of the hydrocarbon and the temperature at which the hydrocarbon fuel was burnt (Furuhata *et al.*, 2012; Sánchez *et al.*, 2012). The homologous series of hydrocarbons molecules ranging from C_1 to C_7 are principal components in fuels which are used for such applications as residential heating, gas turbines and internal combustion engines (Wang & Cadman, 1998). For example, C_1 to C_2 gases (methane and ethane) are the major components of natural gas. C_3 to C_4 gases (propane and butane) are the main components of liquefied petroleum gas (LPG) (Marinov et al., 1997), while C_4 to C_{12} molecules are the principal components of gasoline and form some of the components of diesel fuel (Botero et al., 2016).

Efforts have been made previously by researchers to study PAH emissions formed by C_1 to C_7 fuels. For example, C_1 and C_2 fuels have been studied by Siegmann and Sattler (2000) and Bakali *et al*. (2012); C_3 and C_4 fuels were

studied by Marinov et al. (1997) and Schenk *et al.* (2015) and likewise C_7 fuels were studied by Wang and Cadman (1998), Zhang *et al*. (2010) and

Zhang *et al.* (2009). Nevertheless, systematic studies which investigate the influence of progressively increasing carbon number and the degree of unsaturation on PAH formation of a homologous series of C_1 to C_7 hydrocarbons fuels are rare. It is also evident from the literature that there are relatively few experimental PAH studies of the individual hydrocarbons in the homologous series of C_1 to C_7 in a tube reactor, and only limited published information is available on particulate characterisation and soot formation in a tube reactor for this homologous series.

1.2 Aims and objectives

Research to date on the reduction of PAH emissions has tended to focus almost exclusively on lowering particulates through combustion-based and exhaust after-treatment approaches as for example in low temperature combustion and the use of particulate traps. However, reducing particulates does not necessarily imply lessening the toxicity of the PAHs adsorbed on the remaining particulates. Fuel based approaches that result in lower PAH emissions are crucial but rarely studied (Ballesteros *et al.*, 2010). The few studies published have limited themselves to altering the molecular structure of fossil fuels by blending them with biofuels and by reducing fossil fuel aromatic content (Tsai *et al.*, 2010; Barbella *et al.,*1989). The link between a fuel's molecular structure and PAH emissions has so far remained poorly understood. The general aim of this thesis is to investigate systematically the influence of molecular structure of homologous series of fuel molecules on PAH and particulate formation in a homogenous tube reactor and in a compression ignition engine. The specific objectives of this thesis are described as follows:

i) Develop a robust and systematic methodology for the generation and quantification of particulate PAHs and gas phase PAHs from a homologous series of C_1 – C_7 fuels in a homogenous tube reactor and of C_7 alkane and aromatic fuel molecules in a compression ignition (CI) engine.

ii) Characterise the soot particles produced from the pyrolysis of C_1 – C_7 fuels in the tube reactor and their combustion in a CI engine based on particle size, particle number and particle mass using a differential mobility spectrometer (DMS-500).

iii) Carry out a systematic study on how the molecular structures (unsaturation and carbon number) of C_1 – C_7 hydrocarbons influence the speciation of individual 16 EPA priority PAHs into gas and particle phases under pyrolysis conditions.

iv) Investigate the interdependence of particulate phase PAHs (particularly Group B2 PAHs) on the soot particle size, soot number concentration and soot mass.

v) Evaluate the influence of combustion characteristics (premixed burn fraction of fuels and heat release rates) and fuel composition (fuel aromatic content) on the concentrations of exhaust PAHs in a CI engine at constant injection and constant ignition timings.

vi) Determine the effect of adding ignition improver to the blends of fuel molecules on the concentrations of gas phase and particulate phase PAHs, at the same time assessing the influence of varying and equalising ignition delays on the total PAH concentrations.

vii) To reach conclusions as to which fuel molecular structures (e.g. single, double and triple bonded hydrocarbons, molecules of smaller and higher carbon numbers, straight and branched chain molecules, aliphatic and aromatic molecules of similar carbon number) can lead to lower concentration of PAHs.

1.3 Structure of the thesis

This thesis is split into eight chapters as follows:

Chapter 2 reviews literature on the formation and emission of soot and PAHs from tube reactors and compression ignition engines. It begins with an overview of PAH characteristics, mechanisms of PAH formation and effects of molecular structure of hydrocarbons on the formation and emission of PAHs. The chapter is concluded by identifying gaps in knowledge.

Chapter 3 describes the systems and experimental facilities that were used to conduct the set of experiments in this thesis. It also describes a novel methodology which was employed for systematic generation and collection of particulate and gas phase PAH samples. PAH extraction and identification are also described.

Chapter 4 reports the analytical procedure used to quantify the concentration of particulate and gaseous PAHs. Preparation of analytical calibration standard and the development of calibration curves for each of the individual 16 PAHs are described. Development of methods for analysing and interpreting the EPA 16 priority PAHs is detailed.

Chapter 5 investigates the effects of unsaturation on soot and PAH formation of three C_2 hydrocarbons (ethane, ethylene and acetylene) and two C_3 hydrocarbons (propane and propylene) in a laminar flow reactor.

Chapter 6 examines the influence of carbon number of seven hydrocarbons (methane, ethane, propane, n-butane, i-butane, heptane and toluene) on PAH formation in a laminar flow reactor

Chapter 7 investigates the effects of fuel composition on the exhaust emission of PAHs in a compression ignition engine. The chapter focuses on the emissions of the EPA 16 priority PAHs produced by using fossil diesel fuel and some model binary fuels prepared by blending various proportions of toluene into heptane.

Chapter 8 contains the conclusions of the work carried out in this thesis and includes a summary on how the results obtained have added to the current knowledge on choice of fuels and methods employed for PAH quantification. Recommendations for further work are also included.

1.4 Publications

To this date, this thesis has produced the following peer reviewed journal paper:

Dandajeh, Hamisu Adamu, Nicos Ladommatos, Paul Hellier and Aaron Eveleigh. 2017. “Effects of Unsaturation of C_2 and C_3 Hydrocarbons on the Formation of PAHs and on the Toxicity of Soot Particles.” *Fuel* 194. Elsevier Ltd: 306–20. doi:10.1016/j.fuel.2017.01.015

Chapter 2

2. Literature Review

The purpose of this chapter is to review literature on the formation and emission of soot and polycyclic aromatic hydrocarbons (PAHs) from tube reactors, flames and internal combustion engines. It begins with an overview of the nature of PAHs, their sources and health effects. Mechanisms of PAHs formation, starting with generation of the first aromatic ring are reviewed. Different proposed reaction pathways of PAH growth with various examples are highlighted. The role of PAHs in the overall soot formation process is reviewed. Finally, the effect of molecular structure of fuels on the emission of PAHs generated from pyrolysis and combustion is discussed with a view to identifying gaps in current knowledge.

2.1 Characteristics of PAHs

Polycyclic Aromatic Hydrocarbons (PAHs) are organic compounds containing only carbon and hydrogen with two or more aromatic rings (*usually benzene or cyclo-penta rings*) fused together in various configurations. Most PAHs have high boiling and melting points, and therefore appear as colourless, pale-yellow or white solid particles at ambient temperature (Abdel-Shafy & Mansour, 2015). PAHs are generally soluble in organic solvents (*lipophilic*) and have characteristics Ultraviolet (UV) absorbance spectra. Each PAH ring exhibits a unique UV spectrum (Masih et al., 2010).

The physical properties of PAHs are often dependent on their molecular structures. Although PAHs were reported having low vapour pressure and aqueous solubility which tended to decrease with increasing molecular weight (see Table 2.1), their resistant to oxidation increases with increasing molecular weight (Rengarajan et al., 2015; Wnorowski, 2017). PAHs have high boiling points which tended to increase with increasing molecular weight. Table 2.1 show

a list of 16 PAHs, their chemical abstract number (CAS), molecular weight and physicochemical properties. These 16 PAHs were compiled by the United State Environmental Protection Agency (US EPA) and the European Union (EU) as priority pollutants.

Table 2.1: List of 16 Priority PAHs and their properties (EPA, 1999; Hailwood et al., 2001)

Sn	US EPA 16 PAHs	PAH Abbreviation	Molecular Weight (g/mole)	Boiling Point (°C)	Vapour Pressure at 25 °C(Pa)	CAS Number
1	Naphthalene	NPH	128	218	11.9	91-2 -3
2	Acenaphthylene	ACY	152	265-280	3.86	208-96-8
3	Acenaphthene	ACN	154	278-279	0.50	83-32-9
4	Fluorene	FLU	166	293-295	0.43	86-73-7
5	Phenanthrene	PHN	178	339- 340	9.07×10^{-2}	85-01-08
6	Anthracene	ATR	178	340	3.4×10^{-3}	120-12-7
7	Fluoranthene	FLT	202	375 -393	1.08×10^{-3}	206-44-0
8	Pyrene	PYR	202	360-404	5.67×10^{-4}	129-00-0
9	Benzo[a]anthracene	B(a)A	228	435	6.52×10^{-7}	56-55-3
10	Chrysene	CRY	228	441-448	1.04×10^{-6}	218-01-9
11	Benzo[b]Fluoranthene	B(b)F	252	481	1.07×10^{-5}	205-99-2
12	Benzo[k]Fluoranthene	B(k)F	252	480-471	1.28×10^{-8}	207-08-9
13	Benzo(a)pyrene	B(a)P	252	493-496	6.52×10^{-7}	50-32-8
14	Indeno[1,2,3-cd]pyrene	I(123cd)P	276	536	1.3×10^{-8}	193-39-5
15	Dibenz[a,h]anthracene	D(ah)A	278	524	2.80×10^{-9}	53-70-3
16	Benzo[g,h,i]perylene	B(ghi)P	276	525	1.33×10^{-8}	191-24-2

2.2 Sources of PAHs

PAHs are ubiquitous chemical compounds which are produced generally from three primary sources: pyrogenic, petrogenic and phytogenic. Pyrogenic PAHs are formed either through high temperature pyrolysis or by incomplete combustion of natural and anthropogenic carbonaceous materials. Natural pyrogenic PAHs are produced in high concentration via volcanic eruption while the anthropogenic sources include destructive distillation of coal, thermal cracking of petroleum products, diesel and petrol combustion, coal and wood burning (Tobiszewski and Namie, 2012). Pyrogenic PAHs are also associated

with industrial activities such as foundry, steel and aluminium production, mining operations and petroleum refining (Commins, 1969; Mastral et al., 2000). Pyrogenic PAHs are likewise produced at low concentrations in grilled food, tobacco, candles and vehicle emissions (McGrath et al., 2007; Karavalakis et al., 2011).

Petrogenic PAHs are inherent within the fuel itself, for example in gasoline, lubricating oil and oil spills in water or soil. Phytogenic PAHs are those derived from plants through degradation of vegetative matter (Abdel-Shafy and Mansour, 2015). The physicochemical properties of PAHs (see Table 2.1) make them exceptionally mobile in the environment (water, soil and air) and resistant to environmental degradation (Raquel and Mesquita, 2016).

Intriguingly, PAHs can be used as intermediaries in agricultural products, pharmaceuticals, plastics, dyes, pesticides and other chemical industries. For example, naphthalene is used in mothballs; acenaphthene, fluorene and fluoranthene are used in the manufacture of dyes, pigments, pesticides and pharmaceuticals (Abdel-Shafy and Mansour, 2015).

Since PAHs are emitted in to the environment as a mixture, diagnostic ratios (relative ratios of isomeric PAH concentrations) are often used (purely based on assumptions) by environmentalists to qualitatively ascertain the sources of these PAH pollutant emissions. Diagnostic ratios are associated with PAH isomers which have identical physicochemical properties and possibly the same environmental fate. For example, from the results of correlation analysis of PAH emission sources, Pies et al. (2008) reported that if the concentration ratio of ATR/ (ATR+ PHN) < 0.1 (see Table 2.1 for PAH abbreviations), the PAH source is considered petrogenic and is pyrogenic when the ratio is > 0.1. Similarly Ravindra et al. (2008) described that if the concentration ratio of FLT/(FLT+ PYR) < 0.5, the PAH is considered from petrol emissions and is treated as diesel emissions when the ratio is > 0.5. Further details on diagnostic ratios as PAH source indicators are reviewed by Tobiszewski & Namie (2012).

2.3 Toxicity of PAHs and their health effects

Polycyclic Aromatic Hydrocarbons (PAHs) have long been considered as one of the major precursors for soot particles, while they also form the main toxic components adsorbed onto the particulates (Richter and Howard, 2000). Most PAHs are carcinogenic, mutagenic and teratogenic (Kaden et al., 1979; Kim et al., 2013) and can be present either adsorbed onto the particulates or found as breathable gaseous species in the atmosphere.

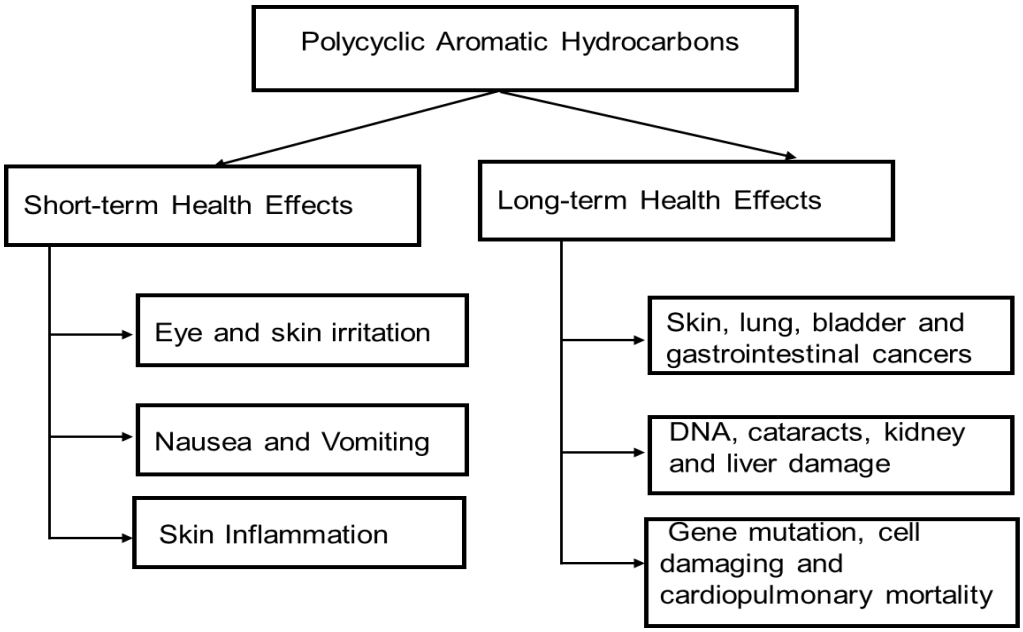

Figure 2.1:Short and long-term effects of PAHs exposure (Kim et al., 2013)

PAHs toxicity could result in short and long-term health effects. These effects depend on the molecular structure of the PAHs, PAH concentration and the level of human exposure. Figure 2.1 summarises the health effects associated with PAH exposure (Yan et al., 2004). Industrial exposure to a mixture of PAHs can induce symptoms such as eye & skin irritation, inflammation, nausea and vomiting. Yet, it is not fully understood exactly as to which PAH is responsible for each effect; for example it has been known for some time that naphthalene, anthracene and benzo(a)pyrene were causative agents for skin irritation (Badger et al., 1964), but the mechanism by which they affect the skin is not precisely known.

Extreme exposure to PAHs could ultimately lead to premature death. For instance, human mortality cases associated with air-bone particulates bearing adsorbed PAHs have been reported in some cities in the United Kingdom (Gowers, Miller and Stedman, 2014) and the United States (Richter et al., 1999).

In light of the above health reports, a number of toxicological assessments of PAHs have been made over several decades by various global agencies (Agency for Toxic Substances and Disease Registry, U.S. department of Health and Human services, 1995; EFSA, 2008). These agencies evaluated and selected several PAHs on the basis of their carcinogenicities. The selection made by the United States Environmental Protection Agency (US EPA) constituted a list of 16 priority PAHs that are now being consistently listed by researchers worldwide in the PAH analysis of environmental samples.

Table 2.2: List of Priority 16 PAHs and their Carcinogenicity groups (Nisbet & LaGoy, 1992; EPA,1993).

Sn	PAHs	Molecular Formula	Toxicity Group	Toxicity Factor	PAH Rings	Structure
1	Naphthalene	$C_{10}H_8$	D	0.001	2	
2	Acenaphthylene	$C_{12}H_8$	D	0.001	3	
3	Acenaphthene	$C_{12}H_{10}$	NA	0.001	3	
4	Fluorene	$C_{13}H_{10}$	D	0.001	3	
5	Phenanthrene	$C_{14}H_{10}$	D	0.001	3	
6	Anthracene	$C_{14}H_{10}$	D	0.01	3	
7	Fluoranthene	$C_{16}H_{10}$	D	0.001	4	
8	Pyrene	$C_{16}H_{10}$	NA	0.001	4	
9	Benzo[a]anthracene	$C_{18}H_{12}$	B2	0.1	4	
10	Chrysene	$C_{18}H_{12}$	B2	0.01	4	
11	Benzo[b]Fluoranthene	$C_{20}H_{12}$	B2	0.1	5	
12	Benzo[k]Fluoranthene	$C_{20}H_{12}$	B2	0.1	5	
13	Benzo(a)pyrene	$C_{20}H_{12}$	B2	1.0	5	
14	Indeno[1,2,3-cd]pyrene	$C_{22}H_{12}$	B2	0.1	6	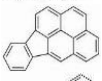
15	Dibenzo[a,h]anthracene	$C_{22}H_{14}$	B2	1.0	5	
16	Benzo[g,h,i]perylene	$C_{20}H_{12}$	D	0.01	6	

The PAH benzo(a)pyrene has been confirmed as being the most carcinogenic of the 16 EPA PAHs (Levin *et al.*, 1977) and, consequently, the most studied (Collins et al., 1998). In earlier years, the toxicity of the rest of the 15 EPA PAHs was considered as potent as that of benzo(a)pyrene by the EPA itself (EPA, 1993).

Nisbet & LaGoy (1992) subsequently evaluated and modified the new toxic equivalence factors (TEF) for each of the 16 EPA PAHs. The TEF indicates the carcinogenic potential of each of the 16 priority PAH relative to benzo(a)pyrene. Nisbet and Lagoy assigned to benzo(a)pyrene and dibenz[a,h]anthracene a TEF of unity, while benzo(a)anthracene, benzo(b)fluoranthene, benzo(k)fluoranthene and indeno(1,2,3-cd)pyrene were assigned a TEF value of 0.1. The remaining 10 PAHs of the US EPA were either 1000 or 100 times less toxic than the aforementioned six PAHs.

A year after Nisbet and Lagoy's study, chrysene was added to the above list of six PAHs by the US EPA itself (EPA, 1993) in the provisional guidance for quantitative risk assessment (EPA/600/R-93/089) and was accorded a TEF value of 0.01. The above aggregate of seven PAHs were then grouped by the US EPA (1993) as Group B2 ('*possibly carcinogenic to humans*'), while 7 out of the remaining 9 PAHs were grouped as '*unclassifiable as to carcinogenicity'* (Group D). Table 2.2 and Table 2.1 list the US EPA 16 priority PAHs, their structures, number of rings, carcinogenicity groups and toxicity equivalent factors (TEFs).

2.4 Formation of PAHs

Evolution of PAHs often begins with the formation of a first aromatic ring (phenyl radical or benzene) via several reaction pathways (Richter & Howard, 2000; D'Anna *et al*., 2000; Frenklach, 2002). The contribution of various intermediate species to PAH formation is often fuel dependent. For example, PAHs can be formed from aromatic fuels such as benzene in large concentration either indirectly, following the breakdown of fuel or by directly polymerising dehydrogenated rings. In aliphatic fuels, such as methane or ethylene, formation of the first aromatic ring is facilitated by series of rudimentary reactions,

eventually leading to the formation of the first aromatic ring, and is preceded by the breaking down of the fuel molecules (Richter & Howard, 2000).

2.4.1 Formation of first aromatic ring

Berthelot (1866) considered formation of the first aromatic ring in the late 19th century and his work was cited by Richter & Howard (2000) who researched the cyclo-trimerisation of acetylene (C_2H_2) to benzene (C_6H_6) at low temperatures of about 400 ^oC. The reaction, represented by $R_{2.1}$, occurs in the presence of a catalyst (nickel and other transition metals). Since then, there has been extensive discussion among researchers regarding different reaction pathways for the formation of the first aromatic ring.

$$3\ (C_2H_2) \rightarrow C_6H_6 \qquad R_{2.1}$$

Cole et al. (1984) were the first to consider quantitatively, the contribution of aliphatic fuels to aromatic ring formation. They established possible kinetic mechanisms by comparing predicted formation rates with the experimental values obtained using premixed flat-flames of 1, 3-butadiene at low pressure. Cole et al. proposed a ring formation mechanism via the vinyl radical (C_2H_3) addition to 1, 3-butadiene (1, 3-C_4H_6) and subsequent cyclization of hexadienyl (C_6H_9) and removal of hydrogen. The reaction sequences are represented by $R_{2.2}$ to $R_{2.5}$.

$$C_2H_3 + 1,3\text{-}C_4H_6 \rightarrow C_6H_9 \qquad R_{2.2}$$

$$C_6H_9 \leftrightarrow c\text{-}C_6H_9 \qquad R_{2.3}$$

$$c\text{-}C_6H_9 \leftrightarrow C_6H_8 + H \qquad R_{2.4}$$

$$c\text{-}C_6H_8 \leftrightarrow C_6H_6 + H_2 \qquad R_{2.5}$$

Shortly after the investigation by Cole *et a*l., the '*even-carbon-atom*' pathways were proposed by Frenklach et al. (1985) based on kinetic modelling of acetylene pyrolysis supported by shock tube experiments. The mechanism involves adding acetylene to the normal-cyclobutadiene (n-C_4H_3) radical and the normal-butadienyl (n-C_4H_5) radical to produce phenyl radicals (C_6H_5) and benzene

molecule (C_6H_6) respectively. The reactions are shown in $R_{2.6}$ and $R_{2.7}$ respectively.

$$n\text{-}C_4H_3 + C_2H_2 \rightarrow C_6H_5 \qquad R_{2.6}$$

$$n\text{-}C_4H_5 + C_2H_2 \rightarrow C_6H_6 + H \qquad R_{2.7}$$

However, Miller & Melius (1992) questioned the validity of reactions $R_{2.6}$ and $R_{2.7}$ on the basis that $n\text{-}C_4H_3$ and $n\text{-}C_4H_5$ can both be converted readily into $i\text{-}C_4H_3$ and $i\text{-}C_4H_5$ stable isomers, which would therefore mean that they could not be available in sufficiently high concentrations for the formation of benzene molecule and phenyl radical. Instead, Miller & Melius and several other investigators proposed the '*odd-carbon-atom'* pathways through the reaction of two propargyl (C_3H_3) radicals. The reactions which produce benzene molecule and phenyl radical are reproduced by reactions $R_{2.8}$ and $R_{2.9}$ respectively.

$$C_3H_3 + C_3H_3 \rightarrow C_6H_6 \qquad R_{2.8}$$

$$C_3H_3 + C_3H_3 \rightarrow C_6H_5 + H \qquad R_{2.9}$$

The implication of propargyl radicals in the formation of aromatic rings and soot has long been long been suspected prior to the formation of the above reaction pathways ($R_{2.8}$ and $R_{2.9}$), due to the exceptional stability of the propargyl radical (Frenklach et al., 1983). Propargyl is a good radical for soot formation as it is known to be a highly resonantly stable free radical, which ensures its survival in hostile flame environments compared to most ordinary radicals. It is also resistant to oxidation by oxygen molecules (Frenklach, 2002).

A number of other '*odd-carbon atom*' pathways to aromatic rings have been proposed (Ikeda et al., 2006; Wang & Brezinsky, 1998) which involve the reaction of cyclopentadienyl radicals ($c\text{-}C_5H_5$). These radicals can be produced by the reaction of the stable propargyl radical and acetylene molecule (which is relatively abundant specie in combustion and flames) as shown by reaction $R_{2.10}$.

$$C_3H_3 + C_2H_2 \rightarrow c\text{-}C_5H_5 \qquad R_{2.10}$$

The cyclopentadienyl radical subsequently reacts with a methyl radical to produce benzene; it is also possible that two cyclopentadienyl radicals can

combine to produce naphthalene ($C_{10}H_8$) directly, avoiding the need for the formation of a first aromatic ring (benzene or phenyl). These reactions are shown in reactions $R_{2.11}$ and $R_{2.12}$ respectively.

$$c\text{-}C_5H_5 + CH_3 \rightarrow C_6H_6 + H + H \qquad R_{2.11}$$

$$C_5H_5 + C_5H_5 \rightarrow C_{10}H_8 + H + H \qquad R_{2.12}$$

Even though evolution of PAHs via the formation of first aromatic rings is probably the most prolific route for PAH growth, the formation of PAHs can also occur by directly forming '*multi-ring*' PAHs as shown in reaction $R_{2.12}$ for naphthalene, thereby avoiding the formation of first aromatic rings (Frenklach et al., 1993). Many other propositions for PAH formation mechanisms have been put forward and these include the formation of aromatics from poly-acetylene condensation and reactions of C_4H_x radicals (Richter & Howard, 2000).

Lastly, it is important to note that the reactant species and radicals mentioned in section 2.4.1 are intermediate products formed by the fragments of a wide variety of fuel molecules. It is therefore possible to produce aromatic rings, PAHs and soot from a very wide variety of fuel molecules, ranging from the very simple methane molecule to larger more complex molecules, as well as from oxygen bearing molecules such as ethanol and fatty acids.

2.4.2 Poly-aromatic growth

Poly-aromatic growth beyond the first ring was initially known to be dominated by the hydrogen-abstraction-acetylene-addition (HACA) mechanism (Frenklach, 2002), but further studies have established that the HACA mechanism is too slow to explain the observed rates of PAH formation (Shukla and Koshi, 2011). Additional proposed PAH growth pathways include: methyl-addition and cyclisation (Shukla et al., 2010), phenyl-addition and cyclisation (Shukla et al., 2008), as well as vinyl -addition and cyclisation (Shukla and Koshi, 2012a). Aromatic radical – radical and radical – molecule reactions were also reported (Shukla et al., 2007).

2.4.2.1 Hydrogen Abstraction Acetylene Addition (HACA)

The HACA mechanism was first introduced in 1991 by Frenklach & Wang. It involves a *repetitive* sequence of reactions which first remove a hydrogen atom from a given aromatic molecule (denoted by A_i, where *i* is the number of condensed rings) by a hydrogen radical (H) thereby making the aromatic molecule a radical denoted by A_i- (see reaction $R_{2.13}$) and subsequently adding a gaseous acetylene molecule (C_2H_2) to the aromatic radical site left by the abstraction of hydrogen. This description of the HACA mechanism and reactions $R_{2.13}$ and $R_{2.14}$ were cited by (Frenklach, 2002). The significance of these reactions is discussed further below.

$$A_i + H \rightarrow A_i - + H_2 \qquad R_{2.13}$$

$$A_i - + C_2H_2 \rightarrow \text{product} + H \qquad R_{2.14}$$

Reaction $R_{2.13}$ converts the molecule by means of hydrogen abstraction into an active radical, so that it can undergo additional growth. Conversion of a molecule to a radical can be implemented in several ways, but hydrogen abstraction by gaseous hydrogen is the dominant pathway observed under flame and shock tube pyrolysis conditions (Frenklach et al., 1983; Frenklach & Wang, 1991). One characteristic of the hydrogen abstraction in HACA is its reversibility. The aromatic radical can be re-stabilised into a molecule by adding to it a gaseous hydrogen (H_2) or through reaction with hydrogen radicals, as shown in reactions $R_{2.15}$ and $R_{2.16}$ respectively. Acetylene addition is also reversible as shown in $R_{2.17}$. The acetylene addition decides to a large extent, the rate of PAH growth (Frenklach, 2002).

$$A_i - + H_2 \rightarrow A_i + H \qquad R_{2.15}$$

$$A_i - + H \rightarrow A_i \qquad R_{2.16}$$

$$A_i - + C_2H_2 \leftrightarrow A_iC_2H + H \qquad R_{2.17}$$

An example of the HACA mechanism can be found in the formation of the smallest tri-cyclic PAH (acenaphthylene) from a phenyl radical (C_6H_5) as shown in $R_{2.18a}$ to $R_{2.18f}$. The phenyl radical can be produced by abstraction of hydrogen from benzene (C_6H_6). The HACA mechanism, as its name states, proceeds

through repetitive reaction in which hydrogen is abstracted and acetylene is added until a PAH is formed.

First, hydrogen is abstracted from the phenyl radical which results in benzyne (C_6H_4) and a hydrogen molecule (H_2) as shown in $R_{2.18a}$. Reaction$R_{2.18b}$ shows the formation of phenyl acetylene (C_8H_5) due to acetylene addition to benzyne. As represented in $R_{2.18c}$, hydrogen is further removed from phenyl acetylene to make it a radical (C_8H_5). Naphthyl ($C_{10}H_7$) is formed in $R_{2.18d}$ by adding acetylene to a phenyl acetylene radical. Reaction $R_{2.18e}$ shows the formation of acepentalene ($C_{10}H_6$) due to hydrogen abstraction. Finally, addition of acetylene to acepentalene as shown in $R_{2.18f}$ produces acenapthylene ($C_{10}H_8$). The entire reaction pathways ($R_{2.18a}$ to $R_{2.18f}$) in forming acenaphthylene from phenyl radical is also reproduced in Figure 2.2.

$$C_6H_5 + H \rightarrow C_6H_4 + H_2 \qquad R_{2.18a}$$

$$C_6H_4 + C_2H_2 \rightarrow C_8H_6 \qquad R_{2.18b}$$

$$C_8H_6 + H \rightarrow C_8H_5 + H_2 \qquad R_{2.18c}$$

$$C_8H_5 + C_2H_2 \rightarrow C_{10}H_7 \qquad R_{2.18d}$$

$$C_{10}H_7 + H \rightarrow C_{10}H_6 + H_2 \qquad R_{2.18e}$$

$$C_{10}H_6 + C_2H_2 \rightarrow C_{12}H_8 \qquad R_{2.18f}$$

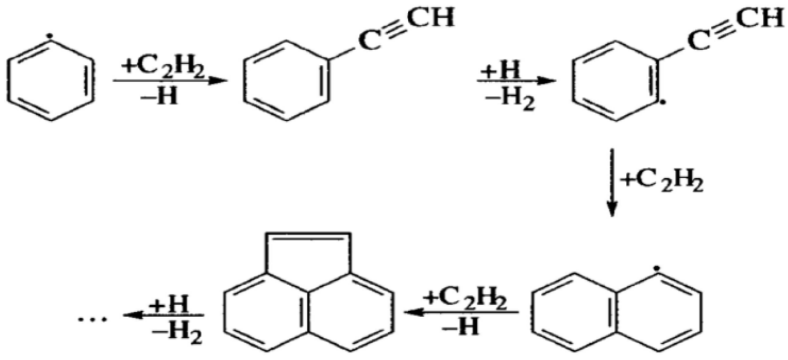

Figure 2.2: Primary reaction pathways for the formation of acenaphthylene from Phenyl radical by HACA mechanism (Frenklach & Bornside, 1984)

While HACA can produce symmetrical PAHs, its major weaknesses as a dominant PAH growth mechanism are: Firstly, HACA may be '*too slow*' to explain

the observed rapid experimental processes of PAH growth and subsequent soot formation, since the atomic mass of the PAH product only increase by 24 atomic mass unit (amu). Secondly, HACA may terminate the PAH growth reactions by producing compounds with alternating single and triple bond (poly-yne) compounds and stable five-membered ring PAHs such as the acenaphthylene produced in Figure 2.2.

2.4.2.2 Phenyl Addition and Cyclisation (PAC)

Since HACA is perceived as a slow reaction mechanism, research was intensified in search for faster reaction routes. In 2008, Shukla et al. proposed phenyl addition and cyclisation (PAC) mechanism observed during pyrolysis of toluene and toluene-benzene mixtures in a tubular reactor. A classic PAC mechanism begins by adding a phenyl radical to any fusing site (e.g. sites A in reactions $R_{2.19}$ and $R_{2.20}$) of an aromatic molecule and then followed by dehydro-cylisation or cyclo-dehydrogenation (loss of hydrogen molecule and cyclisation of the carbon atoms) thereby producing two additional fusing sites.

A typical example of a PAH growth PAC mechanism as provided by Shukla & Koshi (2011) is the formation of ortho-terphenyl (3 x phenyl or $C_{18}H_{14}$) from benzene molecule and also formation of benzo(e)pyrene ($C_{20}H_{12}$), a five ring PAH, from phenanthrene (a three ring PAH). These reactions are represented by $R_{2.19}$ and $R_{2.20}$ respectively. The PAH growth mechanism in reaction $R_{2.19}$ is initiated by adding a phenyl radical (C_6H_5) to a benzene molecule (C_6H_6) followed by dehydrogenation to form biphenyl molecule and then further addition of a phenyl radical to biphenyl to form ortho-terphenyl ($C_{18}H_{14}$). The de-hydro-cyclisation (*i.e, elimination of hydrogen molecule combined with ring formation*) of terphenyl results in the PAH phenanthrene. Further addition of phenyl radical to phenanthrene molecule followed by dehydrogenation converts phenanthrene to benzo(e)pyrene as shown in reaction $R_{2.20}$.

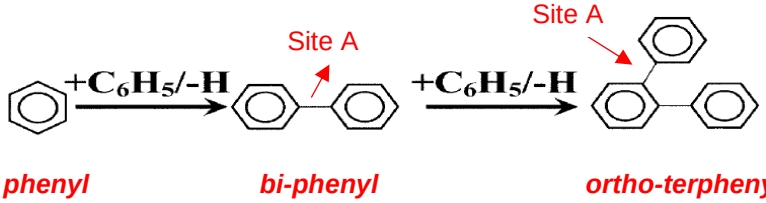

$R_{2.19}$

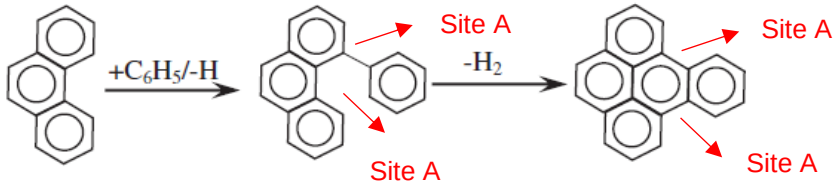

R2.20

phenanthrene ***benzo(e)pyrene***

The advantage of PAC over the HACA mechanism is that PAC can apparently support, in principle, limitless growth of PAH, since each growth step produces two additional fusing sites for further ring growth. The PAC mechanism is also recognised to be faster than HACA, since 77 amu atomic mass is added to each PAH species in a single reaction step. In contrast, PAH growth can be terminated after a limited number of steps in HACA mechanism. A drawback of the PAC approach, is its inability to produce symmetrical PAHs as compared with HACA.

2.4.2.3 Methyl Addition and Cyclisation (MAC)

MAC mechanism was proposed by Shukla et al. (2010) following their experiment on gas phase pyrolysis of toluene and toluene/acetone mixtures in a tube reactor. A conventional MAC mechanism is initiated by adding one or more methyl radicals to an aromatic specie followed by cyclo-dehydrogenation, thereby forming a cyclo-penta fused or benzenoid PAH. An example of MAC mechanism include the formation of indene from toluene and naphthalene from indene. These reaction sequences are shown below in $R_{2.21}$ and $R_{2.22}$. Reaction $R_{2.21}$ starts with addition of two methyl (CH_3) radicals to an aromatic toluene followed by de-hydro-cyclisation to produce the cyclo-penta fused molecule of indene PAH (C_9H_8). In the case of reaction $R_{2.22}$, indene molecule grows through addition of a methyl radical (CH_3) followed by dehydrogenation and re-cyclisation, resulting finally to the two ring PAH naphthalene ($C_{10}H_8$) (Shukla & Koshi, 2011).

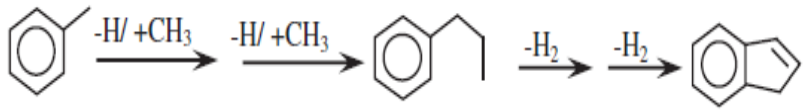

R2.21

Toluene ***Indene***

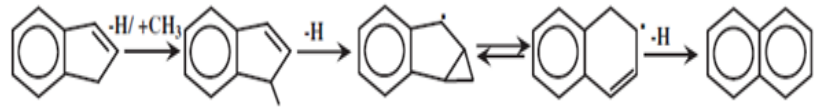

R2.22

Indene ***Naphthalene***

The MAC mechanism is relatively effective for PAH formation, since it can accelerate limitless growth and likewise produce symmetrical PAHs. One key drawback of MAC is that it is even slower than the HACA and, of course, the PAC mechanisms, as the atomic mass of each aromatic molecule can only be increased by 14 amu in each reaction step of the PAH growth. The methyl radicals in MAC mechanism are unstable since they can easily react with other radicals to produce new radicals and stable species.

2.4.2.4 Hydrogen Abstraction, Vinyl Radical Addition (HAVA)

HAVA mechanism was proposed by Shukla & Koshi (2012) based on in-situ direct sampling mass spectrometric studies in toluene pyrolysis. The mechanism is based on the concept of abstracting hydrogen from an aromatic molecule and adding vinyl radical to a fusing site. If one considers the formation of fluoranthene for instance, the HACA stops once acenaphthylene is formed, but the HAVA mechanism can go beyond the formation of acenaphthylene to produce fluoranthene. For example, naphthalene is produced from benzene molecule in reaction sequence $R_{2.23}$ and fluoranthene ($C_{16}H_{10}$) can be formed from naphthalene in reaction sequence $R_{2.24}$.

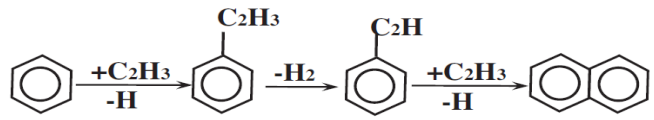

$R_{2.23}$

benzene ***naphthalene***

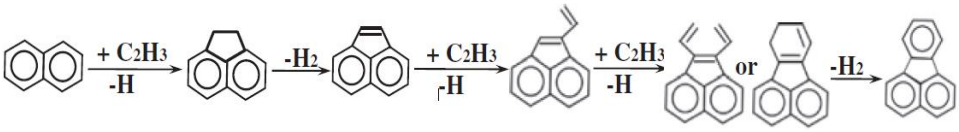

$R_{2.24}$

acenaphthene ***acenaphthylene*** ***fluoranthene***

Reaction sequence $R_{2.23}$ begins with a benzene ring (C_6H_6), which undergoes hydrogen abstraction and vinyl radical addition to produce styrene ($C_6H_5CH=CH_2$ or C_8H_8) followed by dehydrogenation ($-H_2$) of styrene to phenyl-acetylene ($C_6H_5C\equiv CH$or C_8H_6). Further addition of a vinyl radical to phenyl-acetylene, combined with hydrogen abstraction, results in naphthalene ($C_{10}H_8$).

Naphthalene then proceeds via reaction sequence $R_{2.24}$ which involves successive steps of vinyl radical addition and hydrogen abstraction to produce fluoranthene ($C_{16}H_{10}$) as a four-ring PAH.

Reaction sequence $R_{2.24}$ starts with naphthalene and, following hydrogen abstraction and vinyl radical addition, acenaphthene is formed which converts to acenaphthylene with loss of a hydrogen molecule ($-H_2$). Further hydrogen abstraction and vinyl radical addition to acenaphthylene results in 1-ethynylacenaphthylene, to which again a vinyl radical is added following hydrogen abstraction to produce 1, 2-diethynlacenaphthylene or dihydrofluoranthene which reconfigures to the PAH fluoranthene with hydrogen loss ($-H_2$).

Finally, all the reaction pathways discussed are limited on their own, since they are all (in a way) dependent on the local experimental conditions and are often stimulated by one or more reactive species. Considering the complex nature of active radicals produced in a practical combustion system such as internal combustion engine, it would be appropriate to mention that no single mechanism can dominate the growth of PAHs. This is because, none of the above reaction pathways are sufficiently rapid, individually, in comparison to the faster soot formation observed in experiments. A combination of PAC and HACA for instance, occurring simultaneously, could result in PAH growth rates approaching those observed experimentally in soot formation.

2.5 Soot Formation

Although soot cannot be defined distinctly, it has been described by Tree & Svensson (2007) as a solid substance having carbon to hydrogen ratio (C/H) of approximately 8:1. Freshly formed particles have the highest number of hydrogen atoms with C/H ratio up to unity. Choi *et al.* (1994) reported the numerical density of soot as 1.84 ± 0.1 g/cm^3. Soot is mostly formed from unburned fuel and can therefore adsorb hydrocarbons (such as PAHs) and other molecules depending on the prevailing conditions. The combination of soot and other solid and liquid phase matter, which can be collected on a filter from combustion generated exhaust gases is called particulate or particulate matter (Tree and Svensson,

2007). Particulate is usually divided into soluble and insoluble (dry fraction). Soot is often approximated to the insoluble fraction of particulate.

Formation of soot involves a complex series of reactions and physical processes culminating in the formation of agglomerates of soot particles. These particles are formed by numerous de-hydrogenated polymerised hexagonal rings (PAHs) and vary widely in size from single primary particles, formed by condensation reactions, having sizes of roughly 5 to 30 nm and particulates which have sizes from roughly 30 nm to 1000 nm and which comprise coagulated primary particles onto which further soot matter has been added.

Soot formation involves five major processes which are depicted in Figure 2.3. Namely: pyrolysis, nucleation, coalescence, surface growth and agglomeration. Pyrolysis refers to the decomposition of organic compounds such as hydrocarbon fuels at high temperature without considerable oxidation even though oxygen/oxygen bearing molecules may be present. Virtually all hydrocarbon fuels undergo pyrolysis. The rate of hydrocarbon pyrolysis is dependent on temperature and concentration of the fuel. All fuel pyrolysis typically produces the same intermediate products such as unsaturated hydrocarbons (acetylene and poly-acetylenes) and PAHs (Tree and Svensson, 2007). The commonest pyrolysis species include: acetylene, ethylene, methane, propane and benzene (Haynes & Wagner, 1981). These species are generally considered as soot precursors and are produced irrespective of the molecular structure of the starting fuel.

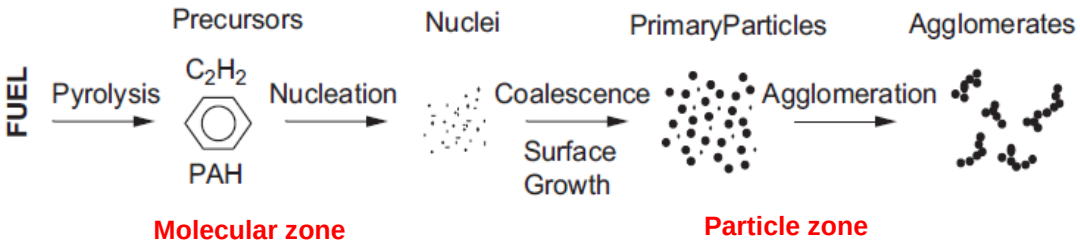

Figure 2.3:Schematics of the soot formation processes (Tree & Svensson, 2007)

The molecular zone in soot formation, which includes the soot precursors, is where large PAHs are formed and grow. The growth process of the first aromatic ring to larger PAHs having 500 – 1000 amu and sizes of 0.5nm is common for most hydrocarbons. Formation of the first aromatic ring is pre-requisite for soot

formation, especially so for hydrocarbons with aliphatic and olefinic nature. The processes of first aromatic ring formation and PAH growth has been described previously in section 2.4 of this thesis.

The particle zone includes the inception of particles from heavy PAHs and nucleation (inception) of solid particles from heavy PAHs having molecular weight of roughly 2000 amu and diameter of 1.5 nm. Such particle nuclei are formed at temperatures around 1300 - 1600K and do not contribute considerably to the total soot mass, since they provide sites for later surface growth (Blacha *et al.*, 2012; Richter & Howard, 2000). The stages of growth to larger PAHs which lead to soot nucleation and growth are similar for all fuels and, in fact, are faster than the rate at which the first aromatic ring is formed. Thus, the rate at which the first aromatic ring is formed determines the soot incipient rates, which ultimately dictates the ease of a hydrocarbon to form soot (Tree and Svensson, 2007).
Immediately after the nascent soot particles are formed, their mass begins to increase (*surface growth*) through addition of gas phase molecules (acetylene and PAHs) to the surface of the particles. During surface growth, the mass of soot increases while the particle number remain the same. The end of nucleation and the start of surface growth were reported to occur simultaneously (Tree & Svensson, 2007), with no observable transition between them. Most of the individual primary soot particle mass is added during surface growth to form primary particles of sizes of roughly 30 nm.

Collision between particles (*coalescence or coagulation*) during *mass growth* result in agglomeration of individual particles into clusters and this greatly increases the particle size. This results in decrease in the number of particles while the total mass of the soot remains constant. During coalescence, two or more particles combine to form one larger particle. Agglomeration begins when the coalesced particles stick together to form larger groups of particles. The size of the agglomerated soot particles depend on the combustion operating conditions, but on average, they fall in the range of 20 – 70 nm (Tree & Svensson, 2007). In diesel engines, Ladommatos and Zhao (1994) reported that these particles agglomerate further towards the end of combustion, and were observed in the exhaust as '*chain-like*' with sizes in the range of 100 nm – 2 µm. The structure of particles undergoes gradual transformation from amorphous soot

material to a more *graphitic carbon.* Smith (1981) added that the '*graphite-like*' structure of soot makes it more resistant to oxidation.

2.6 Soot Oxidation

Oxidation results in conversion of hydrocarbons and soot to CO, CO_2, and H_2O depending on the availability of oxygen or oxygen bearing radical. Active oxidation species depend on the combustion system and fuel/air mixture characteristics (lean, stoichiometric or rich mixture). The major oxidizing agents are OH, O and O_2, with OH and O_2 being the most prevalent contributors in rich and lean combustion respectively. Oxidation occurs at any stage of the soot formation process shown in Figure 2.3., from pyrolysis to agglomeration when the temperature is above 1300 K (Tree and Svensson, 2007). The combination of oxidation and soot formation rates determines the rate at which soot is formed.

2.7 Formation of PAH and Soot in diesel engines

Understanding diesel spray combustion and particulate formation in direct injection (DI) compression ignition (CI) engine has been improved significantly in recent years. A conceptual model that results in soot formation during quasi steady phase of combustion in a heavy duty DI diesel engine was developed by Dec (1995) and cited by Musculus et al. (2012). The Dec model schematics that summarises diesel combustion is shown in Figure 2.4. As a liquid fuel is injected at high pressure through a small hole in the injector nozzle into the engine cylinder containing hot compressed air, it is entrained by the surrounding gases, forming a cone-shape spray as shown as (1) in Figure 2.4.

The injected liquid fuel is then atomised and droplets are formed which, in turn, vaporise completely thereafter by mixing with the hot entrained gases. Images obtained using the Rayleigh Scattering show the vaporised air/fuel mixture downstream of the liquid fuel as overly uniformly rich with equivalent ratio (Φ) ranging from 2 to 4 (Musculus et al., 2012). Fuel pyrolysis is initiated by energy transfer to the fuel by the hot air and pyrolysis is, therefore controlled by the rate of fuel/air mixing.

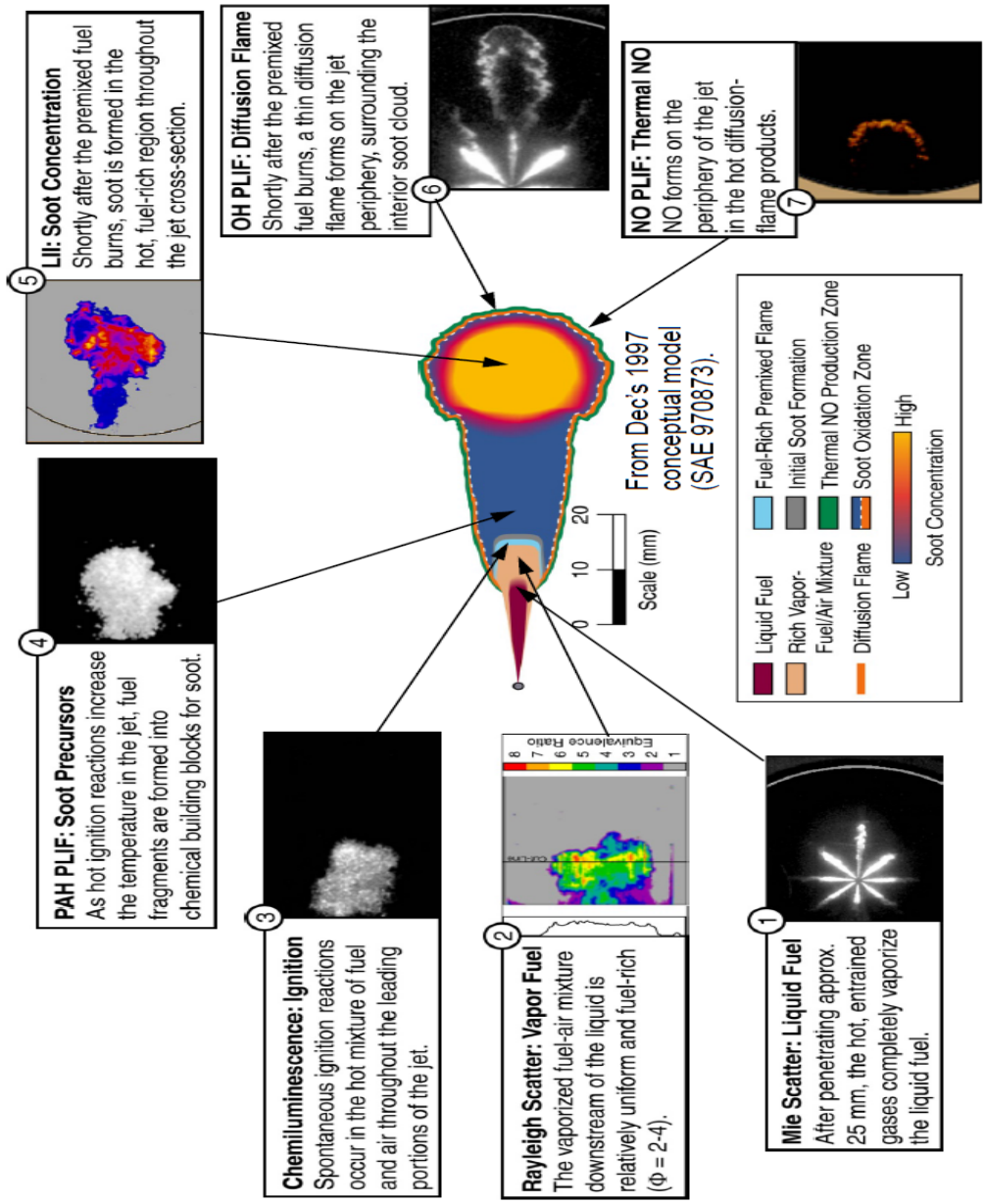

Figure 2.4: Diesel conceptual model describing fuel mixing and combustion, up to the end of injection (Dec, 1997; Musculus *et al*., 2012).

In diesel engine combustion, ignition delay (ID) is described as the interval in crank-angle-degrees (CAD) between the start of injection (SOI) and start of combustion (SOC). The initial detection of heat release after fuel auto-ignition is conventionally designated as the SOC. The premixed combustion phase is characterised follows the occurrence of auto-ignition of fuel/air pockets which pre-mixed during ID period (Heywood, 1988). Figure 2.5 shows typical characteristics of heat release rate. The peak heat release rate in Figure 2.5 is due to rapid combustion of premixed fuel prepared during ignition delay period and it results in rapid rise in in-cylinder temperature and pressure. The premixed combustion

phase is divided by a point which shows the rate of fuel/air mixtures becoming available for combustion (mixing controlled phase), however, this point is not distinctly clear in modern engines (Tauzia *et al.*, 2006)

Turning now back to Figure 2.4, chemiluminescence was used by Dec (1995) to detect the first appearance of heat release following multiple-site ignition of fuel/air mixture (see (3) in Figure 2.4). PAHs and other building blocks for soot formation were detected by Dec (1997) using planar laser induced fluorescence (PLIF), following breaking down of the fuel vapour during the initial stage of premixed combustion (see (4) in Figure 2.4). PAHs have been known for some time to be principal soot precursors (Richter & Howard, 2000) and their formation mechanisms has been described previously in section 2.4 of this thesis. Soot is formed in the hot, fuel rich, regions of the fuel jet and it takes place immediately after the premixed fuel has been burned. A thin layer of diffusion flame forms and encircles the internal soot cloud as can be seen in (5) and (6) in Figure 2.4.

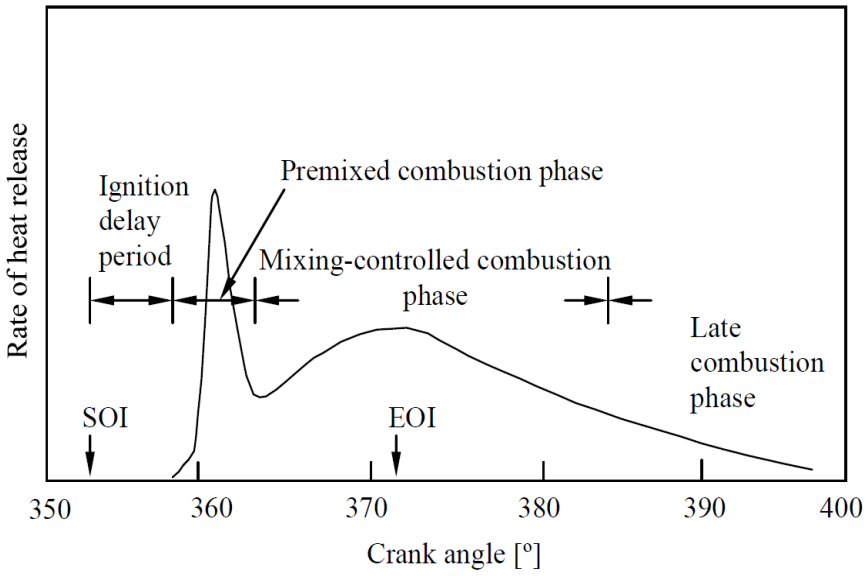

Figure 2.5: Classic heat release rate (J/ deg) curve of a DI compression-ignition engine identifying different combustion phases (Heywood, 1988).

The distance between the injector and the diffusion flame is called the lift-off length (LL) and is a crucial parameter for soot formation in CI engines. A large lift-off length encourages more air and oxygen entrainment which can oxidise the soot precursors in the core of the fuel spray. Larger soot particles were observed by Dec (1995) at the circumference of the premixed region, suggesting that the soot particles must have grown as they approach the edge of the premixed flame.

2.8 PAH emissions from tube reactors

The identity and concentration of PAHs produced from tube reactors and from most practical combustion systems depend on several factors, such as chemical structure of the fuel molecule, temperature distribution in the reactor, residence time and mixing behaviour in the reactor, fuel/air ratio (equivalence ratio) and sites or sinks in the reactor which either converts or adsorb PAHs (Bruinsma and Moulijn, 1988).

Temperature has been reported as one of the most critical parameter in determining the type and concentration of PAHs formed in a reactor. The distribution of temperature in reactors depends primarily upon the size of the reactor and the characteristic heat transfer within the reactor. At high temperatures higher than 1327 ^{o}C for example, heat transfer by radiation might control the temperature inside the reactor (Bruinsma and Moulijn, 1988). Increasing temperature of reactors and combustion systems generally decreases the fuel residence time. Long residence times of fuel in the reactor lead to high conversion of fuel to pyrolysis products (Viteri et al., 2017).

The speciation of individual PAHs into different sizes (number of rings) during fuel pyrolysis is often controlled by the pyrolysis temperature and the molecular structure of the starting fuel molecule. PAHs having two and three rings have been classified as low molecular weights (LMWs). Those PAHs having 4 rings are referred to as medium molecular weights (MMWs), while those with 5 and 6 rings are the high molecular weight (HMW) PAHs (Ballesteros et al., 2015). Low temperature pyrolysis has been reported to favour the formation of LMW and MMW PAHs, whereas high temperature pyrolysis is believed to promote the formation of HMW PAHs (Tobiszewski and Namie, 2012).

Early examples of research into PAH speciation from flow reactors include those of Badger et al. (1964), who investigated pyrolysis of the PAH anthracene, diluted in nitrogen, in a silica tube at low temperatures ranging from 700 to 950 ^{o}C. They detected PAHs and other intermediate pyrolytic products using gas chromatography and ultraviolet/fluorescence spectrometry. Badger et al. reported that increasing pyrolsis temperature from 700 to 950 ^{o}C did not only

favour the production of more PAHs, but also increased the molecular masses of the PAHs. Speciation of the PAHs observed by Badger *et al*. (1964) varried. For example, a 3 ring ATR (see Table 2.1for the definition of acronyms) was the only PAH identified at the lowest temperature of 700 ^{o}C, while greater number of PAHs with sizes ranging from 2 to 4 rings (NPH, ACY, PHN, ATR FLT and PYR) were detected at the highest temperature of 950 ^{o}C. These findings suggest that increasing pyrolysis temperature tended to increase the number and sizes of PAHs.

More than two decades later, Bruinsma and Moulijn (1988) examined the pyrolytic formation of PAHs in a tube reactor in argon-diluted mixture of six hydrocarbon fuels within the temperature range of 627 – 927 ^{o}C. The six fuels examined included 5 aromatic molecuels (toluene, benzene, ethylbenzene, styrene and phenyl-acteylene) and one aliphatic molecule (n-decane). At temperatures below 827 ^{o}C, Bruinsma and Moulijn detected only non condensed intermediate molecules such as biphenyl (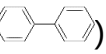) from benzene pyrolysis. At relatively higher temperatures around 927 ^{o}C, however, the non-condensed compounds were found to be unstable and thus converted to stable condensed PAHs. The findings of Bruinsma and Moulijn interestingly appeared to support the results of previous studies that the formation of condensed 3 to 4 rings PAHs (ACY, FLT and PYR) was broadly favoured by the pyrolysis temperature while the preferencial yield of 3 ring PAHs (PHN, FLU and ATR) dependend on the molecular structure of the aromatic hydrocarbon tested. In orther words, at temperatures lower than 827 ^{o}C, the molecular configuration of the test fuels determined the production of LMW PAHs such as PHN and ATR and it was less significant in determining the yield of PAHs at high temperatures. For instance, the PAH yields for n-decane and toluene were found by Bruinsma and Moulijn to be comparatively similar at high temperatures.

Despite the widely-reported view by most researchers that increasing pyrolysis temperature favours the formation of higher molecular weight PAHs, a growing body of literature observed rather contrasting effects on the influence of temperature on the speciation of diverse PAH sizes. For example, during cellulose pyrolysis, McGrath et al. (2003) detected low molecular weight PAHs

dominated by the 2 ring NPH at a low temperature of 400 ^{o}C and the high molecular weight PAHs (B(a)P and B(a)A) at also low temperature of 500 ^{o}C. On the contrary, in toluene pyrolysis at significantly higher temperatures ranging from 1100 to 1800 ^{o}C, Colkert and Seery (1994) identified low and medium molecular weight PAHs having 3 to 4 rings (ATR, PHN, PYR, FLU and ACY) (see Table 2.1 for the definition of acronyms).

Increasing pyrolysis temperature has been reported to substantially increase not only the molecular weight of the PAHs, but also the number of PAH isomers, regardless of the structural complexity of the PAH (Pope *et al.*, 2000). Isomerisation at high temperatures was reported by Pope *et al*. (2000) to partially convert less mutagenic PAHs such as benzo(e)pyrene to its corresponding structural isomer of benzo(a)pyrene; which is highly mutagenic.

The effect of molecular structure of the fuel on PAH sizes obtained from pyrolysis has, sometimes, been reported to be much stronger than the effect of pyrolysis temperature. For example, Wang and Cadman (1998) studied PAH and soot formation from pyrolysis and combustion of three structurally different fuels (toluene, n-heptane and propanol-1) in a reflected shock waves. The experiments were conducted within the temperature range of 727 - 2727 ^{o}C and pressure of 2 - 25 bar. Wang and Cadman Wang and Cadman (1998) carried out pyrolysis and combustion of the hydrocarbon fuels in argon and also in argon/10% oxygen. PAHs were analysed using high pressure liquid chromatography (HPLC) equipped with mass spectrometry. Wang and Cadman (1998) detected similar identities of PAHs from both aromatic toluene and aliphatic heptane soot samples, but the concentration of PAHs and the soot yield from heptane combustion was considerably lower than those obtained from toluene combustion. Wang and Cadman also reported that the PAH mass on the soot samples collected from the oxygen-bearing propanol-1 was very small and it was not even adequate for HPLC analysis. However, when propanol-1 was mixed with 10% tetredecane, Wang and Cadman (1998) observed that the concentration of PAHs emitted from the resulting propanol-1/tetradecane blend was similar to those obtained from heptane and toluene fuels under comparable conditions.

Among the light hydrocarbon species considered as PAH and soot precursors, acetylene has received much attention in the literature. Acetylene is a common product of most hydrocarbon pyrolysis and its reaction pathways for PAH formation has been discussed extensively. For example, Sánchez *et al.* (2012) studied PAH and soot formation from acetylene and ethylene pyrolyses within the temperature range of 800 – 1150 ^{o}C at atmospheric pressure in a tubular flow reactor. Their methodology involved collecting soot and gaseous pyrolysis products, followed by PAH extraction from the soot and gaseous products using classical Soxhlet and rotary evaporation of the solvent and subsequent GCMS analysis of the PAH extracts. Sánchez *et al.* (2012) reported that acetylene pyrolysis produced higher concentration of PAH and soot within the temperature range of 800 - 950 ^{o}C than ethylene pyrolysis. However, at temperatures above 950 ^{o}C, Sánchez et al. observed that the total PAH concentration (sum of gas and particulate phases) was slightly higher in the case of ethylene pyrolysis than in acetylene pyrolysis. These results suggest that the effect on PAH concentration of the molecular structures of acetylene and ethylene is more significant at lower temperatures.

When the oxygen molecule is introduced during pyrolysis of light hydrocarbons such as acetylene, it can either inhibit or promote temperature influences on the total mass of PAHs and soot, depending on whether the temperature is low or high. Inspired by this possibility, Frenklach *et al.* (1990) examined soot formation during oxidation of acetylene, allene, 1,3-butadiene, toluene, benzene and chloro-benzene in a shock-tube at high temperatures ranging from 1157 – 3217 ^{o}C. Frenklach et al. reported that adding small concentration of oxygen to the 6 hydrocarbons encouraged soot formation at lower temperatures and retarded it at very high temperatures. Further observations by Frenklach et al. demonstrated that the effect of oxygen on soot yield depended on the molecular structure of the hydrocarbon fuel examined, and it was most prolific for unsaturated hydrocarbons (acetylene, allene and 1,3-butadiene).

The global effects of oxygen on PAH and soot emissions has been explained by Frenklach et al. (1990) in shock tube experiments using acetylene as a starting hydrocarbon. These effects are summarised as follows: a) oxygen promotes decomposition of fuel molecules b) it encourages production of hydrogen atoms

and other radicals which then promote PAH growth at low temperatures c) stimulation of aromatic radical oxidation by molecular oxygen. Studies in the literature have attempted validating Frenklach et al.'s conclusion. For example, a recent study conducted by Sánchez et al. (2012) involved investigating the presence of oxygen on PAH formation during acetylene pyrolysis within a temperature range of 600 - 1050 ^{o}C. They reported that adding oxygen up to 10,000 ppm to acetylene pyrolysis promoted the formation of soot and PAHs under fuel rich conditions and at the lowest temperature tested (600 ^{o}C). At the highest pyrolysis tempeture (1050 ^{o}C) however, Sánchez et al observed that increasing oxygen level decreased the amount of PAHs, soot and PAH precursors such as benzene. In a related study of acetylene pyrolysis by the same research group under the same temperature range, Sánchez et al. (2013) examined the effects of temperature and fuel concentration on PAH formation in a tubular reactor. They reported increase in PAH yield with increasing fuel concentration from 10,000 – 30,000 ppm. Sánchez et al. (2013) reported that the maximum yield of total PAHs was observed at a temperature of 950 ^{o}C regardless of the acetylene concentration used and the overall PAH concentration declined with rise in temperature above 900 ^{o}C.

The influence of molecular structure of solid fuels such as biomass, coal, pure-PAHs and dry sewage sludge on the concentration of PAHs formed is rather complex due to numerous physical and chemical processes involved in their pyrolysis. For instance, Mukherjee et al. (1994) carried out pyrolysis of argon-diluted pyrene (a 4 ring PAH) in a laminar flow tube furnace within the temperature range of 927 – 1227 ^{o}C. They identified several pyrolysis products including bi-pyrenes, which were believed to be formed from direct polymerisation of aromatics. McGrath et al. (2001) investigated experimentally pyrolysis of biomass materials (cellulose, pectin and chlorogenic acid). They studied PAH formation in a quartz tube at low temperatures ranging from 300 to 850 ^{o}C. McGrath et al. reported that chlorogenic acid produced the highest PAH mass at low temperatures when compared with cellulose and pectin and the higher PAH mass from chlorogenic acid was attributable to its large aromatic content.

In order to further understand PAH formation from complex solid fuels, pyrolysis of model fuels such as catechol (representative structures in wood, coal and

tobacco) were reported. For example, Marsh et al. (2004) investigated pyrolysis of ortho-dihydoxy benzene (catechol) in a laminar flow reactor within the temperature range of 700 -1000 ^{o}C. They identified several pyrolysis products using GC-FID (GC with flame ionisation detector). Marsh et al. reported aromatic intermediates such as indene and benzene dominating the pyrolysis products at low temperatures, while larger benzenoid PAHs were believed to be formed via polymerisation of benzene rings at higher temperatures. In recent years, Dai et al. (2014) studied PAH formation from pyrolysis of dry sewage sludge in a well controlled tubular reactor and within temperatures ranging from 250 to 1250 ^{o}C. They reported that PAHs having 2 - 3 rings (NPH, ACN, FLU) and orginally present in the sewage sludge, influenced the total PAH emission at low pyrolysis temperature of 250 - 550 ^{o}C. However, when the pyrolysis temperature was increased to 950 ^{o}C, Dai et al. observed that the concentration of PAHs having 2- 3 rings decreased while the concentration PAHs having 5-6 rings (B(b)F, B(k)F, B(a)P, I(123-cd)P and B(ghi)P) increased.

Among the molecular structural features of fuel molecules described in the literature, isomerism (molecular compactness) has been reported to influenece the concentration of PAHs formed. Viteri et al. (2017) recently examined PAH and soot formation from pyrolysis of four butanol isomers (tert butanol, 2-butanol, 1-butanol and iso-butanol) at three temperatures: 1002, 1102 and 1202 ^{o}C. They developed a ranking system based on soot and PAH concentyrations produced by the four isomers, which took into account the increase in molecular compactness and the ease of isomer decomposition. The resulting ranking was as follows for PAH and soot concentrations: tert butanol > 2-butanol > 1-butanol > isobutanol. Viteri et al. also observed the total PAH concentration decreasing with increase in pyrolysis temperature from 1002 - 1202 ^{o}C regardless of the fuel isomer examined.

The Influence of carbon number of hydrocarbons on PAH formation has mostly been investigated in flames and rarely examined under pyrolysis conditions. Siegmann and Sattler (2000) investigated PAH formation mechanisms in a laminar diffusion flame in the case of methane (C_1) using time-of-flight mass spectroscopy. They reported abundant concentrations of benzenoid PAHs with hexagonal carbon rings (NPH, ATR and PYR). The modelling results of Bakali

et al. (2012) for a low pressure sooting C_1 flame, validated experimentally, also demonstrated high abundance of benzenoid NPH and PYR under fuel-rich conditions. Vincitore and Senkan (1998) studied PAH formation using heated micro-probe sampling and GCMS. The experiments were conducted in atmospheric opposed flame arrangement using ethane (C_2). PAHs were quantified by directly analysing the gas samples withdrawn within the flame. Vincitore and Senken detected 2 to 4 ring PAHs, with pyrene being the most abundant PAH.

Turning now to C_3 to C_4 fuels, Marinov *et al.* (1997) carried out experimental and detailed kinetic modelling studies on PAH formation in rich premixed (sooting) flames using propane (C_3)/oxygen/argon mixtures under atmospheric conditions. They analysed the gas composition within the reaction and post reaction zones of the flame using GC-MS. Marinov et al reported considerable yield of benzenoid NPH and PHN in the case of these propane (C_3) flames. In the flames of C_4 fuels, Schenk et al. (2015) carried out an experimental investigation on PAH formation and soot morphology in opposed-flow atmospheric pressure premixed C_4 flames (n-butane, i-butane, i-butene and i-butanol). They employed flame sampling molecular beam mass spectrometry (MBMS) with electron ionisation (EI) and in-situ GC-MS. The PAHs identified by Schenk et al were both benzenoids (NPH and PHN) and five membered rings (ACY and FLU). For example, the intensity (and therefore abundance) of NPH detected by the GCMS was ranked in the order: i-butene > i-butane > n-butane > i-butanol.

PAH formation in the case of the C_7 aromatic toluene is somewhat unique. This is because, toluene chemistry is associated with both fuel decomposition and PAH growth (Zhang et al., 2010). This is exemplified in the study of Zhang *et al.* (2009) who carried out experimental and theoretical studies on toluene pyrolysis within the temperature range of 927 to 1527 ^oC. Zhang *et al.* also identified both benzenoid and five-membered ring PAHs having 2 to 3 rings (NPH, ACY, PHN and ATR) (see Table 2.1 for the definition of acronyms).

Lastly, it is apparent from the literature on PAH formation of pyrolysis and flames of C_1 – C_7 fuels that benzenoid PAHs having 2 – 4 hexagonal carbon rings are produced in significantly high concentrations regardless of the carbon number of

the hydrocarbon tested. Furthermore, there are relatively few experimental PAH studies of the individual C_1 to C_7 fuels in tube reactors and systematic studies of increasing carbon number of fuels on PAH formation have not been reported. Influence of increasing carbon number of hydrocarbons was only investigated on soot formation. For example, in diffusion flame, Ladommatos et al. (1996) reported soot propensity of hydrocarbons molecules increasing with carbon number. Crossley et al. (2008) proposed a micro-pyrolysis index (MPI) and threshold sooting index (TSI) for a number of hydrocarbons, and they stated an increase in soot propensity when the carbon number of the hydrocarbons was increased.

2.9 PAH emission from internal combustion engine

PAH formation and emission from internal combustion engines (ICEs) are rather complex when compared to flames and flow reactors. Unlike flow reactors, the conditions in ICEs are usually turbulent, heterogeneous, unsteady, and uncontrollable; the combustion process is often inaccessible for observation and analysis. Factors influencing the yield of PAHs from ICEs include the following: composition of the fuel (saturated, unsaturated, branched, oxygenates etc.), fuel type (diesel, reformulated diesel, biodiesel, gasoline etc.), engine type (light and heavy duty, diesel or gasoline engines), engine operating conditions (cold start, idling, steady state, acceleration), working conditions (temperature, pressure, speed, load, air/fuel ratio) (Lim *et al.*, 2005; Borrás *et al.*, 2009).

PAHs are produced in ICEs from incomplete combustion of fuels, as outlined in the Dec 1997 model described in section 2.7 of this thesis. PAH emissions from ICEs can be grouped according to five possible origins: 1) PAHs originally in the fuel (petrogenic) and surviving combustion 2) pyrolysis of fuels to form PAHs (pyrogenic) 3) pyro-synthesis of PAHs from aliphatic hydrocarbons 4) PAHs from the fuel that accumulated in the lubricating oil and later adsorbed onto particulates 5) PAHs that are stored in the engine deposits and which are later discharged into the exhaust (Elghawi *et al.*, 2010). Investigations into the influence of fuel composition on PAH emissions in ICEs have a long history.

In the 1970s, Valori *et al.* examined PAH emissions from the exhaust of a lift truck powered by both gasoline and liquefied petroleum gas (LPG). The exhaust particulates bearing PAHs were collected on a filter. PAHs from the particulates were soxhlet extracted in cyclo-hexane and later identified and quantified using GC-MS. The prominant PAHs detected by Valori *et al.* in both the gasoline and LPG powered exhausts had 2 - 4 rings (NPH, ACN, FLU, PHN, ATR, PYR, FLT and CRY) (see Table 2.1 for the definition of acronyms). These PAHs, particularly ACN, were found in considerably lower concentrations in the engine exhaust when the lift truck was fuelled with LPG. One significant conclusion reached by Valori *et al.* was that regardless of the fuel combusted, the identity of the PAHs produced were similar, but concentrations of the quantified PAHs were notably lower when the lift truck was powered by LPG compared to when it was fuelled by gasoline.

One decade later, Pedersen *et al.* (1980) studied the effects of fuel composition, types of lubricant and engine operating parameters on the emission of particulate-bound PAHs in an automobile diesel engine fuelled with various fuels and operated under constant load and steady state conditions. The fuels consisted of multi blends of iso-octane, n-heptane, toluene, benzene, o-xylene and heavy aromatics having carbon number of C_9 to C_{10}. Pedersen *et al.* reported that over 90 % of the heavier PAHs such as B(a)P and B(ghi)P were found on the particulates having diameters below 1000 nm, while significant proportions of light PAHs were found in gaseous phase of the exhaust gas. Concentrations of the particle-bound PAHs were strongly influenced by the fuel aromatic content and the proportions of petrogenic PAHs in the fuel. The effect of fresh-lubricant on the concentration of the PAHs was smaller. However, the concentrations of PAHs that accumulated overtime in the used lubricant increased the PAHs adsorbed onto particulates almost linearly.

Several studies have shown that most of the PAHs recovered from the exhaust of diesel and gasoline engines are common, but the concentration of the total PAHs is considerably higher in the diesel than in the gasoline exhaust. For example, Miguel et al. (1998) investigated gaseous and particulate PAH emissions measured from the Caldecott tunnel in San Francisco in the United State. Two different samples were collected from two tunnel bores: the first bore

was used mainly by heavy duty diesel engines while the second bore was used mainly by light duty gasoline engines. Miguel et al. reported that the heavy-duty diesel engines produced substantially higher fine particulate mass and total PAH concentration than the light duty gasoline engines. In particular, diesel trucks formed significantly higher concentrations of medium molecular weight PAHs (FLT, PYR, B(a)A and CRY) than the gasoline vehicles, by a factor up to 76, while gasoline vehicles produced more high-molecular-weight PAHs (B(a)P, I(123-cd)P, D(a)A and B(ghi)P). Size resolved measurements of particulate-bound PAHs suggested that PAHs from diesel exhausts were found in both the ultrafine size mode (< 120 nm) and accumulation size mode (120 – 2000 nm), whereas PAHs were present mostly in the ultrafine size mode in the case of gasoline exhausts.

In a related study, Marr et al. (1999) measured the PAHs in motor vehicle fuels (gasoline and diesel) and in their corresponding exhaust emissions. The predominant PAH detected in the engine exhausts was NPH, amounting to 62% of the total PAH in the gasoline exhaust and 48 % in the diesel exhaust. Marr et al. observed no correlation between the amount of petrogenic PAHs in diesel fuel and the mass of PAHs in the diesel exhaust, while a correlation emerged between the amount of petrogenic PAHs in gasoline fuel and the amount of PAHs in the gasoline exhaust. In a related study, Elghawi *et al.* (2010) studied PAH emissions (gaseous and particulate phase) generated from a V6 gasoline engine operated in homogenous charge compression ignition (HCCI) and spark ignition (SI) modes. The engine was powered by gasoline fuel (winter grade) and run under steady state. Elghawi *et al.* extracted the particulate and gaseous PAHs in an ultrasonic bath and analysed the PAHs from the extracts using GCMS. The particle phase PAHs (B(a)A, CRY, PYR and B(b)F) produced in the SI and the HCCI modes were similar in terms of the type of PAHs, but at relatively lower concentration in the case of SI mode. Elghawi *et al.* observed 3 gas phase PAHs (NPH, ACY and ACN) common to both the SI and HCCI modes, but with additional PAHs (FLU, ATR, PHN, FLT and PYR) detected in the case of HCCI mode. It is interesting to note that most of the gas phase PAHs detected by Elghawi *et al.* in the SI mode were also originally present in the commercial grade gasoline.

The survival rates of petrogenic PAHs present in fuels during combustion have been described by numerous studies. In radiotracer experiments, for example, Tancell et al. (1995) reported that the B(a)P in a diesel fuel accounted for about 80 % of the B(a)P in the exhaust of a diesel engine while pyro-synthesis and lubricating oil only accounted for 20% of the total exhaust B(a)P. Tancell et al. observed that pyro-synthesis of low molecular weight PAHs having 2 and 3 rings influenced the formation of high molecular weight PAHs having 5 and 6 rings. The survival of individual petrogenic PAHs when subjected to combustion differs. For instance, Tancell & Rhead (1996) combusted diesel fuel containing NPH, 2-methyl NPH, PYR, FLUO and B(a)P in a direct injection diesel engine and each of this compound was carbon 14 labelled. They reported PAHs in decreasing survival rates as: FLU > 2-methyl NPH > NPH > PYR > B(a)P (see Table 2.1 for the definition of acronyms).

Research to date on the influence of engine operating conditions on PAH emissions constitutes a relatively small body of the literature. In 2009, Borrás et al. investigated the effect of four engine operating conditions (cold start, idling, acceleration and steady state) on particle phase PAH emissions from a light duty diesel engine. Particulates were sampled on a glass microfiber filter and the PAHs were ultrasonically extracted from the particulate and analysed using GCMS. Borrás et al. observed that the concentrations of high molecular weight PAHs measured when the engine was cold-started were much higher than the corresponding concentrations of PAHs measured when the engine was in idling condition. Higher PAH concentrations were also measured by Borrás et al. when the engine was operated in an acceleration mode than when it was run under steady state conditions.

Fossil fuels with high PAH content have been reported to promote PAH formation (Aakko, 2005), but no definitive conclusions have been reached, as yet, regarding the effect of fuel mono-aromatic contents on the identity and concentrations of PAHs formed. There are divergent views in the literature on the effect of total aromatic content of fuels on PAH emissions, as outlined below. Barbella et al. (1989) investigated the effect of fuel aromatic content on PAH and soot emissions from a single cylinder direct injection diesel engine fuelled with n-tetradecane, a mixture of 70% n-tetradecane + 30 % toluene, and two diesel oils of dissimilar

aromatic contents. The engine was operated at a constant speed and constant injection timing. Barbella et al. observed that the concentration of the exhaust PAHs was dependent on the composition of the fuel tested. Higher PAH mass was found from combusting 70%tetradecane + 30%toluene rather than from combusting pure tetradecane. Diesel fuel oils produced the highest concentration of PAHs among all the fuels tested; and most of these PAHs were believed to have emanated from the unburned PAHs in the diesel oils.

Mi et al. (2000) studied the effect of total aromatic and poly-aromatic contents of fuels on the exhaust PAH emission from a heavy-duty diesel engine under steady state conditions. They added 10% of single ring toluene and 5% of the 3 ring PAH fluorene to a base diesel fuel. The proportions of toluene and fluorene in the diesel blend represented mono-aromatic and poly-aromatic hydrocarbons respectively. Mi et al. reported that adding PAH fluorene to the diesel fuel, increased the emission of total PAHs as well as the PAH fluorene itself. However, there was no significant change in PAH emission when adding toluene to the diesel fuel. Nine years later, Borrás et al. (2009) investigated PAH emissions from different reformulated diesel fuels in a light duty diesel engine. Their results showed that adding 5 – 25 % of mono-aromatics to low sulphur diesel and reference diesel fuels had no considerable effect on the exhaust PAH concentrations when compared with the concentration of exhaust PAHs from combusting pure reference diesel. However, the biodiesel rape oil methyl ester produced greater number of PAHs but at considerably lower concentrations (~ 50% lower) than the PAHs in the reformulated diesel.

More recent attention has focussed on the use of biofuel in reducing PAH emssions, but it is still not understood wether or not the exhaust particulate bound PAHs and their associated toxicity are reduced. For instance, Lin et al. (2006) reported reduction of PAH emissions by 43 – 90 % when palm-biodiesel was burnt in a heavy-duty diesel engine compared to burning premium diesel fuel. On the contrary, Tang et al. (2007) observed no considerable difference in PAH emissions from combusting conventional diesel and a blend of biodiesel/diesel. Kado et al. (1996), surprisingly, reported increase in the concentration of the PAH benzo(a)pyrene when burning rapeseed oil ethyl ester compared to when combusting pure diesel fuel in a diesel engine.

Reduction of PAH emissions resulting from blending biofuel into diesel appears to be associated with the oxygen content of biodiesel, but it is difficult reaching firm conclusions on the toxicity of particle-bound PAHs. This is due to lack of rigor in reporting components of each biofuel and the blending ratios tested (Ballesteros et al., 2010). This results also show variability due to engine test conditions, such as engine load, which further complicates ascribing to fuel any changes in PAH emissions. For example, He *et al.* (2010) measured PAH emissions from the exhaust of a direct injection turbo-charged diesel engine fuelled with biodiesel and diesel. The engine was run at a constant speed of 2300 rpm and various loads. He *et al.* observed that adding biodiesel to diesel fuel reduced the exhaust PAHs, particularly the particulate bourne PAHs as well as their associated toxicity. There was also variation of PAHs with the engine load, which demonstrated that the highest PAH concentration was observed at the highest load and this concentration decreased when the load was decreased.

Increased PAH emissions resulting from blending biofuel into diesel fuel have been associated with the physical properties of biofuels. Ballesteros et al. (2015) recently examined particulate borne PAHs from a single cylinder heavy duty diesel engine fuelled with a commercial diesel fuel and diesel-bioethanol blends. They observed increased PAH emissions with increasing amount of bio-ethanol content in diesel fuel. Ballesteros et al ascribed the results to two influeneces. Firstly, ethanol has high latent heat of vapourisation which could decrease the combustion temperature and this could reduce the bounout of PAHs and soot. Secondly, the power output of the engine was reduced due to ethanol addition to diesel fuel.

More recently, Szewczyńska et al. (2013) investigated the characteristics of particulate PAHs from a diesel engine fuelled with diesel and a number of diesel-bioester blends. They collected particulates on a fibre glass filter from the engine exhaust using electrical low pressure impactor and the PAHs adosorbed onto the particulates were identified by high performance liquid chromatography. Szewczyńska et al. observed that adding 40% of bioester (B40) to diesel fuel reduced the concentration of the total PAH emissions. Further analysis of the exhaust fumes showed that particulates produced from both the diesel and B40 constituted of particles of diameters below 0.25 µm. The PAHs adsorbed onto

these particles had a high concentration of 3 and 4 ring PAHs in the case of diesel fuel and low concentration of 5 and 6 ring PAHs in the case of 40% bioester in diesel fuel. One can deduce from Szewczyńska et al.'s study, that although adding bio-ester to diesel fuel reduced the total particulate mass and total PAH concentrations, it nevertheless shifted the individual PAHs to pottentially more toxic ones.

In the past few years, researchers have started making measurements and analysing the chemistry of incylinder PAHs with engines running on model fuels. This is exemplified in Wang *et al.* (2015), who researched the evolution of in-cylinder PAHs in a direct injection diesel engine fuelled with n-heptane and n-heptane/toluene blends. Wang *et al* sampled the in-cylinder PAHs using a total cylinder sampling system (total cylinder gas damping). The contents of the cylinder were collected in a sampling bag and were later passed through a teflon-coated fiber filter. The PAHs on the particulate filter and gas samples were soxhlet extracted and later analysed using GCMS. With n-heptane as the fuel, Wang *et al* reported progressive increase in the concentration of in-cylinder PAHs while combustion progressed from premixed and to the diffusion phase and then to the late combustion phase. Wang *et al* also observed that adding toluene to n-heptane decreased the total PAH concentrations by 48% in the premixed phase, but increased it by 30% in the early diffusion phase. Individual PAHs detected in significantly high concentrations were 2 ring NPH and 3 ring PAHs of five-membered-ring structures (ACY, CAN and FLU). This suggests that the five-membered-ring PAHs are significant for the growth of in-cylinder PAHs.

2.10 Conclusions and Gaps in knowledge

2.10.1 Conclusions

Polycyclic Aromatic Hydrocarbons (PAHs) are organic compounds with two or more aromatic rings fused together in various configurations. They are considered as toxic pollutants. Sixteen toxic PAHs have been prioritised by the United State Environmental Protection Agency (EPA) and European Union (EU).

Long-term human exposure to particulates bearing these PAHs could result in carcinogenic and mutagenic effects.

PAH formation depends on the molecular structure of the fuel and the combustion/pyrolysis conditions. Evolution of PAHs often starts with the formation of the first aromatic ring from resonantly stabilised hydrocarbon radicals. Poly-aromatic growth proceed through different reaction pathways depending the growth species (acetylene, phenyl, methyl and vinyl).

Soot particles have graphitic-like structures formed from numerous de-hydrogenated polymerised hexagonal rings (PAHs) and vary in size, from the primary particles formed by condensation reactions having sizes roughly 5 to 30 nm, to accumulation particles which have sizes from roughly 30 nm to thousands of nanometres.

In tube reactors, PAH formation and speciation of individual PAHs into diverse number of rings is influenced substantially by temperature effects. The molecular structure of the initial fuel molecule determines not only the formation of the first aromatic ring, but also the growth pathways of smaller PAHs into heavier ones as well as the total amount of particle/gas phase PAHs formed.

In internal combustion engines, the composition of fuel molecule, petrogenic PAHs originally in the fuel, engine operating conditions and PAHs in the lubricant strongly influenced PAH emissions, but the extent to which fuel aromatic content affects PAH emission is still yet to be unravelled.

2.10.2 Gaps in Knowledge

It is apparent from the literature that the influence of molecular structure of fuels on PAH formation has not been fully understood, while the effect of degree of unsaturation of fuels on PAH formation has so far not been investigated.

Diesel and gasoline fuels contain a mixture of saturated, unsaturated, branched, and aromatic hydrocarbons (Pitz and Mueller, 2011). To understand and address

the influence of fuel molecular structure on the formation and emission of toxic PAH molecules, a homologous series of saturated and unsaturated C_1 to C_7 fuel molecules could be assessed; this could lead to insights that could inform the processing of fuels such that they produce fewer toxic PAH emissions.

The characteristics of PAHs in the gaseous phase and those adsorbed onto particles and the relative toxicity of these PAHs with variation in fuel degree of unsaturation are still not precisely understood. Understanding of the linkage between fuel molecular structures and the amount and toxicity of air bone and particulate borne PAHs is still also incomplete.

In terms of the effect of increasing carbon number of hydrocarbons on PAH formation, it was observed from the literature that there are relatively few experimental PAH studies of individual C_1 to C_7 fuels in tube reactors. It apparent that the influence of carbon number of hydrocarbons was only investigated regarding soot formation. No attempt was made to systematically study the influence of carbon number of a homologous series of C_1 – C_7 on PAH formation in a tube reactor. Particulate characterisation and soot formation analyses from tube reactors of these range of hydrocarbons is also limited. Furthermore, it is still not clear whether increasing carbon number of a hydrocarbon molecule has an influence on the carcinogenic Group B2 PAHs adsorbed onto soot particles or those PAHs available in the gas phase.

From the literature regarding PAH emissions from internal combustion engines, there is a view among researchers that switching to alternative fuels is a more effective way of reducing PAH emission than reducing the aromatic content of the fuel. Some investigators express the view that regulating the poly-aromatic content of diesel fuel would be a more suitable means of managing PAH emission than the regulation of the total aromatic content of the fuel, but no definitive conclusions were reached on the effect of fuel aromatic contents on PAH emissions. The extent to which the total aromatic content in fuels influences the total PAH formation is not fully established. In addition, no attempt was made in the literature to study the influence of varying ignition delay of fuels on the PAH formation in a compression ignition engine. Understanding the extent of increasing premixed burnt fractions on PAH emissions is also lacking.

Chapter 3

3. Experimental Systems and Methodology

This chapter describes the systems that were used to conduct the experiments. It also describes the methodology employed for PAH identification and quantification. The chapter begins with methods of generating particulates and gas phase PAHs from a tube reactor and a diesel engine. Characterisation of particulates using a DMS500 particle sizer instrument is described. Collection of particulates and gas phase PAH samples, including the extraction of PAHs from these samples using an accelerated solvent extraction (ASE) system, are also described. PAH identification and quantification using gas chromatography coupled with mass spectrometry (GCMS) is outlined.

3.1 Tube Reactor Facility

Emissions from practical combustion systems such as gas turbines and internal combustion engines consist of a complex mixture of several compounds in the form of solid, liquid and gaseous substances. Among these substances are solid soot particles and gas phase polycyclic aromatic hydrocarbons (PAHs). PAH emissions from diesel engines are known to be affected by combustion characteristics, fuel composition and fuel physical and chemical properties (Martin *et al.*, 2017); similar effects have been reported for gasoline engine (Szewczyńska et al., 2017) and gas turbine combustors (Chen *et al.*, 2017). The main obstacle however in accurately evaluating the chemical effect of fuels in these practical systems, where combustion conditions are complex and poorly controllable, is that the combustion process is less accessible for observation and analysis.

For these reasons, studies into the chemical effects of fuels on soot and PAH emissions often utilise experimental systems which allow good control of combustion and sampling conditions. Such investigations include: flames (Blacha et al., 2012; Rodrigues et al., 2015), shock tubes (Frenklach et al., 1985; Kc et al., 2015), plug flow/stirred flow reactors (Wen et al., 2005; Manzello et al., 2007) and laminar flow reactors (Glarborg et al., 2004; Sánchez et al., 2012; Dandajeh et al., 2017).

In this thesis, a laminar flow reactor was employed to investigate PAH and soot emissions from pyrolysis of liquid and gaseous hydrocarbons. The conditions in the reactor, unlike those in internal combustion engines, were steady, laminar and homogenous. The tube reactor was developed and commissioned by Eveleigh (2015) in the thermodynamics laboratory of UCL Mechanical Engineering Department.

3.1.1 Components of the tube reactor

Figure 3.1 shows a schematic of the tube reactor used throughout the present work. The experimental facility consisted of a reactor temperature control system, oxygen-free nitrogen and fuel gas supplies, mass flow controllers (MFC) (1) for nitrogen and the gaseous fuel, a syringe pump for injecting liquid fuels, a nitrogen heater, fuel inlet (2), nitrogen/fuel, static mixer (3), circulating cooling water (4), insulated heated nitrogen/fuel lines, tube heater (5), DMS 500 particle size spectrometer instrument and its dilution cyclone, DMS 500 sampling probe (6), soot sampling probe (7), particulate filter housing, a stainless steel resin (XAD-2) cartridge holder, volumetric gas meter, vacuum pump, and a PC for system control and storing data. The reader is referred to A 1 in Appendix A for an image of the tube reactor.

3.1.2 Generation of particulate and gas phase PAHs

Using the tube reactor shown in Figure 3.1, liquid and gaseous hydrocarbons ranging from C_1 – C_7 were pyrolysed under oxygen free conditions at temperatures in the range 1050 - 1350 ^{o}C. The oxygen free pyrolysis in the tube reactor and the range of temperatures chosen resemble, to a considerable extent,

the conditions in the core of the fuel spray of a diesel engine where, in the early stages of combustion, there is little oxygen available.

The carrier gas used during the pyrolysis of all the hydrocarbons was nitrogen and was metered at a constant flow rate of 20 L/min (at STP conditions) using a mass flow controller. All hydrocarbon molecules were supplied to the tube reactor at a fixed carbon flow rate of 10,000 ppm on C_1 basis. Thus, for example, the volumetric flow rate of ethane gas was approximately one and half times as high (ml/min) as that of propane. The flow rates corresponded to laminar flow conditions within the reactor (Reynolds number ~ 200) throughout the temperature range of 1050 - 1350 ^{o}C. Ethane was used as the baseline fuel for daily repeat checks, to detect any potential drifts in the reactor systems and associated instrumentation. The fuel molecules were injected into the nitrogen stream via software-controlled solenoid valves. An electrical tape heater surrounded and heated the nitrogen line connected to the fuel inlet (2). A proportional integral derivative (PID) controller maintained the nitrogen gas temperature at 150 °C.

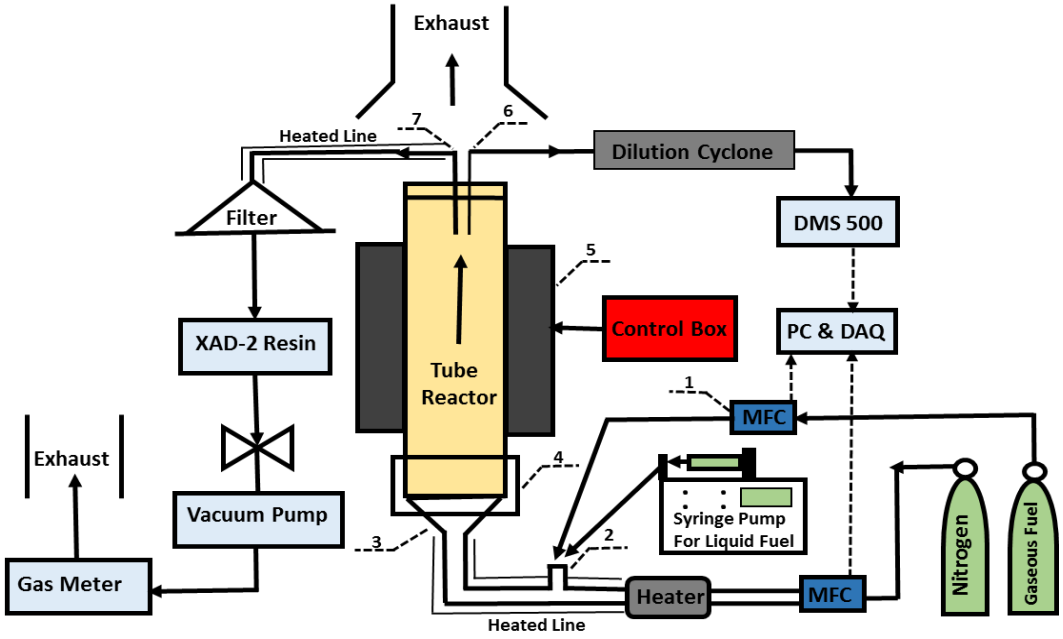

Figure 3.1: Schematics of the pyrolysis tube reactor: 1) mass flow controller (MFC) 2) fuel vaporiser 3) static mixer 4) circulating cooling water 5) tube furnace 6) DMS 500 sampling probe 7) soot sampling probe

Immediately when fuel was introduced into the nitrogen stream, the combined f stream passed through a static mixer (3). The mixer was packed with 8 mm stainless steel ball bearings which were located at the tube reactor inlet. The mixer ensured that the combined streams were homogeneously mixed. The temperature in the mixer was maintained at about 180 °C with the aid of a type K thermocouple. The alumina tube reactor was 1440 mm long and had 104 mm diameter.

The tube was vertically positioned in an electric furnace and about 600 mm of the tube central length was heated, and was found to be uniform. Measurements by Eveleigh (2015) showed a uniform axial temperature distribution profile in the tube reactor over this 600 mm length axis. The profile is typical of such tube reactors (Glarborg et al., 2004). The tube heated section was maintained by an electrical PID controlled system at temperatures within the range of 1050 – 1350 °C. The gas average residence time (t_r) can be calculated using equation 3.1.

$$t_r(s) = \frac{V_r(L)}{Q(L/s)} \qquad \text{Eq3.1}$$

Where V_r is the volume of the 600 mm reaction zone of the reactor, and Q is the volumetric flow rate at the test temperature. The average residence time was

therefore dependent on the reactor temperature (T), and could be expressed using equation 3.2

$$t_r(s) = \frac{4470}{T} \quad \text{Eq3.2}$$

3.1.3 Sampling of particulate and gas phase PAHs

Particulates and gaseous PAHs generated within the reactor were sampled from the exit of the reactor at 100 ^oC intervals, by means of a stainless-steel probe connected to a vacuum pump. To avoid condensation of gas phase PAHs, the soot sampling stainless steel probe (7) that led to the filter housing was heated by a tape heater and controlled at a temperature of 120 °C by a separate PID controller. The probe was placed at the outlet of the reactor and was connected to the filter by a 12.5 mm stainless steel tube (7). The flow rate of the vacuum pump was maintained at < 18 L/min using a control valve. Between the soot sampling probe and the vacuum pump, a particulate filter and a resin PAH adsorption system were placed to collect particulate and gaseous PAHs respectively. The design of the custom-made resin adsorption system is described in A 2 in Appendix A.

Soot samples were collected on a glass micro fibre filter (70 mm diameter, 0.7 µm pore size, 75 g/m^2 mass, 310 s filtration speed) (Fisher Scientific UK). A glass fibre filter was chosen due to its PAH-inertness and heat resistant properties, and was also found suitable by many other studies (EPA Method TO, 1999 ; Sánchez et al., 2012; Sánchez et al., 2013). The mass of the filter was measured before and after sampling on a high precision mass balance (resolution of 0.001 mg) to obtain the soot mass collected. Figure 3.2a shows a sample of soot collected on a glass micro fibre filter during ethane pyrolysis at 1150 ^oC.

The filter was initially baked in an oven, to a temperature of 120 ^oC for 8 hours to minimize the moisture in the filter, prior to a testing session and used immediately upon being removed from the oven. The filter holder was also maintained at a temperature of 120 ^oC. Repeatability tests with ethane as the baseline fuel were conducted at 4 different test days. The repeat results for mass concentration from ethane pyrolysis showed that the measurement process was repeatable, to satisfactory levels, with the standard deviations in soot masses generated from

ethane pyrolysis being 1 mg (coefficient of variation (CoV) of 20 %) at the temperature of 1050 ^{o}C and 14 mg (CoV of 9 %) at the temperature of 1250 ^{o}C.

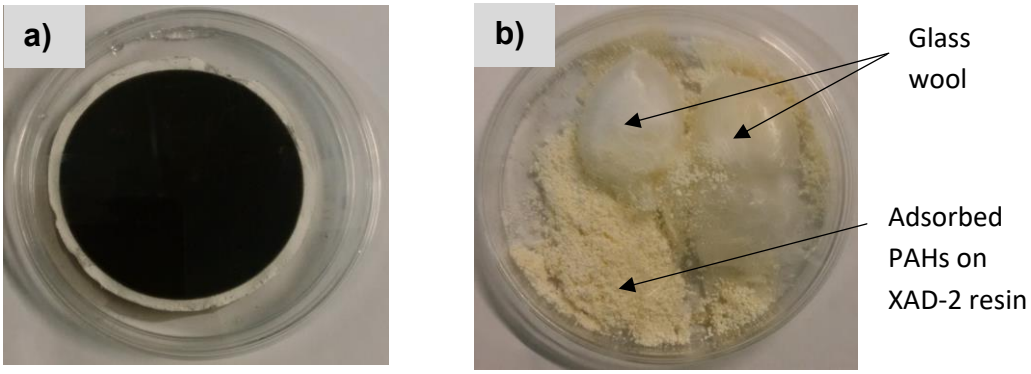

Figure 3.2: Samples of: a) soot collected on a glass micro fibre filter b) gas phase PAHs collected on an XAD-2 resin; samples were collected during ethane pyrolysis at 1150 ^{o}C

The gas phase PAHs were trapped onto a Supelco brand Amberlite XAD-2 resin (~0.65 mL/g pore volume, 90 Å mean pore size, ~300 m^2/g surface area and density of 1.02 g/mL at 25 °C) (Sigma Aldrich, UK). XAD-2 resin was selected since it was reported by EPA (1999) to have higher collection and retention efficiencies compared with other sampling materials such as Tenax® and polyurethane foam (PUF). A preliminary PAH analysis carried out in this study with both the XAD-2 resin and PUF confirmed that the resin adsorbed more PAH mass and was therefore more suitable for trapping gaseous PAHs. Figure 3.2b shows a sample XAD-2 resin bearing adsorbed PAHs during ethane pyrolysis at 1150 ^{o}C.

A glass cartridge was first loaded with 5 g of the XAD-2 resin sandwiched between two pieces of glass wool. The cartridge was then inserted into a custom-made stainless-steel housing. The resin housing was connected in series after the particulate filter. The gas volume passed through both the filter and the XAD-2 resin was measured by a diaphragm volumetric gas meter (Q_{max} = 6 m^3/h) sourced from Bell flow Systems UK.

During ethylene pyrolysis at 1150 °C for example, the DMS 500 particle spectrometer was used to assess the sample in the flow before and after the filter housing. It was found that particles up to 200 nm were sampled before the filter. After the filter, no particle > 10 m was passed onto the XAD-2 resin. Therefore, only clean gases without particles > 10 nm entered the XAD-2 resin holder.

Particles < 10 nm recorded by the DMS 500 were considered to be condensed species (Kittelson, 1998).

The sampling durations for soot and gaseous PAHs was 15 min at all temperatures tested. This duration was chosen after an optimisation exercise to trap sufficient mass of soot for subsequent GCMS analysis. Measurements were made of the filter gravimetric soot mass (M_s) and the cumulative volume of gas (V_g) passed through the particulate filter, and the XAD-2 resin for each test duration. The particulate and the gas phase samples collected were stored separately in 90 mm diameter plastic petri-dishes and wrapped with para-film tape and immediately frozen to -20 ^oC and stored in dark frozen conditions before further analysis (EPA Method TO, 1999).

3.2 Diesel Engine Facility

All engine tests reported in this thesis were conducted on a single cylinder, 4-stroke, compression-ignition engine which was described previously by Talibi (2015). The engine was situated in a purpose-built enclosed test cell and operated from an adjacent control room (B.02) in the thermodynamics laboratory of UCL Mechanical Engineering Department.

3.2.1 Diesel engine specification

The schematic of the single cylinder, 4-stroke, compression-ignition engine used for the all the engine experiments is shown in Figure 3.3. Table 3.1 lists the specifications for the engine assembly. The cylinder head (including intake and exhaust valves), piston and connecting road, were taken from a 2.0 litre 4-cylinder Ford Duratorq donor engine, and were mounted on a single cylinder Ricardo Hydra crankcase. The in-cylinder gas pressure was measured to a resolution of 0.2 crank-angle-degree (CAD) using a Kistler 6056A piezoelectric pressure transducer in conjunction with a Kistler 5018 charge amplifier, 1800 pulse per revolution (ppr) shaft encoder and a digital data acquisition system. The reader is referred to A 3 in Appendix A for an image of the diesel engine.

Table 3.1: Engine Specifications

Description	Specification
Bore	86 mm
Stroke	86 mm
Swept volume	499.56 cm3
Compression ratio (geometric)	18.3 : 1
Maximum in-cylinder pressure	150 bar
Piston design	Central ω – bowl in piston
Fuel injection pump	Delphi single-cam radial-piston pump
High pressure common rail	Delphi solenoid controlled, 1600 bar max.
Diesel fuel injector	Delphi DFI 1.3 6-hole solenoid valve
Electronic fuel injection system	1 µs duration control
Crank shaft encoder	1800 ppr, 0.2 CAD resolution
Oil and coolant temperature	80 ± 2.5 °C

The experimental set-up consisted of an existing special low volume high pressure fuel system which was used to deliver test fuels (heptane and heptane/toluene blends) to the fuel injector at a common rail injection pressure previously described by Talibi (2015). The fuel system facilitated the direct injection of the test fuels, which had low lubricity. The use of lubricity additives which would have been required to avoid damage to the conventional common rail fuel circuit. Similarly, the use of this custom-made system, which require only low fuel volumes, reduced the cost of the fuel tests. Figure 3.3 shows the fuel system which consists of a stainless-steel vessel with capped ends and a free moving piston (3) with circumferential O-rings (2). The circumferential O-rings divided the high-pressure fuel vessel into two chambers (A & B). Chamber ‘A’ contained diesel fuel, while ‘B’ contained the test fuel.

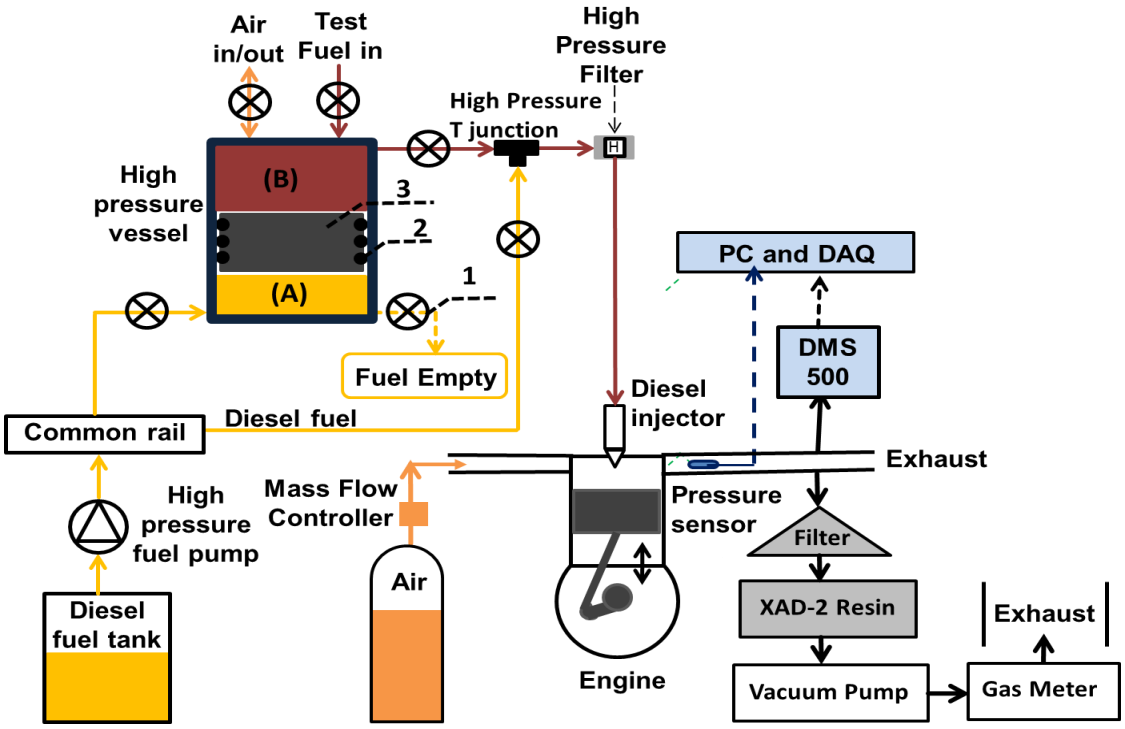

Figure 3.3: Schematics of the engine sampling system: 1) high pressure needle valve 2) O-ring 3) free moving piston.

A conventional diesel fuel system was used as a hydraulic system to deliver pressurised diesel fuel to chamber A of the fuel vessel. The pressurised diesel fuel acted as a hydraulic fluid which created pressure in the test fuel via the moveable free piston, as shown in Figure 3.3. The O-rings (2), installed circumferentially on the surface of the piston, ensured no mixing of test fuel and the diesel fuel. The diesel fuel was pressurised to a precise level using the Emtronix engine control system and the free moving piston always communicated this pressure to the test fuel. A high-pressure filter was installed between the fuel vessel and the fuel injector to prevent any damage to the injector by debris in the test fuel. High pressure needle valves (1) were used to switch between the fossil diesel fuel and the test-fuels, with the diesel fuel providing baseline data.

Pressures and temperatures were monitored in real-time and logged onto PCs using National Instruments (NI) data acquisition systems (DAQ). A NI LabVIEW program, developed in-house, evaluated the real-time in-cylinder pressure data to determine the net apparent heat release rates and indicated mean effective pressure (IMEP).

A Delphi DFI 1.3 six-hole, servo-hydraulic solenoid valve fuel injector was used to inject liquid fuel directly into the combustion chamber. An EmTronix EC-GEN 500 engine control system was used to control the injection pressure, injection timing and duration of injection. The intake air flow rate was measured using a Romet G65 positive displacement volumetric air flow meter.

3.2.2 Generation and sampling of particulate and gas phase PAHs

Particulates and gas phase PAHs generated within the engine cylinder were sampled from the engine exhaust. Particulates and gas phase PAHs were sampled about 1000 mm downstream of the engine exhaust by means of a half-inch diameter stainless steel probe connected to a vacuum pump, which provided a flow rate of 40 L/min through a particulate and gaseous PAH collection system (see Figure 3.3). To avoid condensation of gas phase PAHs and water vapor during sampling, the temperature of the soot sampling stainless steel probe that led to the filter housing was measured by a type K thermocouple and was always found be > 100 °C. Particulate filter and a stainless-steel resin based system, employed previously in the tube reactor shown in Figure 3.1, were also used to collect particulate and gaseous PAHs respectively. The cumulative volume of gas (V_g) passed through the particulate filter and the resin was measured, at each test condition, using a volumetric gas meter (Bell flow Systems UK).

The particulate samples were collected on a glass micro fibre filter (70 mm diameter and 0.7 µm pore size) (Fisher Scientific UK). The filter was first dried in a desiccator for 12 hours and weighed, before sampling with a high precision mass balance (± 0.001 mg). After sampling, the filter was re-dried in the desiccator for the same duration and re-weighed. The particulate mass collected on the filter (M_s) was recorded. To avoid deterioration of the filter in the high temperature, pulsating flow, engine exhaust, the filter was supported by sandwiching it between two stainless steel wire meshes, which were cut to the same diameter as the filter (0.026 mm aperture, 0.025 mm wire diameter) (The Mesh Company, UK). The appearance of the particulate and the XAD-2 resin

samples collected from the diesel engine were similar to those from the tube reactor shown in Figure 3.2a and b respectively.

3.3 Characteristics of particulates

Particulates, sampled from both the tube reactor and diesel engine exhausts were characterised at sub-micron levels using a fast differential mobility spectrometer (Cambustion DMS-500). The DMS-500 was used to determine the size, mass and number distributions of particulates in the range of 5 – 1000 nm. Ultrafine particles (particles < 1000 nm in size) were reported having the potential of causing health complications when they are deposited deep into the human lungs (Brewer *et al.*, 2016).

3.3.1 Sampling of particulates using DMS500

About 200 mm from the exit of the tube reactor, particulates were sampled and conveyed to the DMS500 using a centrally located stainless steel probe (6 mm diameter, 5 00 mm length) as shown in Figure 3.1. In the case of the diesel engine, exhaust gases were sampled for particulate measurements about 300 mm downstream of the engine exhaust valves using the same sampling probe as in the tube reactor and thereafter transported to the DMS500.

Undiluted samples from the reactor and diesel engine were then passed to the remote sampling head (1) of the DMS500 as shown in Figure 3.4. The reader is referred to

A 4 in appendix A for an image of the DMS 500 used for this present work. Exhaust gases were diluted at this point by 4:1 (ratio of air to gaseous exhaust sample) using heated compressed dry air. The purpose of this primary dilution was twofold. Firstly, agglomeration of particles along the sample line were reduced following the dilution of the sample to lower concentration. Secondly, the water dew point of the exhaust gaseous stream was reduced (especially in the diesel engine) to less than the ambient operating temperature in the DMS500 instrument.

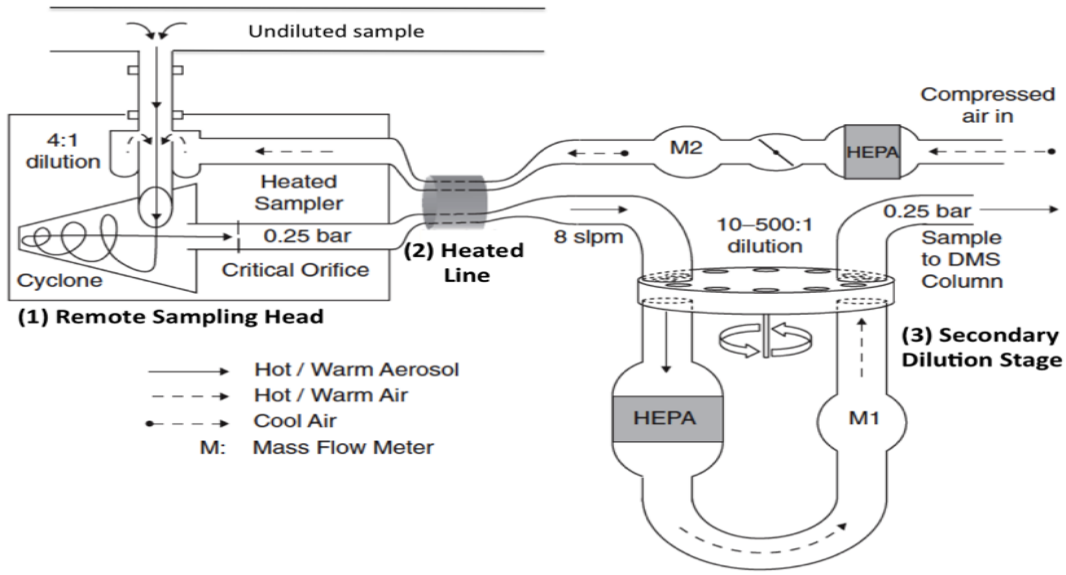

Figure 3.4: Schematic showing sample flow through the DMS500 instrument (Symonds et al. 2007; Cambustion, 2011).

After primary dilution, the sample then flowed into the heated cyclone of the remote sampling head (1) where larger particles > 1000 nm were segregated and removed by impaction. The sample flow subsequently moved via an orifice, which decreased the flow rate of the sample. The pressure downstream of the orifice was maintained at about 0.25 bar (absolute) via an external pump. The sample was then transported from the remote cyclone, via a 5m long polytetrafluoroethylene (PTFE) heated line (2), to the secondary dilution system by means of a rotating disc. The PTFE pipe was maintained at a temperature of 80 ^{o}C. Samples were diluted by compressed air in the secondary diluter in ratios ranging from 10 to 500:1. The flow rates of the sample and that of the compressed air were measured to obtain the precise dilution ratios. High efficiency particulate filters (HEPA) were used to filter some portion of the sample flow (Cambustion, 2011).

The sample then flowed through a corona discharge system shown in Figure 3.5, where particles were charged negatively. The charged particles then moved to the classifier column which consisted of a uniform cylindrical column of air flow. The negatively charged particles were deflected by a high voltage electrode through a sheath flow of free air toward electrometer detector rings. The 22 electrometer detector rings were located at various positions around the high voltage electrode, which was situated along the central cylindrical column axis.

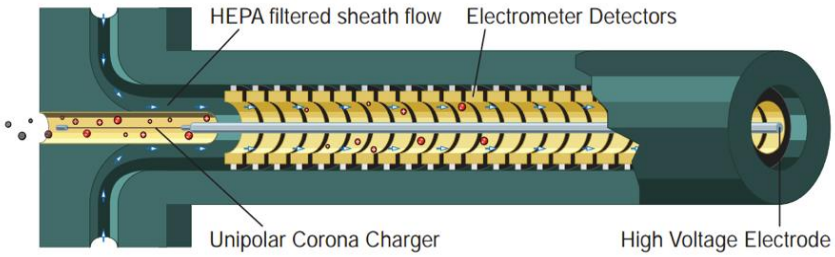

Figure 3.5: Classifier column of the DMS 500 (Cambustion, 2011).

The position from which the charged particles were attached and impacted onto the rings was depended on aerodynamic drag to electrostatic charge ratio. Particles were therefore classified by their mobility (dependent on charge and drag) and also their sizes. Particulate mass was determined by the instrument by assuming that the shape of the particle was spherical and density of the particles (1.8470.1 g/cm^3) using the DMS500 instrument. Previous studies have reported good estimates of diesel particulate mass using the DMS500 instrument and were in agreement with gravimetric filter mass measurements (Symonds *et al.*, 2007).

3.4 Extraction of PAHs

Once particulate and gas phase PAH samples were collected from the exit of the tube reactor and exhaust of the diesel engine, PAHs from these samples could be extracted using various methods. The most commonly available extraction techniques commonly used are: Soxhlet Extraction (Hollender et al., 2003; Oukebdane et al., 2010), Accelerated Solvent Extraction (ASE) (Fisher et al., 1997; Richter et al., 1996), Mechanical Agitation, Ultrasonic Agitation/Sonication (Eiceman et al., 1980), Pressurised Fluid Extraction (PFE) (Rynö et al., 2006), Supercritical and Subcritical Fluid Extraction (SCFE) (Bøwadt and Hawthorne, 1995), Microwave Assisted Extraction (MAE) (Beckerl, 1994; Jain et al., 2009) and Solid Phase Extraction (SPE) (Kiss et al., 1996).

Efficiency of extraction and recovery of the PAHs depends on the extraction process and the type of solvent used. Conventional Soxhlet extraction and accelerated solvent extraction (ASE) techniques were examined further in section 4.6 of this thesis for comparison and subsequent selection based on

recommendations of the US Environmental Protection Agency (EPA) (Richter et al. 1996).

3.4.1 Accelerated Solvent Extraction (ASE)

Extraction of PAH species from the particulate and XAD-2 resin samples was carried out using an Accelerated Solvent Extractor (ASE) (Thermo Scientific Dionex-150). ASE is an automated technique for rapidly extracting molecules such as PAHs at elevated temperature and pressure. It is a recommended technique by the EPA (Method 3545, SW-846, draft update IVA) for extracting PAHs. ASE has several advantages over classical Soxhlet extraction (atmospheric extraction), including large reduction in solvent volume used, faster extraction times by up to an order of magnitude and improved PAH extraction efficiency and PAH recovery (Richter et al., 1996). One unique disadvantage of the ASE however is the high procurement and maintenance cost.

3.4.1.1 Thermo Fisher Dionex ASE 150

Figures 3.6a and b show the Dionex ASE 150, its operating systems and schematic of its flow operation respectively. The ASE machine was installed in room B.09 in the Thermodynamic Laboratory of UCL Mechanical Engineering.

Figures 3.6a and b shows that the Dionex ASE 150 consist of: (1) a solvent reservoir where the solvent was stored (2) an extraction cell where the sample was packed, (3) an oven where the extraction cell was heated (4), a control panel where the extraction conditions (pressure, temperature, static cycles) were monitored (5), the door-open lever that closed both the sample cell and the oven (6), a waste bottle, sealed with a special built-in cap, where the rinsed solvent is collected (7), needle up down switch, which controlled the position of the vent needles and the source to the collection bottle (8), a collection bottle where the PAH extracts were stored (9) a dip tray, installed to collect any solvent that leak during rinsing or running of the ASE 150 (Thermo Scientific, 2011). The ASE system had stainless steel extraction cell sizes ranging from 5, 10, 22, 34, 66 and 100 mL. The extraction cells consisted of a cell body and two interchangeable

end caps (see Figure 3.6b). A 10 mL extraction cell was used throughout this study.

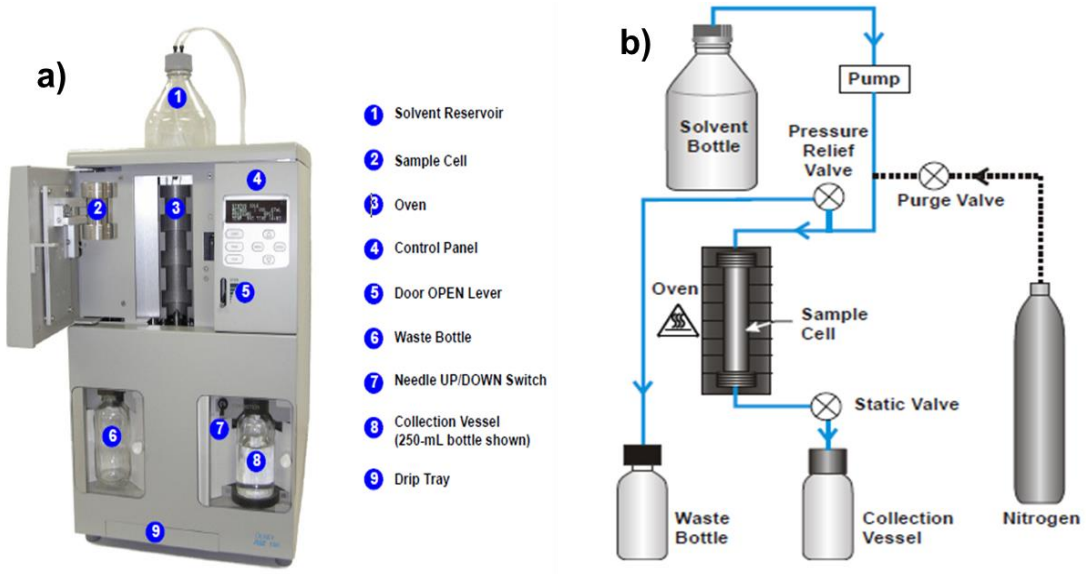

Figure 3.6: a) Operating systems of Accelerated Solvent Extractor (ASE) Dionex b) Schematic of ASE process (Thermo Scientific, 2011).

Particulate and XAD-2 resin samples were first loaded into the extraction cell and packed with fisher brand Ottawa general purpose sand (Lot; 114317). The purpose of the sand was to fill any extra space within the extraction cell, thereby reducing solvent consumption. The solvent reservoir was filled with dichloromethane (DCM). Extraction was usually performed either by filling the sample cell with solvent before heating (*pre-filling method*) or by pre-heating the sample cell before filling with solvent (*pre-heating method*) (Richter et al., 1996). The later method was used throughout this study. The oven was initially heated for 5 minutes prior to loading the sample cell into the oven. After the oven-heating, the loaded sample cell was inserted into the oven and the system door was closed. The pump was turned on and the static valve was closed. DCM was pumped into the sample cell until the pressure in the cell reached 1500 psi (10.35 MPa).

During extraction, the static valve was opened occasionally to maintain the extraction pressure to the set value. Figure 3.6b shows a schematic of the extraction flow chart. The sample cell was heated to a set temperature of 120 ^{o}C. Fresh DCM was pumped through the sample cell and the static valve was opened thereafter to allow the PAH extracts to flow into the collection vial. The purge

valve was opened, and the Nitrogen gas purged the remaining extract into the collection vial. The pressure relief valve was also opened, and the residual pressure was released from the cell.

3.4.1.2 Optimised extraction conditions

All the particulate and XAD-2 resin samples were extracted using DCM as a solvent. DCM was used as a solvent because it has boiling point (40.0 ^{o}C) far lower than that of all the 16 PAHs of interest (218 – 525 ^{o}C) and has long been used (Oukebdane *et al.*, 2010) for PAH recoveries. The extraction process was optimised after several repeats while varying the operating conditions such as temperature, number of static cycle, purge time and rinse volume. The optimised extraction conditions are shown in Table 3.2.

Table 3.2: Optimised conditions for sample extraction

Accelerated Solvent Extraction (ASE) Solvent = Dichloromethane (20 mL) Duration for single extraction = 15 min	
Temperature	125 ^{o}C
Pressure	1500 bar
Static Cycle	1 (at 5 min)
Extraction Cell	10 mL
Purge Time	60 s
Rinse Volume	40 %
Extraction Repeats	3
Final Volume of Extracts	60 mL

Extraction of PAHs from each particulate and resin sample was repeated three times in the same collection vial to ensure that all the extractable PAHs were extracted. The first, second and third extractions accumulate the total extraction volume to 60 mL per sample. Figures 3.7a, b, c and d show images of 60 mL PAH extracts in DCM from the soot samples which were collected from pyrolysis of 85%heptane/15%toluene blend at 1350, 1250, 1150 and 1050 ^{o}C respectively. It can be seen from Figure 3.7 that the colour of the PAH extracts in DCM darkens with decreasing pyrolysis temperature of the reactor (Figures 3.7a, b, c and d). Efficiency of the extraction method was evaluated using 84.6 mg of ethylene soot

generated from the reactor at 1150 ^{o}C and was found to be 90 %. The extraction efficiency was the mean of the 3 consecutive extractions as shown in equation 3.3.

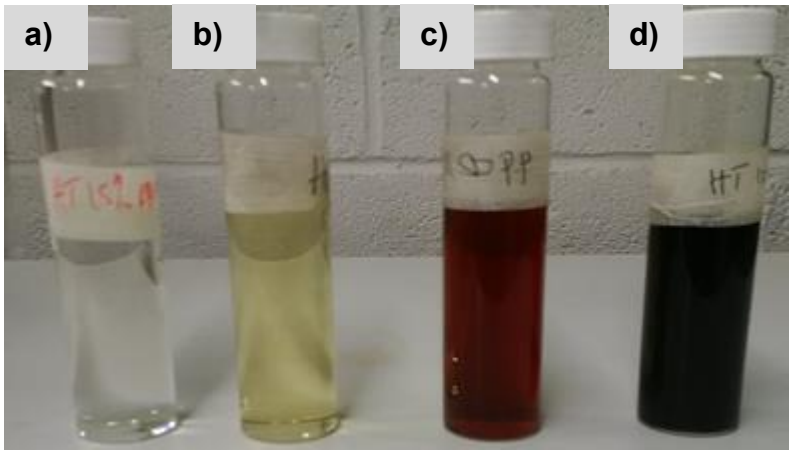

Figure 3.7: Appearance of the 60 mL PAH extracts in DCM. Soot samples were collected from pyrolysis of 85%heptane/15%toluene blend at 4 different temperatures: a) 1350 ^{o}C b) 1250 ^{o}C c) 1150 ^{o}C d) 1050 ^{o}C

$$\text{Extraction efficiency} = \frac{Sum\ of\ PAHs\ from\ first + second + third\ extractions}{3} \qquad \text{Eq.3.3}$$

PAH recoveries of each of the 16 PAHs were calculated relative to the conventional atmospheric Soxhlet extraction and were found to be in the range of 82 – 120 %. Detailed comparison of the Soxhlet and ASE processes will be discussed in chapter 4. Several authors (Oukebdane et al., 2010; Popp et al., 1997) also compared the recovery efficiencies of ASE and conventional Soxhlet and their results were similar to those reported in this thesis. To prevent any deterioration of PAHs during deep-freeze storage, all the samples were extracted within one week of their generation (Oukebdane et al., 2010).

3.5 Solvent evaporation/extract concentration

Following the extraction of PAHs from the particulate and XAD-2 resin samples by the ASE process, most of the DCM in the 60 mL extracted PAH volume was evaporated immediately by bubbling gently a nitrogen stream at 5 L/min through the extraction vial containing the PAH extracts. The extraction vial was situated in a custom-made stainless steel PID controlled heating mantle. The heating mantle was maintained at a temperature close to the boiling point of DCM (~ 40

^{o}C). Each extract was initially concentrated from 60 mL down to about 15 mL and was then transferred into a graduated glass tube (0 to 15 m L) (VWR, UK). The 15 mL extract was then concentrated further, down to about 1 mL (V_c, mL) for subsequent GCMS analysis. Figure 3.8 shows the set-up for solvent evaporation while Figure 3.9 shows the images of the concentrated PAH extracts (V_c, mL) of the extracts shown in Figure 3.7.

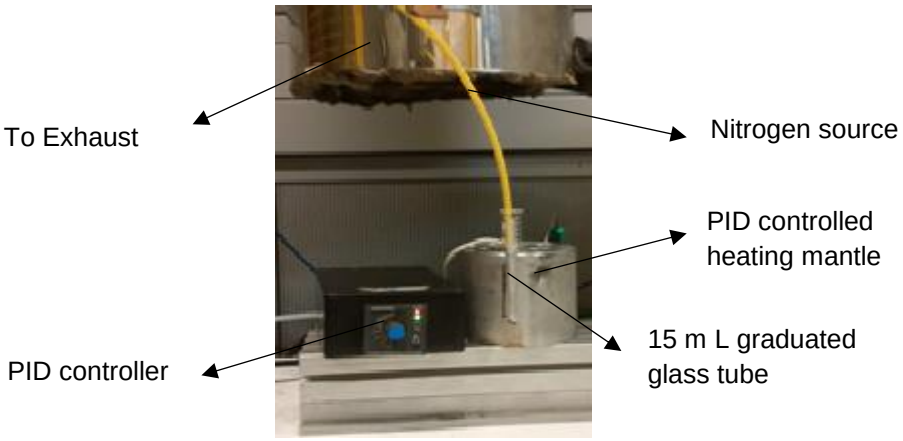

Figure 3.8: A set-up for sample concentration / solvent evaporation

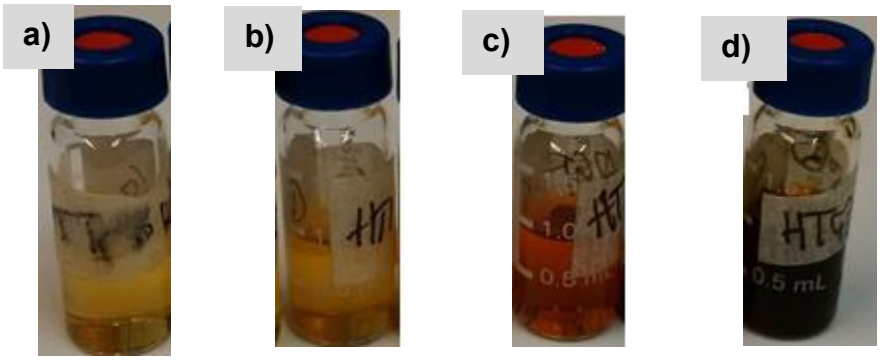

Figure 3.9: Appearance of 1 mL concentrated PAH extracts following solvent evaporation of extracts shown in Fig.3.7. Soot samples were collected from pyrolysis of 85%heptane/15%toluene blend at 4 different temperatures: a) 1350 ^{o}C b) 1250 ^{o}C c) 1150 ^{o}C d) 1050 ^{o}C.

Gas Chromatography Mass Spectrometry (GC-MS) is an analytical technique which allows a complex mixture of unknown molecules (such as PAHs) in a sample to be separated, identified and quantified with the aid of analytical standards. The GC component separates the mixture of each PAH as a distinct peak, while the MS element identifies the PAH peak based on its mass to electrical charge ratio (m/z).

3.6.1 Operating principle of GC 7890B coupled with 5977A MSD

The GCMS model used for the PAH analysis throughout this present study is GC 7890B coupled with 5977A MSD (mass selective detector) procured from Agilent Technologies, UK and was also installed in room B.09 of the Thermodynamic Laboratory at UCL Mechanical Engineering. Figure 3.11 shows a schematic of the operational features of a typical GCMS. The GCMS model used Helium carrier gas, and consist of an automatic liquid sampler (ALS) for injecting samples, capillary column, transfer line, ionization source, detector and a PC for data analysis. The reader is referred to A 5 in appendix A for an image of the GCMS model used for this present work. The GC uses a capillary column which is coated with a polymer material. The column is situated in an oven. The capillary column is specified usually, based on its dimensions (length, diameter and thickness) and its phase properties. The GC column is known as the *stationary phase* while the Helium carrier gas is known as the *mobile phase*. The GC 7890B consist of HP-5MS column (30 m x 250 µm x 0.25 µm, 5% Phenyl Methyl Silox) which can withstand a maximum temperature of 325 °C. The capillary column, through absorption and subsequent desorption, helps separate individual gaseous species, in a mixture, and cause them to emerge at different times from the outlet of the column.

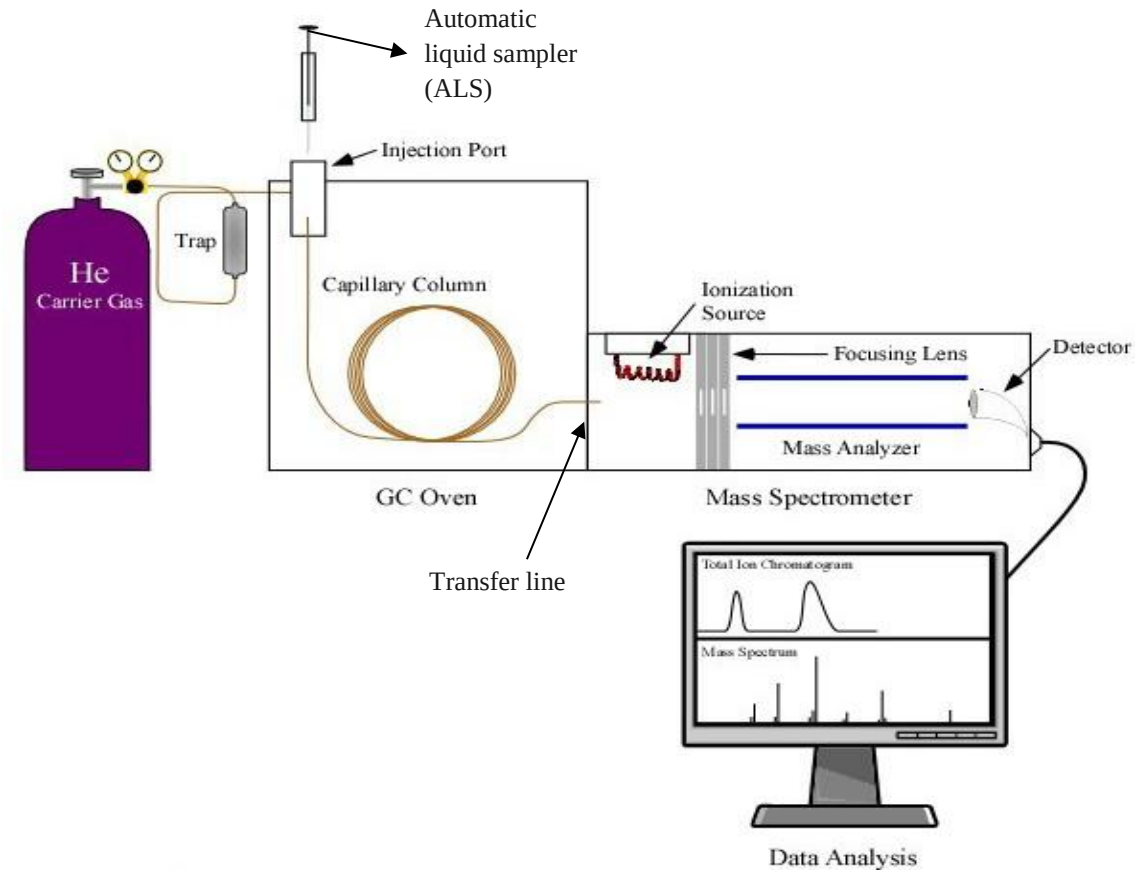

Figure 3.11: Schematics of the operational features of a typical GC-MS (Wu et al., 2012).

Figure 3.10: A screen shot of a Thermo- Lab GCMS software for data acquisition

Table 3.3: Optimised conditions for GCMS analysis.

GC Operating Conditions	
GC Model	7890B GC coupled with 5977A MSD
GC Column	Agilent HP-5MS, 5% Phenyl Methyl Silox, 30m x 250µm x 0.25µm connected to the front inlet and heated by the oven.
Carrier Gas	Helium (He), 1.2 mL/min
Injection Source	Automatic Liquid Sampler (ALS)
Injection Volume	1µL,
syringe capacity	10 µL
Injection Type	Standard
Solvent wash	Pre-injection and Post-injection (2 times) with a volume of 2 µL at fast plunger speed and zero dwell time each.
Inlet	Front Inlet, Split-Splitless,
Inlet Liner	Agilent 5190-2293 ultra-inert, split less, single taper, glass wool
Gas Saver	Off
Injection Mode	Split less
Inlet Temperature	300°C
Pressure	14.105psi
Septum Purge Flow Mode	Standard
Septum Purge Flow	3mL/min
Oven Heating	
	Initial temperature of 50°C, hold for 1min, then a ramp rate of 25°C/min increased to 150°C hold for 1min. Ram rate of 25°C/min increased to 200°C hold for 1min. Ram rate of 3°C/min increased to 230°C hold for 1min. Ram rate of 8°C/min increased to 310 °C hold for 3 min. **Total run time = 33.0 minutes**
Transfer line Temperature	290°C
Make-up Flow	Nitrogen (20mL/min)
MS Operating Conditions	
MS type	Single Quadrupole
Tune File	Atune.U
Tune type	Electron Ionization (EI)
Tune EMV	1129V
MS Source	230°C
MS Quad	150°C
Acquisition type	Scan
Scan Frequency	5.5 (scans/sec)
Start and End Mass (m/z)	50 – 550 m/z
Cycle Time	181.35 (ms) with m/z step size of 0.1
Solvent Delay	4 minutes
Gain Factor	1

Following solvent evaporation of PAH extracts shown in Figure 3.8, injection of the concentrated PAH extract (V_c, mL) to the capillary column of the GC was

carried out with an automatic liquid sampler (ALS) via an inlet port. Agilent thermo-Lab. acquisition software was used to facilitate sample injection, and its screen shot is shown in Figure 3.10. Additional information regarding the operation of the GC 7890B is given in (Agilent, 2013).

Single and multiple samples can be run on the GC with the aid of an automatic liquid sampler (ALS). An analysis method, which specifies the GC oven temperature profile, was initially developed and optimized on the thermo-Lab software. The optimized method that was used throughout this study is shown in Table 3.3. Prior to running the unknown PAH sample, the GC was initially calibrated using analytical standards which will be described later in chapter 4. A preliminary injection of the solvent (as a blank), with which the unknown PAH samples were prepared, was run before injecting the samples. Injecting a 'blank sample' to the GC column prior to the sample injection ensures clearing contaminants within the column.

Shortly after the sample was injected into the GC column, it was vaporised and swept onto a chromatographic column by the inert mobile carrier gas. Separation of the 16 PAHs (see Table 2.1 for their list) in the GC column was achieved based on their differences in chemical properties and their relative affinity to the mobile carrier gas and the stationary GC column. The PAHs were subsequently retained in the column and later come-off (*elute*) from the column at different times known as *retention time.* Two PAHs (especially isomers) may have relatively close retention times (*co-elution*). PAHs with lower molecular weight usually elute prior to those with higher molecular weight due to differences in boiling points; but properties such as vapor pressure and polarity of the PAH could also influence their retention times. Molecules separated by the GC were carried by the instrument to the MS (via a heated *transfer line)* where they were ionized, accelerated, deflected and detected separately.

The ion source in the MS converts compounds into *ionized fragments.* Two modes of ionization often encountered in MS are the electron ionization (EI) and chemical ionization (CI). The former is most widely used. In EI mode, the molecules are bombarded by a beam of electrons resulting to loss of one electron (molecular ion, M^+). The resulting peak of a molecular ion observed from a mass

spectrum designates the molecular weight of the compound. The high energy transmitted to the molecular ion also generates fragment molecules with a unique relative abundance which further provides a 'fingerprint' to the molecular structure of the compound. The fragmentation pattern of the molecules depends on the amount of energy, in electron volt (eV), applied by the system.

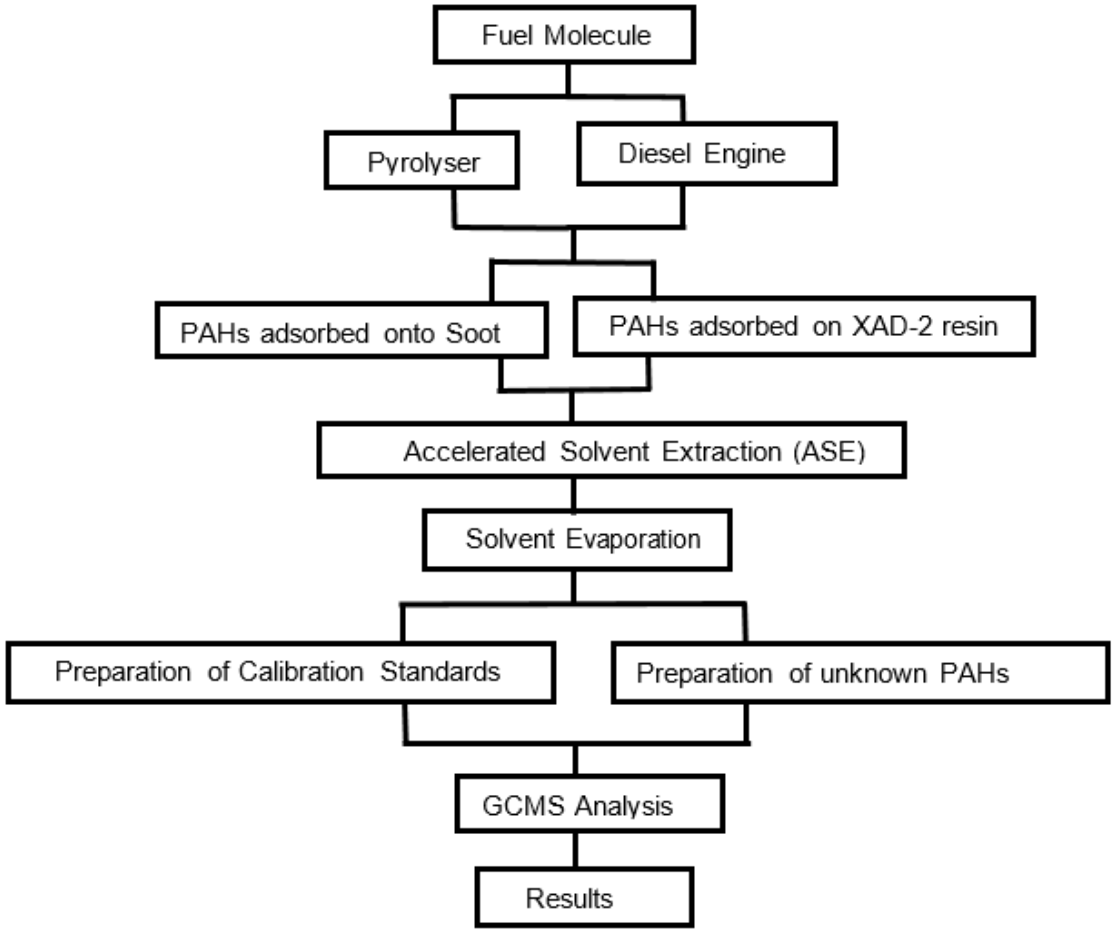

Figure 3.12: Summary of the methodology for the quantification of the US EPA 16 priority PAHs.

Once ionised, the positively charged ions then enter a mass analyzer (detector) where they are separated based on their mass related properties and also on the detector employed. Different types of detectors exist, and they include: quadrupoles, time-of-flight, ion trap, magnetic sector, tandem quadrupoles (MS – MS) etc. The mass spectrometer used in this study incorporated a single quadrupole analyzer (mass selective detector – MSD). The output of the separated molecules was produced as a signal which was monitored on a PC.

Spectra of the separated PAH molecules were then generated with each of the PAHs having a distinct peak showing individual PAH abundance. Comparison of the spectra with a mass spectral library provided by the national institute of standard (NIST) enables identification of the name and structures of the individual PAHs. Table 3.3 summarizes the entire methodology used through this thesis. Detailed analysis for GCMS calibration and PAH analysis of unknown PAH samples will be discussed in chapter 4.

In conclusion, the methodology for PAH quantification involved generating particulate and gas phase PAH samples from a tube reactor and a diesel engine. Characteristics of particulates were determined using DMS 500 instrument. PAHs in the particulate and gas phase samples were then extracted using an accelerated solvent extraction system (ASE). Following the sample extraction, the PAH extracts were further concentrated to down to about 1mL ($V_{c,}$ mL). The concentrated unknown PAH extracts were later analysed and quantified using gas chromatography coupled to mass spectrometry (GCMS).

Chapter 4

4. Methodology for speciation of the gaseous and particulate borne PAHs

This chapter reports the analytical procedure that was used to qualitatively and quantitatively analyse the concentration of unknown particulate and gaseous PAHs following their identification by the GCMS. Development of method for analysing and interpreting the EPA 16 priority PAHs is detailed. Preparation of analytical calibration standard and processing of calibration curves for each of the individual 16 PAHs are described. Quantification of unknown PAHs from particulate and XAD-2 resin extracts in relation to the calibration curves is outlined. The procedure has certain novel features that will be described in the subsequent section of this chapter.

4.1 Development of GCMS method

The optimised method developed for the GCMS analysis of the unknown PAH and calibration samples was shown previously in Table 3.3 of chapter 3. Gas Chromatography, Mass Spectrometry (GCMS) was chosen for PAH identification due to its reliability for detecting PAHs of relatively low molecular weights (m/z), from as low as 2 atomic mass unit (amu) to as high as 400 amu. GCMS also provides identification and quantification of PAH isomers such as phenanthrene (178 amu) and anthracene (178 amu) (Faccinetto et al., 2015). One limitation, however, to the use of GCMS is its decreasing detection reliability when heavier PAH masses (> 400 amu) are analysed. The method used throughout this thesis employed scanning through all the ionized fragments detected by the mass selective detector (MSD) in a sample within the range of 50 – 550 m/z, but at the

same time selectively monitoring the ions for the EPA 16 priority PAHs shown in Table 4.1. The maximum ion quantified from the 16 PAHs was 278 amu for benzo(a,h)anthracene, which falls within the range of reliable detection by GCMS.

4.2 Preparation of PAH calibration standards

Prior to quantification of the unknown PAHs from the batch of particulate and XAD-2 resin samples, the GC 7890B, 5977A MSD was initially calibrated. An external analytical standard mixture containing the 16 EPA priority PAHs (Supelco brand, TCL PAH Mix, 1 x1mL in dichloromethane) (part number of CRM48905) was procured from Sigma Aldrich, UK. The certificate of analysis of the standard is shown in A 6 in appendix A. The certified reference standard PAH solution had a nominal concentration of 2000 µg/mL and was subsequently diluted in dichloromethane (DCM). The DCM used for the dilution was high purity liquid chromatography (HPLC) grade sourced from Fisher Scientific, UK. Each PAH in the calibration mix had a certified purity ranging from 98.2 to 99.7%.

Table 4.1: Selected ions monitored during PAH analysis

PAH	Quantifier Ion	Qualifier Ion(s)
Naphthalene	128	129,127
Acenaphthylene	152	151,153
Acenaphthene	154	152,153
Fluorene	166	165, 167
Phenanthrene	178	176,179
Anthracene	178	176,179
Fluoranthene	202	101,203
Pyrene	202	101,203
Benz(a)anthracene	228	226,229
Chrysene	228	226,229
Benzo(b)Fluoranthene	252	126,253
Benzo(k)fluoranthene	252	126,253
Benzo(a)pyrene	252	126,253
Indeno(1,2,3cd)pyrene	276	138, 227
Dibenz(a,h)anthracene	278	139,279
Benzo(g,h,i)perylene	276	138,277

Bearing in mind the wide range at which PAHs are present in the particulates and XAD-2 resin samples, the PAH standard solution was first diluted in DCM in the ratio of 1:100 and thereupon subsequently diluted further into five calibration levels in the ratio of 1:5 (20, 4, 0.8, 0.16 and 0.032 µg/mL). The equation used for the serial dilution is shown below as Eq.4.1. Dilution of the PAH stock solution was carried out in DCM using high precision, high accuracy pipettes (1 – 1000 µL), 16 mL vials and 250 mL volumetric flasks.

Table 4.2: Deuterated internal standards and their corresponding target PAHs

SN	Deuterated Internal Standards	Quantifier Ions	CAS No	PAHs
1	1,4-Dichlorobenzene-d4	151.03	3855-82-1	-
2	Naphthalene-d8	136.1		Naphthalene
3	Acenaphthene-d10	164.27	15067-26-2	Acenaphthylene Acenaphthene Fluorene
4	Phenanthrene-d10	188.29	1517-22-2	Phenanthrene Anthracene Fluoranthene
5	Chrysene-d12	240.36	1719-03-5	Pyrene Benzo(a)anthracene Chrysene
6	Perylene-d12	264.38	1520-96-3	Benzo(b)fluoranthene Benzo(k)fluoranthene Benzo(a)pyrene Indeno(1,2,3-cd)pyrene Dibenz(a,h)anthracene Benzo(g,h,i)perylene

$C_1V_1 = C_2V_2$ Eq.4.1

Where:

C_1 = Nominal concentration of the stock PAH standard (µg/mL)

V_1= Volume of the stock PAH standard used to make the calibration standards (mL)

C_2 = Final concentration of the PAH calibration standard (µg/mL)

V_2 = Final diluted volume to produce the needed PAH calibration (mL)

An internal standard mixture (Sigma Aldrich, UK) of concentration equivalent to the middle calibration level (0.8 µg/mL) was added to each calibration vial based on the guidelines for PAH quantification as suggested by EPA Method TO (1999). The internal standard mixture contained 6 deuterated PAH compounds; and their corresponding target PAH compounds which are shown in Table 4.2. The deuterated internal standard under each target PAH was used to quantify the unknown target PAH.

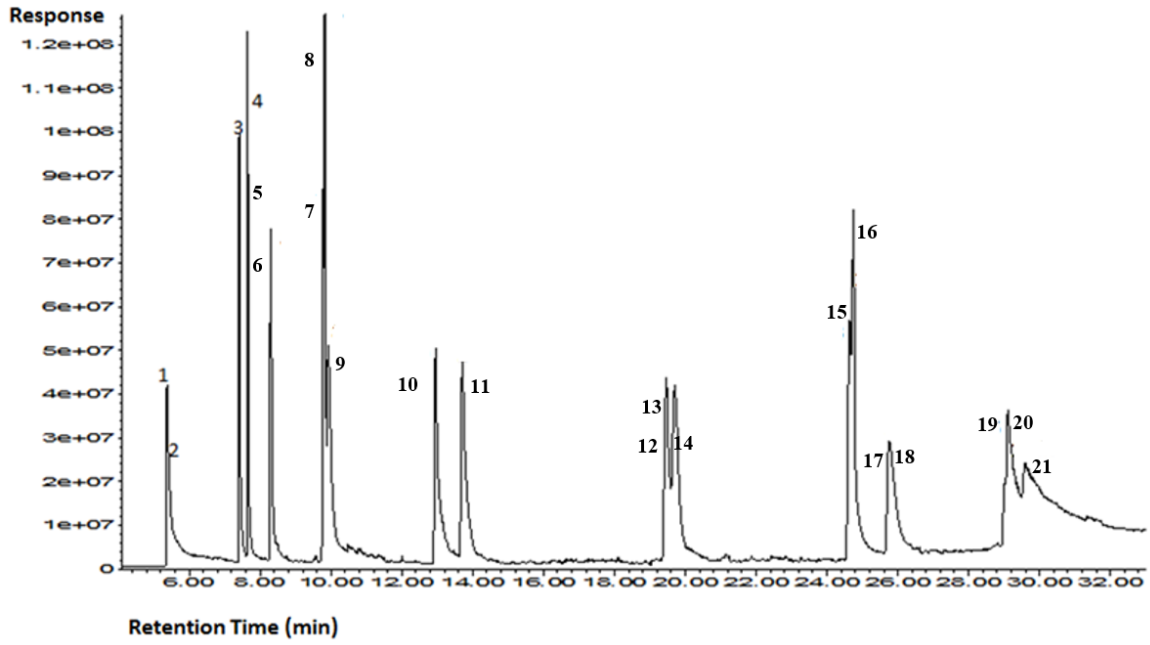

Figure 4.1: Typical Total Ion Chromatograph (TIC) of the calibration standard (20,000 µg/L) with the highest concentration spiked with 800 µg/L of an internal standard. 16 PAHs and 5 Deuterated internal standards were identified as follows: 1 = Naphthalene-d8, 2 = Naphthalene, 3 = Acenaphthylene, 4 = Acenaphthene-d10, 5 = Acenaphthene, 6 = Fluorene, 7 = Phenanthrene-d10, 8= Phenanthrene, 9 = Anthracene, 10 = Fluoranthene, 11= Pyrene, 12 = Benzo(a)Anthracene, 13 = Chrysene-d12, 14=Chrysene, 15 = Benzo(b)Fluoranthene, 16= Benzo(k)Fluoranthene, 17 = Benzo(a)Pyrene, 18=Perylene-d12, 19 = Indeno(1,2,3-cd)Pyrene, 20 = Dibenz(a,h)Anthracene and 21= Benzo(g,h,i)Perylene.

Further successive dilution of the lowest concentration/calibration level (0.032 µg/mL) revealed the minimum threshold concentration below which a PAH compound cannot be detected by the GCMS. This minimum threshold

concentration is called limit of detection (LOD) of the PAH. The LOD for each of the EPA 16 PAHs identified by the 7890B GC was found to be always lower than the lowest calibration level (< 0.032 µg/mL).

Preliminary analyses of pure dichloromethane solvent (blank), extracts from unused glass microfiber filter and XAD-2 resin showed no considerable contamination either within the GCMS column or in the syringe used for injecting samples. The integrated peak area of all these preliminary samples on the GC/MSD was below the detection limit, largely due to high signal to noise ratio (S/N = 50/1). The five calibration levels were run on the GCMS using an Agilent Thermo Lab software described previously in Chapter 3. The data files of the five calibration levels were subsequently stored, after the GCMS run, on the analysis PC for subsequent qualitative PAH analysis. Typical total ion chromatograph (TIC) of the highest concentration (20 µg/mL) of the calibration levels, spiked with 0.8 µg/mL of an internal standard is shown in Figure 4.1.

4.3 Qualitative PAH Analysis

Qualitative analysis of the data files corresponding to the five calibration levels, each containing the EPA 16 priority PAHs and 5 PAH internal standards, was carried out using the Agilent mass Hunter software. The data file of the calibration level with the highest concentration was initially uploaded using the software and its Total Ion Chromatogram (TIC) displayed on the GCMS analysis PC screen. A screen shot of the mass hunter qualitative analysis software interface displaying a typical TIC is shown in Figure 4.2. PAH compounds were found by integrating each peak on the TIC and the response (area under each peak) was noted. A Library search was then run on the data file to identify each peak as a distinct PAH. However, in the likely case of PAH isomers co-eluting, the PAH ions shown in Table 4.1 were at first extracted by chromatographic deconvolution prior to the library search. It is important to note that only when two PAH isomers (e.g. FLT and PYR) co-eluted as a single peak, at relatively close retention time, then those PAHs were found by "*Chromatographic Deconvolution Algorithm*".

Deconvolution is a method of separating co-eluting PAHs by developing a pure spectrum for each PAH (Du and Zeisel, 2013). Immediately after the TIC was de-

convoluted and all the fragment ions extracted, the resulting sample file was saved as an extracted ion chromatogram (EIC). The library installed in the MS is the National Institute of Standard (NIST) library. Spectral library search involves matching known mass spectra of PAH compounds in the library with that of the unknown PAH compounds in the sample. After the library search, each identified PAH ion was associated with a name, score, molecular formula, molecular mass, retention time and Chemical Abstract Service (CAS) number. A ‘score’ shows the likelihood of a PAH compound being identified correctly. The closer a score is to 100%, the greater the certainty that the PAH compound has been identified correctly. It is noteworthy mentioning that the score of all the 16 PAHs identified was 70% or higher; suggesting that the correct PAHs have been identified. Following the PAH identification, the sample file was then exported as a compound extraction file (.cef) and thereafter saved on the GCMS analysis PC.

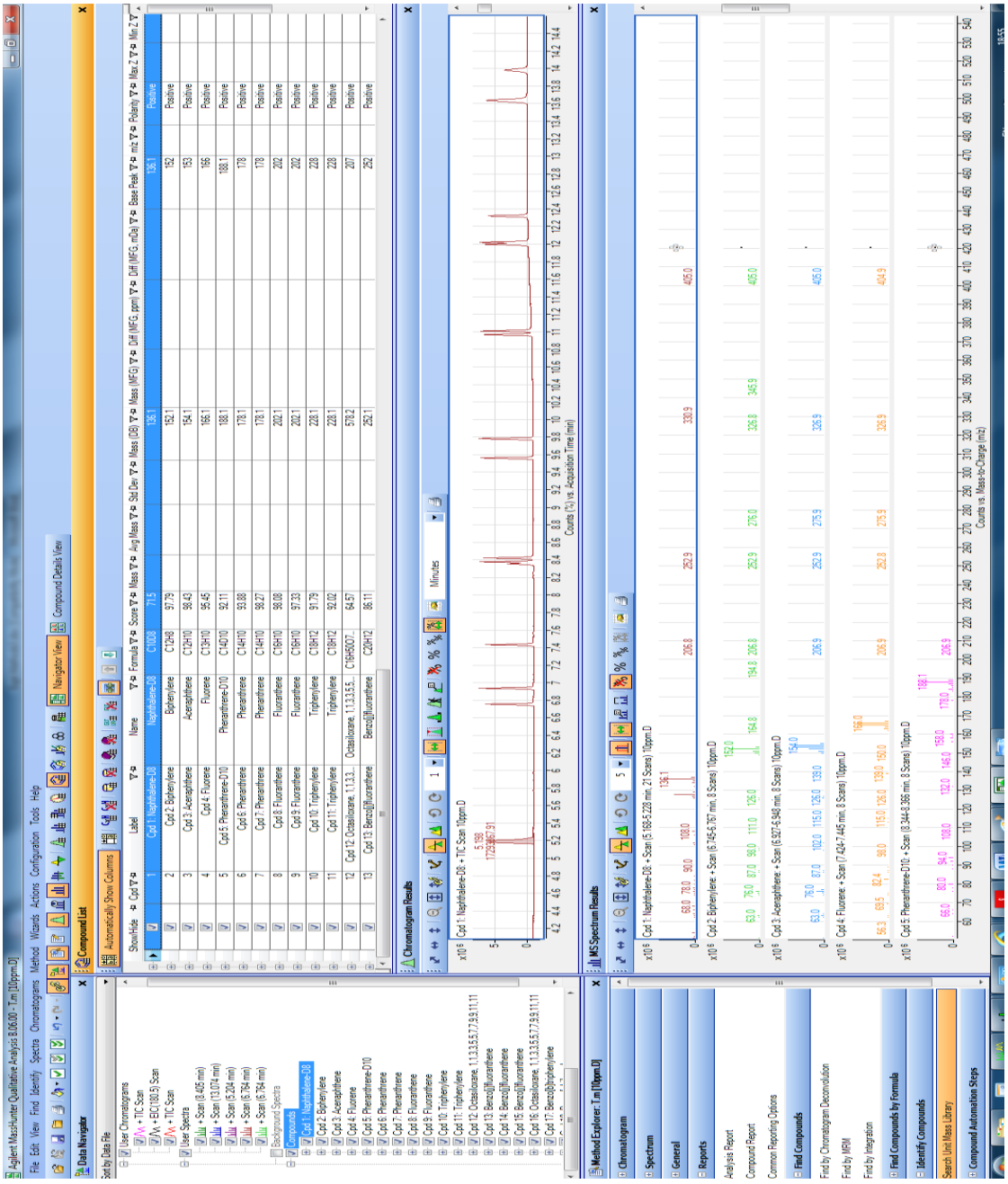

Figure 4.2: A screen shot of a typical Mass Hunter qualitative analysis software for PAH identification.

4.4 Quantitative PAH Analysis

The quantitative PAH analysis was carried out using the MSD Mass Hunter software. A screen shot of the MSD quantitative analysis interface is shown in Figure 4.3. The Mass Hunter software worked by initially creating a quantification method from either an acquired scan data or from an already stored compound extraction file (.cef) saved previously during qualitative analysis. The latter was

used in this case. The method set-up task was performed by setting up the following PAH parameters: PAH compounds, retention times, internal standards, PAH concentration, quantifier ions and calibration curve. A batch of the five calibration levels (20000, 4000, 800, 160 and 32 µg/L) was created and saved in (.bin) file format. A batch was a group of related data files that were processed using the same analysis method. The quantitative method, which was saved earlier, was applied later to the batch generated.

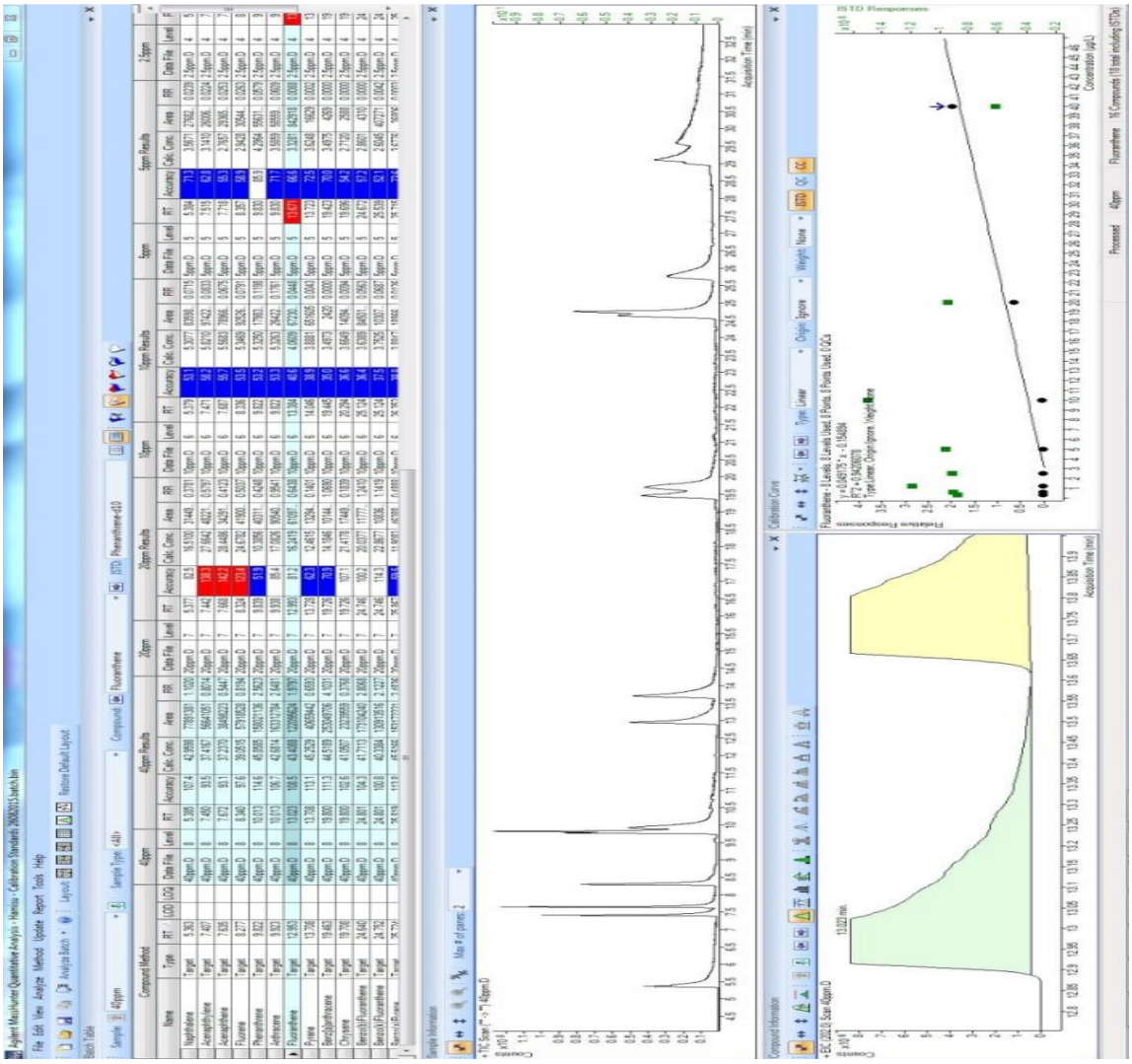

Figure 4.3: A Screen shot of a typical MSD Mass Hunter software (Agilent, UK).

Analysis and quantification of the batch produced the calibration curves for each of the EPA priority 16 PAHs. Detailed description of the method development and PAH quantitation procedure can be found in the Agilent MassHunter workstation Guide (2010). Calibration curves for all the PAHs were developed by plotting the

concentrations of the five calibration levels against their responses (integrated area under each peak).

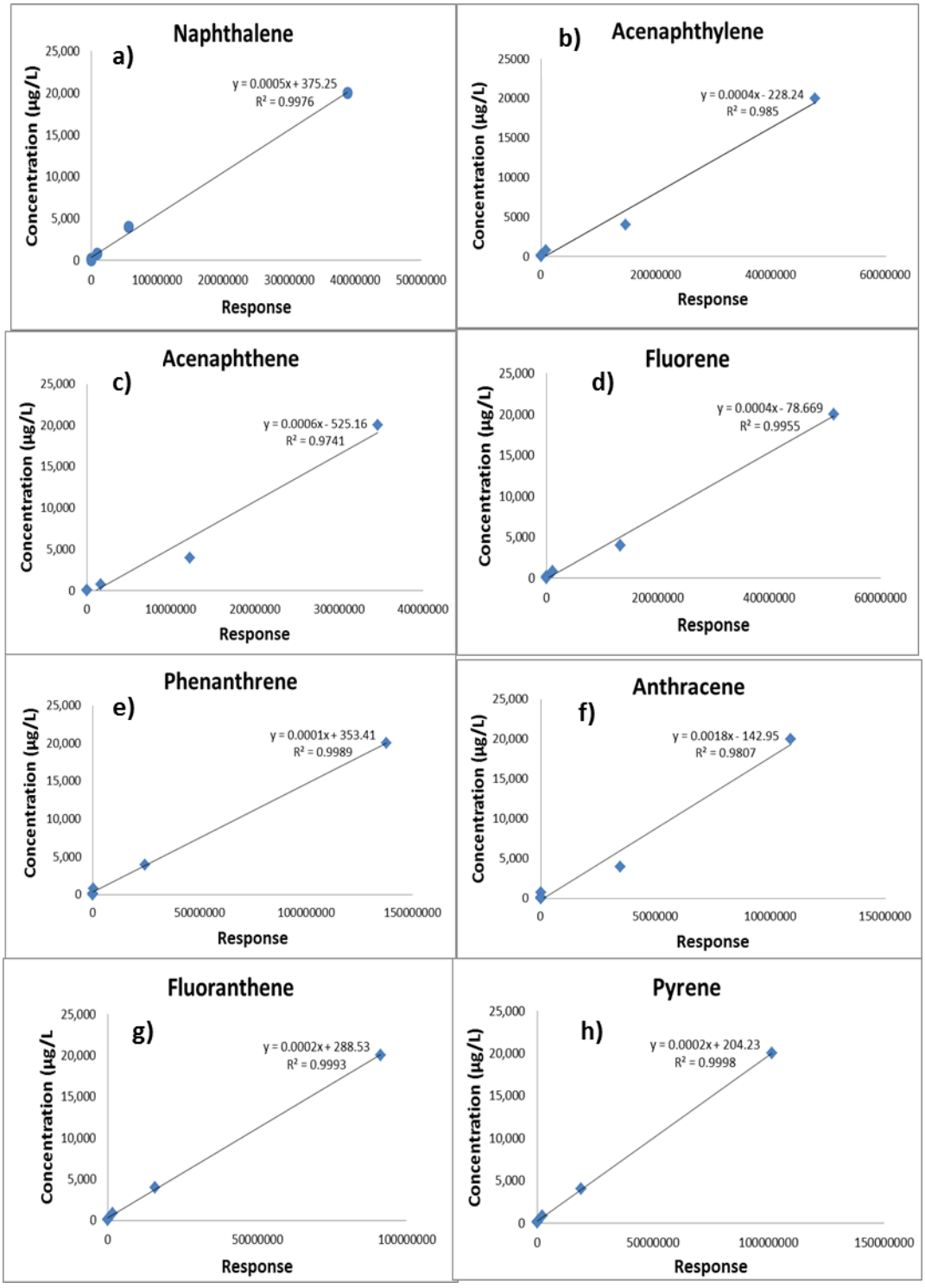

Figure 4.4: Typical calibration Curves for the US EPA 16 priority PAHs. Calibration curves were developed from 5 concentrations levels (20, 4, 0.8, 0.16 and 0.032 µg/mL): a) Naphthalene b) Acenaphthylene c) Acenaphthene d) Fluorene e) Phenanthrene f) Anthracene g) Fluoranthene h) Pyrene.

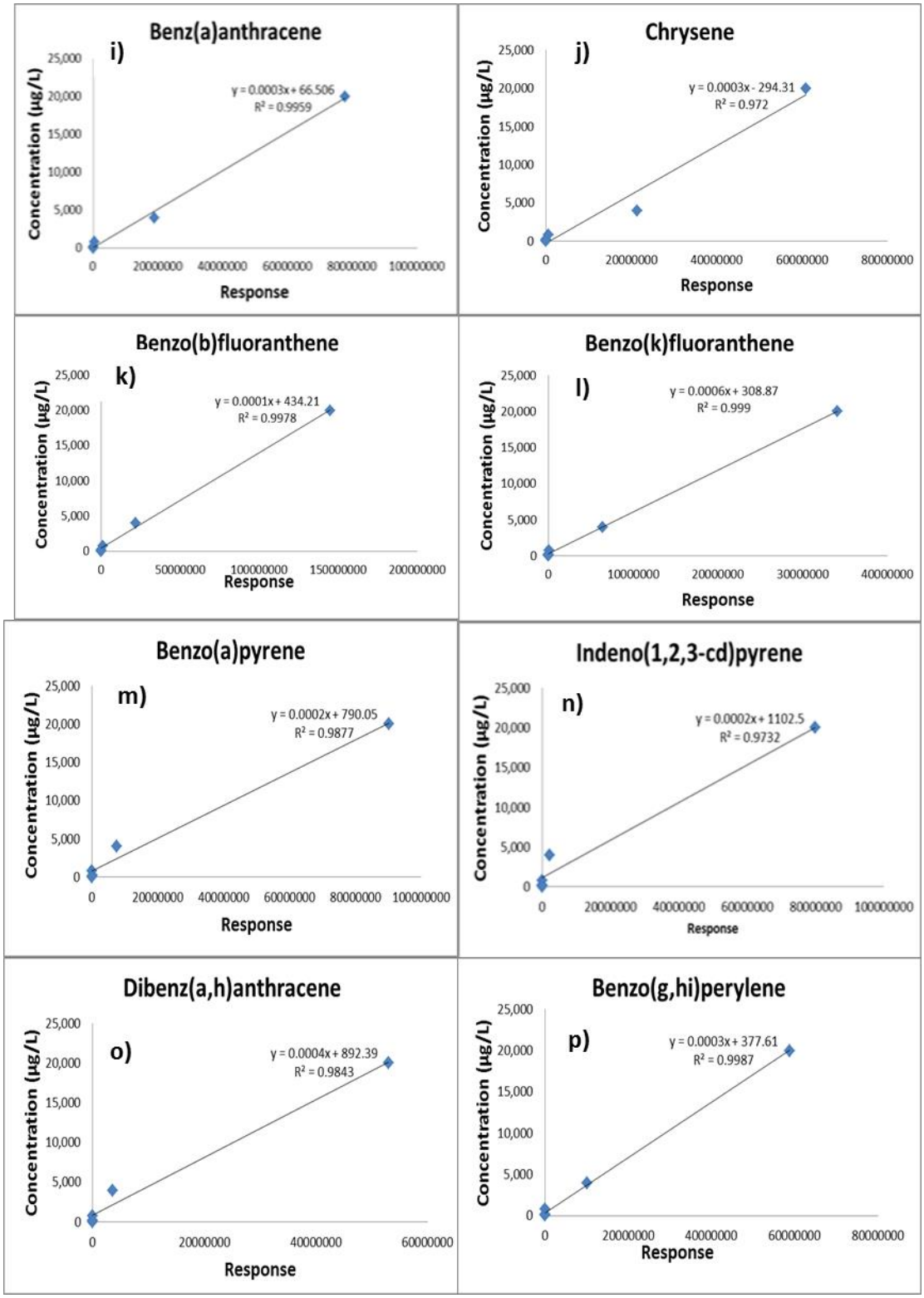

Figure 4.5: Typical calibration Curves for the US EPA 16 priority PAHs. i) Benzo(a)Anthracene j) Chrysene k) Benzo(b)Fluoranthene l) Benzo(k)Fluoranthene m) Benzo(a)Pyrene n) Indeno(1,2,3-cd)Pyrene o) Dibenz(a,h)Anthracene p) Benzo(g,h,i)Perylene.

Response factors (ratio of peak area of a PAH /concentration of the PAH) of all the 16 PAHs was calculated by the Mass Hunter software. The relative response

factor (RRF) of each PAH was also computed with the aid of equation 4.2 based on the recommendations of the EPA Method TO (1999). RRF is an indication of the relative response of the GC-MS to PAH concentration compared to the internal standard of the PAH.

$$RRF = \frac{A_T C_{iS}}{A_{iS} C_T} \qquad \text{Eq.4.2}$$

Where:

A_T = Area/response of the primary quantitation target ion of the target PAH

A_{is} = Area/response of the primary quantitation ion for the internal standard

C_T = Concentration of each target PAH extrapolated from the calibration curves shown in Figure 4.4.

C_{is} = Concentration of the internal standard (µg/mL)

The average relative response factor ($\overline{RRF}$) of the EPA 16 priority PAHs was calculated and used for the PAH quantification. $\overline{RRF}$ for all the calibration levels (in fact for all the calibration curves) was found to be within the range of 0.5 – 2.5, which was within the minimum criteria set by the EPA Method TO (1999).

Calibration curves were developed within the PAH concentration range of 32 – 20,000 µg/L for each of the 16 PAH compounds and were found be linear with correlation coefficient (R^2) values higher than 97% for all the PAHs. Figures 4.4 and 4.5 shows the calibration curves for each of the EPA 16 priority PAHs while the summary of the calibration equations is shown in Table 4.3. The highest calibration level (highest calibration concentration) was run in triplicate. The standard deviation (±δ) of the retention times was calculated and shown in Table 4.3. It can be seen from the table that the lowest retention shift was ±0.002 for acenaphthene-d10 and perylene-d12 while the highest was ±0.064 for napthalene-d8.

Table 4.3: The summary of the 16 Calibration results of the 16 PAHs

*EP	EPA/EU 16 PAHs	Retention Time (RT) (Min)	Concentration Range (µg/L)	Calibration Equation
1	Napthalene-d8	5.606±0.064	1,000	-
2	Naphthalene	5.633±0.039	32-20,000	y = 0.0005x + 275.25
3	Acenapthylene	7.592±0.004	32 - 20,000	y = 0.0004x – 228.24
4	Acenaphthene-d10	7.783±0.002	1,000	-
5	Acenaphthene	7.812±0.019	32-20,000	y = 0.0006x –525.16
6	Fluorene	8.472±0.005	32 - 20,000	y = 0.0004x – 78.67
7	Phenanthrene- d10	10.027±0.013	1,000	-
8	Phenanthrene	10.054±0.010	32 - 20,000	y = 0.0001x + 353.41
9	Anthracene	10.195±0.015	32 - 20,000	y = 0.0018x –142 .95
10	Fluoranthene	13.356±0.034	32 - 20,000	y = 0.0002x + 288.53
11	Pyrene	14.158±0.050	32 - 20,000	y = 0.0002x + 204.23
12	Benz(a)anthracene	20.002±0.018	32 - 20,000	y = 0.0003x + 66.5
13	Chrysene-d12	20.074±0.03	1,000	-
14	Chrysene	20.263±0.011	32 - 20,000	y = 0.0003x – 294.31
15	Benzo(b)fluoranthene	24.948±0.037	32 - 20,000	y = 0.0001x + 234.21
16	Benzo(k)fluoranthene	25.078±0.063	32 - 20,000	y = 0.0006x + 308.87
17	Benzo(a)pyrene	26.076±0.003	32 - 20,000	y = 0.0002x + 790.05
18	Perylene-d12	26.251±0.002	1,000	-
19	Indeno(1,2,3cd)pyrene	29.252±0.013	32 - 20,000	y = 0.0002x + 1102.5
20	Dibenz(a,h)anthracene	29.325±0.026	32 - 20,000	y = 0.0004x + 892.39
21	Benzo(g,h,i)perylene	29.88±0.045	32 - 20,000	y = 0.0003x + 377.61

EP designates Elution Precedence

4.5 Quantification of unknown PAHs

Each unknown target PAH compound in the particulate and XAD-2 resin extracts was processed using the same method shown in Table 3.3. Unknown target PAHs were quantified by selectively monitoring the quantifier PAH ions shown in

Table 4.1 with the corresponding quantifier ions for the internal standards shown in Table 4.2. This analysis was implemented by identifying the unknown target PAHs based on detection of the ions in each PAH molecule and subsequent comparison of their retention times with those of the QTM PAH Mix calibration standards. The limit of quantification (LOQ) was described as the ratio of the limit of detection (LOD) to the sampling volume of gas or sampling soot mass. The mass of gas phase (GP) and particulate phase (PP) PAHs, both normalised by the volume of gas passed through the particulate filter and the XAD-2 resin in series, are shown in Eq.4.3 and Eq.4.4 respectively. The mass of PP PAHs, normalised by the mass of soot from which the PAHs were extracted, is shown in Eq.4.5.

$$C_{GP,\,Vg} = \frac{A_T\, C_{iS}\, V_c}{\overline{RRF}\, A_{iS}\, Vg} \quad (\mu g \text{ of PAH/m}^3 \text{ of gas}) \qquad \text{Eq.4.3}$$

$$C_{PP,\,Vg} = \frac{A_T\, C_{iS} V_c}{\overline{RRF}\, A_{iS}\, x\, Vg} \quad (\mu g \text{ of PAH/m}^3 \text{ of gas}) \qquad \text{Eq.4.4}$$

$$C_{PP,\,Ms} = \frac{1000\, A_T C_{iS}\, V_c}{\overline{RRF}\, A_{iS} Ms} \quad (\text{ng of PAH/mg of soot}) \qquad \text{Eq.4.5}$$

Where:

$C_{GP,\,Vg}$ = Mass of the target gas phase PAH (µg) normalised by the volume of gas (m^3) passed through the particulate filter and XAD-2 resin in series.

$C_{PP,\,Vg}$ = Mass of the target particle phase PAH (µg) normalised by the volume of gas (m^3) passed through the particulate filter and XAD-2 resin in series.

$C_{PP,\,Ms}$ = Mass of the target particle phase PAH (ng) normalised by the mass of soot (mg) collected on the particulate filter.

$\overline{RRF}$ = Average relative response factor of the EPA 16 priority PAHs

A_T = Area/response of the primary quantifier target ion of the unknown PAH in a sample

A_{is} = Area/response of the primary quantifier ion for the internal standard corresponding to the target PAH

C_{is} = Concentration of the internal standard (µg/mL) added to the unknown sample

V_c = Volume of the concentrated PAH extracts following solvent evaporation prior to GC run (mL)

V_g = Volume of gas passed through the particulate filter and XAD-2 resin in series

M_s = Mass of soot collected on the particulate filter (mg)

It should be noted here that the calibration curves reported in this chapter are representative only of those developed throughout the course of quantitating the PAHs described in chapters 5 – 7 of this thesis. Generally, before any batch of particulate and XAD-2 resin samples generated from either the tube reactor or diesel engine were quantified, new calibration curves were developed on each occasion. The highest calibration level employed was 100,000 μg/L.

4.6 Comparative analysis between Soxhlet extraction and accelerated solvent extraction (ASE)

A soot sample of 100 mg was collected on a glass microfiber filter. The soot was generated from toluene pyrolysis using the tube reactor at a temperature of 1150 ^oC and hydrocarbon concentration of 10,000 ppm on C_1 basis. The particulate filter, containing 100 mg of the soot sample, was cut symmetrically into two pieces. The PAHs on the first half of the filter were Soxhlet extracted while the PAHs on the second half were extracted using the ASE process. Extraction of both samples was carried out in dichloromethane (DCM) as the solvent. The volume of DCM used during Soxhlet extraction was 150 mL while only 60 mL of DCM was used during the ASE method. Both the Soxhlet and ASE extracts were later concentrated down to 5 mL by evaporating most of the DCM using a rotary evaporator set-up. An approximate volume of 1.0 mL of each extract was transferred by means of pipette into an Agilent 2.0 mL vial for analysis by the GCMS. Since the PAH results from the Soxhlet and ASE processes were to be compared only, the PAHs were not quantified using internal standards. Each PAH extract from the soot sample was run on the GCMS in a full scan mode using the operating conditions shown in Table 3.3. The peak area of each of the 16 PAHs detected and the ratio of each PAH based on the area from ASE sample to the area of the Soxhlet sample are shown in Table 4.4. Seven PAHs common to

both Soxhlet and ASE were identified ranging from ACY, PHN, FLT, PYR, B[a]A, B[k]F, I[1,2,3-cd]P and B[g,h,i]P, while B[b]F was only detected in the Soxhlet extracted sample.

Table 4.4: Comparison between PAHs Soxhlet and ASE (Nd denotes PAHs that are 'not detected' by the GCMS).

EP	US EPA/EU 16 PAHs	Soxhlet Area	ASE Area	% (ASE area / Soxhlet area)
1	Naphthalene	Nd	Nd	-
2	Acenapthylene	20308947	16776212	82.6
3	Acenaphthene	Nd	Nd	-
4	Fluorene	Nd	Nd	-
5	Phenanthrene	317865686	343920868	108.2
6	Anthracene	Nd	Nd	-
7	Fluoranthene	342916814	342812725	100
8	Pyrene	302804545	361072022	119.2
9	Benzo[a]anthracene	619228314	587416241	94.9
10	Chrysene	Nd	Nd	-
11	Benzo[b]Fluoranthene	109324049	Nd	-
12	Benzo[k]Fluoranthene	694934709	587759948	84.6
13	Benzo[a]Pyrene	Nd	Nd	-
14	Indeno[1,2,3-cd]Pyrene	709613930	832891252	117.4
15	Dibenz[a,h]anthracene	Nd	Nd	-
16	Benzo[g,h,i]Perylene	8099620	5106272	63.0
	Total	**3125096614**	**3077755540**	**-**

EP designates Elution Precedence and 'nd' means 'not detected' by the GCMS

It can be observed from Table 4.4 that the peak area of most of the particulate phase PAHs from both the Soxhlet and ASE were reasonably close. For example, the proportions of ACY extracted by Soxhlet and ASE were calculated as 0.64 and 0.54 % respectively; while those of B(a)A extracted by Soxhlet and ASE are 19.8 and 19.1 % respectively. The recovery of the ASE relative to the soxhlet was found within the range of 63 – 119.2%. These results suggest that, bearing in mind the complex and multiple processes involved, the agreement between Soxhlet and the ASE is satisfactory. It is noteworthy that the ASE has somewhat higher recovery.

Chapter 5

5. Effects of Unsaturation of C_2 and C_3 Hydrocarbons on the Formation of PAHs and on the Toxicity of Soot Particles

This chapter concerns the effect of unsaturation on soot and PAH formation of three C_2 hydrocarbons (ethane, ethylene and acetylene) and two C_3 hydrocarbons (propane and propylene). Pyrolysis of the five gaseous fuel molecules in a heated nitrogen was carried out within the temperature range of 1050 - 1350 ^oC under oxygen free condition and a fixed fuel concentration of 10,000 ppm on C_1 basis. The experimental results showed that, depending on the temperature at which a fuel is pyrolysed, its degree of unsaturation plays an important role on the type and concentration of PAHs generated and, on the overall carcinogenic potential of the gaseous and particulate effluent.

5.1 Introduction

Engineering systems such as gas turbines and internal combustion engines utilise gaseous fuels which produce toxic substances when they are burnt. Among these substances are solid soot particles and gas-phase polycyclic aromatic hydrocarbons (PAHs). The link between soot and PAHs has long been established. Firstly, PAHs assemble themselves into larger structures which are the soot particles themselves. Secondly, PAHs are mostly found adsorbed on the surfaces of soot particles and form their toxic components.

PAHs produced by some C_2 and C_3 fuels were investigated previously in flames (Crittenden & Long, 1973; Olten & Senkan, 1999; Smyth et al., 1997) and tube reactors (Sánchez et al., 2012; Sánchez et al., 2013; Shukla & Koshi, 2012). Advances have also been made using kinetic modelling (Frenklach, 2000; Norinaga et al., 2009; Lacroix et al., 2010; Frenklach et al., 1985).

However, the characteristics of PAHs in the gaseous phase and those adsorbed onto particles including the relative toxicity of these PAHs with variation in fuel degree of unsaturation, are still not precisely understood. Understanding of the linkage between fuel molecular structures and the amount and toxicity of air-borne and particulate-borne PAHs is still also incomplete.

Diesel and gasoline fuels contain a mixture of saturated, unsaturated, branched, and aromatic hydrocarbons (Pitz and Mueller, 2011). In order to understand and address the influence of fuel molecular structure on the formation and emission of toxic PAH molecules, a homologous series of saturated and unsaturated C_2 and C_3 fuel molecules have been assessed; this has contributed to insights that could inform the processing of fuels so that they produce fewer toxic PAH emissions.

This chapter presents, a systematic study of both the gas-phase and particle-phase PAHs generated from the pyrolysis of C_2 and C_3 fuels in a laminar flow reactor. The PAHs studied were the 16 listed by the US EPA as priority PAHs (see Tables 2.1 and 2.2 in chapter 2). Special attention was given to Group B2 PAHs which are classified as possible carcinogens to humans. Pyrolysis of the gaseous fuel molecules was carried out within the temperature range of 1050 - 1350^{o}C under oxygen free condition and a fixed fuel concentration of 10,000 ppm on C_1 basis. Soot and gas phase products generated within the reactor were sampled from the exit of the reactor. The PAHs from the samples were then extracted using an accelerated solvent extractor (ASE) and their analysis was carried out using gas chromatography coupled to mass spectrometry (GCMS).

5.2 Experimental Approach

5.2.1 Gaseous Fuel Molecules Tested

Five, chemically pure (CP) grade, single components gaseous fuel molecules, sourced from BOC UK, were tested and their properties are shown in Table 5.1. They included three C_2 fuel molecules (ethane, ethylene and acetylene) and two C_3 fuels (propane and propylene). The percentage purity of each of the gas molecules was 99 % or greater. Ethane is a significant component of natural gas, while propane is a principal component of Liquefied Petroleum Gas (LPG).

Table 5.1: The five fuel molecules tested with their properties at 1.013 bar and 15 ^oC.

Sn	Fuel Molecules	Molecular Structure	C/H	Molecular Mass (g/mole)	Boiling point (^oC)	Density (kg/m^3)
1	Ethane	H_3C-CH_3	0.33	30.07	-88.6	1.28
2	Ethylene	$H_2C=CH_2$	0.5	28.05	-103.7	1.19
3	Acetylene	$HC\equiv CH$	1	26.04	-84.7	1.11
4	Propane	$H_3C-CH_2-CH_3$	0.375	44.10	-42.1	1.90
5	Propylene	$H_3C-CH=CH_2$	0.5	42.08	-47.6	1.81

The purpose of this chapter is to investigate the influence of unsaturation of C_2 and C_3 Fuels on PAH formation as follows:

i) Confirm the influence of the degree of unsaturation on the propensity of a fuel to form soot in the tube reactor used for this study

ii) Characterise the soot particles produced from (i) above in terms of size, mass and number using the DMS 500 particle size spectrometer

iii) Study the influence of fuel unsaturation on the condensation of PAHs on soot particles and the production of PAHs as gas phase species

iv) Study the influence of fuel unsaturation on the toxicity of the Group B2 PAHs found on soot particles under pyrolytic conditions

v) Consider mechanisms that lead to the formation of gas and particle phase PAHs, and in particular, those mechanisms that lead to the formation of Group B2 PAHs

5.2.2 Sample Generation

Soot and gaseous PAH samples were generated by means of pyrolysis at temperatures ranging from 1050 -1350 °C using a tube reactor described ealier in chapter 3. The carrier gas used during the pyrolysis of all the gaseous fuel molecules was nitrogen and was metered at a constant flow rate of 20 L/min. All five fuel molecules were supplied to the pyrolyser at a fixed carbon flow rate of 10,000 ppm on C_1 basis. The flow rate of each fuel molecule is shown in Table 5.2. Ethane was also used as the baseline fuel for daily repeat checks, and to detect any potential drift in the reactor systems and associated instrumentation. Particulate generation from the tube reactor has been described in detailed in chapter 3.

Table 5.2: The concentrations of five fuel molecules tested.

Sn	Fuel Molecule	Fuel Flow rate (mL/min)	Fuel Flow rate on C_1 basis (ppm)
1	Ethane	99.80	10,000
2	Ethylene	99.95	10,000
3	Acetylene	98.90	10,000
4	Propane	69.90	10,000
5	Propylene	64.80	10,000

The filter gravimetric soot mass measurements and calculated soot mass concentrations at each temperature are shown in Table 5.3 and Table 5.4 respectively. The particulate and the gas phase samples collected were stored separately in 90 mm diameter plastic petri dishes and wrapped with para-film tape and immediately frozen and stored in dark frozen conditions for later analysis.

5.2.3 Sample Extraction

The extraction of PAH species from the soot and from the resin samples was carried out using an Accelerated Solvent Extractor (ASE) (Thermo Scientific Dionex-150) described previously in chapter 3 of this thesis.

5.2.4 Sample Concentration

The ASE provided the PAHs in solution with 60 mL of DCM. Most of the DCM was evaporated by bubbling gently a nitrogen stream through the vial containing the DCM and PAH extracts. The detailed sample concentration was described in chapter 3.

5.2.5 Sample Analysis

The concentrated 1 mL extracts of both the particulate and gas phase PAHs were analysed using gas chromatography coupled to mass spectrometry (GCMS) (Agilent 7890B GC coupled with 5977A MSD), and has been described previously in chapter 3. PAH quantification from the extracts has been discussed in chapter 4 of this thesis.

5.3 Results and Discussion

5.3.1 Effect of unsaturation on Soot Mass

Measured soot masses from the pyrolyses of the C_2 and C_3 fuels are shown in Tables 5.3 and 5.4 respectively. The results from Tables 5.3 and 5.4 showed that, for all the fuels examined, increase in temperature of the reactor from 1050 – 1250 ^{o}C resulted in increase in the mass of soot collected per unit volume of sample gas. This trend was consistent with similar trends reported in the literature (Sánchez et al., 2013; Ruiz et al., 2007a; Mathieu et al., 2007).

It can be observed from Table 5.3 that the single bonded ethane and the doubled bonded ethylene produced roughly similar soot mass concentrations, indicating that under the experimental conditions tested, the presence of double bond was not significant in determining the rate of soot formation. In an oxygen/fuel environment (Markatou, Wang and Frenklach, 1993), one would expect ethylene to soot substantially more than ethane, probably because of increased tendency for ethylene to become acetylene by means of hydrogen abstraction due to oxygen radicals. The absence of oxygen, in the pyrolytic conditions reported here, did not promote such hydrogen abstraction by means of oxygen radicals.

Table 5.3: Gravimetric filer mass measurements of C2 hydrocarbons.

	Ethane		Ethylene		Acetylene	
Temperature (°C)	Soot Mass, M_s,(mg)	Soot Conc. M_s/V_g (mg/m^3)	Soot Mass, M_s,(mg)	Soot Conc. M_s/V_g (mg/m^3)	Soot Mass, M_s,(mg)	Soot Conc. M_s/V_g (mg/m^3)
1050	5.100±1.000	16.00	8.000	25.70	36.30	119.0
1150	75.00±11.00	433.5	84.60	485.5	142.4	863.0
1250	153.0±14.00	956.3	155.4	953.4	202.6	1282
1350	124.5±11.00	793.0	135.0	849.1	169.3	1092

It is also apparent from Table 5.3 that when the triple bonded acetylene was pyrolysed, the soot formation, in comparison to the other two C_2 fuels, increased considerably. For instance, the soot concentrations generated in acetylene pyrolysis at the temperatures of 1050 °C and 1150 °C were, respectively, 5 and 2 times those for ethylene. The above observations are supported by the results of other investigations. For example, Ruiz et al. (2007) carried out pyrolysis of ethylene and acetylene within the temperature range of 1000 – 1200 °C in a similar tube reactor and they found that the amount of soot generated from acetylene was significantly higher than that from ethylene at all temperatures.

Table 5.4: Gravimetric filer mass measurements of C3 hydrocarbons.

	Propane		Propylene	
Temperature (°C)	Soot Mass, M_s, (mg)	Soot Conc. (M_s/V_g) (mg/m^3)	Soot Mass, M_s, (mg)	Soot Conc. (M_s/V_g) (mg/m^3)
1050	31.40	88.20	45.90	173.2
1150	146.3	774.1	202.0	1080
1250	202.9	1222	221.4	1366
1350	157.5	966.3	222.6	1436

***Conc. is equivalent to concentration*

The enhanced soot propensity of acetylene could be that it is directly involved as a reactive species in the HACA (hydrogen abstraction, acetylene addition) mechanism, which contributes to, both, PAH and particle growth (Frenklach, 2002). Several mechanistic studies highlighted the significance of the HACA mechanism in fuel rich hydrocarbon flames (e.g. Violi et al., 1999) and under

pyrolysis conditions (e.g. Shukla and Koshi, 2012). Acetylene has also been identified as directly involved in the formation of the first aromatic ring (Richter & Howard, 2000). This sets acetylene apart from ethane and ethylene, which must first both undergo dehydrogenation to form acetylene. It can also be observed from Table 5.3 that the large differences in the soot concentrations for ethane, ethylene and acetylene, at low temperature, reduced significantly at the higher temperatures.

Similarly, it can be seen from Table 5.4 that propylene yielded more soot concentrations than propane at all conditions tested. This could also be expected, since propylene (C_3H_6) is a doubled bonded unsaturated C_3 fuel that can produce propargyl radicals (C_3H_3) during pyrolysis (Norinaga and Deutschmann, 2007a). Propargyl radicals are known to be highly instrumental in the formation of the first aromatic ring (Miller & Melius, 1992), thus speeding up subsequent PAH growth and soot particle inception. This is probably why propylene formed soot prolifically. Higher soot propensity for propylene, when compared with propane, was also reported for flames by Wang & Chung (2014). It is noteworthy mentioning that the relative importance of acetylene over propargyl radical in forming the first aromatic ring depends on the starting hydrocarbon fuel molecule.

Finally, considering all the results for the C_2 and C_3 fuels in Tables 5.3 and 5.4 together, it could be concluded that the tendency of a fuel molecule to soot increases when its unsaturation level increases within the homologous series of the fuels shown in the Tables; however, this does not seem to apply in the case of ethane and ethylene.

5.3.2 Particulate characterisation of C_2 and C_3 hydrocarbons

Figure 5.1 shows the size distribution of soot particles (on number basis) produced from pyrolysis of C_2 and C_3 hydrocarbons, as measured with the DMS 500. Figures 5.1a, b, c and d show the size and number spectra for the C_2 and C_3 hydrocarbons at temperatures of 1050, 1150, 1250 and 1350 ^oC respectively. It can be seen from Figures 5.1a, b, c and d that there is a shift toward larger soot particles with increasing pyrolysis temperature from 1050 to 1350 ^oC, but ethylene pyrolysis was an exception for reasons which are not clear. For example,

pyrolysis of ethane at a temperature of 1050 ^{o}C resulted in particles in the size range of 13 – 86 nm, whereas at the higher temperature of 1350 ^{o}C, particles were broadly distributed in the range of 86 – 562 nm. Similar observations have been reported by Eveleigh (2015) during pyrolysis of ethane, ethylene and ethanol.

Figure 5.2 summarises the DMS data for the C_2 and C_3 hydrocarbons in terms of influence of temperature on (a) soot particle mean diameter (b) total soot mass concentration (mass per unit volume of N_2 carrier gas at N_2 inlet conditions and (c) total soot particle number concentration.

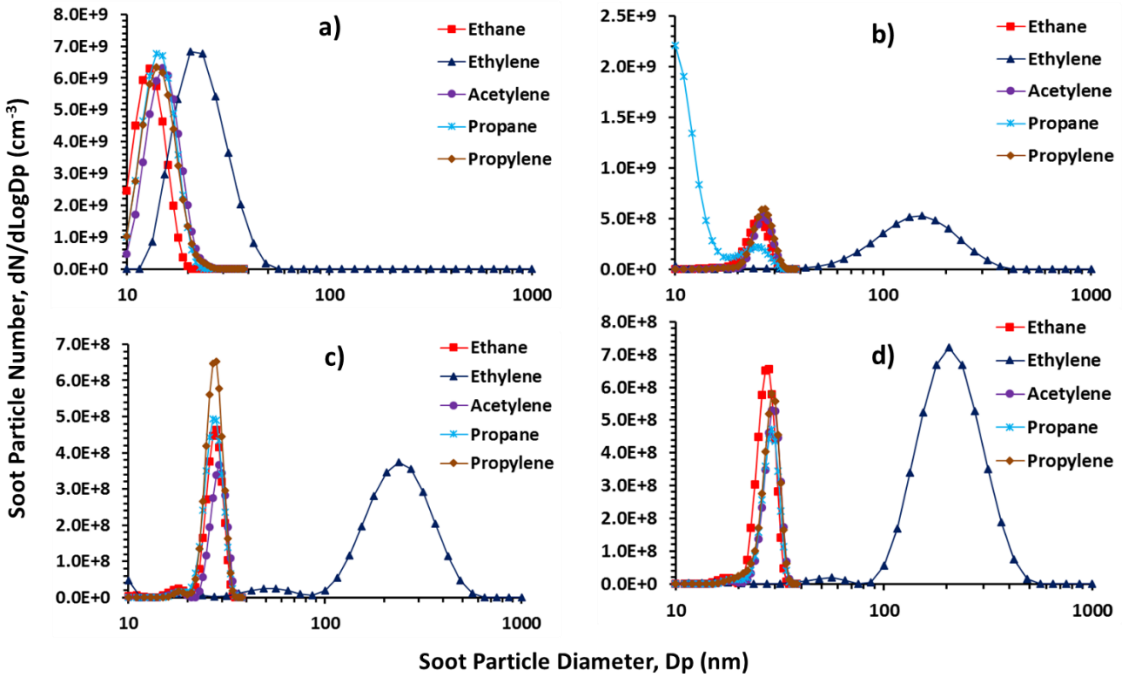

Figure 5.1: Number distribution of particulates formed from C2 and C3 hydrocarbons at 4 different temperatures a) 1050 ^{o}C b) 1150 ^{o}C c) 1250 ^{o}C d) 1350 ^{o}C

Figure 5.2a shows that the soot particle mean diameter increased with temperature increase, regardless of the degree of unsaturation of the hydrocarbon. It is apparent from Figure 5.2a that the average soot particle size of acetylene increases from 77 to 378 nm when the temperature increases from 1050 to 1350 ^{o}C and thereafter levelled-off up to 1350 ^{o}C. Similar observation can be made within the same temperature range of 1050 –1350 ^{o}C, for ethane and ethylene in terms of trends, although the particle size range was somewhat lower at 40 to 305 nm. Apparent from Figure 5.2a is the trend for larger soot particle

mean diameter with increase in degree of unsaturation of the C_2 and C_3 hydrocarbons within the temperature range of 1050 to 1150 ^oC. In Figure 5.2a, propylene formed slightly bigger soot particles than propane within the temperature range of 1050 to1250 ^oC.

Comparing Figure 5.2b and Table 5.3, similar variations can be observed for the degree of unsaturation of the C_2 and C_3 fuels for soot particle mass concentrations respectively measured by the DMS 500 and gravimetric filter mass measurements at all temperatures. Figure 5.2c shows that the number concentrations of C_2 fuels increased with increasing unsaturation of the fuels only at a temperature of 1050 ^oC.

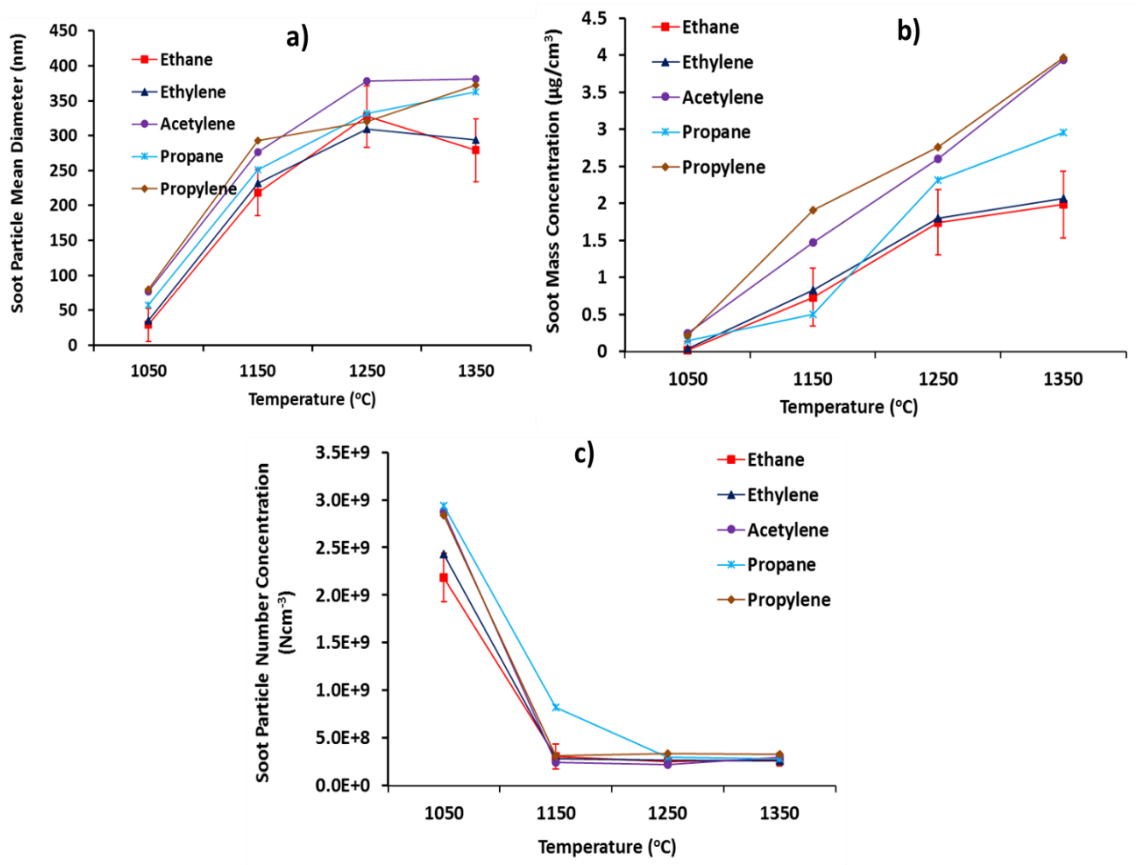

Figure 5.2: Temperature Variations of C2 and C3 hydrocarbons with (a) Particle Mean Diameter (b) Total Soot Particle Mass (c) Particle Number

All the C_2 hydrocarbons can be observed from Figure 5.2c to have approximately the same particle number in the temperature range of 1150 to 1350 ^oC regardless of the unsaturation of the hydrocarbon. This result suggests that within this temperature range, soot particle agglomeration may not be dependent on the fuel

molecular structure. Increasing unsaturation in C_3 fuels decreased the total number concentration within the temperature range of 1050 to1350 ^oC.

Considering now Figures 5.2a and c together, it its apparent that as the pyrolysis temperature was increased from 1050 to 1350^oC, the particles became bigger (Figure 5.2a – larger diameter) and also the total number of particles become fewer (Figure 5.2c – smaller particle number), irrespective of the degree of unsaturation of the fuels. This finding of increasing particle diameter and decreasing particle number concentration can be attributed to the primary particles agglomerating into larger, fewer, particles of several hundred nm in size (Heywood, 1988) as the pyrolysis temperature was increased.

Therefore, looking at Figure 5.2 as a whole, it could be concluded that as the temperature rose, the particles agglomerated into fewer larger particles, but with the larger particles still growing, with the result that the total mass of the particles increases. So, while agglomeration produced fewer larger particles, the fewer particles continued to grow through agglomeration but also new soot deposition on them. Figure 5.2c also shows that this observation applies mainly to the temperature increase from 1050 to 1150 ^oC, beyond which soot particle agglomeration may be less significant within the temperature range of 1150 to 1350^oC. Nevertheless, Figure 5.2a shows that in the temperature range of 1150 to 1350 ^oC, agglomeration may have ceased, but particle growth continues through new soot deposits on the particles already formed.

Taking together Figures 5.2a, b and c, it is evident that the soot mass concentration is determined by the bigger soot particle sizes of smaller number, than the many smaller particles of smaller sizes. It is also important to note that changing the bond of a C_2 and C_3 fuel from single to double and to triple bonds, increases the propensity of the fuel molecule to produce soot particles of bigger sizes.

5.3.3 Gas and Particle phase PAH Distributions

Figure 5.3 shows the PAH results for ethane. The figure shows the PAHs extracted from the XAD-2 resin and from the particulate collected on the filter. In

Figure 5.3, the results of the PAHs extracted from the resin are labelled “GP” (gas phase) PAHs while those extracted from the particulate are labelled “PP” (particle phase) PAHs. The error bars in Figure 5.3 denote standard deviations. Figure 5.3a shows the gas phase PAH mass normalised with the volume of gas passed through the resin and the filter (in series) (i.e., gas phase PAH concentration), while Figure 5.3b shows the corresponding concentration of the mass of PAH extracted from the particulate per unit volume of gas passed through the filter. Figure 5.3c shows the mass of PAH extracted from the particulate but this time normalised with the particulate mass. Finally, Figure 5.3d shows the combined total PAH (gas and particulate borne PAHs) normalised by the volume of gas.

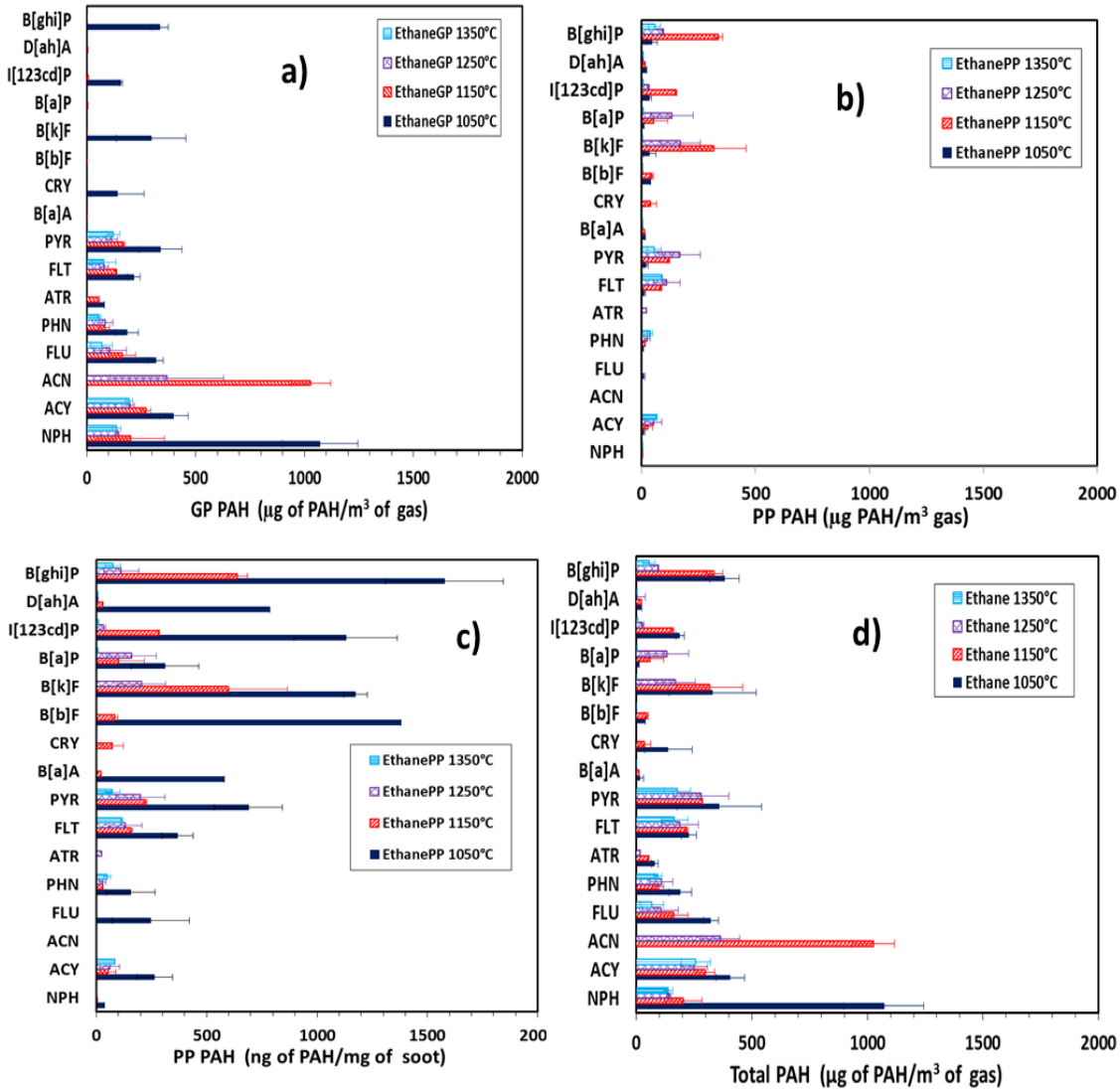

Figure 5.3: The distributions of PAHs during ethane pyrolysis from temperature range of 1050 to 1350oC: a) Gas Phase (GP) (µg of PAH/m3 of gas) b) Particle Phase (PP) (µg of

PAH/m^3 of gas) c) Particle Phase (ng of PAH/mg Soot). d) Total PAHs (GP +PP) (µg of PAH/m^3 of gas). Error bars denote the standard deviation.

It can be observed from Figure 5.3a that smaller PAHs ranging from naphthalene (MW = 128 g/mole) to pyrene (MW = 202 g/mole) were consistently identified in the gas phase (GP) in relatively high concentrations at all the temperatures tested. This trend was consistent with those reported in the literature (Sánchez et al., 2012; Sánchez et al., 2013). The GP PAHs have higher vapour pressures and lower boiling points which reduces their condensation and adsorption rates onto the particulates. The GP PAH concentration (Figure 5.3a) decreased with temperature rise from 1050 to 1350 ^{o}C.

One possible explanation for this decrease in the concentrations of GP PAH with temperature rise was that, at the temperature of 1050 ^{o}C for example, the kinetics for their growth into larger PAH was slower, hence, they continuously accumulated in the gas phase in relatively high concentrations. At higher temperatures, it is expected that the rate of growth of a specific PAH into larger PAH accelerated (relative to the rate at which the specific PAH was formed from smaller PAHs). In this way, one would expect the concentration of a specific PAH to be dependent on the balance between its formation through smaller PAHs and its change through growth into larger PAHs. As PAHs grew to larger structures, these were incorporated into new or nascent soot particles.

Figure 5.3a shows that at a temperature of 1050 ^{o}C, heavier PAHs (CRY, B(k)F, I(123cd)P and B(ghi)P) occur in both GP and PP. This could be due to greater particulate surface area becoming available for PAH condensation at lower temperatures. However, at temperatures of 1150 ^{o}C and above, these heavier PAHs were predominantly found in the PP. The disappearance of these four PAHs from the GP at higher temperatures (>1150 ^{o}C) could therefore, be due to the increased rate of soot and particle surface area becoming available for PAH condensation and adsorption. Figure 5.3b shows that five lighter PAHs (NPH, ACY, FLR, PHN and FLT – see Tables 2.1 for PAH abbreviations) were found in the particle phase (PP) and these were at low concentrations. Also, heavier PAHs ranging from PYR to B(ghi)P (MW = 276 g/mole) were found in the particle phase (PP) at high concentrations.

The PP PAHs normalised with the mass of soot from which they were extracted is shown in Figure 5.3c. It can be observed that both the lighter and heavier PAHs on the soot particles decreased with temperature rise. For example, the concentrations of B(g,h,i)P per unit mass of soot at a temperature of 1050 ^{o}C decreased by 2.5 times at 1150 ^{o}C, 14 times at 1250 ^{o}C and 21 times at 1350 ^{o}C. This decline in larger and smaller per unit mass of soot is believed to be related to a decrease, with rising temperature, in the number of soot particles and increase in their sizes, caused by agglomeration of primary soot particles (Heywood, 1988). This had the consequence that the surface area available for the PP PAHs to condense onto decreased.

Another explanation for the decrease in the PAH mass on the soot particles is that temperature increase led to large PAHs becoming soot at greater rates; hence, fewer PAHs were available in the gas phase for condensation on the soot particles. It is also possible that the decrease in the amount of PP PAHs at higher temperature was due to more organised soot particle micro-structure (Mathieu *et al.*, 2007) which made them less reactive (Ruiz *et al.*, 2007) and thus, they might have therefore accommodated smaller amounts of PAHs.

Figure 5.3d combines the GP and PP PAHs; the total PAHs per unit volume of gas is shown in the figure, which was drawn by adding the GP PAHs in Figure 5.3a to the PP PAHs in Figure 5.3b. The total PAH distribution includes most of the 16 EPA priority PAHs. It can be observed from Figure 5.3d that the trend in the concentrations of the total PAHs resembled more that of the GP than that for the PP PAHs. Thus, the total PAH found in the gaseous and particulate phases in ethane pyrolysis was dominated by the GP PAHs.

The variations of GP and PP PAHs per unit volume of gas, and of the PP per unit mass of soot for ethane pyrolysis was broadly similar with those found for the other C_2 fuels and all the C_3 fuels tested. Tables 5.5, 5.6 and 5.7 summarise the variations of the GP and PP PAHs for all the fuels tested. Among all the PAH results displayed in those Tables, only ethane results are shown in Figure 5.3 as an example, and also as a guide for discussion.

The relative contributions of the GP and PP PAHs to the total PAH are shown in Figure 5.4 for the C_2 and C_3 fuels investigated. It can be seen from Figure 5.4a

that at the temperature of 1050 ^{o}C, for example, the proportion GP from ethane pyrolysis was 95 %. This proportion decreased to 64 % and 58 % at 1150 ^{o}C and 1250 ^{o}C, respectively. In the case of ethylene (Figure 5.4b), the proportion of GP dropped gradually from 93 % to 66 % when the temperature was raised from 1050 – 1350 ^{o}C. However, Figure 5.4c shows that the pattern for acetylene pyrolysis was largely dominated by the GP PAHs in the temperature range of 1050 – 1250 ^{o}C by a constant proportion of approximately 84 %, followed by a marked drop of this proportion to 50 % at 1350 ^{o}C.

The decrease in the proportion of GP PAHs due to temperature increase seen in Figures 5.4a, b and c could generally be linked with a corresponding increase in the mass of soot generated and to increasing PP PAHs condensed on the soot particles. For example, in the case of ethylene pyrolysis, the soot mass concentration sampled at 1050 ^{o}C was 25.7 mg/m^{3} and it increased remarkably by a factor of 19 and 37 at temperatures of 1150 ^{o}C and 1250 ^{o}C, respectively.

Owing to the fact the C_3 fuel molecules yielded substantially higher soot masses, Figure 5.4d showed that the proportion of the GP PAHs in propane pyrolysis was relatively low at only 68 % at a temperature of 1050 ^{o}C and then decreased to 40 % at 1150 ^{o}C. Figure 5.4d shows that, at temperatures higher than 1150 ^{o}C for propane pyrolysis, the proportion of the PP PAHs on propane soot particles overtook those in the GP PAHs and dominated the total PAH distribution up to 1250 ^{o}C. The temperature at which the PP PAHs crossed-over the GP PAHs was observed earlier in propane (1150 ^{o}C) than in acetylene (1350 ^{o}C), hence, the PP PAHs were only greater than the GP PAHs in acetylene pyrolysis at temperatures higher than 1350^{o}C (see Figure 5.4c).

The proportions of GP and PP PAH for propylene pyrolysis are shown in Figure 5.4e. It can be seen from the figure that the GP and PP PAHs were almost equal at a temperature of below 1050 ^{o}C with relative proportions of 43 % and 57 % respectively. However, the PP PAHs in propylene pyrolysis dominated the total PAHs at higher temperatures. One could hypothesise from Figure 5.4e that the GP PAHs probably have higher concentrations at temperatures lower than 1050 ^{o}C.

Table 5.5: Normalised Gas phase (GP) and Particle Phase (PP) PAHs of C2 Fuels (µg of PAH/m3 of gas) (*bdl denotes 'below detection limit' of the PAH)

	Ethane								Ethylene								Acetylene PAHs							
	1050°C		1150°C		1250°C		1350°C		1050°C		1150°C		1250°C		1350°C		1050°C		1150°C		1250°C		1350°C	
PAHs	GP	PP	GP	PP	GP	PP	GP	PP	GP	PP	GP	PP	GP	PP	GP	PP	GP	PP	GP	PP	GP	PP	GP	PP
NPH	1071	1.04	201.7	2.139	141.5	1.77	137	1.84	300	1.24	212	2.7	246	2.2	215	2.08	1337	1.62	1280	2.7	685	2.09	279	2.31
ACY	399.6	7.73	272.0	27.51	199.5	51.3	194	64.2	315	bdl	258	bdl	276	bdl	229	9.84	407.8	bdl	341	41	352	14.5	160	bdl
ACN	bdl	bdl	1030	bdl	368.1	bdl	bdl	bdl	853	bdl	698	bdl	473	bdl	bdl	bdl	530.6	bdl	627	bdl	412	bdl	bdl	bdl
FLU	316.7	7.22	163.9	bdl	106.7	bdl	69.6	bdl	176	bdl	162	bdl	120	bdl	bdl	bdl	190.9	bdl	206	bdl	99.6	bdl	86.6	bdl
PHN	186.5	4.54	81.69	15.28	85.97	23.2	57.2	37.3	71.0	1.59	69	3.47	73.9	2.82	68.3	2.67	77.04	2.09	70.6	3.4	72.6	10.7	44.7	32.7
ATR	bdl	bdl	bdl	bdl	bdl	bdl	bdl	bdl	281	bdl	219	bdl	bdl	101	bdl	83.2	574.9	bdl	bdl	bdl	bdl	bdl	bdl	190
FLT	216.8	10.7	135.1	83.11	79.1	111	78.8	87.8	165	11.2	123	57.8	164	34.0	135	56.9	173.2	24.7	167	47	111	46.3	61.2	110
PYR	339.8	20.2	167.4	117.9	114.1	166	122	55.5	283	23.1	174	102	153	67.6	150	67.5	335.3	58.9	295	86	215	82.7	56.9	212
BjaA	0.204	0.25	0.448	0.517	0.427	0.43	0.48	0.443	0.24	0.30	0.4	0.65	0.49	0.53	0.54	0.5	0.283	0.39	0.56	0.6	0.51	0.51	0.60	0.56
CRY	140.9	bdl	bdl	37.91	bdl	bdl	bdl	bdl	34.7	bdl	bdl	bdl	bdl	bdl	bdl	16.3	74.89	27.3	bdl	bdl	bdl	bdl	bdl	bdl
BjbjF	0.718	0.88	1.578	1.82	1.503	1.5	1.70	1.56	0.82	1.05	1.5	2.3	1.72	1.87	1.91	1.77	0.998	33.8	1.98	2.3	1.79	1.78	2.11	1.96
BjkjF	296.1	34.3	2.08	315.2	1.982	170	2.25	2.06	138	40.9	2.0	235	2.27	2.46	2.53	2.33	174.3	104	2.62	88	2.35	55.9	2.78	2.59
BjaP	2.422	9.09	5.32	53.45	5.07	133	5.75	5.30	63.4	9.45	5.0	55.1	5.82	6.3	6.46	5.96	95.14	97.3	6.71	175	6.00	44.1	7.13	35.4
Ij123cdjP	157.3	33.1	7.43	149.5	7.075	28	8.02	7.35	3.90	29.6	7.1	217	8.12	27.3	9.01	15.6	26.58	143	9.35	47	8.37	17.9	9.96	9.25
DjahjA	2.736	3.37	6.01	6.936	5.727	5.73	6.49	5.95	3.20	4.02	5.7	8.77	6.57	7.12	7.30	6.74	3.803	5.26	7.57	8.7	6.78	6.78	8.06	7.48
BjghiP	336.7	46.1	bdl	337.3	2.423	93.5	2.75	57.0	205	70.8	2.4	367	2.78	271	3.09	162	35.25	261	3.23	219	2.87	137	3.41	3.17

Table 5.6: Normalised Particle Phase (PP) PAHs of C2 and C3 Fuels (x 10 ng of PAH/mg of soot) (*bdl denotes 'below detection limit' of the PAH).

	1050 °C					1150 °C					1250 °C					1350 °C				
PAHs	C_2H_6	C_2H_4	C_2H_2	C_3H_8	C_3H_6	C_2H_6	C_2H_4	C_2H_2	C_3H_8	C_3H_6	C_2H_6	C_2H_4	C_2H_2	C_3H_8	C_3H_6	C_2H_6	C_2H_4	C_2H_2	C_3H_8	C_3H_6
NPH	3.56	4.3	1.37	2.6	1.79	0.41	0.62	0.3	0.28	0.23	0.22	0.23	0.18	0.14	0.2	0.24	0.27	0.14	0.21	0.14
ACY	26.4	bdl	bdl	bdl	87.8	5.21	bdl	4.8	7.3	11.8	6.15	Bdl	1.23	1.93	2.9	8.5	1.26	bdl	6.61	4.84
ACN	bdl	bdl	bdl	bdl	bdl	bdl	bdl	bdl	bdl	bdl	bdl	bdl	bdl	bdl	bdl	bdl	bdl	bdl	bdl	bdl
FLU	24.7	bdl	bdl	bdl	bdl	bdl	bdl	bdl	bdl	bdl	bdl	bdl	bdl	bdl	bdl	bdl	bdl	bdl	bdl	bdl
PHN	15.5	5.5	1.75	3.4	43	2.9	0.8	0.39	2.53	3.9	2.78	0.3	0.91	1.92	2.2	4.9	0.34	1.94	3.68	3.31
ATR	bdl	bdl	bdl	bdl	332	bdl	bdl	bdl	bdl	bdl	bdl	10.8	bdl	13.3	2.8	bdl	10.6	11.2	50.5	2.24
FLT	36.7	38.7	20.7	39	64.6	15.7	13.3	5.5	8.78	10.6	13.3	3.62	3.91	7.93	5.8	11.6	7.26	6.5	10.5	5.77
PYR	69.0	79.8	49	83	109	22.3	23.5	10	14.5	16.7	19.9	7.2	6.99	12	20	7.3	8.62	12.5	8.25	15.0
B[a]A	0.86	1.03	0.33	0.6	0.41	0.1	0.15	0.07	0.07	0.06	0.05	0.06	0.04	0.03	0.04	0.06	0.06	0.03	0.05	0.03
CRY	bdl	bdl	23	27	78.9	7.18	bdl	bdl	bdl	6.5	bdl	bdl	bdl	bdl	bdl	bdl	2.08	bdl	bdl	bdl
B[b]F	3.02	3.64	28	2.2	1.43	0.35	0.53	0.26	0.24	0.2	0.18	0.20	0.15	0.12	0.13	0.21	0.23	0.12	0.18	0.12
B[k]F	117	141	87	239	306	59.7	54.1	10.2	50	55.2	20.4	0.26	4.73	8.82	3.7	0.27	0.30	0.15	0.24	0.15
B[a]P	31.1	32.7	82	154	121	10.1	12.7	20.2	7.42	16.9	15.9	0.67	3.73	9.85	3.5	0.70	0.76	2.09	0.61	0.39
I[123cd]P	113	106	120	241	104	28.3	50.1	5.44	22	28.3	3.36	2.91	1.51	1.61	0.6	0.97	2.0	0.55	0.84	0.55
D[ah]A	11.5	1.39	4.42	109	52	1.31	2.02	0.1	0.91	0.75	0.69	0.76	0.57	0.44	0.48	0.79	0.86	0.44	0.68	0.44
B[ghi]P	158	245	220	238	244	6.39	84.7	25.3	33.4	40.6	11.2	28.9	11.6	13	5.04	7.53	20.7	0.19	0.29	0.19

Table 5.7: Normalised Gas and Particle Phase PAHs of C_3 fuels (µg of PAH/m^3 of gas).

	Propane PAHs								Propylene PAHs							
	1050 °C		1150 °C		1250 °C		1350°C		1050°C		1150 °C		1250 °C		1350°C	
PAHs	GP	PP	GP	PP	GP	PP	GP	PP	GP	PP	GP	PP	GP	PP	GP	PP
NPH	207	2.31	195	2.19	131	1.68	121	2.03	426	2.91	198	2.50	146	2.04	94	1.95
ACY	346	bdl	266	56.6	241	23.6	162	63.9	275	152	263	127	166	39.5	138	69.4
ACN	326	bdl	bdl	bdl	bdl	bdl	bdl	bdl	791	bdl	653	bdl	bdl	bdl	bdl	bdl
FLU	193	bdl	138	bdl	69.8	bdl	bdl	bdl	238	bdl	197	bdl	93.5	bdl	bdl	bdl
PHN	71.7	2.97	46	19.6	32.3	23.4	24	35.6	73.8	74.5	52	42.5	2.18	29.9	29	33.1
ANT	bdl	bdl	bdl	bdl	331	163	bdl	487	bdl	576	bdl	bdl	bdl	384	bdl	322
FLR	172	34.1	120	67.9	69.5	96.9	58.5	101	149	112	114	114	58.9	79.3	26	82.6
PYR	360	72.9	155	112	96.7	147	90.1	79.7	208	188	156	180	39.3	274	26	215
B[a]A	0.22	0.56	0.4	0.53	0.52	0.40	0.45	0.48	0.33	0.71	0.5	0.60	0.41	0.49	0.5	0.47
CRY	bdl	24.0	bdl	29.4	bdl	bdl	bdl	bdl	53.8	137	bdl	69.9	bdl	bdl	bdl	bdl
B[b]F	0.78	1.97	1.5	1.85	1.83	1.41	1.58	1.72	1.15	2.47	1.6	2.13	1.44	1.73	1.8	1.66
B[k]F	260	211	1.9	387	2.42	108	2.08	2.27	148	531	2.1	597	1.91	50.0	2.4	2.19
B[a]P	60.6	136	5.1	57.5	6.19	120	5.33	5.82	34.5	209	5.5	183	4.88	47.6	6.1	5.6
I[123cd]P	57.3	213	7.0	171	8.63	19.6	7.44	8.12	5.41	181	7.7	306	6.81	8.17	8.6	7.82
D[ah]A	3.08	95.9	5.7	7.08	6.99	5.37	6.02	6.57	4.38	90.1	6.2	8.11	5.51	6.61	6.9	6.33
B[ghi]P	101	210	2.4	258	2.95	159	2.54	2.78	1.85	422	2.6	438	2.33	68.9	2.9	2.67

It is useful at this point to consider results from published sources and compare them with results reported in this thesis for PAH emissions from various fuels. The results in this thesis show that lighter PAHs up to and including pyrene were generally found to be more abundant in the gaseous phase, while the heavier PAHs were found to be more abundantly adsorbed on the particulates. This is consistent with previous studies (Sánchez et al., 2012; Sánchez et al., 2013; Ballesteros et al., 2015) and Figure 5.5 summarises these observations. The 6 PAHs in Figure 5.5 (NPH, ACN, ACY, FLU, PHN, ATR) having 2 and 3 rings are categorised as the lighter PAHs. The four PAHs (FLT, PYR, B[a]A, CRY) having 4 rings are grouped as medium PAHs, while the 6 PAHs (B(b)F, B(k)F, B(a)P, I(123cd)P, D[ah]A and B(ghi)P) having 5 and 6 rings are classified as the heavier PAHs (Ballesteros, Guillén-Flores and Barba, 2015).

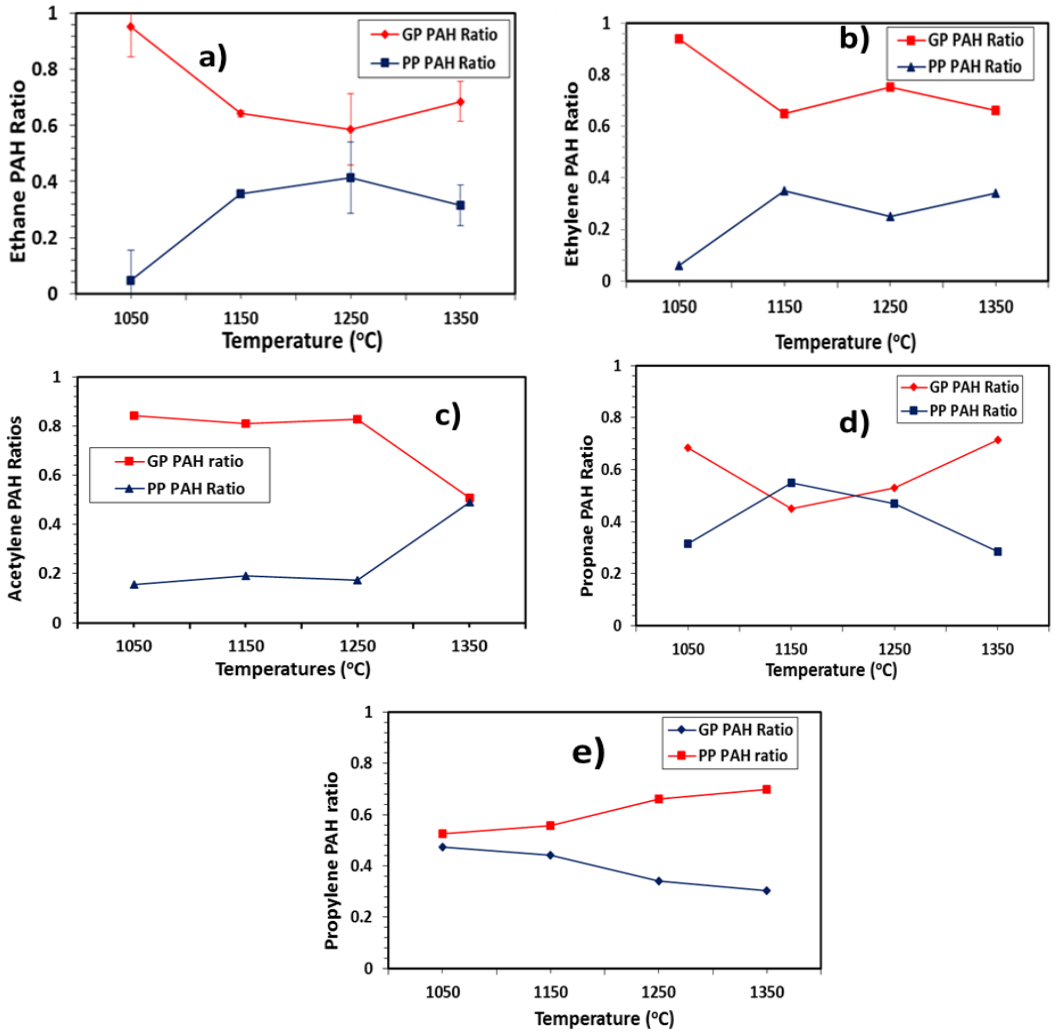

Figure 5.4: Gas phase (GP) and Particle phase (PP) PAH Ratios of C2 and C3 Fuels: a) Ethane b) Ethylene c) Acetylene d) Propane e) Propylene ("Ratio" on the Y- axis refers to the fractional contribution of GP and PP PAHs to the total PAHs, hence, GP ratio + PP ratio = 1)

Figure 5.5 demonstrates that as the molecular weight of the PAHs increased from that of naphthalene to that of benzo (g,h,i)perylene, the econcentrations of gas phase PAHs decreased while those of the PP PAHs increased. Pyrene (a 4 ring PAH) was found in both the gaseous and the particulate phases in an approximately 1:1 ratio and marks the transition between the lighter PAHs (mostly found in the gas phase) and the heavier PAHs found (mostly on the particulates).

Frenklach (2000) also reported pyrene as the principal 'precursor to soot particle nucleation' which might imply that in addition to being adsorbed on the particulate, pyrene also contributes directly to the formation of larger PAHs which eventually lead to soot particle nucleation. Therefore, the transition between GP and PP

PAHs occurs around 4-ring PAHs and interestingly, this observation is in agreement with that reported by Alam et al. (2013) who measured atmopsheric PAHs in the city of Birmingham, UK.

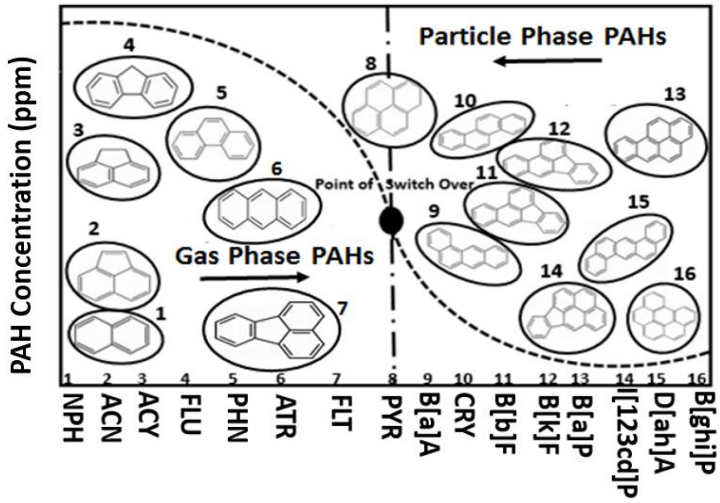

Figure 5.5: Summary on the increase or decrease of the particulate and gas phase PAHs as the molecular weight increases.

One limitation of the phenominological PAH distribution in Figure 5.5 is that it is most applicable within the tempeture range of 1150 to 1250 ^{o}C and for the results obtained in the tube reactor (and under the conditions studied), where significant proportions of both gas phase and particle phase PAHs were detected.

5.3.4 Growth of Individual Total PAHs

The total mass concentration of the gaseous and particulate PAHs was found by adding together the gas phase (GP) and particle phase (PP) PAH concentrations for each of the 16 individual PAH. Figure 5.6 shows the total concentrations of individual PAHs for all the C_2 and C_3 fuels tested. It can be observed from Figure 5.6a that naphthalene concentration in acetylene pyrolysis was substantially higher when compared with the levels of naphthalene for the other fuels investigated. The abundance of naphthalene in acetylene pyrolysis agreed with the findings of other published works (Sánchez et al., 2012; Sánchez et al., 2013) and was expected, since acetylene contribute significantly to the formation of the first aromatic ring (benzene or phenyl radical). Formation of napthalene often follows the formation of the first aromatic ring through a number of possible pathways (Richter & Howard, 2000; Frenklach, 2002, Miller & Melius, 1992;

Norinaga & Deutschmann, 2007b). One of the pathways to formation of benzene is the reaction of vinyl acetylene (C_4H_4) with acetylene (C_2H_2). Shukla and Koshi, (2012) reported the formation of vinyl acetylene via acetylene dimerisation. Similar mechanisms to benzene formation in acetylene pyrolysis were also reported in ethylene pyrolysis (Frenklach et al., 1985; Frenklach et al., 1988).

Returning to Figure 5.6a, at the high temperature of 1350 ^oC for example, naphthalene concentrations for both ethylene and acetylene were almost the same and this agrees with the findings that the behaviour of ethylene and acetylene is very similar at high temepature (Ruiz et al., 2007; Frenklach et al., 1988). Ethane also showed significant amount of naphthalene at 1350 ^oC, and it is likely that this is because ethane could readily yield ethylene (Shokrollahi et al., 2013). Furthermore, Figure 5.6 shows that various PAHs from two to four rings were obtained at mostly similar concentrations for ethane and ethylene.

Turning attention to the C_3 fuel molecules now, the formation of the first aromatic ring from propane and propylene was reported via propargyl radical (C_3H_3) recombination (Norinaga & Deutschmann, 2007a; Miller & Melius, 1992). Following the formation of the first aromatic ring, the growth process to two-ring naphthalene from phenyl radicals could readily occur via the two-stage HACA mechanism (Frenklach et al., 1985; Bittner & Howard, 1981). Although it was reported that the route to naphthalene via phenyl-acetylene was dominant, Bittner & Howard (1981) and Shukla & Koshi (2012) supported that the growth to naphthalene occurs from phenyl radicals via the two stage HACA mechansim. Naphthalene could also be formed by the self-reaction of cyclopentadenyl radicals (C_5H_5) (Richter & Howard, 2000). All the routes outlined above are likely to contribute to naphthalene formation with the 2-stage HACA and phenyl-acetylene pathways contributing perhaps the most.

Once naphthalene has been formed, it could then grow further by means of the HACA mechanism to the four-ring pyrene either through the five membered ring PAH acenaphthylene, shown in Figure 5.6b, or via the benzenoid PAH phenanthrene (Figure 5.6c) (Frenklach et al., 1985). Both acenaphthylene and phenanthrene could be formed from naphthalene via the HACA mechanism. The appreciable amounts of biphenyl compounds identified by GCMS in the products

of pyrolysis of most of the fuels examined suggests that phenanthrene could have grown via biphenyl through the HACA mechanism. Richter et al. (1999) also reported phenathrene formation via the biphenyl route, but in premixed benzene flames.

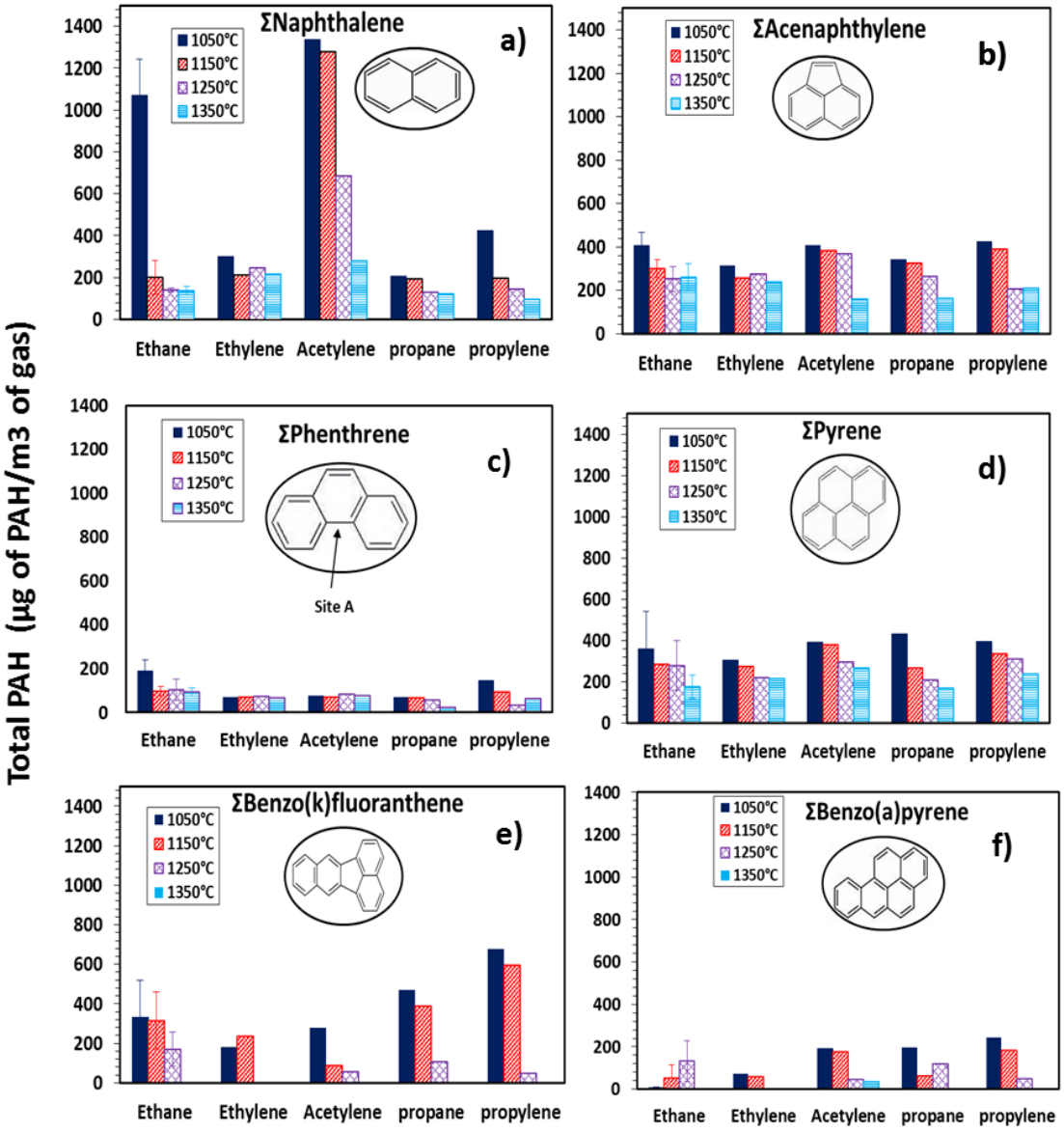

Figure 5.6: Distributions of total PAHs produced during the pyrolysis of C2 and C3 Fuels a) Naphthalene b) Acenaphthylene c) Phenanthrene d) Pyrene e) Benzo(k)fluoranthene and f) Benzo(a)pyrene.

Looking at Figure 5.6c more closely, it can be seen that the concentrations of phenanthrene in the pyrolysis of all the fuels examined were much lower than those of pyrene (Figure 5.6d). This comparison may imply that phenathrene was not available in sufficiently high concentrations to support abundant pyrene

formation. It is therefore possible that pyrene might have instead grown via the acenaphthylene pathway by means of HACA, since the concentrations of acenaphthylene in the pyrolysis of the five fuels examined was high relative to that of phenanthrene.

Abundance of acenaphthylene over phenantherene in ethylene and acetylene pyrolyses was also reported previously by other researchers (Crittenden & Long, 1973; Sánchez et al., 2012). An alterative, contrasting, possibilty was that bezenoid-phenanthrene was observed in low concentration because it was significantly depleted through readily being converted to benzenoid-pyrene. Nevertheless, the growth of naphthalene to pyrene by the HACA mechanism, principally via the acenaphthylene pathway, was found to be the dominant route (Frenklach et al., 1985).

A possible route for the growth of acenaphthylene to fluoranthene by HACA was recently reported (Shukla and Koshi, 2012a). It can also be seen from Figure 5.6d that pyrene was found in approximately equal concentrations in the pyrolysis products of all the 5 fuel molecules investigated, regardless of their degree of unsaturation. An explanation for this observation is that probably all 2 and 3 ring PAHs pass through pyrene in order to grow further to heavier PAHs.

Once pyrene or fluoranthane has been formed, further PAH growth from either of them to heavier PAHs, especially the Group B2 PAHs, could be achieved either by HACA or HAVA (hydrogen abstraction, vinyl radical addition) (Shukla and Koshi, 2012a). Other growth pathways, depending on intermediate precursors, include phenyl addition and cyclisation (PAC) as well as methyl addition and cyclisation (MAC) (Shukla and Koshi, 2011).

Further growth of the Group B2 PAHs could occur either within thesemselves or via Group D PAHs. For example, the five ring benzo(k)fluoranthene (Figure 5.6e) a member of Group B2 PAHs, could be formed from the three ring fluoranthene via HAVA (Shukla and Koshi, 2012a). Chrysene, also a four ring member of Group B2 PAHs, could grow from the three ring phenathrene radical by one-stage HACA. Similarly, the four ring benzo(a)anthracene could grow from the three ring anthracene and then benzo(a)anthracene could be converted to the five ring benzo(a)pyrene (Figure 5.6f) by means of further dehydrogenation and acetylene addition ($-H_2/+C_2H_2$) (Keller et al., 2000).

It is noteworthy mentioning that the conversion of the three-ring anthracene to the four-ring benzo(a)anthracene and then to the highly mutagenic five ring benzo(a)pyrene increases toxicity by 10 times at each growth stage. A two-stage HACA starting with the two ring naphthalene radical (2-naphthyl) could lead to three ring anthracene (Richter et al., 1999). Also, isomerisation of the three ring phenanthrene to the three ring anthracene was found to be possible at temperatures > 1327^{o}C (Colket and Seery, 1994). This agrees with the increasingly high concentrations of anthracene detected over phenanthrene at a temperature of 1350 ^{o}C (see Table 5.5, Table 5.6 and Table 5.7) suggesting isomerisation at this higher temperature of phenanthrene to anthracene.

From a view point of the stability of anthracene, it is worth mentioning here that anthracene was not detected at most of the pyrolysis temperatures for most of the fuels, since the kinked-phenanthrene was already known to be more stable than the linear-anthracene (Poater et al., 2007). This notable absence of anthracene could be associated with the consistent partial sublimation inherent with it (Richter et al., 1999).

The five-ring mutagenic benzo(a)pyrene (Figure 5.6f) could be produced through a number of pathways, including from the pyrene radical (2-pyrenyl) via two consecutive steps of the HACA mechanism (Richter et al., 1999). The six ring indeno(1,2,3-cd)pyrene, another Group B2 toxic PAH, could be formed from a pyrene radical (4-pyrenyl) by phenyl addition to 4-pyrenyl. Finally, it is possible for the six ring benzo(g,h,i)perylene to be produced from the four ring pyrene via several consecutive HACA steps (Frenklach et al., 1985).

5.3.5 Number of PAH Rings

Figure 5.7 groups, for each fuel, the total PAH concentration according to number of rings. The resulting PAH concentration for the different number of rings helps observe the growth of PAHs. Figure 5.7 shows that regardless of the degree of unsaturation of the fuel molecules investigated, the concentrations of the PAHs increased from those for two rings, peaked at three rings and then tended to decrease in the case of four to five and then to six rings.

For exmple, in ethylene pyrolysis at temperature of 1050 ^{o}C (Figure 5.7 b), the concentrations of 2 ring PAHs was about 200 µg/m^3, increasing more than eightfold to >1500 µg/m^3 for the 3 ring PAHs and then reduced drastically to around 500 µg/m^3 for the 4 rings, 200 µg/m^3 for the 5 rings and slightly increased to about 250 µg/m^3 for the 6 ring PAHs. A similar trend was observed for all the fuels and at most temperatures investigated.

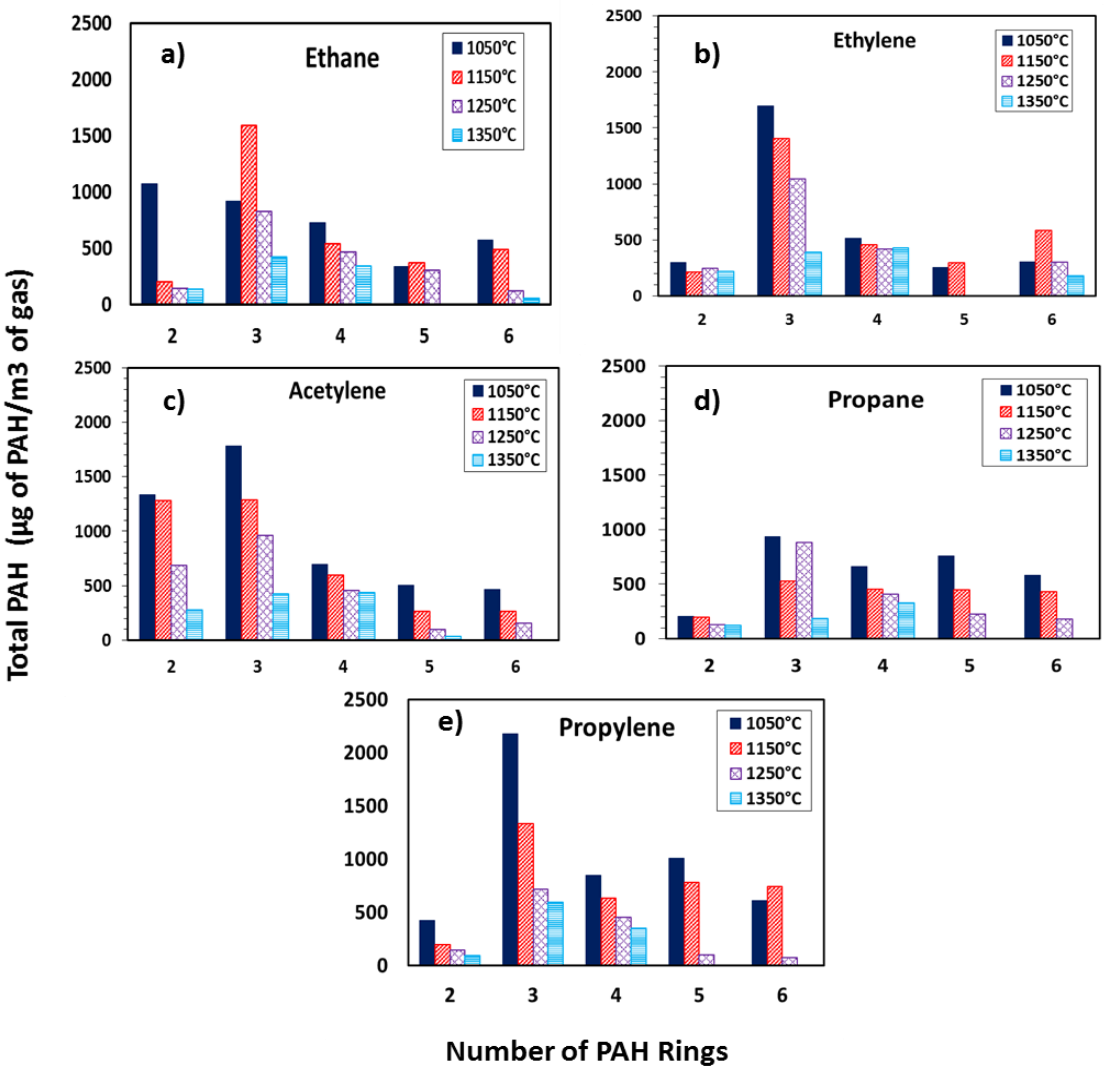

Figure 5.7: Number of PAH rings of C2 and C3 Fuels: a) Ethane b) Ethylene c) Acetylene d) Propane e) Propylene

It is evident, therefore, from Figure 5.7, that pyrolysis of the C_2 and C_3 fuels yielded substantially higher concentrations of the 3 ring PAHs than the PAHs having 2 rings or 4 to 6 rings. The three ring PAHs were discussed ealier (in relation to Figure 5.6) and are believed to have major impact on the growth of the 4 - 6 ring PAHs. Probably because they have more growth sites *'arm chairs'* (site

A in Figure 5.6c) at which a new ring could be completed readily through the HACA mechanism. Furthermore, considering Figure 5.7a, b and c, ethane, ethylene and acetylene had respectively significant number of two ring PAH, and the concentration of the 2 ring PAHs tended to increase with increased degree of unsaturation of the fuel.

Figure 5.7d and e show that propane and propylene respectively had lower concentrations of two ring PAHs when compared with the C_2 fuels. The concentrations of the two ring PAH in the C_3 fuels also increased somewhat with increase in unsaturation of the fuel particularly at the lower temperature of 1050 ^oC. The concentrations of four ring PAHs (pyrene, fluorathene, chrysene and benzo(a)anthracene) were fairly close to each other irrespective of the C_2 or C_3 fuel used.

Regarding the 5 and 6 ring PAHs, Figure 5.7 shows that the concentrations of 5 and 6 ring PAHs in the C_3 fuels were somewhat higher than those in the C_2 fuels. Another observation from Figure 5.7 is that for the C_2 fuels, the concentration of the 6 ring PAHs was greater than that for the 5 ring PAHs, while the converse was true for the C_3 fuels. These variations in 5 and 6 ring PAH concentrations could possibly be attributed to the rate at which the 5 and 6 rings PAHs were consumed for soot formation in the C_2 and C_3 fuels. In the C_2 fuels for example, the production rates of the 5 ring PAHs was, possibly, faster than the consumption rates of the 6 rings to heavier PAHs and eventually into, nascent soot particles. The oppsosite could possibly be the case for the C_3 fuels. It is worth mentioning that the majority of the mutagenic group B2 PAHs are either 5 or 6 rings, with the exception of benzo(a)anthracene and chrysene, which are 4 ring PAHs and can be seen from Figure 5.7 to be presenet in substantial concentrations.

5.3.6 Total PAH Analysis

The total concentrations of gas phase (GP) and particulate phase (PP) PAHs are shown Figures 5.8a and b respectively. The total PAHs in Figure 5.8 were found by summing-up, for each fuel, the individual concentrations of all the 16 PAHs that were detected at each temperature. It can be observed from Figure 5.8a that

the GP PAH concentrations per unit volume of gas of all the C_2 and C_3 fuels decreased with rise in temperature from 1050 – 1350 ^oC. Also, it can be seen from Figure 5.8a that the triple bonded acetylene had the highest concentrations of GP PAHs in the temperature range of 1050 – 1320 ^oC, followed by also high concentrations in the case of ethane and ethylene.

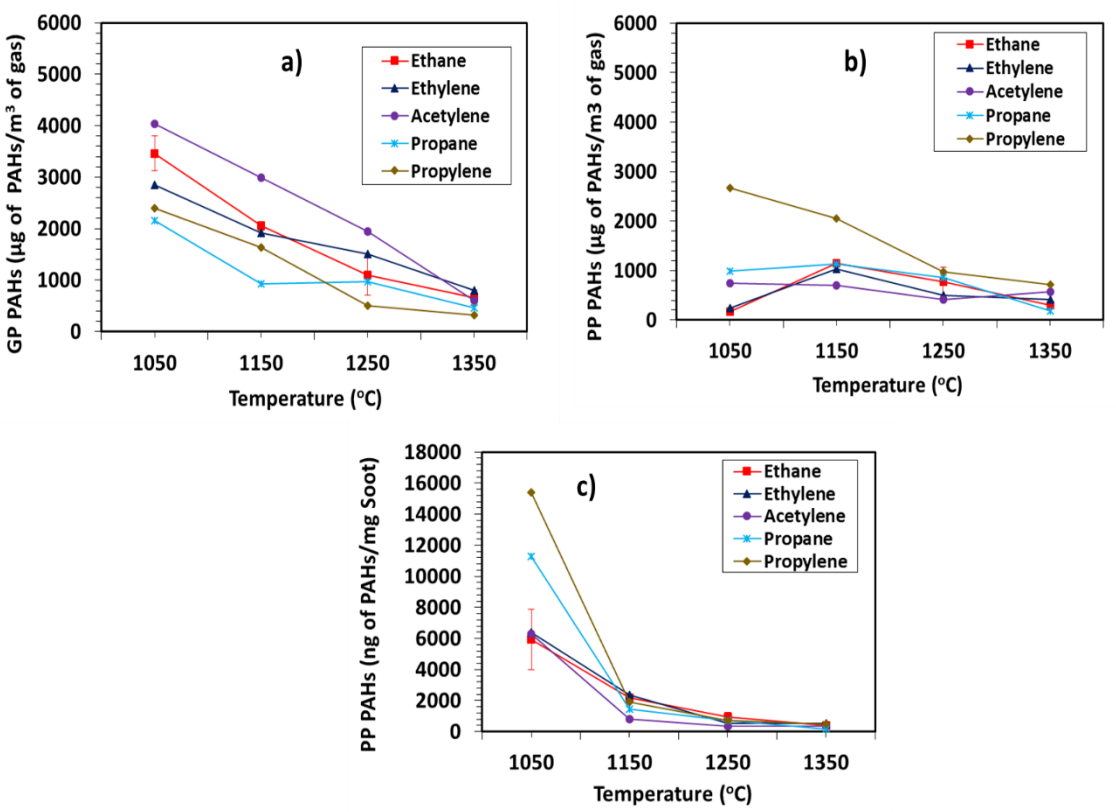

Figure 5.8: Normalised Total PAH Concentrations: a) Gas Phase (µg of PAH/m3 of gas) b) Particle Phase (µg of PAH/m3 of gas) c) Particle Phase (ng of PAH/ mg of soot).

Figure 5.8a also shows that the concentrations of GP PAHs for the C_3 fuels were lower than those for the C_2 fuels at all the temperatures examined. Propylene shows higher GP PAH concentration than propane up to a temperature of 1200 ^oC. It would therefore appear from Figure 5.8a that the highly unsaturated acetylene, which is also a key growth specie in the HACA mechanism shows consistently the highest concentration of PAH at all temperatures; however, there is no such clear trend for the unsaturated C_2 and C_3 fuels (ethylene and propylene) when compared with the saturated C_2 and C_3 fuels (ethane and propane).

The particle phase (PP) PAH concentrations per unit volume of gas, shown in Figure 5.8b, indicate that the double bonded C_3 propylene yielded the highest concentrations of PP PAHs at all temperatures compared with the other fuels investigated. The results shown in Figure 5.8b suggest that apart from the case of propylene, the particle phase concentrations of PAHs per unit volume of gas were affected less by rising temperature than the GP PAHs shown in Figure 5.8a. The normalised PP PAH concentrations per unit mass of soot are shown in Figure 5.8c. The figure shows high abundance of PAH mass concentrations at the low temperature of 1050 ^oC, but the concentrations decreased drastically when the tempetature rose to 1150 ^oC. Further decrease in the PAH mass concentrations can be seen as the temperaure was increased to 1350 ^oC. This observation suggests that the condensation of PP PAHs on soot particle does not only result in solvent-extractable PAH, but also that it results in incorporation of the condensed PAHs into soot particle structure.

The high mass concentration of PP PAHs at the lowest temperature of 1050 ^oC might additionally be related to the total surface area of the soot particles available for condensation of the PP PAHs. Measurements made with a DMS 500 particle size spectrometer in the case of ethane pyrolysis provided estimates of the total surface area at 1050 ^oC of 6 x 10^6 $\mu m^2/cm^3$ of soot and at 1350 ^oC of 7 x10^2 $\mu m^2/ cm^3$. The total surface area decreased substantially (up to four order of magnitude) with temperature increase as a result of increased soot particle agglomeration which resulted in fewer, larger particles.

It is apparent from Figure 5.8c that propylene yielded the highest amount of PP PAHs per unit mass of soot at 1050 ^oC, followed by propane. The C_2 fuels formed similar amounts of PP PAHs at 1050 ^oC, ethane and ethylene maintained PAH mass concentrations of similar magnitude even at higher temperatures. It is interesting to note that this closeness in the mass concentrations of PAHs for ethane and ethylene from 1050 to 1350 ^oC coincides with similar soot masses for these two fuels recorded in Table 5.3 for the range of 1050 to 1350 ^oC.

Finally, returning to Figures 5.8a and b, as mentioned above, the GP PAH concentrations are seen to decrease in Figure 5.8a as temperature rises, while the PP PAH concentrations are seen to be less sensitive to rising temperature. A posssible explanation for this is that the rate at which GP PAHs grow and become

carbonaceous soot is greater than the rate at which GP condense on particles and remain extractable by the ASE process.

5.3.7 Toxicity of Soot Particles

This section focuses on the Group B2 PAHs extracted from the soot particles and assesses the carcinogenicity of the particulate generated by the various fuels used. The weighted carcinogenicity of PAHs (WC-PAHs), taken together, was defined as shown in equation 5.1; that is, as the sum of the product of each of the EPA16 priority PAH concentration (C_i) and their toxicity equivalent factor (TEF). The TEFs adopted, shown in Table 2.2, were those proposed by Nisbet & LaGoy (1992) which are widely used by investigators to assess PAH toxicity. Since TEF is a relative factor and dimensionless and C_i has unit of concentration, WC-PAH also has units of concentration.

WC- PAHs = $\sum_{i=1}^{16}(\mathrm{TEF_i} * \mathrm{Ci})$ 5.1)

The weighted carcinogenicity (WC- PAHs) of the soot particles for the C_2 and C_3 fuels, on volume of gas and mass of soot bases, is shown in Figures 5.9a and b respectively. Considering Figure 5.9a first (gas volume basis), It is apparent that the soot particles produced from propylene pyrolysis had the highest carcinogenicity in the temperature range of 1050 – 1250 ^oC and the carcinogenicity decreased with temperature increase. For example, the weighted carcinogenicity of propylene soot particles at temperature of 1050 ^oC was 1.5 times that of propane, 3 times that of acetylene and 20 times that of ethane and ethylene. This trend is due to the significantly higher amount of benzo(a)pyrene condensed on propylene soot particles. Other Group B2 PAHs that contributed to the carcinogenicity of propylene soot particles can also be seen in Tables 5.6 and 5.7.

Propane soot particles had the second highest carcinogenicity at a temperature of 1050 ^oC, while their carcinogenicity was the highest at 1250 ^oC. This result reflects high concentrations of both B(a)P and D(a,h)A on propane produced soot particles. The trends of carcinogenicities for ethane and ethylene soot particles shown in Figure 5.9a were similar to their PAH concentrations shown in Figure 5.8b.

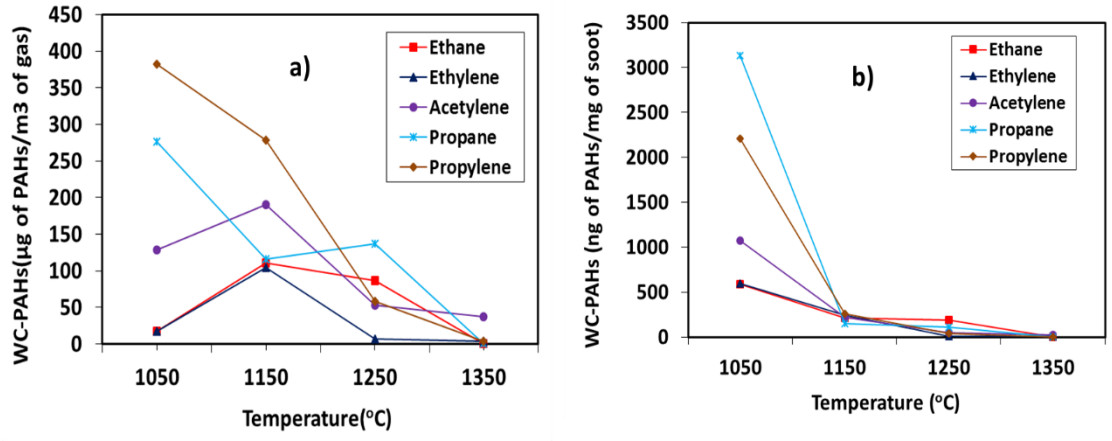

Figure 5.9: Normalised Weighted Carcinogencity: a) weighted carcinogenicity of PP PAHs (µg PAH/m3 gas) b) weighted carcinogenicity of PP PAHs (µg PAH/ g soot).

Considering now Figure 5.9b, which is plotted on soot mass basis, this shows that the soot particles generated from propane had the highest carcinogenicity per unit mass of soot at 1050 ^{o}C and it was found to be approximately 1.5 times that for propylene, 3 times acetylene and 5 times that of ethane and ethylene.

In conclusion, while low pyrolysis temperature was associated with low abundance of soot particles, the toxicity of soot particles generated at low temperature was found to be much higher than the toxicity levels at higher temperatures. Potential implication of this observation might be that lower temperature combustion systems, for example, those designed for NOx control, may have higher overall levels of particulate WC- PAH toxicity.

5.4 Conclusions

The results of both gas-phase and particle-phase PAHs generated from the pyrolysis of ethane, ethylene, acetylene, propane and propylene were presented.

- The degree of unsaturation of the fuels tested was observed to have a significant impact on the resulting amount of soot concentration in the effluent gas (nitrogen). The amount of soot and the gas phase PAHs generated from the C_2 fuels were found to be increasing with increasing unsaturation in the fuels.
- The C_3 fuels also followed a similar trend with those of the C_2 fuels, but they had greater soot yield and particle phase PAHs. The double bonded

C_3 propylene produced the highest amount of soot and particle-phase PAHs per unit mass of soot and per unit volume of gas. Propylene also produced soot particles with the highest carcinogenicity in the temperature range of 1050 - 1250 ^oC and the carcinogenicity decreased with temperature increase.

- Soot particle mean diameter increased while the number concentration decreased with increasing pyrolysis temperature from 1050 to 1350 ^oC regardless of the degree of unsaturation of the hydrocarbon investigated. This was believed to be attributed to primary soot particles agglomerating into larger, fewer, particles of several hundred nm in size as the pyrolysis temperature was increased
- The particle phase PAHs included, invariably, Group B2 members, while the gas phase PAHs included members of Group D. Even though Group D PAHs are unclassifiable by the EPA in terms of carcinogenicity, however, they contribute substantially to the mechanisms of growth of the carcinogenic Group B2 PAHs.
- There was greater abundance of PAHs (including those of Group B2) at low temperature, while higher temperatures promoted increased soot yield but lower PAH concentration in both the gas and particulate phases.
- The total PAH concentration increased from two rings, peaked at three rings and then tended to decrease in the case of four to five and then to six rings, regardless of the degree of unsaturation of the fuel molecules investigated.
- The toxicity of soot particles generated at low temperature was found to be much higher than the toxicity levels at higher temperatures. Potential implication of this observation might be that lower temperature combustion systems, for example, those designed for NOx control in diesel engines, may have higher overall levels of particulate with higher toxicity

Chapter 6

6. Influence of carbon number of C_1 – C_7 hydrocarbons on PAH formation

This chapter considers the influence of carbon number, in the case of seven hydrocarbons (methane, ethane, propane, n-butane, i-butane, heptane and toluene), on PAH formation in a laminar tube reactor. The hydrocarbons underwent oxygen-free pyrolysis within the temperature range of 1050 – 1350 ^oC, all at a fixed carbon concentration of 10,000 ppm on C_1 basis. Particulate and gas phase PAHs were collected at the outlet of the reactor when the pyrolysis temperature was increased at intervals of 100 ^oC. The particulates generated were characterised at sub-micron levels in terms of size, number and mass using a differential mobility spectrometer (DMS-500). The PAHs studied were the US EPA 16 priority PAHs with particular attention given to group B2, which are possible human carcinogens. The experimental results showed that increasing the carbon number of hydrocarbons from C_1 to C_7 had significant impact on the soot propensities, gas and particulate phase PAH concentrations, and on the carcinogenicity of soot particles.

6.1 Introduction

Atmospheric air quality is continually degraded by particulate emissions from different combustion sources, and stringent global particulate legislation has largely been enacted due to the adverse health effects of these emissions (Richter & Howard, 2000). Understanding particulate production requires detailed knowledge of the formation and growth of particulate molecular precursors. Such

understanding can aid the design of particulate controls in practical combustion systems (Longwell, 1982).

Polycyclic aromatic hydrocarbons (PAHs), known for some time as major particulate precursors (Graham et al., 1975), have received substantial attention in the last few decades due to their toxicity. However, PAH formation mechanisms and, in particular, effects of fuel composition on PAHs are yet not fully understood, despite a considerable volume of experimental, theoretical and numerical studies published in the literature.

Evolution of PAHs often begins with the formation of the first aromatic ring (phenyl or benzene) via several reaction pathways (D'Anna et al., 2000; Frenklach, 2002). Poly-aromatic growth beyond the first ring was initially known to be dominated by the hydrogen-abstraction-acetylene-addition (HACA) mechanism (Frenklach, 2002), but further studies have established that the HACA mechanism is too slow to explain the observed rates of PAH formation (Shukla and Koshi, 2011). Additional proposed PAH growth pathways include: methyl-addition and cyclisation (Shukla, Miyoshi and Koshi, 2010), phenyl-addition and cyclisation (Shukla *et al.*, 2008), as well as vinyl -addition and cyclisation (Shukla and Koshi, 2012a). Aromatic radical – radical and radical – molecule reactions were also reported (Shukla *et al.*, 2007).

Toxicity of particulate is influenced by the molecular structure of the hydrocarbon and the temperature at which the hydrocarbon is burnt (Bruinsma & Moulijn, 1988; Furuhata et al., 2012). Hydrocarbons ranging from C_1 to C_7 are used as fuels for such applications as residential heating, gas turbines and internal combustion engines, while they also form principal components of other fuels (Zhang et al., 2013; Marinov et al., 2016; Zhang et al., 2010; Botero et al., 2016; Marinov et al., 1997). For example, C_1 to C_2 gases (methane and ethane) are the major components of natural gas. C_3 to C_4 gases (propane and butane) are the main components of liquefied petroleum gas (LPG) (Marinov *et al.*, 1997), while C_4 to C_{12} molecules are the principal components of gasoline (Zhang et al., 2013).

Efforts have been made in the literature to study PAH emissions of some hydrocarbons belonging to the range of C_1 to C_7 fuels, as for example, C_1 and C_2 fuels by Siegmann & Sattler (2000) and El Bakali et al. (2012), C_3 and C_4 fuels by

Marinov et al. (1997) and Schenk et al. (2015), and likewise C_7 fuels by Wang & Cadman (1998) and Zhang et al. (2010). Nevertheless, systematic studies which investigate the influence of increasing carbon number on PAH formation of a homologous series of these fuels are rare. Particularly, the influence of carbon number was only investigated in the case of soot formation, for example, in diffusion flames, Ladommatos et al. (1996) reported that soot propensity of hydrocarbons molecules increased with carbon number. Crossley et al. (2008) proposed a micro-pyrolysis index (MPI) and threshold sooting index (TSI) for a number of hydrocarbons. They reported increase in soot propensity when the carbon number was increased. McEnally & Pfefferle (2011) also reported increase in yield sooting index (YSI) for several hydrocarbons when the carbon number was increased.

It is evident from the foregoing discussion that there are relatively few experimental PAH studies of the individual hydrocarbons in the homologous series of C_1 to C_7 when pyrolysed in a tube reactor; and also, only limited published information is available on particulate characterisation and soot formation in a tube reactor for this homologous series. There is also incomplete information on whether increasing carbon number has an influence on the carcinogenic Group B2 PAHs when they are adsorbed onto soot particles or when they are available in the gas phase.

6.2 Experimental Systems and Methods

6.2.1 Hydrocarbon molecules investigated

Seven, single component hydrocarbon molecules were investigated. This included five single gaseous fuels (methane, ethane, propane, n-butane and i-butane) (BOC, UK) and two liquid fuels (heptane and toluene) (Sigma Aldrich, UK). The molecular structures and flow rates of these test fuels are shown in Table 6.1.

Table 6.1: Molecular structures and flow rates of the C1 – C7 hydrocarbons at STP.

Sn	Fuel Molecule	Molecular Structure	Nomenclature	C/H	Flow rate (mL/min)
1	Methane	CH_4	C_1	0.250	206
2	Ethane	$H_3C{-}CH_3$	C_2	0.333	99.80
3	Propane	$H_3C{-}CH_2{-}CH_3$	C_3	0.375	69.90
4	n-butane	$H_3C{-}CH_2{-}CH_2{-}CH_3$	nC_4	0.400	48.99
5	i-butane	$H_3C{-}CH_2{-}CH_2{-}CH_3$	iC_4	0.400	48.41
6	Heptane	$H_3C{-}(CH_2)_5{-}CH_3$	nC_7	0.4375	0.175
7	Toluene	$C_6H_5\ CH_3$	arC_7	0.875	0.127

The hydrocarbons listed in Table 6.1 allowed the following influences of fuel molecular structure to be assessed:

i) Evaluate and confirm the soot propensities of a homologous series of C_1 – C_7 hydrocarbons under oxygen free pyrolysis in the tube reactor used for this study

ii) Characterize the soot particles produced from the range of C_1 – C_7 hydrocarbons based on size, number and mass using the DMS500 particle size analyser.

iii) Study PAH formation of the C_1 – C_7 hydrocarbons

iv) Correlate the soot propensities in (i) with the DMS data in (ii) and the PAH formation data in (iii) above

v) Whether increase in carbon number influences the identity of PAHs formed, and whether they tend to be found in the gas phase (GP) or particle phase (PP), particularly the B2 sub-group of PAHs.

vi) Whether isomers of hydrocarbons with the same carbon number but different molecular configurations result in altered PAH formation and toxicity of soot particles under pyrolysis conditions.

6.2.2 Generation of particulate matter and gas phase PAHs

Particulate and gaseous PAH samples were generated by means of pyrolysis at temperatures ranging from 1050 -1350 °C using the tube reactor described earlier in chapter 3. The carrier gas used during the pyrolysis of all the gaseous fuel molecules was nitrogen and was measured at STP conditions using a mass flow controller at a constant flow rate of 20 L/min for all the tests conducted. The flow rates corresponded to laminar flow within the reactor (Reynolds number ~ 200) throughout the temperature range of 1050 - 1350 ^{o}C. The hydrocarbon molecules were injected into the Pyrolyser at a fixed carbon flow rate of 10,000 ppm on C_1 basis. Therefore, the volumetric flow rate of methane, as shown in Table 6.1, was approximately twice as high as that of ethane and three times that of propane. Detailed particulate generation in the tube reactor and sampling procedures have been described previously in chapter 3 of this thesis.

Size and number distributions of soot particles at sub-micron level were determined by a differential mobility spectrometer (Cambustion DMS 500) instrument. Analysis of the particle size distribution was implemented via a sampling probe (6) and a dilution cyclone situated before the DMS 500. The sampling conditions of the DMS 500 have been described previously in chapter 3 of this thesis.

The cumulative gas volume (V_g) that passed through the filter and the resin was measured by a volumetric diaphragm gas meter (Bell flow Systems, UK). Soot and gaseous PAH sampling duration was maintained at 15 min for all test conditions. Table 6.2 shows, at each temperature, the mass of soot (M_s) collected and calculated soot mass concentrations (M_s / V_g) for the C_1 – C_7 hydrocarbons. The soot and the gas phase PAH samples were stored in plastic petri-dishes and immediately deep-frozen in the dark before subsequent PAH extraction and GCMS analysis.

6.3 Sample extraction and solvent evaporation

The extraction of PAH species from the soot and resin samples was carried out using an Accelerated Solvent Extractor (ASE) (Thermo Scientific Dionex-150)

describe previously in chapter 3 of this thesis. The dichloromethane containing the extracted PAHs was evaporated, so as to concentrate the PAH mixture, by bubbling gently a stream of nitrogen through the solvent vial which was situated in a custom-made PID controlled heating mantle. Detailed solvent evaporation has been described previously in chapter 3 of this thesis.

6.4 GCMS analysis of concentrated PAH extracts

The concentrated 1 mL extracts of both the particulate and gas phase samples were analysed using gas chromatography coupled to mass spectrometry (GCMS) (Agilent 7890B GC coupled with 5977A MSD) and has been described previously in chapter 3. Methodology for speciation and quantification of gaseous and particulate borne PAHs from the extracts has been discussed in chapter 4 of this thesis.

6.5 Results and Discussion

6.5.1 Soot propensities of C_1 –C_7 hydrocarbons

Gravimetric filter mass measurements and calculated soot mass concentrations (mg/m^3) obtained from pyrolysis of C_1 – C_7 hydrocarbons are shown in Table 6.2. The table shows that soot mass concentrations for the various hydrocarbons tested increased when the pyrolysis temperature was increased from 1050 – 1350 ^oC. These results match those observed in earlier studies (Dandajeh et al., 2017; Sánchez et al., 2012; Ruiz et al., 2007; Murphy, 1997). Methane however stands-out as having zero soot mass collected at the lowest temperature of 1050 ^oC. Similar observation was made by Murphy (1997), who observed carbon film deposition in methane pyrolysis commencing at temperatures > 1000 ^oC. As the pyrolysis temperature was raised from 1050 to 1250 ^oC, the soot concentration for methane became unexpectedly high. The high soot concentration of methane at 1250 ^oC may have been influenced by the fact that methane pyrolysis at temperatures of 1200 ^oC and 1300 ^oC is dominated by production of acetylene and ethylene respectively (Guéret et al., 1997). Large production rate of acetylene at the temperature of 1250 ^oC is a likely reason why methane shows

slightly higher mass concentration of soot at 1250 ^{o}C than those of ethane, propane and n-butane, though considerably lower than the concentrations for i-butane and toluene.

Table 6.2: Gravimetric filter soot mass measurements (conc. denotes concentration).

Temperature(^{o}C)	1050 ^{o}C		1150 ^{o}C		1250 ^{o}C		1350 ^{o}C	
Hydrocarbons	Soot Mass, M_s (mg)	Mass Conc. M_s/V_g (mg/m^3)	Soot Mass, M_s (mg)	Mass Conc. M_s/V_g (mg/m^3)	Soot Mass, M_s (mg)	Mass Conc. M_s/V_g (mg/m^3)	Soot Mass, M_s (mg)	Mass Conc. M_s/V_g (mg/m^3)
Methane (C_1)	-	-	49.4	282	202	1253	159	1002
Ethane (C_2)	5.1	16.0	75	434	153	956	125	793
Propane (C_3)	31.4	88.2	146	774	203	1222	158	966
n-butane (nC_4)	30.6	74.6	164	837	215	1187	173	969
i-butane (iC_4)	113	304	217	1113	247	1396	196	1114
Heptane (nC_7)	7.5	20.3	72.8	362	134	727	117	658
Toluene (arC_7)	251	745	228	1300	232	1379	206	1286

As the carbon number of the hydrocarbons was increased, it can be observed from Table 6.2 that the soot mass concentrations also tended to increase at all temperatures. At the temperature of 1150 ^{o}C for example, the soot mass concentration of methane (C_1) was 282 mg/m^3, which then increased by factors of 1.5, 2.6, 3.0, 3.9, 1.3 and 4.6 when C_2, C_3, nC_4, iC_4, nC_7 and arC_7, respectively, were pyrolysed. There was a slight departure from this trend in the mass concentration of heptane (nC_7) for reasons which are not clear, since the pyrolysis of all the fuels was carried out at a fixed carbon concentration.

Prior studies in the literature also reported increase in soot propensity of hydrocarbons with increasing carbon number of the fuel (Ladommatos et al., 1996; McEnally & Pfefferle, 2011; Calcote & Manos, 1983), although under flame environments and not always at fixed fuel C_1 supply rates. For example, Ladommatos et al. (1996) employed variable flow rates of hydrocarbons in diffusion flames in order to achieve critical sooting heights, from which a similar

trend was deduced, that is, an increase in sooting tendency as the carbon number of the fuel was increased.

Comparing the soot propensities of the two C_4 hydrocarbons, Table 6.2 shows that iC_4 produced a significantly higher soot concentration at the temperature of 1050 ^oC, by a factor of at least 3 times relative to nC_4, and remained higher at all temperatures. This result is consistent with previous studies (Zhang et al., 2013). The relative difference in soot concentrations for nC_4 and iC_4 decreased when the temperature was increased to 1350 ^oC. The reason for the increased soot concentration for iC_4 compared with nC_4 is likely to be that pyrolysis of iC_4 produces intermediate radicals such as propargyl and C_4 species (Oehlschlaeger et al., 2004) which are key to the formation of the first aromatic ring, and subsequent growth of PAHs and soot.

Table 6.2 also shows that the soot concentration of arC_7 at the temperature of 1050 ^oC is approximately 37 times greater than that for nC_7. This result is in line with those of previous studies (Ladommatos et al., 1996; Calcote & Manos, 1983). The exceptionally high soot concentration of toluene, as an aromatic molecule, was expected, since its decomposition produces phenyl and benzyl radicals via self-de-methylation and hydrogen-abstraction respectively (Zhang et al., 2010). Phenyl radicals are PAH growth species in the phenyl addition and cyclization (PAC) mechanism (Shukla *et al.*, 2008). Abundance of acetylene in toluene pyrolysis (Zhang et al., 2010) could also accelerate the growth of PAHs and soot surface growth via the HACA mechanism (Frenklach, 2002).

6.5.2 Particulate characteristics of C_1 –C_7 hydrocarbons

Soot particles produced by pyrolysis of the seven hydrocarbons at an inlet concentration of 10,000 ppm were characterised in terms of particle mass, size and number concentrations using a differential mobility spectrometer (Cambustion DMS500). Figure 6.1 shows the number distribution of soot particles produced from pyrolysis of the C_1 – C_7 hydrocarbons. Figures 6.1a, b, c and d show the size and number spectra for the C_1 – C_7 hydrocarbons at temperatures of 1050 ^oC, 1150 ^oC, 1250 ^oC and 1350 ^oC respectively. It can be seen from the

spectra in Figures 6.1a, b, c and d that increasing pyrolysis temperature from 1050 to 1350 ^{o}C shifted soot particle sizes towards larger diameters.

For example, pyrolysis of C_2 ethane molecule at a temperature of 1050 ^{o}C resulted in larger number of particles in the size range of 13 – 86 nm, whereas at higher temperature of 1350 ^{o}C, smaller number of particles were broadly distributed in the range of 86 – 562 nm. Similar shift in particle diameter can be seen from the pyrolysis of C_7 toluene. The particle diameters from toluene pyrolysis at temperatures of 1050 ^{o}C and 1350 ^{o}C ranged from 87 – 649 nm and 100 – 866 nm respectively. This result is in line with previous studies by Eveleigh (2015) who carried out pyrolysis of C_2 hydrocarbons (ethane, ethylene and ethanol) at an inlet fuel concentration of 8000 ppmv (0.8% v).

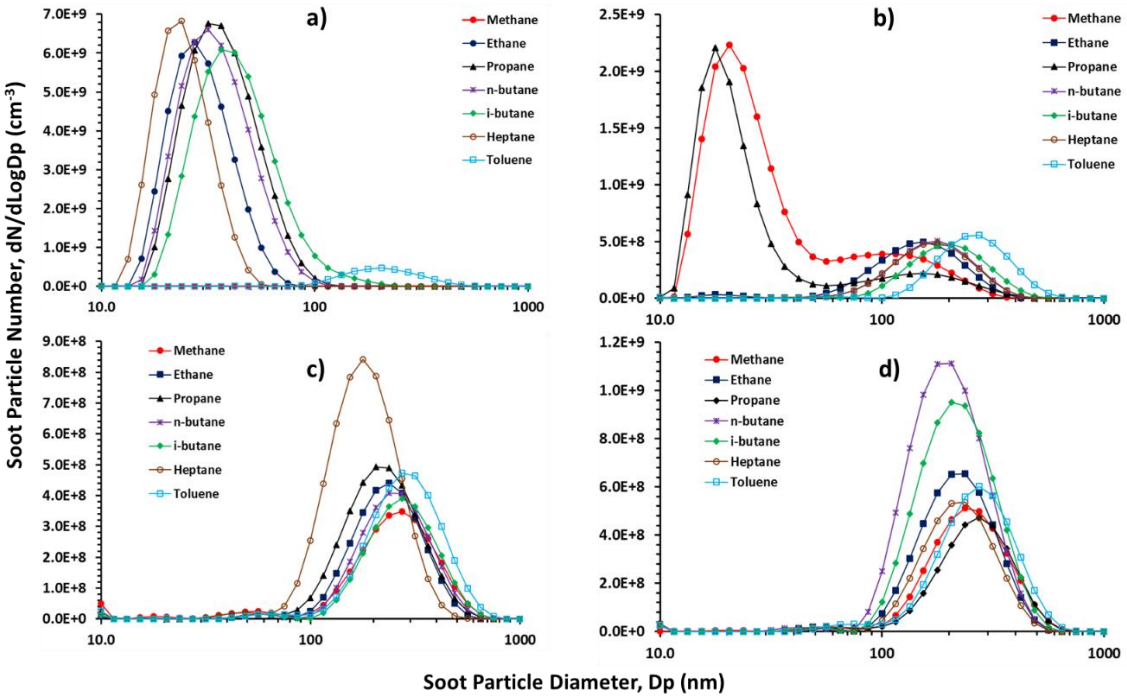

Figure 6.1: Number distribution of particulates formed from C1 - C7 hydrocarbons at 4 different temperatures a) 1050 ^{o}C b) 1150 ^{o}C c) 1250 ^{oC} d) 1350 ^{o}C.

Tables 6.3 and 6.4 summarise measured DMS data. The Tables present the influence of temperature on soot particle mean diameter (nm), total soot particle number concentration (particle number per unit volume of N_2 carrier gas at N_2 inlet conditions) and soot mass concentration. It can be seen from Table 6.3 that at the temperature of 1050 ^{o}C for example, soot particle mean diameter (D_{pm}) of the hydrocarbons increased as their carbon number was increased from C_1 to C_3

and iC_4 to arC_7. However, nC_4 and nC_7 departed to a degree, from this trend. As the temperature was increased to 1150 ^oC, D_{pm} appeared to increase with increasing carbon number of the hydrocarbons, but became almost independent of carbon number at the temperature of 1350 ^oC. This is believed to be due to agglomeration of soot particles which could have resulted in increase in soot particle sizes (Heywood, 1988). The mean diameter for toluene at 1050 ^oC can be seen to be roughly similar to the mean diameter for heptane at 1350 ^oC.

Table 6.3: Soot particle size and number concentration measurements using DMS500.

	Mean Particle Size, D_{pm} (nm)				Number Concentrations (dN/dDp)(1/cm^3)			
Temperature(^oC)	**1050**	**1150**	**1250**	**1350**	**1050**	**1150**	**1250**	**1350**
Methane (C_1)	38.7	191	381	356	1.8E+07	1.1E+09	2.6E+08	2.2E+08
Ethane (C_2)	40.3	223	323	306	2.3E+09	2.8E+08	2.4E+08	3.9E+08
Propane (C_3)	58.0	251	332	362	2.9E+09	8.2E+08	2.9E+08	2.8E+08
n-butane (nC_4)	55.0	247	353	287	2.8E+09	2.5E+08	2.4E+08	5.9E+08
i-butane (iC_4)	90.0	287	379	312	2.8E+09	2.3E+08	2.3E+08	5.2E+08
Heptane (nC_7)	31.0	246	256	304	2.3E+09	2.6E+08	4.2E+08	3.1E+08
Toluene (arC_7)	308	356	410	375	2.3E+08	2.6E+08	2.8E+08	3.4E+08

Similarly, Table 6.3 shows that the soot particle number concentration for all the hydrocarbons decreased when the temperature was increased from 1050 to 1350 ^oC. It can also be observed from the Table that both iC_4 and nC_4 had nearly the same soot particle number concentration at all the temperatures. Soot particle agglomeration for the C_4 fuels increased with temperature increase at apparently similar rates. These results would seem to suggest that branching a straight chain nC_4 to iC_4 still produces similar number of soot particles, but with considerably larger mean particle size.

The variation of soot particle number for nC_7 and arC_7 suggests that the soot particle number for toluene is almost independent of temperature. The implication of this observation is that toluene soot particles appear to grow individually, rather than through agglomeration, by means of deposition of gaseous species on the particles already formed. It is important to note the trends of soot mass

concentrations shown in Table 6.4, measured using the DMS500, agree with those from the gravimetric filter measurements shown in Table 6.2. The trend also shows increased soot mass concentrations with increasing carbon number of the hydrocarbons at all temperatures.

Table 6.4: Particle mass (µg/cm3) measurements from DMS500.

Temperature (°C)	1050	1150	1250	1350
Methane (C_1)	0.00001	0.43	2.55	3.04
Ethane (C_2)	0.048	0.75	1.95	2.53
Propane (C_3)	0.15	0.50	2.31	2.96
n-butane (nC_4)	0.11	1.02	2.39	3.45
i-butane (iC_4)	0.32	1.50	2.78	3.87
Heptane (nC_7)	0.03	0.98	1.78	2.00
Toluene (arC_7)	1.76	3.26	4.27	4.14

In conclusion, soot formation for the C_1 – C_7 hydrocarbons has several distinct features, with methane and toluene departing somewhat from these characteristics. Methane had the smallest number of primary particles at 1050 °C, suggesting that reactions were too slow at this temperature for soot formation, compared with most of the other C_2 – C_7 fuels. Toluene on the other hand had a relatively larger mean particle size (308nm) even at the low temperature of 1050 °C. The particle size for toluene at the lowest temperature of 1050 °C was similar to that for most of the other aliphatic C_1 – C_7 hydrocarbons but at the higher temperature of 1350 °C. These findings imply that of the molecules tested, methane and toluene are at the two extreme ends in terms of soot formation rates, with methane the least and toluene the most prolific soot producer.

6.5.3 Influence of carbon number on GP and PP PAHs

Figure 6.2 presents PAH concentrations of C_1 – C_7 hydrocarbons which resulted from summing up, for each hydrocarbon, all the 16 EPA PAHs shown in Table 2.1. Figure 6.2a shows gas phase (GP) PAH mass extracted from the XAD-2 resin and normalised with the volume of gas (V_g) passed through the resin

which was positioned in series and after the particulate filter. Figure 6.2b shows particulate phase (PP) PAH mass, extracted from the particulates collected on the filter, also normalised with V_g. Figure 6.2c shows normalised PP PAH plotted against normalised GP PAHs.

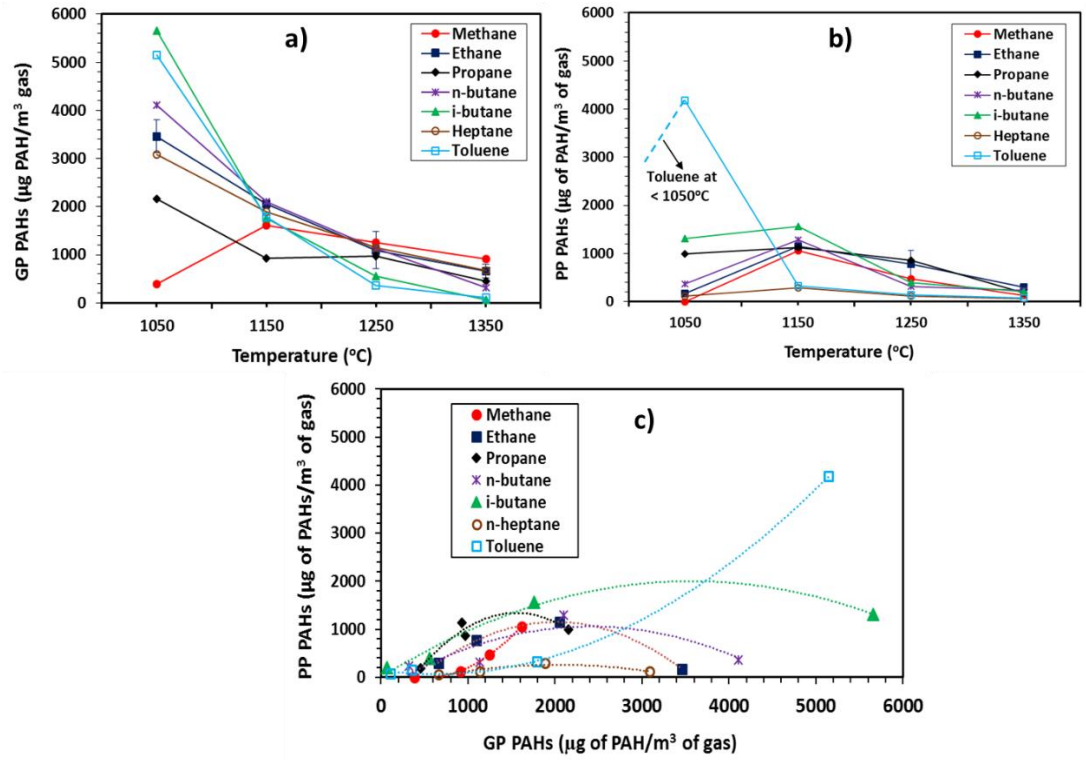

Figure 6.2: Normalised Total PAH Concentrations: a) Gas Phase (µg of PAH/m3 of gas) b) Particle Phase (µg of PAH/m3 of gas) c) PP and GP at four different temperature points: 1050°C, 1150°C, 1250°C and 1350°C.

It can be seen from Figure 6.2a that increasing the temperature of the reactor from 1050 to 1350 °C resulted in lower GP PAH concentrations for all the fuels. This effect of temperature on the GP PAHs is consistent with other published works (Sánchez et al., 2013; Dandajeh et al., 2017). Methane was an exception though, with a near zero GP PAH mass at the temperature of 1050 °C. This is likely due to slower formation rates of intermediate precursors (such as acetylene) during methane pyrolysis at 1050 °C. It can also be observed from Figure 6.2a at the temperature of 1350 °C that the GP PAH concentrations decreased with increasing carbon number of the hydrocarbons but the trend is unclear at other temperatures.

The PP PAH mass concentration shown in Figure 6.2b increase within the temperature range of 1050 to 1150 °C for all the fuels except toluene, but as the

temperature was raised further from 1150 to 1350 ^{o}C, the PAH concentration subsequently decreased. This decreasing trend of PP PAH concentrations above 1150 ^{o}C is believed to be due to incorporation of PP PAHs (particularly Group B2) into soot; and has been reported previously by (Aracil et al., 2005) in pyrolysis of polyvinyl-chloride. Comparing Figures 6.2a and b at the temperature of 1050 ^{o}C, it can be seen that both the GP and PP PAHs on volume of gas basis increase with increasing carbon number of the hydrocarbons examined. Although this does not seem to apply in the case of propane and heptane pyrolyses.

Figure 6.2c shows the GP and PP PAHs concentrations of the seven hydrocarbons plotted against each other at four different temperatures (1050 ^{o}C, 1150 ^{o}C, 1250 ^{o}C and 1350 ^{o}C) and the curves suggest that the abundance of both GP and PP PAHs is influenced by temperature. That is, the abundance of both reduces with temperature and this is possibly due to more rapid conversion of GP to soot (see Table 6.2). More detailed observation of Figure 6.2c shows that both the PP PAH and GP PAH concentrations increased and this relation held up to the temperature of 1150 ^{o}C; as the temperature rose further to 1350 ^{o}C, both GP and PP PAH concentrations reduced together (methane and toluene are exceptions to this trend). Considering now Figures 6.2a, b and c together, concentrations of higher GP and PP PAHs can be observed at the temperature of 1050^{o}C for iC_4 over nC_4 as well as for arC_7 over nC_7. This observation suggests that isomerisation and aromatisation of the respective C_4 and C_7 fuels at 1050 ^{o}C, both promote formation of molecular precursors of soot as well as higher soot concentration and larger soot particle sizes (see Table 6.2).

PP PAH mass was normalised in two ways, in Figure 6.3a by the soot mass (see Table 6.2) and in Figure 6.3b by the soot particle number (see Table 6.3). Figure 6.3a shows that the concentration of PP PAHs per unit mass of soot decreased substantially with increasing temperature of the reactor from 1050 – 1350 ^{o}C for all the fuels. That is, a relatively smaller amount of PAHs was deposited on soot particles, per unit mass of soot, while the amount of soot increased as the temperature rose. Figure 6.3a shows that at the temperature of 1150 ^{o}C, the PP PAH concentrations (as well as the Group B2 PAH concentration) at a temperature of 1150 ^{o}C decreased with increasing carbon number. It can also be seen in Figure 6.3a that the PP PAH concentration at a temperature of 1050 ^{o}C

during methane pyrolysis was zero due to absence of soot at such temperature (see Table 6.2).

What stands out in Figures 6.3b and 6.2b is the PP PAH concentration of toluene at a temperature of 1050 ^{o}C. Toluene is a source of large number of intermediates (phenyl and benzyl radicals) at low temperatures (Shukla *et al.*, 2008), which can contribute to PAH and soot particle growth. This is reflected by the appreciable soot mass concentrations for toluene at the temperature of 1050 ^{o}C relative to the other hydrocarbons examined (see Table 6.2). It is expected that at temperatures lower than 1050 ^{o}C (see Figures 6.3b and 6.2b) toluene will exhibit an increasing trend in the PP PAH concentrations with rising temperatures to 1050 ^{o}C.

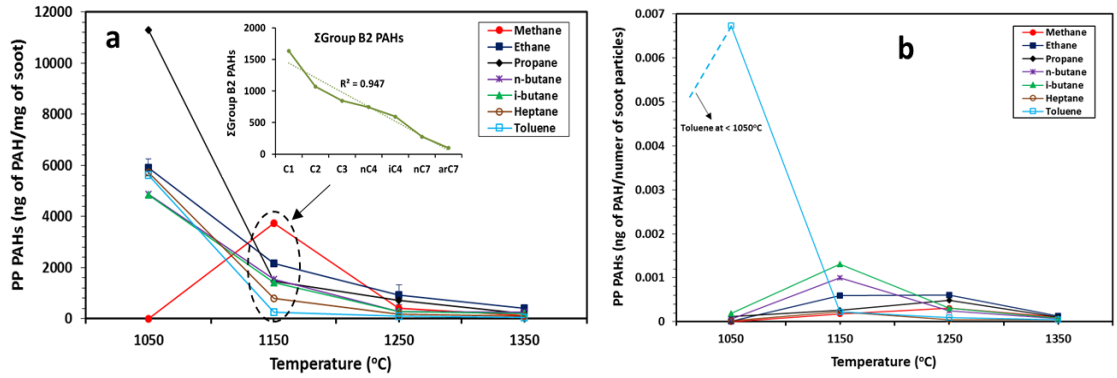

Figure 6.3: Normalised Total PAH Concentrations: a) Particle Phase (ng of PAH/mg of soot) b) Particle Phase (µg of PAH/soot particle number).

The above extrapolation for toluene PAH mass for temperatures lower than 1050 ^{o}C is supported by the findings of other published studies. For example, Sánchez et al. (2013) reported increasing trend in PAH concentrations of C_2 fuels within the temperature range of 700 – 950 ^{o}C and a corresponding decrease in PAH mass at temperatures above 950 ^{o}C.

Figure 6.3a suggests that different structures of hydrocarbons with the same carbon number (nC_4 & iC_4 and nC_7 & arC_7) produced roughly similar PP PAH concentrations per unit mass (M_s) of soot at all temperatures. The PP PAHs normalised with the number of soot particles are shown in Figure 6.3b. The concentrations of PAHs per soot particle increased when the pyrolysis temperature was increased from 1050 to 1150 ^{o}C and drastically decreased

when the temperature was raised to 1350^{o}C (toluene was still an exception). Fig.6.3b shows that hydrocarbons with the same carbon number (nC_4 & iC_4 and nC_7 & arC_7), yielded identical PAH mass within the temperature range of 1250 to 1350 ^{o}C.

6.5.4 Influence of carbon number on Individual total PAHs

This section examines the PAH distribution for the individual C_1 – C_7 hydrocarbons. Table 6.5 presents the distributions of the 16 EPA priority PAHs for each hydrocarbon fuel, while Figures 6.4a, b, c and d show the PAH concentrations of PHN, PYR, B(k)F and I(1,2,3-cd)P respectively. These four PAHs were selected from Table 6.5 as examples for further discussion. It can be seen from Figures 6.4a and b that lighter benzenoid PAHs (PHN and PYR) were detected in roughly similar concentrations, at all temperatures, regardless of the carbon number of the hydrocarbon. A similar observation can be seen in Table 6.5 for lighter five-membered ring PAHs (ACY and FLT). Formation of lighter PAHs at low temperatures of 1050 ^{o}C was reported to be dominated either by aromatic radical-radical or radical-molecule reactions (Shukla *et al.*, 2007). For example, kinked PAHs, such as phenanthrene, with one arm chair feature (site X in Figure 6.4) could grow to pyrene via reaction of phenanthrene radical and acetylene molecule. However, the growth of pyrene to heavier PAHs was reported to be inefficient through the HACA mechanism (Shukla *et al.*, 2007) due to its multiple double fusing sites (site Y in Figure 6.4).

Figures 6.4c and d show at the temperature of 1050 ^{o}C, an increasing trend of heavier five-membered ring PAHs of B(k)F and I(1,2,3-cd)P respectively with increasing carbon number of the hydrocarbon. This observation however, does not seem to apply in the case of heptane pyrolysis in Figure 6.4c and heptane and toluene pyrolyses in Figure 6.4d. On the contrary, Table 6.5 shows no such clear trend for the heavier benzenoid PAHs (B(a)P, D(a,h) and B[ghi]P) at temperature of 1050 ^{o}C. It should be noted here that the five-membered ring PAHs have a common feature of multiple triple fusing sites/arm-chairs, making it easier for PAH growth via the HACA mechanism.

One striking characteristic of the heavier PAHs (together with few of the lighter PAHs) shown in Table 6.5, is their disappearance at the higher temperature of 1350 ^{o}C. Smith (1979) and Shukla *et al.* (2007) both also reported this observation in the case of toluene pyrolysis. The disappearance of these PAHs at high temperatures has been ascribed to insufficient soot surface area /number of soot particles available for PAH condensation (Dandajeh *et al.*, 2017).

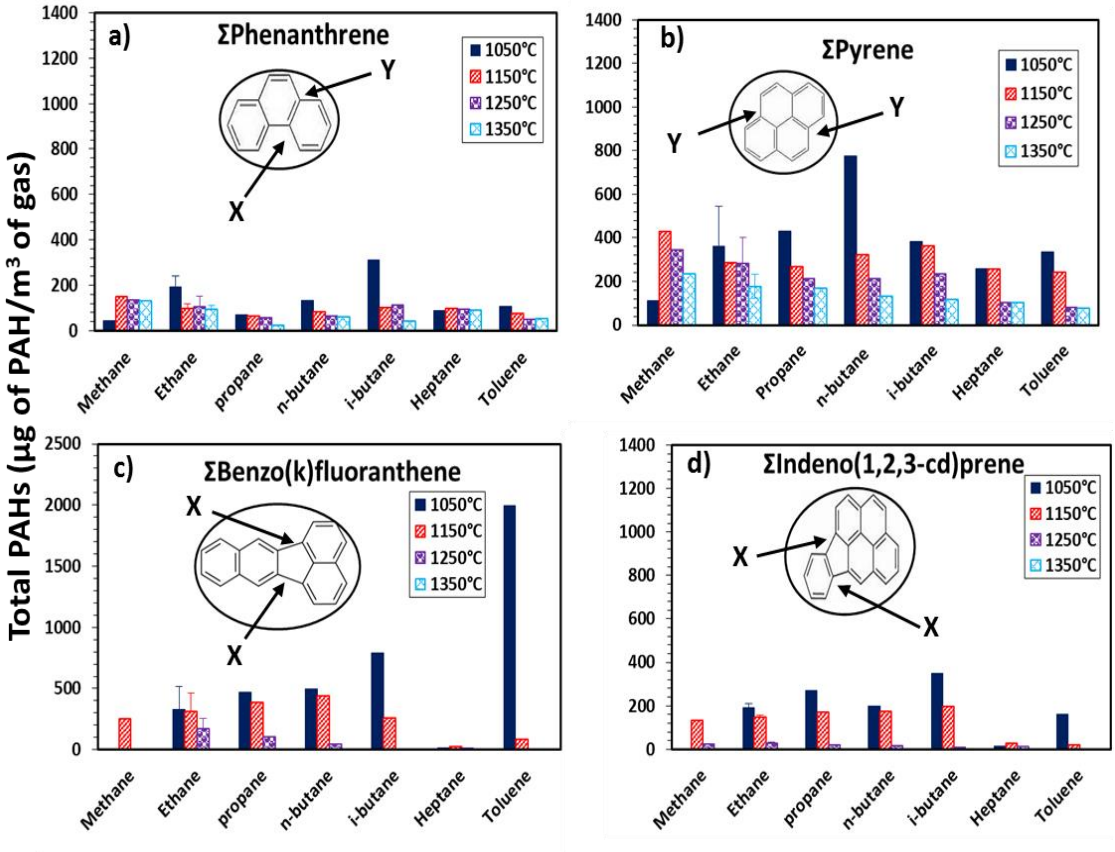

Figure 6.4: Distributions of total PAHs produced during the pyrolysis of C1 – C7 hydrocarbons a) Phenanthrene b) Pyrene c) Benzo(k)fluoranthene d) Indeno(1,2,3-cd) pyrene.

The soot particle number concentrations of the hydrocarbons shown in Table 6.3 showed remarkable decrease with temperature increase to 1350 ^{o}C. For example, when the pyrolysis temperature was increased from 1050 to 1350 ^{o}C, the soot particle number concentrations decreased approximately by factors of 6, 10, 5, 5 and 7 in the case of the C_2, C_3, nC_4, iC_4 and nC_7 hydrocarbons, respectively. Shukla *et al.* (2007) reported that the kinetics for the formation of heavier PAHs at high temperatures of 1350 ^{o}C is dominated by the HACA mechanism.

It is interesting to note that most of the PAHs detected in this chapter at high concentrations in the pyrolysis of the individual C_1 – C_7 hydrocarbons (see Table 6.5), were also reported in high concentrations in previous published works under oxygen-free pyrolysis (Shukla *et al.*, 2007; Zhang *et al.*, 2010; Zhang *et al.*, 2009) and flame environments (Siegmann and Sattler, 2000; El Bakali *et al.*, 2012; Marinov *et al.*, 1997; Schenk *et al.*, 2015).

6.5.5 Effects of carbon number on total PAHs and on the PAH rings

Figure 6.5 shows the concentrations of PAHs in terms of number of rings (size of PAHs) for the seven hydrocarbon fuels. Figures 6.5a, b, c and d show the total PAH concentrations at temperatures of 1050, 1150, 1250 and 1350 ^oC respectively. It can be seen from Figure 6.5a that the concentrations of the total number of PAH rings at a temperature of 1050 ^oC, particularly those of 3, 4 and 5 rings, increased with increase in carbon number of the hydrocarbons from C_1 – C_7, but surprisingly this does not seem to apply in the case of heptane pyrolysis.

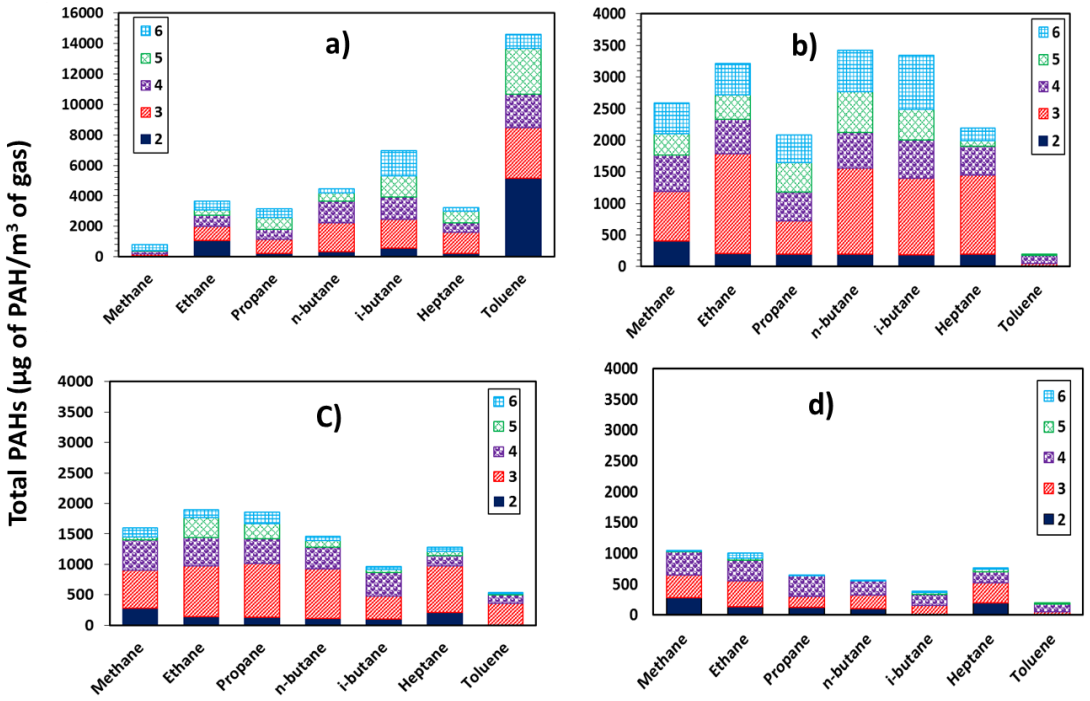

Figure 6.5: Total PAH concentrations with respect to their number rings for the C1 – C7 hydrocarbons at four different temperature points: a) 1050 ^oC b) 1150 ^oC c) 1250 ^oC d) 1350 ^oC. The legend on the graphs denotes number of PAH rings.

Table 6.5: Total PAH (GP +PP) distributions of C1 – C7 hydrocarbons (µg of PAHs/ m3 of gas); where 'nd' denotes PAHs that were 'not detected' by the GC.

	1050 °C							1150 °C							1250 °C							1350 °C						
PAHs	C1	C2	C3	nC4	iC4	aIC7	arC7	C1	C2	C3	nC4	iC4	aIC7	arC7	C1	C2	C3	nC4	iC4	aIC7	arC7	C1	C2	C3	nC4	iC4	aIC7	arC7
NPH	44.7	1073	210	326	580	220	344	407	204	197	195	189	197	344	278	474	132	116	97.8	209	4.3	277	139	123	107	3.9	196	4.1
ACY	68.3	407	344	342	1294	355	340	421	299	324	244	276	303	340	388	632	285	181	193	297	317	254	259	226	271	117	249	nd
ACN	nd	nd	322	520	8.09	754	11	9.3	1025	7.5	635	702	678	nd	nd	827	nd	492	7.42	305	8.3	nd	nd	nd	nd	nd	nd	nd
FLU	41.8	324	193	255	297	178	397	220	163	138	143	135	172	397	108	252	69	75.9	nd	68.1	nd	nd	68.1	nd	nd	nd	nd	nd
PHN	46.2	191	74.7	133	311	89.3	109	154	97	65.9	83	100	97.6	109	136	219	56	63.3	112	94	51	130	94.5	58.6	94.4	41	91.2	55
ATR	1.07	nd	1.69	640	2.2	1.5	2473	2.5	2.1	2.0	259	1.0	1.92	2473	nd	257	494	nd	81.7	1.9	nd	nd	nd	487	nd	nd	nd	nd
FLT	71.9	228	200	285	1046	170	642	147	218	188	237	241	163	642	158	395	166	141	160	73	53	138	167	160	101	60	74.2	54
PYR	113	380	433	777	384	260	334	430	285	267	322	385	256	334	344	686	244	212	235	104	82	236	178	170	134	120	103	76
B[a]A	0.5	0.45	0.56	0.58	1.02	0.45	180	1.18	0.96	0.95	1.5	1.8	0.89	180	0.54	2.03	0.9	0.51	0.45	0.87	0.5	0.5	0.44	0.94	0.49	0.9	0.86	0.5
CRY	2.19	140	23	381	22.4	196	1043	nd	35.9	29.4	4.5	8.0	38.8	1043	2.38	nd	4.1	2.3	2.0	3.84	nd	nd	nd	4.2	nd	nd	nd	nd
B[b]F	1.75	1.6	1.97	2.06	3.61	1.59	272	4.15	3.4	3.35	5.3	4.66	3.15	272	1.89	7.15	3.2	1.81	1.59	3.055	1.9	1.9	1.56	3.3	1.71	3.3	3.04	1.6
B[k]F	2.3	330	470	496	791	720	1985	258	317	389	442	282	51.1	1985	2.49	444	110	44.8	4.36	24.41	4.9	2.5	2.06	4.36	2.28	4.4	4.01	2.1
B[a]P	5.89	11.5	197	45.6	571	58.2	404	65	58.8	62.5	177	218	20.8	404	42.3	219	127	56.2	28	22.73	13	8.5	5.27	11.1	5.77	11	28.1	12
I[123cd]P	8.22	190	270	198	348	13.8	161	142	157	178	180	206	33.8	161	27.2	207	28	14.2	7.47	17.11	9.0	9	7.35	15.6	8.05	16	14.3	7.8
D[ah]A	6.85	6.1	95.9	7.84	13.7	6.05	348	15.8	12.9	12.7	20	24.2	12	348	7.21	27.2	12	6.9	6.05	11.64	7.3	7.3	5.95	12.6	6.52	13	11.6	6.1
B[ghi]P	404	383	311	97.1	1320	192	764	337	337	261	476	842	173	754	118	594	162	58.1	44.7	55.19	3.1	70	57	5.33	5.52	5.4	4.91	2.6

Table 6.6: Particulate Phase (PP) PAH distributions of C1 – C7 hydrocarbons (ng of PAHs/mg of soot); where 'nd' denotes PAHs that were 'not detected' by the GC.

	1050 °C							1150 °C							1250 °C							1350 °C						
PAHs	C1	C2	C3	nC4	iC4	alC7	arC7	C1	C2	C3	nC4	iC4	alC7	arC7	C1	C2	C3	nC4	iC4	alC7	arC7	C1	C2	C3	C4	iC4	alC7	arC7
NPH	0.0	35.5	28.3	18.2	11	44.04	8.03	10.03	4.05	2.82	6.55	4.95	5.3	1.3	1.8	2.12	1.4	1.8	1.3	2.7	1.5	2.2	2.4	2.1	2.1	1.8	2.8	1.5
ACY	0.0	264	nd	nd	nd	nd	nd	nd	52.1	73.1	nd	nd	nd	nd	nd	61.5	19	nd	10	nd	nd	nd	85	66.1	114	58	nd	nd
CAN	0.0	nd	nd	nd	nd	nd	nd	nd	nd	nd	nd	nd	nd	nd	nd	nd	nd	nd	nd	nd	nd	nd	nd	nd	nd	nd	nd	nd
FLU	0.0	247	nd	nd	nd	nd	nd	nd	nd	nd	nd	nd	nd	nd	nd	nd	nd	nd	nd	nd	nd	nd	nd	nd	nd	nd	nd	nd
PHN	0.0	155	33.77	55.35	47.1	58.55	88.2	12.88	28.9	25.3	22.4	23.7	8.8	1.7	2.3	27.8	19	9.8	2.7	3.4	7.0	21	49	36.8	36	20	3.6	1.9
ATR	0.0	nd	nd	nd	nd	nd	1334	nd	nd	nd	nd	nd	nd	nd	nd	nd	133	nd	59	nd	nd	nd	nd	505	nd	nd	nd	nd
FLT	0.0	367	385.7	209	225	247.6	339	10.51	157	87.8	95.3	88.1	23	20	36	133	79	48	62	10	35	45	116	105	102	1.9	29	19
PYR	0.0	689	826.1	424.1	471	377.3	206	557.9	223	145	133	150	47	33	93	199	120	69	94	2.0	55	55	73	82.5	137	106	36	36
B[a]A	0.0	8.58	6.354	3.912	2.66	10.64	241	2.423	0.88	0.68	1.22	1.2	1.3	0.3	0.4	0.51	0.3	0.4	0.3	0.6	0.4	0.5	0.6	0.51	0.5	0.4	0.7	0.4
CRY	0.0	nd	272.2	79.99	87.8	162.1	279	3.04	71.8	38	1.4	2.3	1.3	3.1	nd	1.1	0.4	1.1	2.0	1.2	2.8	nd	nd	nd	nd	nd	nd	nd
B[b]F	0.0	30.2	22.38	13.78	9.37	37.47	364	8.534	3.45	2.4	4.28	4.21	4.5	1.1	1.5	1.8	1.2	1.5	1.1	2.3	1.3	1.9	2.1	1.78	1.8	1.6	2.4	1.3
B[k]F	0.0	1174	2388	1229	891	1861	1383	904.9	597	500	355	235	135	66	2.0	204	88	38	1.5	31	1.7	2.5	2.7	2.35	2.3	2.0	3.2	1.7
B[a]P	0.0	311	1541	564.2	698	707.1	538	209.4	101	74.2	161	158	43	9.0	34	159	99	42	18	25	4.4	6.4	7	6.02	6	5.2	21	4.2
I[123cd]P	0.0	1131	2414	1027	735	488.5	211	474.7	283	221	206	178	74	15	22	33.6	16	12	5.4	14	6.2	9	9.7	8.4	8.3	7.3	11	5.9
D[ah]A	0.0	115	1087	52.49	35.7	142.8	462	32.52	13.1	9.15	16.3	16	17	4.3	5.7	6.88	4.4	5.8	4.3	8.7	5.0	7.3	7.9	6.8	8.7	5.9	9.2	4.8
B[ghi]P	0.0	1578	2383	1279	1686	1875	812	1582	639	334	565	577	471	109	112	112	130	49	32	73	2.1	70	75	2.88	2.8	2.5	3.9	2.0

It can also be seen from Figure 6.5a that pyrolysis of iC_4 produced higher number of 2, 5 and 6 rings compared to the corresponding nC_4. Similarly, Figure 6.5a shows that pyrolysis of aromatic toluene (arC_7) produced substantially higher number of 2 - 6 ring PAHs compared to the aliphatic heptane molecule (nC_7).

As the temperature of the reactor was increased from 1150 to 1350 ^oC, the concentrations of the PAHs decreased, but especially apparent in the case of the hydrocarbons with larger carbon numbers (iC_4 and arC_7). This trend is particularly notable at the temperature of 1350 ^oC (see Figure 6.5d), suggesting rapid consumption of 2, 3 and 4 ring PAHs in soot particle growth at higher temperatures. The heptane, once again, departed from this general behaviour. Considering Figure 6.5 in its entirety, it can be seen that the concentrations of 4, 5 and 6 ring PAHs (especially Group B2 members) decreased when the temperature of the reactor was raised from 1050 to 1350 ^oC.

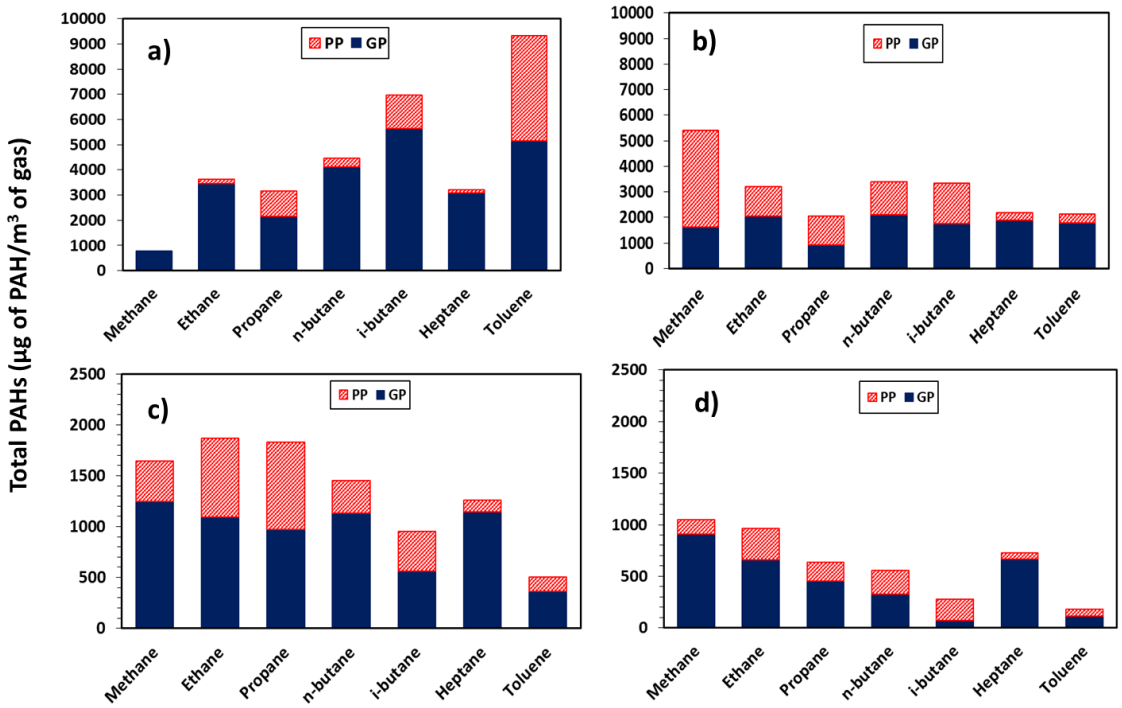

Figure 6.6: Total PAH concentrations of the C1 – C7 hydrocarbons partitioned into gas phase (GP) and particulate phase (PP) PAHs at four different temperature points: a) 1050 ^oC b) 1150 ^oC c) 1250 ^oC d) 1350 ^oC.

Figures 6.6a, b, c and d show the total PAH concentrations partitioned into gas and particulate phases at tempeartures of 1050, 1150, 1250 and 1350 ^oC respectively. It can be seen from Figures 6.6a, b, c and d that the proportions of

gas phase PAH concentrations dominated the total PAH concentrations regardless of the carbon number of the hydrocarbon investigated. Considering Figure 6.6 in its entirety, it can be seen that Figures 6.6a and d show increasing and decreasing trends in the total PAH concentrations with increasing carbon number of the hydrocarbons at lowest and highest temperatures of 1050 and 1350 ^{o}C, respectively; however, Figures 6.6b and c show no clear trend of the influence of carbon number on the total PAH concentrations at the intermediate temperatures of 1150 ^{o}C and 1250 ^{o}C respectively.

One possible explanation for the increase in total PAH concentrations with increasing carbon number at the temperature of 1050 °C is that the kinetics for the growth of PAHs to soot was slow; hence, PAHs of various sizes (number of rings) continuously accumulate in comparatively high concentrations. This result is supported by the lower soot concentrations shown in Table 6.2 for all the hydrocarbons tested. At higher temperature of 1350 ^{o}C however, the total PAH concentrations decreased with increasing carbon number since the rate of growth of PAHs to soot accelerated, exceeding the rate at which the PAHs were formed and grown (Dandajeh *et al.*, 2017). This is also supported by the increased soot mass concentrations of the C_1 - C_7 hydrocarbons shown Table 6.2.

6.5.6 Error analysis

Repeatability checks were conducted during 4 different pyrolysis test periods with ethane as the control hydrocarbon. This was done to detect any daily drift in the experimental equipment and instrumentation and also in order to check the repeatability of the procedures involved. The standard deviations reported in this thesis are thus calculated from these daily repeat tests with ethane.

Table 6.7 shows the summary of the percentage variations (100% δ/mean) for all the parameters investigated, where δ is the standard deviation. For example, the percent variation in measuring soot mass of ethane is 20% at a temperature of 1050 ^{o}C and 9 % at 1350 ^{o}C. The percentage variations in measuring gas and particulate phase PAHs are shown by the highest (H) and lowest (L) variations of the individual PAHs. Visible error bars on the graphs throughout this thesis denote the standard deviations of the measured parameter. These data therefore

provided a measure of daily variability in the PAH analysis of the hydrocarbons investigated and the results that were discussed earlier in this chapter are subject to these variabilities.

Table 6.7: Percentage Variations (100% δ /mean) for the test parameters ('H' and 'L' denotes the highest and lowest percentage variations for each PAH specie respectively).

	Temperature (°C)			
Pwercentage Variation (±%)	**1050**	**1150**	**1250**	**1350**
Soot Mass, M_s (mg)	20	15	9	9
Mean Particle Diameter, D_{pm} (nm)	33	15	14	15
Particle Number (dN/dD_p) ($1/cm^3$)	9	36	18	45
GP PAHs	H: NPH (16)	H: NPH (22)	H: ACN (45)	H: FLU (40)
(µg of PAH/m^3 of gas)	L: I[123cd]P (5)	L: FLU (3)	L: NPH (6)	L: PHN (13)
PP PAHs	H: B[ghi]P (28)	H: B[k]F (42)	H: B[a]P (45)	H: PYR (31)
(µg of PAH/m^3 of gas)	L: B[a]P (21)	L: PHN (0.2)	L: B[ghi]P (3)	L: FLT (2)
PP PAHs	H: B[ghi]P (23)	H: B[k]F (44)	H: B[a]P (40)	H: B[ghi]P (46)
(ng of PAH/mg of soot)	L: B[k]F (5)	L: PHN (2)	L: I[123cd]P (32)	L: ACY (0.9)

6.5.7 Toxicity of soot particles produced by C_1-C_7 hydrocarbons

This section examines the toxicity of soot particles generated from pyrolysis of the seven hydrocarbons. The weighted carcinogenicity of PAHs (WC-PAHs), was defined in Dandajeh *et al.* (2017) (see Eq.6.1) as the summation of the product of individual EPA16 priority PAH concentrations (C_i) and their corresponding toxicity equivalent factors (TEF). The TEFs selected have been shown previously in Table 2.2 as proposed by Nisbet and LaGoy (1992) and are widely used for assessing PAH toxicity.

$$\text{WC- PAHs} = \sum_{i=1}^{16}(TEF_i * Ci) \qquad \text{Eq.6.1}$$

Figures 6.7a and b show the WC- PAHs on volume of gas and soot mass bases, respectively. It is apparent from Figure 6.7a that soot particles produced from toluene (arC_7) pyrolysis produced the highest WC-PAHs at a temperature of 1050 ^oC. The WC-PAH of arC_7 on volume of gas basis at a temperature of 1050 ^oC was 3.5 times that of C_3, 4 times that of iC_4, 16 times that of nC_4 and 49 times that of the C_2 and nC_7 hydrocarbons. This result is not due to the high soot mass produced by toluene pyrolysis at 1050 ^oC, as the result is normalised by soot mass, but due to the substantial concentrations of Group B2 PAHs (particularly B(a)P, D(a,h)A and B(k)F) generated from toluene soot particles. PAHs contributing to the toxicity of soot particles from the seven hydrocarbons are shown in Tables 6.5 and 6.6.

Figure 6.7b shows that propane soot particles produced the highest WC - PAHs on soot mass basis at a temperature of 1050 ^oC, and there was a clear decreasing trend of carcinogenicity with temperature increase. The weighted carcinogenicity of propane soot particles (soot mass basis) at 1050 ^oC was 2.4 times that of arC_7, 3.3 times that of nC_7, 3.9 times that of nC_4, 5.3 times that of C_2 and 13.2 times that of the iC_4 hydrocarbon. It is also apparent from Figure 6.7b that the WC – PAHs decreased with increasing carbon number of the hydrocarbon at the temperature of 1150 ^oC.

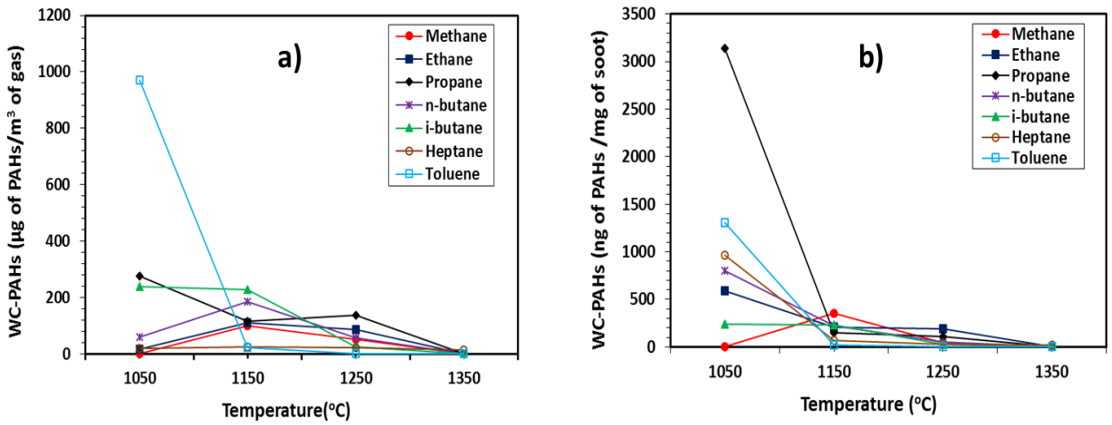

Figure 6.7: Normalised Weighted Carcinogenicity: a) weighted carcinogenicity of PP PAHs (µg of PAH/m3 of gas) b) weighted carcinogenicity of PP PAHs (ng of PAH/ mg of soot).

It is interesting to note that the trend of the WC-PAHs in Figure 6.7b, reflects that for soot particle number concentrations in Table 6.3. This analogy could mean

that increasing carcinogenicity of soot particles is not only dependent on the mass of soot particles, but also on their number. Individual PAHs contributing to the WC - PAHs on soot mass basis are shown in Table 6.6. In Table 6.6, the contribution of Group D PAHs (low ring number and relatively low carcinogenicity factors) to the WC-PAHs stands out as being relatively small, either because those PAHs were not detected (nd) on the soot extracts or their concentrations on the soot particles were low. Group D PAHs have higher vapour pressure (0.0006 – 10.4 Pa at 25 ^{o}C) and lower boiling points (218 – 404 ^{o}C) relative to Group B2 (boiling of 435 – 536 ^{o}C), which may have reduced their condensation rates on the soot particles (Dandajeh *et al.*, 2017).

Closer inspection of Figures 6.7a and b shows that aromatisation in the C_7 hydrocarbons increased the toxicity of soot particles at a temperature of 1050 ^{o}C, but the converse can be observed at the temperature range of 1150 to 1350 ^{o}C. Figure 6.7a shows that the WC-PAH of iC_4 soot particles within temperatures of 1050 to 1150 ^{o}C is higher than those for nC_4, suggesting that isomerisation of the C_4 hydrocarbon is significant in contributing to the abundance of Group B2 PAHs. Again, as in the case of aromatisation of the C7 hydrocarbons, the opposite is true for the C_4 isomerised hydrocarbon when the temperature was increased from 1250 to 1350 ^{o}C. A potential implication of these observations is that hydrocarbons with higher carbon number, which are known to have higher cetane numbers and shorter ignition delays in compression ignition engines (Koivisto et al., 2015), produce substantial particulate mass, but the PAHs on the particulates are generally of lower toxicity. However, where diesel fuel ignition delays decrease, this can also reduce in-cylinder temperatures, which might be expected to increase the WC-PAHs in Figure 6.7b.

6.6 Conclusions

The conclusions from the results reported can be summarised as follows:

- Increasing carbon number of C_1 – C_7 hydrocarbons was observed to increase their propensities to form soot particles in the effluent gas (nitrogen) at all temperatures investigated, except for heptane which was observed to be outside this trend.

- Methane pyrolysis was observed to have the smallest number of primary soot particles at the temperature of 1050 ^{o}C when compared with most of the C_2 – C_7 hydrocarbons. At the lowest temperature of 1050 ^{o}C, the particle average size for toluene (308 nm) was roughly similar to that produced at the highest temperature of 1350 ^{o}C by the C_1 – C_7 aliphatic hydrocarbons.
- Increasing temperature of the reactor from 1050 – 1350 ^{o}C, decreased the total PAH concentrations regardless of the carbon number of the hydrocarbons investigated.
- Increasing carbon number from C_1 to C_7 decreased the gas phase PAH concentration at the temperature of 1350 ^{o}C. Similarly, the particulate phase PAH concentration (including those of the Group B2 PAHs) decreased at a temperature of 1150 ^{o}C when the carbon number was increased from C_1 to C_7. No clear trends were observed at temperatures of 1050 and 1250 ^{o}C.

- The total PAH concentrations tended to increase with increasing carbon number (excluding heptane) at the temperature of 1050 ^{o}C but an opposite (decreasing) trend was observed at 1350 ^{o}C.
- Isomerisation in the C_4 hydrocarbons and aromatisation in the C_7 hydrocarbons increased substantially the soot propensities, the abundance of particle phase PAHs and carcinogenicity on volume of gas basis at the temperature of 1050 ^{o}C.
- Toluene and propane soot particles had the highest weighted carcinogenicities at the temperature of 1050 ^{o}C on gas volume and soot mass bases respectively. At the temperature of 1150 ^{o}C, the weighted carcinogenicity (soot mass basis) was observed to decrease with increasing carbon number of the hydrocarbon.

Chapter 7

7. Influence of combustion characteristics and fuel composition on exhaust PAHs in a compression ignition engine

This chapter describes an investigation into the effects of fuel composition on the exhaust PAHs in a compression ignition engine. The approach adopted involved collecting exhaust particulate matter and gas phase PAHs from a single cylinder, light duty, diesel research engine which was based on a commercial, high speed, automotive engine. The engine was operated at both constant fuel injection and constant fuel ignition modes. The fuels employed were fossil diesel and a number of model binary fuels prepared by blending various proportions of toluene into heptane. PAHs from both the particulate and gas phase samples were extracted using an accelerated solvent extraction (ASE) system. The composition of the PAH extracts was analysed and quantified using gas chromatography coupled to mass spectrometry (GCMS). The PAHs studied were the US EPA 16 PAHs and emphasis was given to the carcinogenic Group B2 PAHs.

7.1 Introduction

While diesel engines are continued to be used due to their fuel economy and potential for high power output, they still suffer from high level of NOx and particulate emissions (Williams et al., 1989; Tancell et al., 1995; Dec, 2010). Even though the advent of EURO 6 emission legislation has so far aided the reduction of NOx and particulates levels via the incorporation of diesel particulate filters (DPF) and other after treatment systems in diesel engine, particulates emission

is still of great concern in terms of health effects (Ã, 2008;Tree and Svensson, 2007; Borrás et al., 2009). The health effect of diesel particulates is principally owing to the polycyclic aromatic hydrocarbons (PAHs) associated with them.

PAHs, which are not directly regulated by diesel emissions regulations, are known human carcinogens (Dec, 2010; Richter and Howard, 2000). They are precursors to soot particles and abundant in atmospheric aerosols (Ballesteros et al., 2010). Coarse soot particles of diameters (Dp) < 10µm could be deposited in the superior respiratory airways, while Inhalable particles at sub-micron levels and bearing carcinogenic-PAHs could be deposited into the human lung pulmonary alveoli of an individual causing various health complications (Pedersen *et al.*, 1980).

PAHs can be found as constituents of fossil fuels (*petro-genic PAHs*) (Aakko, 2005; Collier et al., 1995) and they also are generated during combustion (*pyrogenic* PAHs) (Ang et al., 1985; Kado et al., 2005). Evidence has long been available on the survival of petro-genic PAHs during combustion and their tendency of being carried over to the engine exhaust (Williams et al., 1989; Tancell et al., 1995; Rhead and Hardy, 2003). This mostly happens to fossil fuels such as diesel fuel which contains significant proportions of aromatic compounds, including PAHs. In the case of pyrogenic PAHs, their formation involves complex series of reactions which often begins with the formation of the first aromatic ring, as a result of fuel breakdown, and culminating in the formation of fused aromatic ring structures and PAHs through various reaction pathways (Frenklach, 2002; Shukla and Koshi, 2011). Emission quantities of pyrogenic PAHs depend on the engine operating conditions (Borrás et al., 2009 ; Vojtisek-Lom et al., 2015) and the type of fuel used (Pedersen et al., 1980 ; Lim et al., 2005).

Fossil fuels with high poly-aromatic content have been reported to promote PAH formation (Aakko, 2005 ; Mi et al., 2000). However, no definitive conclusions have been reached, as yet, regarding the effect of fuel mono- aromatic content on the formation of PAHs. Divergent views in the literature on the effect of total aromatic content of fuels on PAH formation exist among researchers, as outlined in chapter 2 of this thesis.

Research published in the literature leads to the conclusion that the poly-aromatic content of fuels has greater effect on the exhaust PAHs than the total aromatics, but the extent to which the total aromatic content in the fuels affects PAH formation is not fully established. It is still not clear from the literature whether the total aromatics in the fuel influences the Group B2 PAHs (*PAHs that are possible human carcinogens as classifiable by the US EPA*).

7.2 Test Fuels

The test fuel for the engine experiments included a reference fossil diesel (Haltermann Carless Ltd, UK), heptane, toluene and methyldecanoate (Sigma Aldrich, UK). The molecular structures of these test fuels are shown in Table 7.1. The fossil diesel fuel had 22.2 % total aromatics and 3.4 % by mass of poly-aromatic contents. The properties of the test fuels are shown in Table 7.2; while other properties of the reference diesel fuel are listed in A 7 in Appendix A.

Table 7.1: Fuels and Additive.

Fuel and Additive	Structure
Heptane	
Toluene	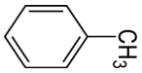
Methyl-decanoate	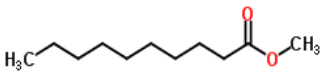
2 Ethylhexyl nitrate (2-EHN)	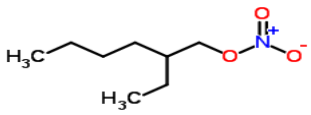

In view of the complex composition of the fossil diesel fuel, heptane was also used for comparison of the results with fossil diesel fuel. Heptane has cetane number close to that of the diesel fuel (see Table 7.2) and there is a significant body of information in the literature on PAH chemistry for heptane as well as for toluene (Mi et al., 2000 ; Sivaramakrishnan et al., 2004). Aromatics constitute substantial proportion of commercial diesel fuel and toluene is a model to several of these aromatics; therefore, heptane/toluene blends have been recommended

as convenient model fuels for compression ignition engines (Wei et al., 2014; Luo et al., 2012). The specifications of the diesel engine used can be found in chapter 3 of this thesis.

Table 7.2: Properties of test fuels (Po et al., 2016; Hellier et al., 2013; Knothe, 2008).

Fuel Properties	Diesel	Heptane	Toluene	Methyldecanoate
Assay (%)	-	99	> 99.8 (GC)	> 99
Fuel Nomenclature	Diesel	H	T	MD
H/C Ratio	1.771	2.28	1.143	2
PAH Content (% mass)	3.4	-	-	-
Boiling Point (^oC)	271.0[a]	98.3	110.6	224
Density (g/mL, 20 ^oC)	0.835	0.684	0.867	0.871
Cetane Number	52.7	54.4	7.4	51.6
Lower heating value (MJ/kg)	43.14	44.5	40.6	36.7

[a] Point of 50% (v/v) recovery obtained according ASTM D86

7.2.1 GC-MS Analysis of PAHs in Reference Diesel Fuel and Lubricating Oil

Qualitative PAH analysis of the diesel fuel (Haltermann Carless), used in this work, was carried-out on the GC-MS prior to the analysis of the pyrogenic exhaust PAHs. A sample of 1,000 ppm of diesel fuel, diluted in dichloromethane, was run on the GCMS. The GC-MS results from the sample showed that, out of the 16 EPA priority PAHs, only naphthalene and fluorene were present in the reference diesel fuel. Other PAHs detected were mainly alkylated species and not members of the 16 EPA PAHs. Previous analysis conducted by He et al. (2010a) and Williams et al. (1989) also detected similar PAHs, but with further detection of phenanthrene and anthracene reported by He et al. (2010a) and Williams et al. (1989) respectively. A wider range of PAHs in diesel fuel was recently reported by Lea-Langton et al. (2013), who identified 7 PAHs, ranging serially (see Table 2.1) from naphthalene to pyrene, but excluding fluoranthene.

A GC run of 1,000ppm each of fresh and used lubricating oil (Castrol Magnetic, SAE 10W-40) samples were also qualitatively analysed as part of the work

reported in this thesis. No PAHs were identified in both the fresh and used lubricating oil. The primary reason for not identifying PAHs in the lubricant is that it only spent a short period of time in the engine; it was previously reported in the literature by Pedersen et al. (1980) that the PAH content in the used lubricant is usually generated during engine usage. Pedersen et al. (1980) reported zero PAH content in an un-used lubricating oil, but some relatively high PAH concentrations due to the continuous use of the lubricant. Pedersen et al. also reported that the amount of exhaust PAHs contributed by the lubricating oil increased with the time of use of the lubricant. Therefore, it is considered un-likely that petro-genic PAHs from the lubricant used in this work contributed significantly and directly to the pyrogenic exhaust PAHs. However, it should be noted that petro-genic PAHs such as chrysene were reported by Grimmer et al. (1981) in both fresh and used lubricants.

7.3 Experimental Layout

Mixtures of single/binary/tertiary fuels were formulated by blending toluene and methyldecaoate into heptane. The proportions of toluene and methyldecoante (on volume basis) added to heptane are shown in Table 7.3. The highest proportion of toluene adopted in the fuel mixtures was 22.5 % and is similar to the percentage of mono-aromatics in commercial diesel fuel (Aakko, 2005). Fuel mixtures were combusted in the diesel engine and their ignition delays were noted. To assess the influence of ignition delay on exhaust PAHs, equalisation of ignition delay durations for different blends was achieved by applying a given amount (in ppm) of an ignition improving additive (2-ethylhexylnitrate) to the fuel mixtures. For example, it can be seen in Table 7.3 that 850 and 1500 ppm of 2-EHN were added to 77.5%H22.5%T to reach ignition delays of 9.8 and 9.4 CAD respectively.

The equalised ignition delays only differed by the resolution of the engine shaft encoder (0.2 CAD) used for measuring engine in-cylinder pressure. The necessary dosages of the ignition improver that was added to the heptane/toluene mixtures to equalise ignition delay was found using an iteration procedure.

Table 7.3: Experimental matrix for the test fuels run in a CI engine at a constant IMEP of 7 bar and a fixed speed of 1200 rpm.

Blend number	Fuel/ Fuel Blend	Ignition Delay (CAD)	2-EHN Dosage (ppm)	Ignition Delay after addition of 2-EHN (CAD)
0	Diesel start	9.4	-	-
1	100%H	9.4	-	-
2	85%H15%T	9.8	400	9.4
3A	77.5%H22.5%T	10.8	850	9.8
3B			1500	9.4
4	65%H15%T20%MD	9.8	-	-
0	Diesel Finish	9.4	-	-

The molecular structures of the fuels shown in Table 7.1 and the experimental conditions outlined in Table 7.3 allowed the following objectives to be achieved:

i) Assess the combustion characteristics of the single/binary/tertiary fuels at constant injection and constant ignition timings.

ii) Calculate the percentage of premixed and diffusion combustion phases from the combustion of heptane/toluene/methyldecanoate mixtures.

iii) Characterise the particulates produced from the combustion of the fuel mixtures in (i) in terms of mass, number and size using DMS 500 instrument

iv) Highlight the PAH distributions of fuel mixtures in (i) from diesel engine and understand the influence of combustion characteristics of the fuels on PAH emissions.

v) Determine the effect of ignition improver on the concentrations of gas phase and particulate phase PAHs

vi) Assess the influence of ignition delays and premixed burn fraction on the total PAH concentrations

vii) Evaluate the potential carcinogenicity of soot particles in diesel engine with and without addition of ignition improving additive.

7.4 Particulate generation in Diesel Engine

7.4.1 Experimental Set-up

The experimental facility of the diesel engine was described in chapter 3.

7.4.2 Experimental Conditions

Two sets of experiments were conducted at a constant IMEP of 7 bar, a fixed engine speed of 1200 rpm and a constant fuel injection pressure of 450 bar:

i) Constant injection timing tests were conducted on the engine with start of fuel injection at 10 crank-angle-degrees (CAD) before-top-dead-centre (BTDC).

ii) Constant ignition timing tests were conducted by maintaining the 10^{o} CAD BTDC injection timing but in addition, by adding 2-EHN to the fuels to equalise the ignition delays.

7.4.3 Characterisation and sampling of particulates

Particulates in the diesel engine exhaust were characterised at sub-micron levels using a differential mobility spectrometer (Cambustion DMS 500), which gave real time outputs of particle mass, number and size. The exhaust gas was sampled by the DMS500 about 300 mm downstream of the engine exhaust valves and conveyed to the particulate analyser (DMS500) via a heated line maintained at 80 °C. Tables 7.4 and 7.5 show the summary of the soot particle mean diameter and particle surface area as measured by the DMS 500 instrument.

Exhaust gas was also extracted about 1000 mm downstream of the engine exhaust by means of a half-inch diameter stainless steel probe connected to a vacuum pump; this sample, which had a steady flow rate of 40 L/min, was passed through a particle and gaseous PAH collection system. The system comprised a particulate filter followed by a resin cartridge for collection of particulate and gaseous PAH respectively. Detailed description of the engine sampling systems have been described previously in chapter 3 of this thesis. For each test fuel, two

samples for both particulates and gas phase PAHs were collected. The gravimetric filter mass measurements (M_s, mg) from the engine exhaust and calculated soot mass concentration (M_s/V_g, mg/ m^3) of all the fuels tested are shown in Tables 7.4 and 7.5. Where V_g (m^3) is the cumulative volume of gas that passed through the particulate and resin measured at each test condition using a cumulative volumetric gas meter.

Table 7.4: Filter soot mass measurements without 2-EHN.

Fuel	soot mass (M_s) (mg)	soot concentration (M_s/V_g) (mg/m^3)	particle mean diameter (D_p) (nm)	soot surface area ($\mu m^2/cm^3$)
100%H	23.0	48.0	176	2720005
85%H15%T	19.3	40.0	178	1865106
77.5%H22.5%T	23.5	45.0	181	2367265
65%H15%T20%MD	6.90	13.7	160	1210826
Reference Diesel	28.7	58.0	177	1846044

Table 7.5: Filter soot mass measurements with 2-EHN.

Fuel + 2-EHN (ppm)	soot mass (M_s) (mg)	soot concentration (M_s/V_g) (mg/m^3)	particle mean diameter (D_p) (nm)	Soot surface area ($\mu m^2/cm^3$)
77.5%H22.5%T + 1500ppm	13.7	28.9	171	1889521
85%H15%T + 400ppm	16.6	34.3	171	1833473
77.5%H22.5%T + 850ppm	14.8	30.8	178	1841702

7.5 Sample Preparation/GCMS Analysis

The sample preparation has been described previously in chapter 4 and included sample extraction and solvent evaporation, as well as GCMS analysis.

7.6 Error Analysis

Engine test and subsequent PAH analysis for each test fuel listed in Table 7.3 was repeated twice and the average value of the test parameter is reported in this work. A reference fossil diesel was tested at the start and end of each daily test. These repeats produced daily variabilities in engine performance and instrumentation as well as provision of baseline data for comparison with the results of the fuel blends. The cumulative standard deviations (δ) of the parameters investigated were thus generated from results of the diesel fuel repeats. Table 7.6 shows the summary of the percentage variations (100% δ/mean) for all the parameters examined. The results that will be discussed in section 7.6 will therefore be subject to the variabilities shown in Table 7.6.

Table 7.6: Percentage Variations (100% δ /mean) for the test parameters investigated.

Parameter	Percent Variation (±%)
Soot concentration, M_s/V_g (±mg/m^3)	18
Peak heat release rates (±J/s)	2.4
Peak in-cylinder pressure (±bar)	0.7
Particle Number, dN/dD_p (±1/cm^3)	15
GP PAHs (±µg of PAH/m^3 of gas)	17
PP PAHs (±µg of PAH/m^3 of gas)	29
PP PAHs (±ng of PAH/mg of soot)	0.2
Total PAHs (±µg of PAH/m^3 of gas)	19

7.7 Results and Discussion

7.7.1 Combustion characterisation at constant injection timing

This section presents combustion characterisation of the test fuels listed in Table 7.3. The experiments were carried out at start of fuel injection (SOI) of 10 CAD before TDC. Figures 7.1a and b show the profiles of the in-cylinder pressures and apparent heat release rates for the test fuels respectively. Table 7.7 shows an

analysis of the main combustion parameters for the various fuels investigated. It can be seen from Figure 7.1a that the 85%H/15%T and 65%H15%T20%MD blends, both having ignition delay (ID) of 9.8 CAD (see Table 7.7), showed the highest peak in-cylinder pressure of 69.3 bar relative to the other fuels investigated. Also visible in Figure 7.1b, is the identical peak heat release rates (69.8 J/s) of the 85%H/15%T and 65%H15%T20%MD blends. As one might expect, the identical ignition delay of these fuels resulted in similar values of peak heat release rate and percentage of premixed fuel burned. These results suggest that replacing 20% by volume of a C_7-heptane, with 20% of methyl-decanoate (an oxygenated C_{11} molecule) does not affect ignition delay and, therefore, the peak in-cylinder pressure and peak heat release rates. Another possible inference might be that the proportion of toluene (15%) in both blends could be responsible for the identical peak in-cylinder pressure and peak heat release rates.

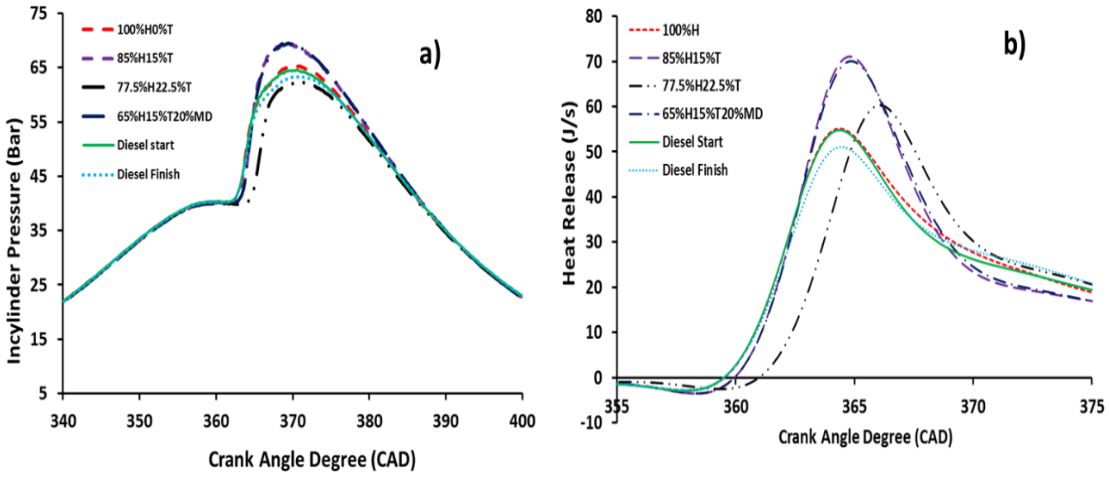

Figure 7.1: Profiles of: a) in-cylinder pressure (bar) b) apparent heat release rate (J/s) for the single/binary/tertiary fuel blends and a reference diesel fuel run in CI engine at speed of 1200 rpm and IMEP of 7 bar.

It can also be seen from Figure 7.1 that the binary mixtures of 77.5%H/22.5%T exhibited the least in-cylinder pressure (63.2 bar) and the second highest peak heat release rate (60.3 J/s), which are consistent with the observation in Table 7.7 that this mixture had the longest ignition delay of 10.8 CAD. Lower peak heat release rate of the 77.5%H/22.5%T blend can be attributed to a start of combustion after TDC, which resulted in heat release at larger in-cylinder

volumes and higher rates of heat transfer to the cylinder walls (Hellier *et al.*, 2013).

It is noteworthy to mention that increasing the amount of toluene from 15 to 22.5% in the heptane/toluene mixture increased the ignition delay by 0.4 CAD due to decrease in reactivity of the mixture with increased toluene. Toluene has higher density and boiling point than heptane (see Table 7.2). The increased in ignition delay is consistent with results from previous studies (Hellier et al., 2013; Di Sante, 2012; Xiao et al., 2000; Andrae et al., 2005). For example, Hellier et al. (2013) researched binary mixtures of heptane/toluene blends in a direct injection compression ignition engine at toluene levels up to 52% (wt/wt). They reported increased ignition delay by 0.5 CAD due to increase in amount of toluene from 10 to 20% in heptane/toluene blends. (Di Sante, 2012) also reported increased ignition delay times with increasing volume of toluene in heptane/toluene mixture measured in a rapid compression machine.

Observations during the experiments showed consistently that increasing toluene level up to 22.5% into heptane/toluene blend inhibited the ignition process significantly. This hindrance of ignition due to toluene addition can be explained using the results of previous studies (Andrae et al., 2005;Wang et al., 2015). It was reported that toluene can be oxidised at low temperatures through abstraction of hydrogen atom (H) by either OH radicals or oxygen molecule (O_2) to form benzyl radicals (Andrae *et al.*, 2005). These reactions are shown below in $R_{7.1}$ and $R_{7.2}$ respectively. The benzyl radicals react further with oxygen atom (O) to form phenyl radicals in reaction $R_{7.3}$ (Wang et al., 2015).

$$C_6H_5CH_3 + OH \rightarrow C_6H_5CH_2 \text{ (benzyl)} + H_2O \qquad R_{7.1}$$

$$C_6H_5CH_3 + O_2 \rightarrow C_6H_5CH_2 \text{ (benzyl)} + HO_2 \qquad R_{7.2}$$

$$C_6H_5CH_2 + O \rightarrow C_6H_5 + CH_2O \qquad R_{7.3}$$

$$C_7H_{16} + O_2 \rightarrow C_7H_{15}O + OH \qquad R_{7.4}$$

It may appear therefore that H-abstraction from n-heptane by O_2, shown in reaction $R_{7.4}$, could be the only possible source of OH radicals that was consumed by toluene in $R_{7.1}$. Reaction $R_{7.4}$ is considered to be the first step in radical

branching, which is important part of ignition chemistry of long alkyl chains and which marks the start of large increase in heat release and ignition of the air/fuel mixture (Westbrook, 2000). Inferences from the preceding reactions suggest that toluene can delay the start of combustion by consuming radicals in reaction $R_{7.1}$ which would otherwise be used to propagate the reaction of heptane in the heptane/toluene blend.

Returning now to Figure 7.1, two fuels of the fossil diesel and 100% heptane (pure heptane) in Figures 7.1a and b exhibited the same peak in-cylinder pressure and peak heat release rate and identical ignition delay of 9.4 CAD. This result was also reported in previous studies (Hellier *et al.*, 2013) and is expected, since both the reference fossil diesel and pure heptane have cetane numbers and lower heating values which are way close to each other (see Table 7.2). However, the reference diesel run at the end of each daily test schedule demonstrated slightly lower in-cylinder pressure and heat release rates; 1.2 bar and 4J/s, respectively, lower than those of the fossil diesel. These test to test variations were largely due to the daily drift in the engine performance.

Taking Figure 7.1 as a whole, it is apparent that increasing the volume of toluene in the heptane/toluene mixture from 0 to 15%, resulted in slight increase in the peak cylinder pressure and peak heat release rate by approximately 4 bar and 16 J/s respectively. Additional increase in the proportion of toluene from 15 to 22.5% in the heptane/toluene mixture, decreased slightly, the peak cylinder pressure and peak heat release rate by approximately 7 bar and 11 J/s respectively. These results are consistent with the corresponding increase in ignition delay, as the percentage of toluene in the blends was increased, and are in agreement with the results of previous studies at constant injection timings (Hellier *et al.*, 2013).

An increased duration of ignition delay allows more time for fuel and air pre-mixing prior to the start of combustion and thus, larger premixed burn fraction. The proportion of premixed phase was defined by Heywood (1988) as the “combustion of fuel and air mixture to combustible stoichiometry during the ignition delay period”. Proportions of premixed and diffusion phases were calculated using Eqs.7.1 and 7.2 respectively. Table 7.7 shows a trend of

increasing proportions of premixed phase and decreasing diffusion phase when the percentage of toluene blended into heptane was increased. The main reason for this is the increasing ignition delay which allows for greater period for air/fuel mixing to occur and a greater amount of premixed mixture to be ready for combustion upon ignition. In addition, higher viscosity and density of toluene, in comparison with heptane, was reported to decrease the rate of air and fuel mixing for toluene (Hellier *et al.*, 2013), hence, increased heptane percentage of premixed phase.

Table 7.7: Proportions of premixed and diffusion phases of fuels without 2-EHN.

Fuels with no EHN	ID	CAD_{switch}	$CHRR_{switch}$	$CHRR_{max}$	%Premixed	%Diffusion
100%H	9.4	370.8	2628	4325	61	39
85%H15%T	9.8	372.6	2992	4323	69	31
77.5%H22.5%T	10.8	373.2	3096	4360	71	29
65%H15%T20%MD	9.8	372.6	3021	4319	70	30
Diesel Start	9.4	370.2	2503	4394	57	43
Diesel Finish	9.4	370.8	2526	4380	58	44

$$\text{Premixed Phase (\%)} = \frac{\text{CHRR}_{\text{swich}}}{\text{CHRR}_{\text{max}}} \times 100 \qquad \text{Eq.7.1}$$

$$\text{Diffusion phase (\%)} = \frac{\text{CHRR}_{\text{max}} - \text{CHRR}_{\text{swich}}}{\text{CHRR}_{\text{max}}} \times 100 \qquad \text{Eq.7.2}$$

Where; CAD_{switch} is the crank angle degree at the point of switch from premixed to diffusion phase, $CHRR_{switch}$ is the cumulative heat release rate at the point of switch from premixed to diffusion phase and $CHRR_{max}$ is the maximum cumulative heat release rate.

Combining the observations from Figure 7.1 and Table 7.7 together, one could deduce that the highest heat release rates occur during premixed combustion. This can be noticeable from the speedy rise and subsequent decline in profiles of heat release rates after the fuel ignited. It is also evident that greater ignition

delay causes a greater proportion of the fuel to be burned during the premixed combustion phase.

7.7.2 Combustion characteristics at constant ignition timing

To isolate the effect of ignition delay of the heptane/toluene mixtures, an ignition improving additive 2-ethylhexyl nitrate (2-EHN) was used to equalise the ignition delays of the various heptane/toluene blends. Dosages of 2-EHN added to the heptane/toluene mixtures to achieve identical ignition delays are shown in Table 7.3. Removing the influence of varying periods of ignition delay allows other influences such as those of the physical properties of the fuels to be investigated.

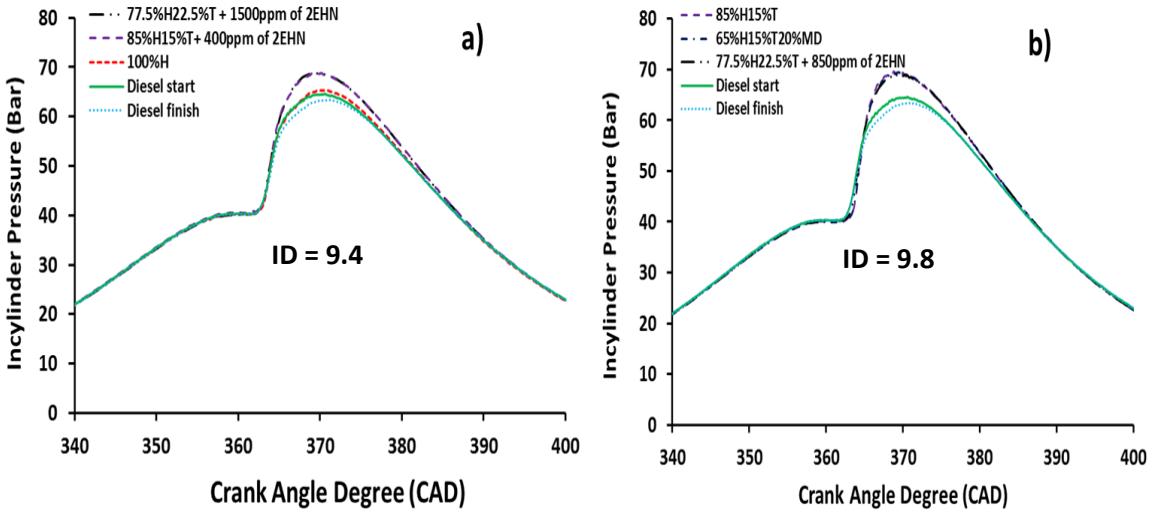

Figure 7.2: Profiles of in-cylinder pressures (bar) at constant ignition delays (ID): a) ID = 9.4 b) ID = 9.8.

Figures 7.2a and b show the profiles of in-cylinder pressure at constant ignition delays of 9.4 and 9.8 respectively. The figures show that equalising the ignition delay of the heptane/toluene blends resulted in identical peak in-cylinder pressures. For example, the peak in-cylinder pressure in Figures 7.2a and b at ignition delays of 9.4 and 9.8 CAD are 69.2 and 68.8 bar respectively. This observable feature of equal peak in-cylinder pressures (as well as pressure profile) suggest that the pressure profile and its peak pressure are influenced primarily by ignition delay and, thereby, the percentage of premixed combustion, with other fuel properties (such as physical properties) having only a secondary and apparently insignificant influence.

Figures 7.3a and b show the profiles of heat release rates at constant ignition delays of 9.4 and 9.8 CAD respectively. As it was observed previously, in the case of in-cylinder pressure, it can also be seen in Figure 7.3 that peak heat release rates of the heptane/toluene blends with 2-EHN is also similar, but this does not seem to apply in the case of fuels with ID of 9.8 CAD. This inconsistency was due primarily to the ignition delays of the fuels not being identical, and it is possibly due to the resolution of the shaft encoder (0.2 CAD) used in measuring the in-cylinder pressure.

Comparing Figure 7.1a and Figures 7.2a and b, it can be observed that, under high load (IMEP of 7bar), the peak in-cylinder pressure is slightly higher in those fuel mixtures with 2-EHN. This finding was also observed by Li et al. (2014) in methanol/biodiesel blend and is anticipated since 2-EHN could produce chain initiation/pre-ignition radicals via thermal decomposition (Higgins et al., 1998).

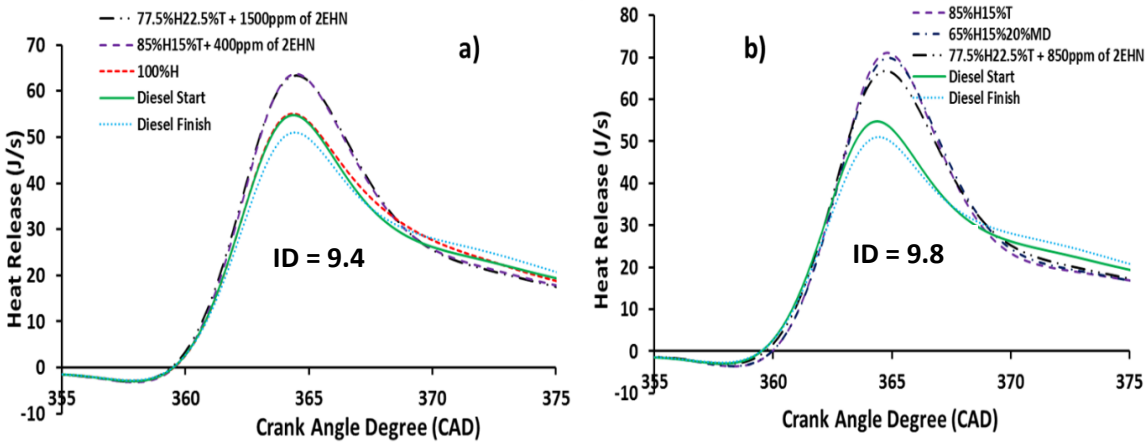

Figure 7.3: Profiles of heat release rates at constant ignition delays (ID): a) ID = 9.4 b) ID = 9.8.

Typically, the C-H and C-C bonds in the heptane/toluene blends have higher bond energies than those of C-O and N-O in the 2-EHN (Li *et al.*, 2014). After addition of 2-EHN to the heptane/toluene, the C-O and N-O bonds in the 2-EHN may be dissociated prior to the C-H and C-C bonds in the fuel blend, thereby culminating to earlier ignition reactions with liberation of large amount of energy (Toland and Simmie, 2003; Ghosh, 2008; Kidoguchi et al., 2000).

Table 7.8 shows that the fuel blends with equal ignition delays exhibited very similar percentages of premixed burnt fraction (within 1% difference). For instance, fuel blends with ID of 9.4 CAD, exhibited proportion of premixed phase

within the range of 61 - 62%, while those with ID of 9.8 CAD showed proportion of premixed phase within the range of 69 - 70%. Comparing the results of the percentage of premixed phase in Tables 7.7 and 7.8, it can be seen that adding 2-EHN to the fuel blends, did not only lower the ignition delay, but also shortened the proportions of premixed burnt fraction. This result agrees well with other earlier works (Jian-guang et al., 2013).

Table 7.8: Proportions of premixed and diffusion phases of fuels with 2-EHN.

Fuels + 2-EHN (ppm)	ID	CAD_{switch}	$CHRR_{switch}$	$CHRR_{max}$	% Premixed	% Diffusion
77.5%H22.5%T + 1500ppm	9.4	370.2	2694	4363	61	39
85%H15%T + 400ppm	9.4	370.2	2724	4367	62	38
100%H	9.4	370.8	2628	4325	61	39
77.5%H22.5%T + 850ppm	9.8	372.8	3013	4335	70	30
85%H15%T	9.8	372.6	2992	4323	69	31
65%H15%20%MD	9.8	372.6	3021	4319	70	30

7.7.3 Soot formation characteristics at constant injection and ignition timings

The profiles of soot particle number concentrations for the test fuels, sampled using the DMS500 particle spectrometer, are shown in Figure 7.4. Figures 7.4a and b present the distributions of soot particle number concentrations of the fuels without and with 2-EHN, respectively. Figure 7.4a shows that the soot particle sizes for all the fuels ranged from 30 – 360 nm without 2-EHN and, similarly, the range 13 – 316 nm when 2-EHN was added to the fuel blends.

The mean soot particle size and the soot volume-normalised surface area ($\mu m^2/cm^3$) of each test fuel with and without 2-EHN are also shown Tables 7.4 and 7.5 respectively. It is apparent from Table 7.4 that toluene addition to heptane increased slightly the mean size of the soot particles generated; from 176 nm for 100%H to 178 nm and 181 nm for 85%H15%T and 77.5%H22.5%T respectively.

Increasing soot mean particle sizes subsequent to toluene addition to heptane was also reported by Wei et al. (2014) for in-cylinder soot generated from toluene/n-heptane combustion in a diesel engine. Table 7.4 also shows the gravimetric filter measurements of soot masses (M_s) and calculated soot concentrations (M_s/V_g) of the test fuels as sampled from the engine exhaust; where V_g is the cumulative volume of gas that passed through the particulate and the XAD-2 resin in series. It is pertinent to note here that the trend of the soot mass concentration based on the gravimetric filter soot mass measurements is consistent with the trend of soot mass concentration measured using the DMS500 instrument.

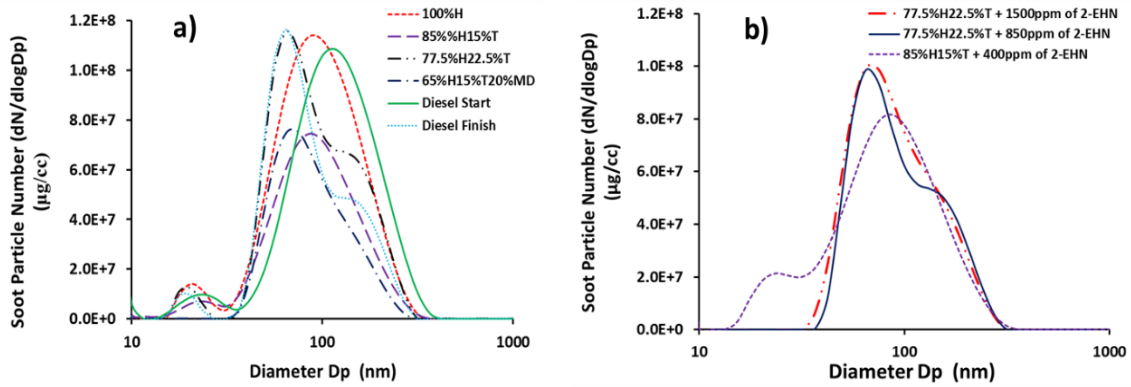

Figure 7.4: Distribution of soot particle number concentrations (dN/dLogDp (cm-3)) for the fuel blends and reference diesel fuel a) without 2-EHN b) with 2-EHN.

Table 7.4 shows that the soot mass concentration of heptane/toluene blend increased from 40 to 45mg/m^3 when the proportion of toluene in heptane was increased from 15% to 22.5%. The soot concentration of 48 mg/m^3 for 100%H was unexpectedly high and should be interpreted with caution. Table 7.4 shows a drastic reduction in soot concentration by 66%, mean particle size by 10% and soot surface area by 35%, when the 20% (by volume) of a C_7 heptane in 85%H15%T blend was replaced with 20% (by volume) of a C_{11} methyl-deconoate (an ester molecule). This result was as expected since oxygenated fuels, such as alcohol and esters, were reported to have much lower particulate emissions when burned in an internal combustion engines, compared with their alkanes/aromatic counterparts (Koivisto et al., 2015a ; Koivisto et al., 2015b).

Generally, pyrolysis of n-heptane leads to generation of large quantities of C_2- C_6 species such as acetylene and propargyl radicals (Ding et al., 2013) which are

highly instrumental in the formation of the first aromatic ring (Richter & Howard, 2000) and subsequent PAH/soot surface growth. Adding 15 % of toluene to heptane (85%H15%T) raised the soot concentration by 10.6 times at a temperature of 1050 ^{o}C, 2.25 times at 1150 ^{o}C, 1.54 times at 1250 ^{o}C and 1.69 at 1350 ^{o}C. This result confirmed that toluene, as an aromatic molecule, is a promoter of soot formation. Some backing to this finding from the literature is the study of Alexiou and Williams (1995) using reflected shock-tube pyrolysis, who reported a decrease in the soot propensity of toluene, when heptane was blended into it. Toluene is a prolific sooter owing to its nucleation rate increasing exponentially with temperature (Division D, 2009). Additionally, toluene pyrolysis is associated with abundance of C_2 - C_6 radicals including acetylene, propargyl and phenyl radicals (Zhang et al., 2010) and blending it into heptane can be expected to increase the radical pool that would serve as soot precursors; hence the subsequent increase in soot yield.

Furthermore, the fact that toluene is an abundant source of phenyl-radicals, via de-methylation, could trigger PAH growth by the phenyl-addition and cyclisation (PAC) pathway (Shukla *et al.*, 2008) and consequently accelerate the soot yield of the resulting heptane/toluene blend. The increased abundance of acetylene in toluene pyrolysis could also speed-up the growth of PAHs and soot surface growth via the well-known hydrogen-abstraction, acetylene, addition mechanism (HACA) (Frenklach, 2002). In diffusion flames however, Ladommatos et al. (1996) reported the soot propensity of toluene being substantially higher than heptane, with toluene having a threshold sooting index of 18.5 times higher than that of heptane.

Table 7.5 shows that adding 2-EHN to the heptane/toluene fuel blend decreased the mean soot particle diameter, soot surface area and, surprisingly, soot mass concentration. The decreasing trend of soot concentration after adding ignition improver is contrary to was reported in earlier works (Kidoguchi et al., 2000; Ladommatos et al. 1996). The reason for this discrepancy is not clear, since the experimental conditions employed in this work were different from those of Kidoguchi et al. (2000) and Ladommatos et al. (1996).

7.7.4 PAH Distributions in Diesel Engine at constant injection timing

This section focuses on the analysis of the EPA 16 priority PAHs collected from the diesel engine exhaust at constant fuel injection timing of 10 CAD BTDC, speed of 1200 rpm and load of 7 bar. Figure 7.5 shows the distributions of exhaust PAHs following combustion of the fuels shown in Table 7.3. Measured PAHs in the exhaust included both those in the gaseous phase as well as those on the particulate surfaces. The gaseous PAHs shown in Figure 7.5, were those extracted from the XAD-2 resin, and are designated as gas phase (GP) PAHs, whereas those PAHs extracted from the soot particles are designated as particle phase (PP) PAHs.

The mass of gas phase PAHs was normalised with the volume of gas (V_g) passed through both the filter and the XAD-2 resin (positioned in series with the filter), and is shown in Figure 7.5a. The mass of PAH extracted from the soot particles was also normalised with volume of gas (V_g) passed through the filter and the XAD-2 resin, and is shown in Figure 7.5b. Figure 7.5c shows the PAH mass extracted from the soot particles but this time normalised with the soot particle mass (M_s) (see Table 7.8). Lastly, Figure 7.5d shows the total PAH (sum of gas and particle phase) and this was normalised by the volume of gas (V_g) passed through the filter and the XAD-2 resin.

In Figure 7.5a, the most abundant exhaust PAHs found in the gas phase (GP) had 2 and 3 rings, irrespective of the fuel combusted. These PAHs included NPH, ACY, ACN, FLU, PHN and ATR. It is interesting to note the 6 most abundant PAHs listed are group D members and, therefore considered to be non-mutagenic. The total sum of these 6 PAHs in the GP accounted for the bulk of the total PAHs in the case of all the fuels. For example, 91 % in the case of the fuel 100%H, 94 % in the case of the fuel 85%H15%T, 91% in the case of the fuel 77.5%H22.5%T, 80 % in the case of the fuel 65%H15%T20%MD and 83% in the case of the fossil diesel fuel. These results of high proportions of the 6 PAHs (NPH, ACY, ACN, FLU, PHN and ATR) are consistent with those observed by He et al. (2010a) in a diesel engine fuelled with biodiesel and diesel.

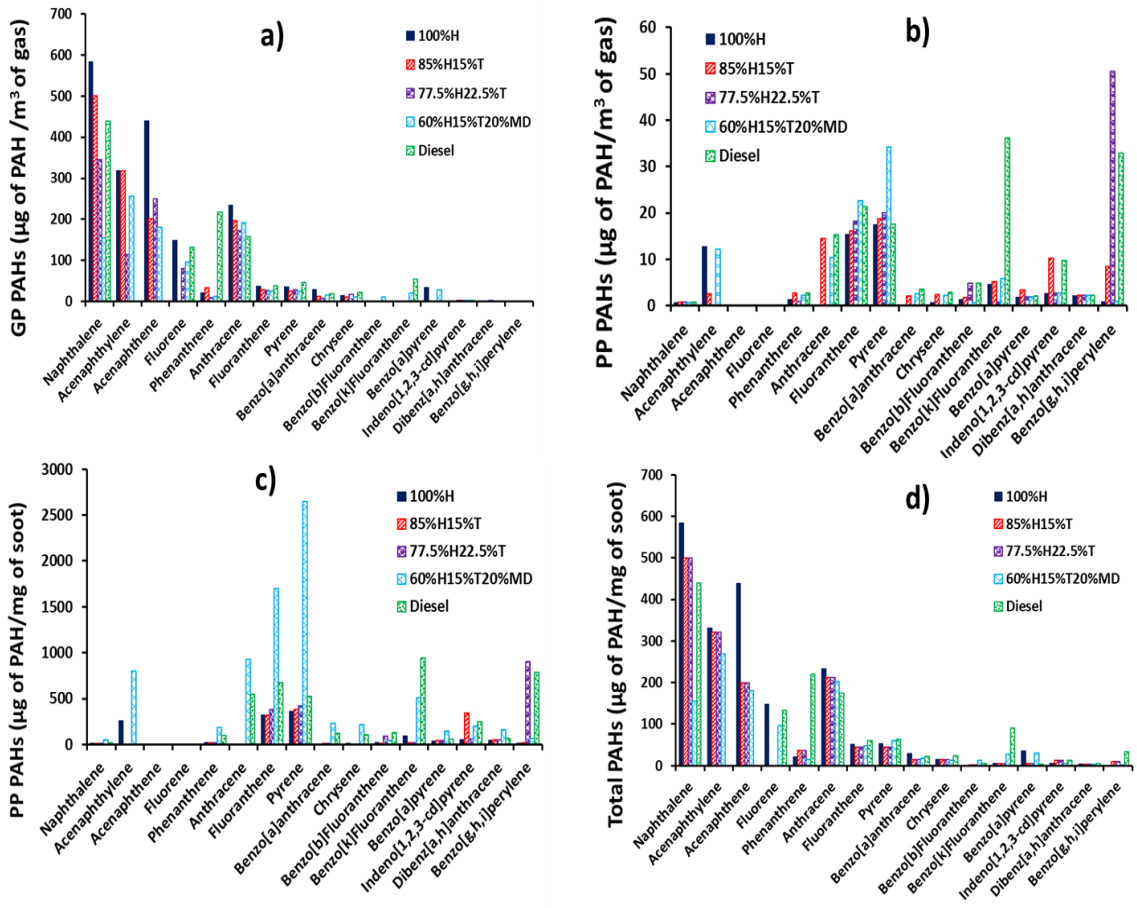

Figure 7.5: The distributions of exhaust PAHs in diesel engine: a) Gas Phase (GP) (µg of PAH/m3 of gas) b) Particle Phase (PP) (µg of PAH/m3 of gas) c) Particle Phase (ng of PAH/mg of Soot) d) Total PAHs (GP +PP) (µg of PAH/m3 of gas).

It is interesting to note that in Figure 7.5a, only four heavier PAHs having 4 and 5 rings (CRY, B(b)F, B(k)F and B(a)P) were detected in the GP in low concentrations, and these four PAHs are highly mutagenic (Group B2 members). It can be further observed in Figure 7.5a that the GP PAH concentrations decreased to near-zero when the number of PAH ring increased from 5 to 6 regardless of the fuel investigated. The observation of decreasing PAH concentrations in the GP with increasing molecular weight of the PAHs (increasing number rings) resembled those observed by Dandajeh et al. (2017) in a tube reactor at a temperature of 1050 ^{o}C and under oxygen free conditions.

Figure 7.5b shows that the 6 smaller PAHs with 2 to 3 rings (NPH, ACY, ACN, FLU, PHN and ATR) detected earlier in the gas phase at high concentrations (see Figure 7.5a) were now identified in the particle phase at low concentrations (lower by several magnitude). These results suggest that the 6 lighter PAHs might have

been consumed in the growth of larger PAHs and subsequently to soot. Conversely, Figure 7.5b shows that the concentrations of PP PAHs increased with increasing molecular weight of the PAH regardless of the fuel combusted. This result also matched with observations in tube reactors by Sánchez et al. (2012) and by Dandajeh et al. (2017).

Figure 7.5c presents the concentration of PAHs adsorbed on the soot particles per unit mass of soot. It can be seen from Figure 7.5c that the PP PAH mass increased with increasing proportions of toluene added to heptane. This result was anticipated since adding toluene to heptane could create more PAH formation routes which aid in PAH growth. Such reaction pathways include phenyl addition and cyclisation (PAC) (Shukla and Koshi, 2012a). The trend in Fig.7.5c further exhibits substantial increase in the PAH mass produced from diesel fuel combustion.

Abundance of PAHs produced from diesel combustion is not surprising, since the fossil diesel used in this work had up to 3.4 % PAHs (including naphthalene, fluorene and other alkylated PAHs). It is likely that the PAHs in the diesel fuel contributed to the pyrogenically formed exhaust PAHs. An example to support this conjecture is the fact that the total naphthalene and fluorene concentrations out of the total PAHs identified from diesel fuel combustion were unusually high; 34 % in the case of naphthalene and 10 % in the case of fluorene. The implication of the above findings could be that some of the naphthalene and fluorene originally present in the fossil diesel could have survived combustion. Several studies have highlighted the possibility of petrogenic PAHs in a fuel surviving combustion. For example, Rhead and Pemberton (1996) observed that 23.8% of the naphthalene detected in the exhaust of a direct injection diesel engine originated from the fuel combusted. Similarly, Tancell et al. (1995) also reported high PAH survival rates of fluorene (0.87%) and naphthalene (0.47%); and the survival rate of each PAH was found to proportionally increase with the energy level of the lowest un-occupied molecular orbital.

The concentrations of total PAH per unit volume of gas is shown in Figure 7.5d, and the figure corresponds to the sum of the gas phase PAHs in Figure 7.5a and the particle phase PAHs Figure 7.5b. It can be seen from Figure 7.5d that the

trend of the total PAH mass resembles to a significant extent, those of the GP PAHs in Figure 7.5a regardless of the fuel tested. It is also apparent from Figure 7.5d that the six PAHs (NPH, ACY, ACN, FLU, PHN and ATR), which were most abundant in the gas phase, also dominated the total PAH distribution. Four out of these 6 PAHs (NPH, FLU, PHN and ATR) constituted over 75 % of the PAHs identified in the diesel combustion and, interestingly, this finding corresponds with those observed by Jin et al. (2014) who reported that 50 to 92 % of the exhaust PAHs of a heavy-duty diesel engine had 2 to 3 rings. The finding that 2-3 ring PAHs dominated the exhaust PAHs is also in agreement with the findings reported by Wang et al. (2015), who researched in-cylinder and exhaust PAHs in a diesel engine fuelled with heptane and heptane/toluene blends.

7.7.5 Total PAH analysis at constant injection timing

Figure 7.6 shows the total PAHs obtained by summing up all the EPA 16 priority PAHs produced for each fuel. Figure 7.6a shows the concentrations of total GP PAHs. It can be seen from the figure that the GP PAH mass for the 100%H was 1906 µg/m^3. The PAH mass concentration decreased linearly to 1336 µg/m^3 and 1067 µg/m^3 when 15% and 22.5% of toluene were, respectively, blended into heptane.

The total PP PAHs in Figure 7.6b shows rather increasing PP PAH concentrations with increasing proportion of toluene added into heptane. A comparison between Figure 7.6a and b suggest that while toluene addition to heptane inhibits ignition of the resulting fuel mixture, it also suppresses the formation of exhaust gaseous PAHs, and at the same time promotes the PAH to proceed onto particulate. In order words, the GP PAHs were more rapidly consumed and converted to soot, following toluene addition to heptane. For example, the PP PAH concentration was 60µg/m^3 in the case of 100%H, and it later increased by 48% and 67% respectively, when 15% and 22.5% of toluene were respectively blended into heptane.

One unanticipated finding that emerged in both Figures 7.6a and b is that the fuel blends of 77.5%H22.5%T and 65%H15%T20%MD exhibited roughly similar concentrations of GP and PP PAHs on volume of gas basis. It is difficult to explain

these results, but it might be related to the resulting opposing effects of both increasing the carbon number of the heptane/toluene blend due to addition of methyl-decanoate ($C_{11}H_{22}O_2$) while also introducing oxygen to the fuel blend.

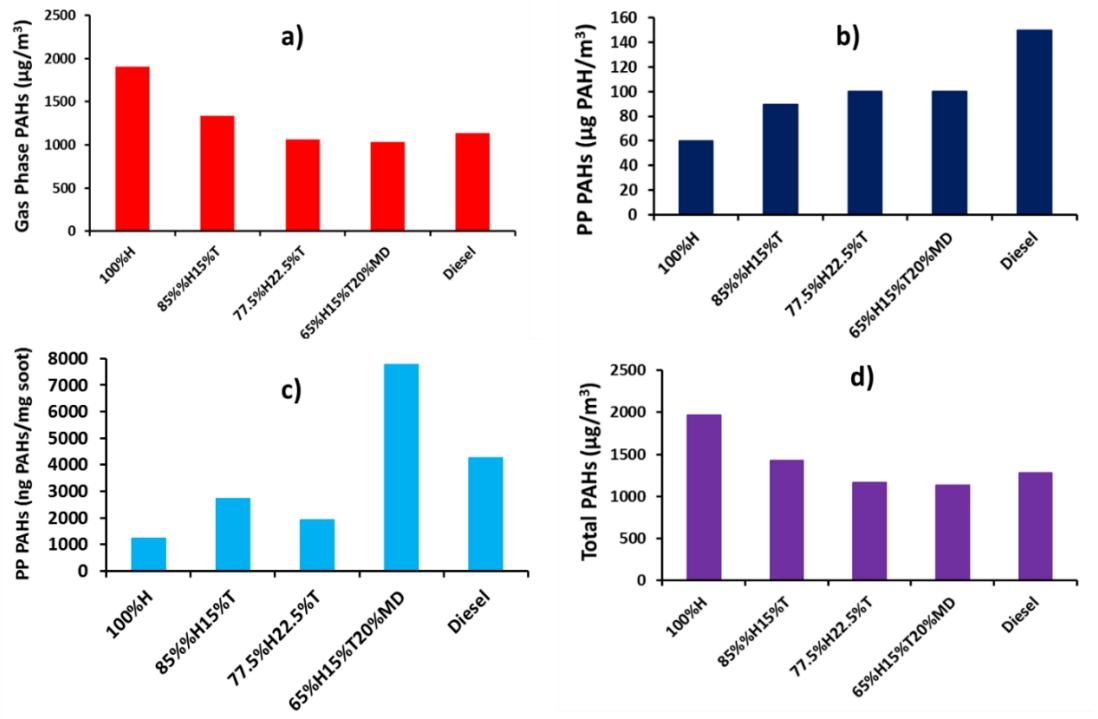

Figure 7.6: Normalised total PAH concentrations in diesel engine: a) Gas Phase (µg of PAH/m3 of gas) b) Particle Phase (µg of PAH/m3 of gas) c) Particle Phase (ng of PAH/ mg of soot) d) Total PAH (µg of PAH/m3 of gas).

The particle phase PAH mass from diesel fuel combustion shown in Figure 7.6b was found to be higher than those from 100%H and in fact, for all the blends. The result for diesel PAH mass is consistent with observations from previous studies (Barbella et al.,1989). The propensity of the fossil diesel fuel used to form both soot and PP PAHs is believed to be attributable to the fossil diesel fuel having 22.2% total aromatic and 3.4% PAH content, which included several single ring aromatics (benzene and toluene) and alkylated PAHs (methyl-naphthalenes). The aromatics, originally from the diesel fuel, could have facilitated the formation of particle phase PAHs and soot, by serving as precursors to soot formation processes.

Comparing Figure 7.6b and Table 7.8, it would appear that the particle phase PAH concentrations, regardless of the fuel combusted, are strongly positively

correlated with the soot particle sizes onto which the PAHs were attached and extracted from. Further comparison shows a negative correlation between the PP PAHs Figure 7.6b and the soot surface area ($\mu m^2/cm^3$) (see Table 7.8) on to which the PAHs were deposited. These results suggest that more PP PAHs were present when particle surface area decreased, possibly due to decrease in soot mass concentration or an increase in mean particle diameter.

Figure 7.6c shows the mass of PAHs (mostly group B2) extracted from the soot particles normalised with the mass of soot particles (see Table 7.8). The trends in the Figure 7.6c appear to correlate positively with those of peak in-cylinder pressures and peak heat release rates shown in Figure 7.1. However, this trend does not seem to apply in the case of 65%H15%T20%MD blend.

The total PAH concentrations shown in Figure 7.7d and it arise from summing-up the GP and PP PAH concentrations. Comparing Figures 7.7a, b and d, suggests that the GP PAHs dominated the total PAHs in the diesel engine, regardless of the fuel combusted. For example, the proportion of GP PAHs generated during combustion of 100%H was 97%, while this proportion decreased to 94% and 91% when 15% and 22.5% of toluene were, respectively, blended into heptane. Combustion of fossil diesel generated only 88% of the GP PAHs. Similar proportions of GP PAHs were reported by He et al. (2010b) in a diesel engine fuelled with diesel and biodiesel as well as by Jin et al. (2014) in a heavy duty diesel engine.

Returning now to Figure 7.6d, a clear decreasing trend of PAH concentrations can be seen with increasing proportions of toluene added to heptane. This result is in line with previous studies (Wang et al., 2015), and could be explained in two ways. Firstly, toluene breakdown mostly results in the production of active reactants such as phenyl, benzene and methane (Sivaramakrishnan et al., 2004; Ledesma et al., 2005) which are instrumental in the growth of PAHs via several reaction pathways. These reaction routes include methyl addition and cyclisation (MAC), phenyl addition and cyclisation (PAC) as well as hydrogen abstraction, acetylene addition (Shukla et al., 2008; Shukla and Koshi, 2012). Secondly, co-oxidation reactions due to interaction of heptane and toluene, as reported by Andrae et al. (2005), can also stimulate the growth of smaller PAHs to larger

PAHs and subsequently to soot. For example, reactions $R_{7.1}$, $R_{7.2}$ and $R_{7.3}$ in section 7.6.1 describe the production of phenyl radicals (through toluene consumption) following oxidation of benzyl radicals. Reaction $R_{7.1}$ illustrates the formation of heptyl radicals through heptane oxidation. Considerable concentrations of phenyl radicals can speed-up the growth of PAHs via phenyl addition and cyclisation reaction pathways (Shukla and Koshi, 2011).

Heptane and toluene decompose via entirely different reaction routes. In the case of n-heptane, after hydrogen abstraction shown in reaction $R_{7.4}$, heptyl radicals decompose thereby yielding intermediates such as acetylene, ethylene and methyl radicals (Xu et al., 2013). Toluene on the other hand is relatively more stable than heptane and its aromatic ring opens at low rates at low temperature (Ledesma *et al.*, 2005). Reaction $R_{7.1}$ therefore dominate toluene pyrolysis and this explains why substantial amounts of phenyl radicals are produced. Furthermore, heptane oxidation is inhibited since it has been reported earlier in reaction $R_{7.4}$ in section 7.6.1 that both heptane and toluene compete for OH radicals. The inhibition of heptyl radicals in $R_{7.4}$ could signify lower concentrations of intermediates such as acetylene and ethylene for the growth of PAHs and this is especially why toluene addition to heptane decreased the concentrations of PAHs.

7.7.6 Effect of Ignition delay and premixed phase on total PAH emissions

Figures 7.7a and b show the variations of total PAHs with ignition delay and percentage premixed phase respectively. It is apparent from Figure 7.7a that increase in ignition delay due to corresponding increase in the proportion of toluene added to heptane was associated with decreased with total PAH mass concentration. For example, the total PAH concentration for 100%H was 1966 $\mu g/m^3$ and it decreased by 27% when the ignition delay was increased from 9.4 to 9.8 CAD in the case of 85%H15%T. This trend saw a further reduction by 41% in the total PAH emissions when the ignition delay was increased from 9.8 to 10.8 CAD in the case of 77.5%H22.5%T.

The finding that the total PAH emission was associated with decreased with increasing ignition delay can be explained by the fact that the maximum average in-cylinder temperature also increased with increasing ignition delay (Koivisto et al., 2015a). This is expected, since the total PAHs were reported to decrease with increasing temperatures (Sánchez et al., 2012; Dandajeh et al., 2017). Further extrapolation from these results would suggest that the relatively low in-cylinder temperature inhibits the consumption of PAHs. It is somewhat surprising that combusting 65%H15%T20%MD does not seem to affect the total PAH concentration significantly from those of 77.5%H22.5%T, even though the ignition delay was increased by 0.4 CAD.

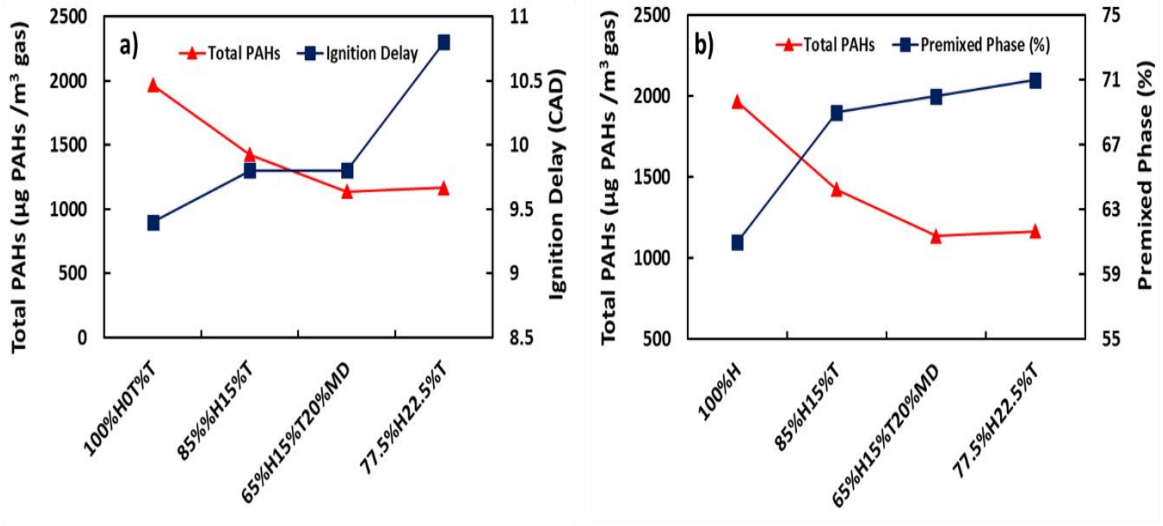

Figure 7.7: Correlation of total PAH (µg PAH/m3 gas) with: a) Ignition delay (CAD) b) premixed phase (%).

Apparent from Figure 7.7b is the decreasing trend of total PAH concentration with increasing percentage of premixed phase. It can be observed from Figure 7.7b that at lower premixed burnt fraction of 61% for example, combustion of 100%H produced the highest PAH mass, with the PAHs presumably made from significant concentration of free radicals generated via heptane pyrolysis at relatively low in-cylinder temperatures. As the proportion of the premixed phase was increased and the diffusion phase decreased, it can be noticed from Figure 7.7b that the total PAH concentration also decreased. This results matched those observed by Wang et al. (2015). Wang et al reported decrease in total in-cylinder PAH mass while the combustion mode shifted from premixed to diffusion and

finally to late combustion phase as the crank angle was advanced after TDC from 0 to 40 CAD.

Taking Figures 7.7a and b together, it is apparent that increasing ignition delay of the heptane/toluene blends also increased the proportion of fuel burnt in the premixed phase. This observation is consistent with earlier studies (Ladommatos et al., 1996; Koivisto et al., 2016).

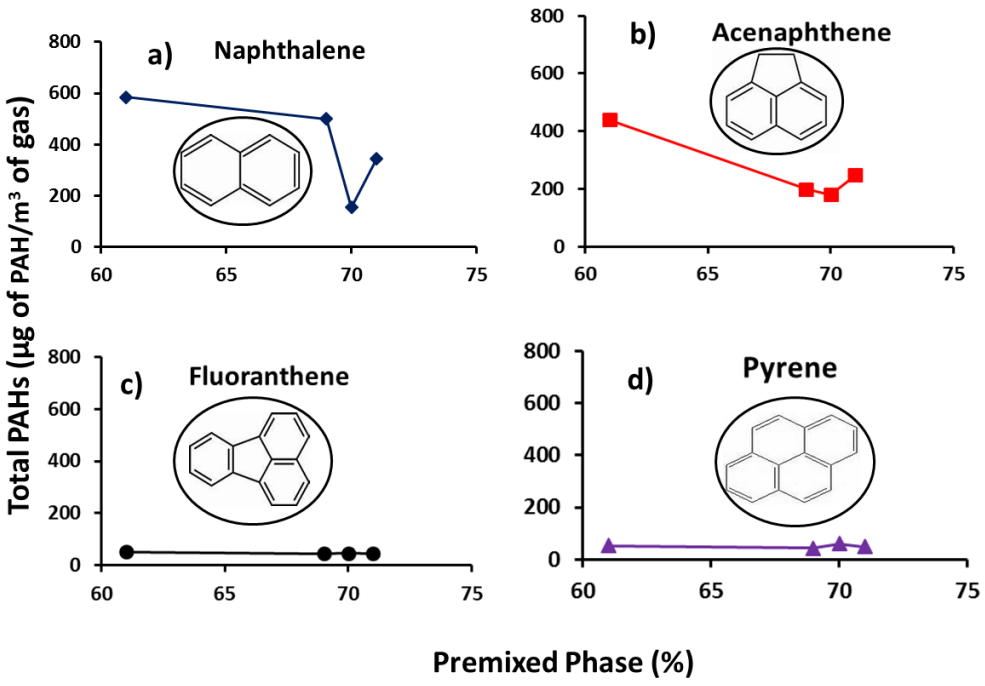

Figure 7.8: Profiles of Group D individual total PAH (µg PAH/m3 gas) with premixed phase (%) a) naphthalene b) acenaphthene c) fluoranthene d) pyrene.

Figure 7.8 presents the profiles of individual total concentrations of group D PAHs (PAHs with low toxicity factors) with percentage premixed phase. It can be seen from the figure that the concentration of the individual PAHs decreased with increasing percentage premixed burn fraction. Premixed phase is characterised as high temperature regime, where fuel and air react in a near-stoichiometric fuel air mixture (Dec, 2010). Lower percentage premixed therefore signifies pockets of richer mixture and higher PAHs formed, since the concentration of PAH increases with increasing fuel concentration (Sánchez et al., 2013). Closer inspection at Figures 7.8a, b, c and d shows progressive reduction in the PAH mass while increasing the number of PAH rings regardless of the percentage premixed phase. Namely; from 2 rings for benzenoid naphthalene (Figure 7.8a) to 3 rings for five-membered-ring acenaphthene (Figure 7.8b), to 4-rings for five-

membered-ring fluoranthene (Figure 7.8c) and finally to 4-ring for a benzenoid pyrene (Figure 7.8d).

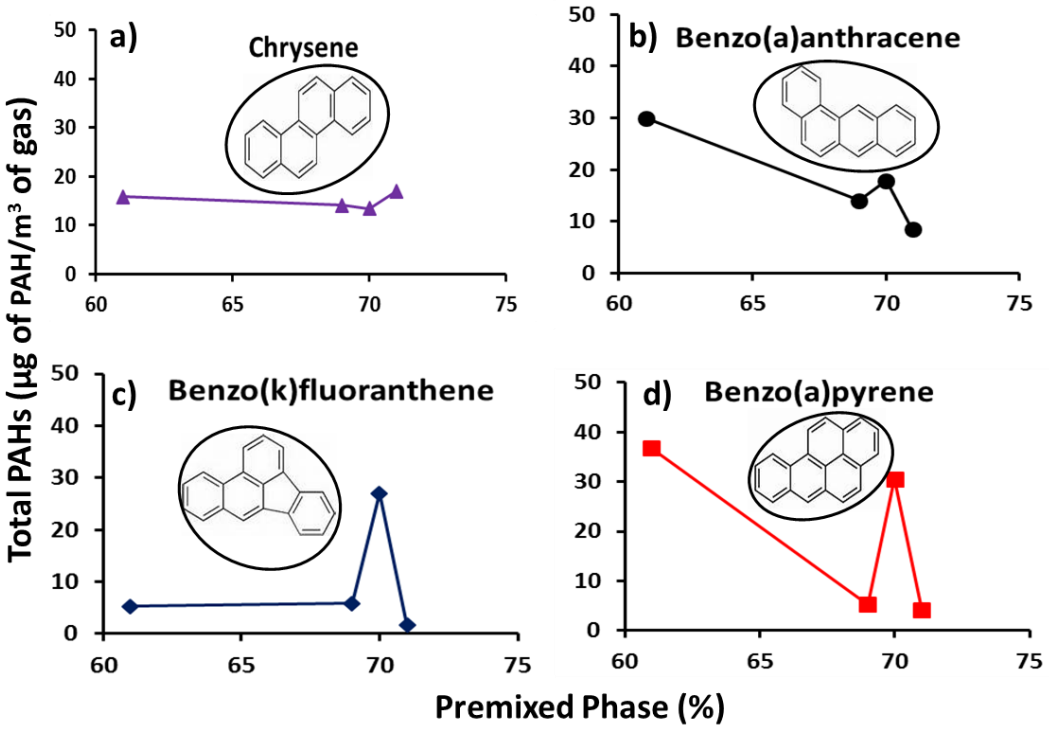

Figure 7.9: Profiles of Group B2 individual total PAH (µg PAH/m3 gas) with premixed phase (%) a) chrysene b) benzo(a)anthracene c) benzo(k)fluoranthene d) benzo(a)pyrene.

Figure 7.9 shows the profiles of individual total concentrations of the group B2 PAHs (PAHs with high toxicity factors) with percentage premixed phase. The figure shows a decreasing trend of PAH mass with increasing percentage premixed phase, but at markedly lower concentrations (by a factor of 16) when compared with those in Figure 7.8 for group D PAHs. One striking feature of PAH concentrations at premixed phase of 70% is the low PAH mass in Figure 7.8 and comparatively higher PAH mass in Figure 7.9. This point is not likely to be an outlier, as it corresponds to a fuel blend with a slightly different molecular configuration due to addition of 20% methyldecanoate to the heptane/toluene blend. The effects of the low and high PAHs concentrations at premixed phase of 70% in Figures 7.8 and 7.9 respectively, were offset in the total PAH concentrations shown in Figure 7.7b.

7.7.7 PAH distribution at constant Ignition timing and constant ignition delay

Figure 7.10 presents the total PAH distribution at constant ignition delay. Figures 7.10a and b show the total PAH distribution at ignition delays of 9.4 and 9.8 respectively. It can be seen from both Figures 7.10a and b that equalising the ignition delays for the heptane/toluene blends did not result in identical PAH concentrations as intuitively anticipated. It instead lessened the mass of individual PAHs due to addition of ignition improving additive (2-EHN). For example, the total PAH concentration of naphthalene in Figure 7.5d for the 85%H15%T was 500μg/m^3 and it decreased by 20% in Figure 7.10a when 85%H15%T + 400ppm of 2-EHN was combusted. Similar correlation applies to the naphthalene concentration of 77.5%H22.5%T blend in Figure 7.5d.

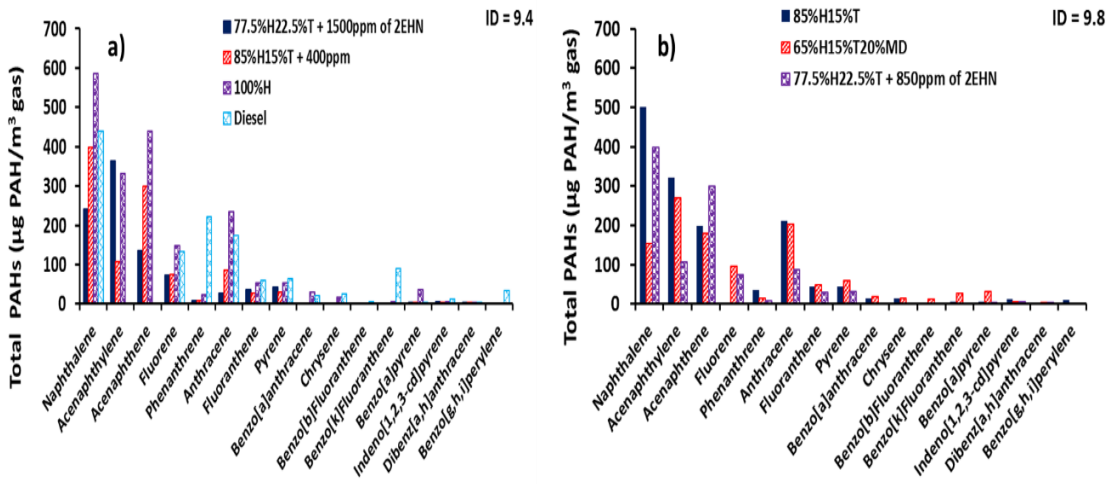

Figure 7.10: Distributions of total exhaust PAHs (GP +PP) (μg of PAH/m3 of gas) at constant ignition delay a) ID = 9.4 b) ID = 9.8.

Similarly, the total PAH concentration of naphthalene in Figure 7.5d for 77.5%H22.5%T was 500μg/m^3, and it decreased by 20% when 850 ppm of 2-EHN was added to 77.5%H22.5%T and 52% for when 1500ppm of 2-EHN was added to 77.5%H22.5%T as shown in Figures 7.10b and a respectively. Closer inspection at Figures 7.10a and b shows decline in PAH concentration of most of the 16 PAHs due to addition of 2-EHN to fuel blends at both ignition delays of 9.4 and 9.8.

7.7.8 Total PAH analysis at constant Ignition timing and constant ignition delay

The total PAH concentration at constant ignition timing is shown in Figure 7.11 and was found by summing up all the EPA 16 priority PAHs at both gas and particulate phases. While Figure 7.10 shows reduction in concentration of the individual total PAH due to addition of 2-EHN, Figure 7.11 rather shows the cumulative reductions in PAH concentration after adding 2-EHN for each fuel.

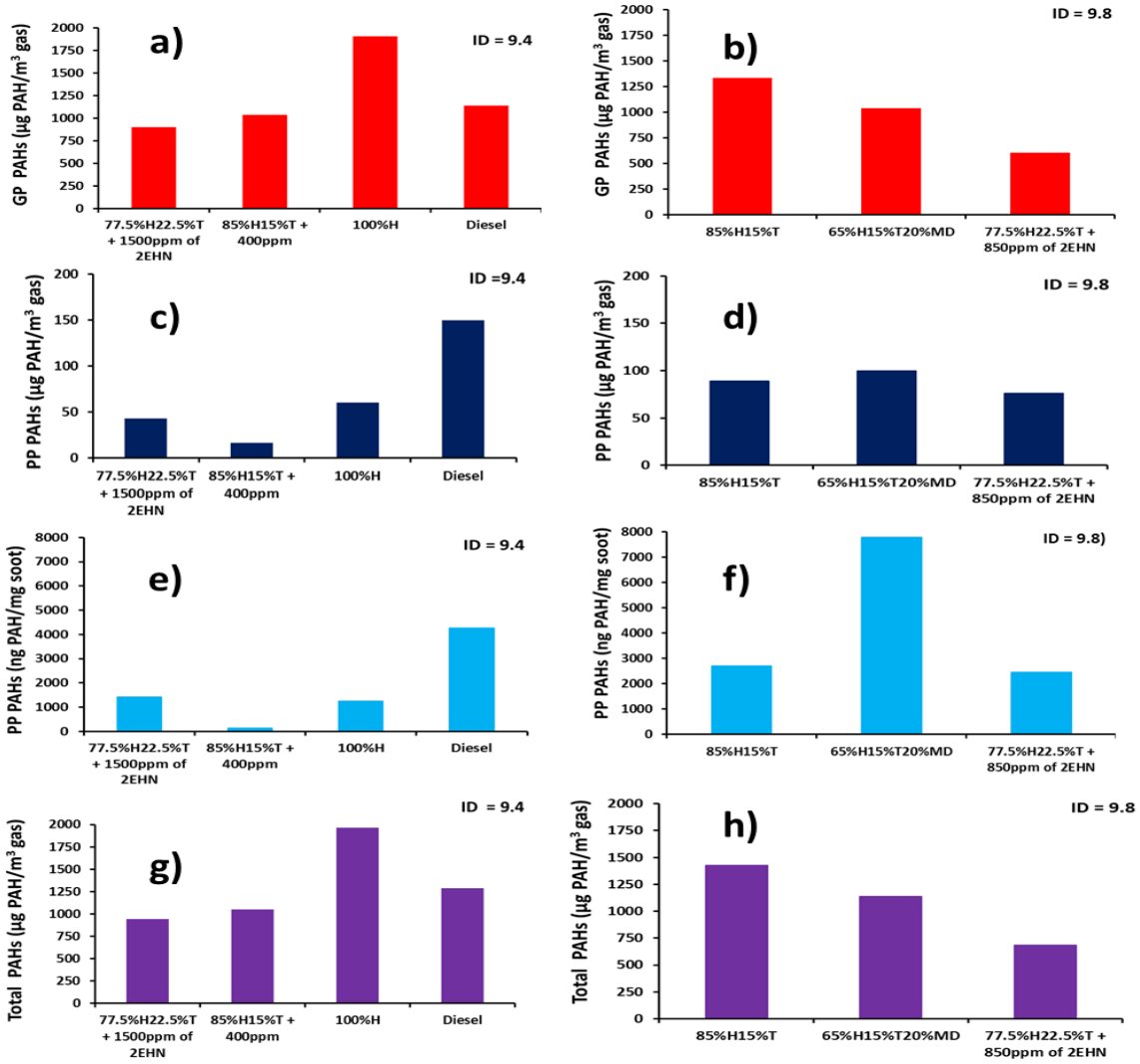

Figure 7.11: Normalised total PAH concentrations at constant ignition delays: a) Gas Phase PAH at ID = 9.4 b) Gas Phase PAH at ID = 9.8 c) Particle Phase PAH at ID = 9.4 d) Particle Phase PAH at ID = 9.8 e) Particle Phase at ID = 9.4 f) Particle Phase PAH at ID = 9.8 g) Total PAH at ID = 9.4 h) Total PAH at ID = 9.8.

Comparing together Figures 7.11a, b, c & d, one can observe that adding 400 ppm of 2-EHN to 85%H15%T decreased the GP PAH concentration (µg /m^3) by

23% (Figures 7.11a & b) and the PP PAH concentration (µg /m^3) by 82% (Figure 7.11c &d). Similar observation can be seen when Figures 7.11e, f, g & h were compared. The PP PAH concentration on soot mass basis (ng /mg) decreased by 95% (Figures 7.11e & f) while the total decreased by 26% (Figures 7.11g & h) when 400 ppm of 2-EHN was added to 85%H15%T blend. The implication of this observation is that while addition of 2-EHN to the fuel blends results in early ignition reaction with high amount of energy liberated, the PAHs associated with exhaust particulates and the gaseous species are considerably abated.

Finally, Figures 7.7 and 7.11 were compared since equalising the ignition delays for the fuel blends did not result in identical PAH concentrations. The conclusion that emerged from Figures 7.7 and 7.11 is that fuel composition seems to have more influence on the propensity/identity of PAHs formed than the combustion characteristics such as ignition delay, heat release rates and premixed burnt fraction of the fuel.

7.7.9 Soot Particle Toxicity

This section presents results of the Group B2 PAHs extracted from the soot masses generated from various fuels tested in the diesel engine. It also includes an assessment of the carcinogenicity of the soot particles from those fuels. It is worth mentioning that the model fuels (heptane and toluene) are not practical fuels, but are intended to give an indication of influence of aromatics/ignition improver on carcinogenicity of soot particles. Table 7.9 presents the sum of the Group B2 PAHs on the soot particles and their respective proportions in the particle phase and the total PAHs. It can be seen from Table 7.9 that the proportion of the Group B2 PAHs for the fossil diesel was 41% in the particle phase and 13% in the total PAHs. However, the proportion of Group B2 PAHs on the soot particles from the various heptane/toluene blends increased from 22% for the 100%H, peaked at 30% for 85%H/15%T and decreased to 12% for 77.5%H/22.5%T and 18% for 65%H15%T20%MD.

The trends for the highest PAH concentration in the Group B2 PAHs when 15 % toluene was blended into heptane and decrease in the PAH concentration when 22.5 % toluene was blended into heptane interestingly correspond, broadly, to

similar trends in the peak apparent heat release rates. In Figure 7.1a for example, the peak heat release rate was 54J/s for 100%H; increased to 71J/s for 85%H/15T; and thereafter decreased to 59J/s for the 77.5%H/22.5%T. This analogy may suggest that the formation of Group B2 PAHs in diesel engine combustion may be influenced by the variations in the heat release rates.

Table 7.9: Sum of Group B2 PAHs and their proportions in total PAHs.

	ΣGroup B2 in PP PAHs (µg/m^3)	ΣGroupB2/ ΣPP PAHs (%)	ΣGroup B2 in Total PAHs (µg/m^3)	ΣGroupB2/ Total PAHs (%)
100%H	13	22	100	5
85%%H15%T	27	30	59	4
77.5%H22.5%T	12	12	47	4
65%H15%T20%MD	18	18	110	10
Diesel	61	41	163	13

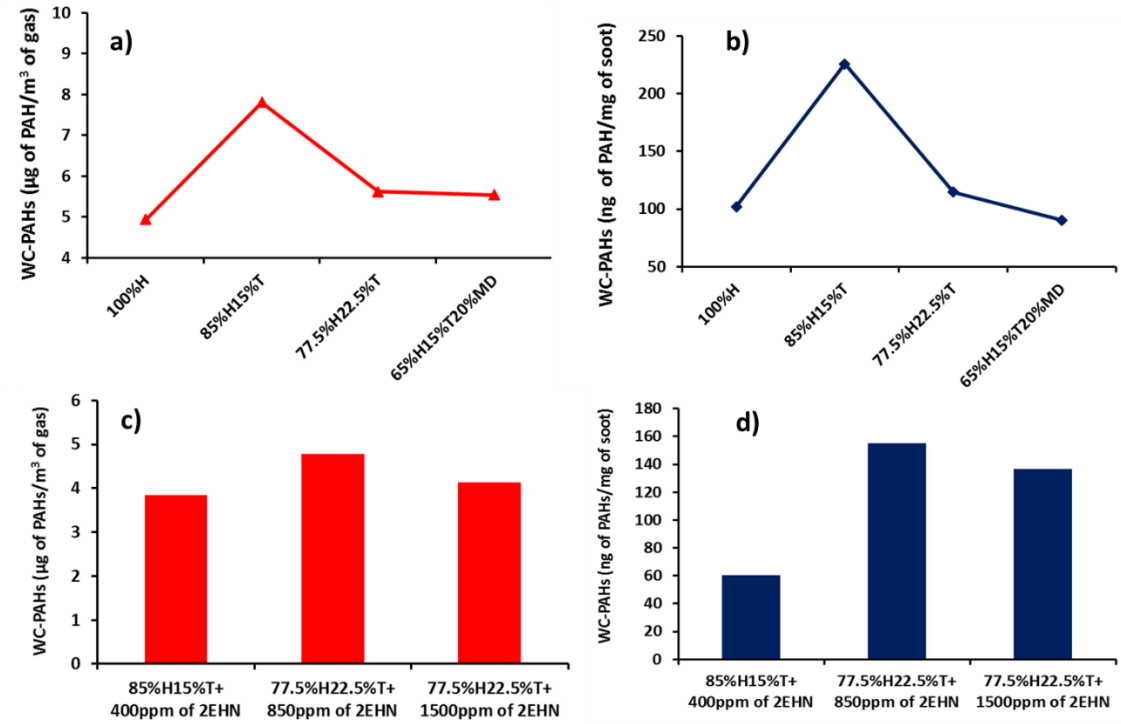

Figure 7.12: Weighted Carcinogenicity of PAHs a) (µg of PAH/m3 of gas) b) Phase (ng of PAH/mg of Soot) c) (µg of PAH/m3 of gas) with 2-EHN d) Phase (ng of PAH/mg of Soot) with 2-EHN.

The weighted carcinogenicity of PAHs (WC-PAHs) was defined as the sum of the product of concentration (C_n) of each of the 16 EPA PAH and their toxicity equivalence factor (TEF_n). The relation on the WC-PAHs is as shown equation 1.

WC- PAHs = $\sum_{n=1}^{16}(TEF_n * C_n)$ Eq.7.3

Figure 7.12 shows the weighted carcinogenicity of soot particles for all the fuels tested. Figures 7.12a and b show the WC- PAHs of the fuel blends without 2-EHN, on volume of gas and mass of soot bases respectively. Figures 7.12c and d show the WC- PAHs of the fuel blends with 2-EHN, on volume of gas and mass of soot bases respectively.

It can be seen from Figures 7.12a and b that the WC- PAHs increases from 100%H peaked at 85%H/15%T and thereafter decreased to 77.5%H/22.5%T and 65%H/15%T20%MD. The WC-PAH was higher for the 85%H/15%T blend because the soot particles generated from 85%H/15%T had substantial concentrations of benzo(a)pyrene, benzo(k)fluoranthene, diben(a,h)anthracene and indeno(1,2,3-cd)pyrene; which have high toxicity factors. Figures 7.12c and d show that the WC- PAHs of the fuel blends decreased due to addition of 2-EHN.

It is interesting to note that the WC-PAHs for all the fuels investigated reflect the particle phase PAH concentrations of the B2 subgroup shown in Table 7.9. The findings from these results suggest that the WC-PAHs for the heptane/toluene blends may also be influenced by their heat release rates shown in Figure 7.1b.

7.8 Conclusions

In an attempt to investigate the influence of combustion characteristics and fuel composition on exhaust PAHs in a compression ignition engine, diesel and blends of heptane/toluene/methyldecanoate were tested. The results presented of both gas-phase and particle-phase PAHs generated from combustion of these fuels can be summarised as follows:

- Increasing toluene proportion in heptane/toluene mixture increased the ignition delay due to decrease in reactivity of the mixture. An increased

duration of ignition delay allows more time for fuel and air pre-mixing prior to the start of combustion and thus, larger premixed burn fraction.

- Equalising ignition delay by adding ignition improving additive (2 ethylhexyl nitrate) resulted in roughly similar peak heat release rates, peak in-cylinder pressure and proportions of premixed burn fractions
- Increasing toluene proportion in heptane/toluene mixture resulted in increase in the mean soot particle sizes and decrease in overall soot surface area. An opposite decreasing trend of mean soot particle size and increasing soot surface area was observed when ignition improving additive was added to the heptane/toluene blend so as to keep ignition delay constant.
- Group D PAHs (naphthalene, acenaphthylene, acenaphthene, fluorene, phenanthrene and anthracene) dominated the GP PAHs as well as the total PAH distributions (> 90%) regardless of composition of the fuel tested. The fraction of group D PAHs in both the gas phase and total PAHs decreased with increase in the proportion of toluene blended into heptane. Fossil diesel had the lowest proportion of gas phase PAHs at 88% and, invariably, the highest particle phase PAHs.
- The total PAHs decreased with increase in the ignition delays and proportions of premixed phase of the various heptane/toluene blends. This suggested an influence on PAHs of the corresponding shift in combustion phasing from premixed to diffusion modes and subsequent changes in in-cylinder conditions.
- The apparent heat release rates of the heptane/toluene blends from diesel engine combustion may have an influence on the concentrations of the GroupB2 PAHs deposited onto the soot particles, and their corresponding weighted carcinogenicities.
- The particle phase PAHs were observed to be strongly positively correlated with the soot particle sizes from which the PAHs were extracted, regardless of the fuel combusted.
- The total PAH concentration decreased with increase in the amount of ignition improver (2-ethylhexyl nitrate) added to the heptane/toluene fuel

blend. Ignition improving additive impacted more significantly on the reduction of particle bound PAHs than those PAHs in the gas phase.

- The weighted carcinogenicity on volume of gas and soot mass bases increased from 100%H, peaked at 85%H/15%T and thereafter decreased to 77.5%H/22.5%T and 65%H/15%T20%MD. Adding 2 ethylhexyl nitrate to the fuel blends also decreased the weighted carcinogenicity of soot particles.
- Fuel composition seems to have more influence on the concentration of PAHs formed than the combustion characteristics (ignition delay, heat release rates and premixed burn fractions).

Chapter 8

8. Conclusions

The results on the influence of molecular structures of a homologous series of fuel molecules on PAH formation have been described and discussed in the preceding chapters. In this chapter, the conclusions that emerged from these results are outlined and recommendations for future work are made.

8.1 Summary of conclusions

It was reported in the literature review that the influence of molecular structure on PAH formation has not been fully understood, while the effect of degree of unsaturation and carbon number of hydrocarbon fuels on PAH formation has not been investigated in tube reactors. Effects of fuel composition on PAH emissions in diesel engine has remained unresolved. This work presented the results of both gas-phase and particle-phase PAHs generated from pyrolysis of a homologous series of C_1 – C_7 hydrocarbons in a homogenous laminar flow reactor and C_7 fuel blends in diesel engine. The PAHs studied were the US EPA 16 priority PAHs, but emphasis was given to those PAHs classified as possible carcinogens to humans (Group B2). The novel methodology employed for the PAH quantification involved sampling particulates and gas phase PAHs from the exit of a tube reactor and from the exhaust of a diesel engine. The PAHs from these samples were then extracted using an accelerated solvent extractor (ASE) and their analysis was carried out using gas chromatography coupled to mass spectrometry (GCMS). The general conclusions reached in this thesis are that, in the case of the tube reactor, increasing the unsaturation of C_2 and C_3 fuels increases their gas phase PAHs in the case of the C_2 fuels and particle phase PAHs in the case of the C_3 fuels. When the carbon number of the hydrocarbon fuels was increased from C_1 – C_7, the total PAH concentrations tended to increase at the temperature of 1050 ^oC but an opposite (decreasing) trend was

observed at 1350 ^{o}C. Temperature increase from 1050 – 1350 ^{o}C decreased the total PAHs regardless of the molecular structure of the fuel. In the diesel engine, fuel composition appeared to have more influence on the concentration of total exhaust PAHs formed than on the combustion characteristics.

8.2 Specific conclusions

The following section summarises the main conclusions that emerged from the work in this thesis.

8.2.1 Effects of Unsaturation of C_2 and C_3 Hydrocarbons on the Formation of PAHs and on the Toxicity of Soot Particles

The effect of unsaturation of fuel molecules on soot and PAH formation of three C_2 hydrocarbons (ethane, ethylene and acetylene) and two C_3 hydrocarbons (propane and propylene) were investigated in a laminar flow reactor under oxygen free pyrolysis and within the temperature range of 1050 – 1350 ^{o}C. Particulates were characterised at sub-micron levels in terms of size, number and mass using a differential mobility spectrometer (DMS-500). The following key observations and conclusions were drawn:

- The degree of unsaturation of the fuels tested was observed to have a significant impact on the resulting amount of soot concentration in the effluent gas (nitrogen). The amount of soot and the gas phase PAHs generated from the C_2 fuels were found to be increasing with increasing unsaturation in the fuels.
- The C_3 fuels also followed a similar trend with those of the C_2 fuels, but they had greater soot yield and particle phase PAHs. The double bonded C_3 propylene produced the highest amount of soot and particle-phase PAHs per unit mass of soot and per unit volume of gas. Propylene also produced soot particles with the highest carcinogenicity in the temperature range of 1050 - 1250 ^{o}C and the carcinogenicity decreased with temperature increase.

- Increasing pyrolysis temperature from 1050 to 1350 ^{o}C increased the soot particle mean diameter, while the soot number concentration decreased regardless of the degree of unsaturation of the hydrocarbon investigated. This result is believed to be attributable to primary soot particle agglomerating into larger, fewer, particles of several hundred manometers in size.
- The particle phase PAHs included, invariably, the Group B2 members, while the gas phase PAHs included members of Group D. Even though Group D PAHs are unclassifiable by the EPA in terms of carcinogenicity, they contribute substantially to the mechanisms of growth of the carcinogenic Group B2 PAHs.
- There was greater abundance of PAHs (including those of Group B2) at low temperature, while higher temperatures promoted increased soot yield but lower PAH concentration in both the gas and particulate phases.
- The total PAH concentration increased from two rings, peaked at three rings and then tended to decrease in the case of four to five and then to six rings, regardless of the degree of unsaturation of the fuel molecules investigated.
- The toxicity of soot particles generated at low temperature was found to be much higher than the toxicity levels at higher temperatures. Potential implication of this observation might be that low temperature combustion systems, for example, those designed for NOx control, may have higher overall levels of particulate with higher toxicity

8.2.2 Influence of carbon number of C_1 – C_7 hydrocarbons on PAH formation

In chapter 6, the influence of carbon number of seven hydrocarbons (methane, ethane, propane, n-butane, i-butane, heptane and toluene) on PAH formation was investigated in a laminar tube reactor within the temperature range of 1050 – 1350 ^{o}C. The hydrocarbons underwent oxygen free pyrolysis at a fixed carbon concentration of 10,000 ppm on C_1 basis. Particulates were characterised at sub-micron levels using a differential mobility spectrometer (DMS-500). The main findings and conclusions are summarised as follows:

- Increasing the carbon number of C_1 – C_7 hydrocarbons was observed to increase their propensities to form soot particles in the effluent gas (nitrogen) at all temperatures investigated, except for heptane which was observed to be outside this trend.
- Methane pyrolysis was observed to have the smallest number of primary soot particles at the temperature of 1050 ^oC when compared with most of the C_2 – C_7 hydrocarbons. At the lowest temperature of 1050 ^oC, the particle average size for toluene (308 nm) was roughly similar to that produced at the highest temperature of 1350 ^oC by the C_1 – C_7 aliphatic hydrocarbons.
- Increasing the temperature of the reactor from 1050 – 1350 ^oC, decreased the total PAH concentrations regardless of the carbon number of the hydrocarbons investigated.
- Increasing carbon number from C_1 to C_7 decreased the gas phase PAH concentration at the temperature of 1350 ^oC. Similarly, the particulate phase PAH concentration (including those of the Group B2 PAHs) decreased at the intermediate temperature of 1150 ^oC when the carbon number was increased from C_1 to C_7. No clear trends were observed at temperatures of 1050 and 1250 ^oC.

- The total PAH concentrations tended to increase with increasing carbon number (excluding heptane) at the temperature of 1050 ^oC but an opposite (decreasing) trend was observed at 1350 ^oC.
- Isomerisation in the C_4 hydrocarbons and aromatisation in the C_7 hydrocarbons increased substantially, the soot propensities, the abundance of particle phase PAHs and carcinogenicity (volume of gas basis) at the temperature of 1050 ^oC.
- Toluene and propane soot particles had the highest weighted carcinogenicities at the temperature of 1050 ^oC on gas volume and soot mass bases respectively. At the temperature of 1150 ^oC, the weighted carcinogenicity (soot mass basis) was observed to decrease with increasing carbon number of the hydrocarbon.

8.2.3 Influence of combustion characteristics and fuel composition on exhaust PAH emissions in a compression ignition engine

In chapter 7, two major tests were carried out in a diesel engine to understand the effects of combustion characteristics and fuel composition on PAH emissions. The first test was conducted at constant injection timing when the engine was fuelled with single, binary and tertiary fuels formulated by blending various proportions of toluene and methyldecanoate into heptane. The second experiment was performed at constant ignition timings by equalising the ignition delays of the fuel blends using an ignition improving additive (2-ethylhexyl nitrate). The following main conclusions were drawn:

- Increasing toluene proportion in the heptane/toluene mixture increased the ignition delay due to decreasing reactivity of the mixture. An increased duration of ignition delay allowed more time for fuel and air pre-mixing, prior to the start of combustion and, thus larger premixed burn fraction.
- Equalising ignition delay by adding ignition improving additive (2-ethylhexyl nitrate) resulted in roughly similar peak heat release rates, peak in-cylinder pressure and proportions of premixed burn fractions
- Increasing toluene proportion in the heptane/toluene mixture resulted in an increase in the mean soot particle sizes and decrease in soot overall surface area. An opposite decreasing trend of mean soot particle size and increasing soot surface area was observed when the ignition improving additive was added to the heptane/toluene blend.
- Group D PAHs (naphthalene, acenaphthylene, acenaphthene, fluorene, phenanthrene and anthracene) dominated the GP PAHs as well as the total PAH distributions (> 90%) regardless of the composition of fuel tested. The fraction of group D PAHs in both the gas phase and total PAHs decreased with increase in the proportion of toluene blended into heptane. Fossil diesel had the lowest proportion of gas phase PAHs at 88% and, invariably, the highest particle phase PAHs.
- The total PAHs emitted from the various heptane/toluene blends decreased with increase in the ignition delays and proportions of premixed

phase, suggesting that the shift in combustion phasing from diffusion to premixed modes influenced the formation rates of PAHs and their conversion rates to soot.

- The apparent heat release rates of the heptane/toluene blends from diesel engine combustion may have an influence on the concentrations of the GroupB2 PAHs deposited onto the soot particles, and their corresponding weighted carcinogenicities.
- The particle phase PAHs were observed to be strongly positively correlated with the soot particle sizes from which the PAHs were extracted, regardless of the fuel combusted.
- The total PAH concentration decreased with increase in the amount of ignition improver (2-ethylhexyl nitrate) added to the heptane/toluene fuel blend. Ignition improving additive impacted more significantly on the reduction of particle bound PAHs than those PAHs in the gas phase.
- The weighted carcinogenicity on volume of gas and soot mass bases increased from 100%H, peaked at 85%H/15%T and thereafter decreased to 77.5%H/22.5%T and 65%H/15%T20%MD. Adding 2-ethylhexyl nitrate to the fuel blends also decreased the weighted carcinogenicity of soot particles.
- Fuel composition seems to have more influence on the concentration of PAHs formed than the combustion characteristics (ignition delay, heat release rates and premixed burn fractions)

8.3 Recommendations for future work

Despite the significance of the results presented in this thesis, many questions remain unanswered.

The present work has shown that the degree of unsaturation of fuel molecules plays an important role on the type and concentration of gas and particulate phase PAHs. Therefore, the influence of other functional group chemistries such as the position of hydroxyl group in the primary, secondary and tertiary alcohols, on PAH formation could be explored. The implication of larger moieties such as aldehydes, ketones, esters and carboxylic acids on PAH formation could also be

the subjects of future investigations. Furthermore, isomerism in the saturated C_4 hydrocarbons has been reported in this work and other similar related works (Schenk et al., 2015; Viteri et al., 2017) to impact strongly positively on PAH formation, however, the cis/trans isomerism (position of alkyl groups in unsaturated alkene molecules) is still unexplored.

Effect of increasing carbon number of hydrocarbons ranging from C_1 to C_7 in the tube reactor was found to decrease the concentration of PAHs formed at temperatures (1350 ^oC) approaching that of diesel engine combustion. However, increasing the carbon number of hydrocarbons fuels in a diesel engine was reported to increase ignition delay of the fuel (Koivisto et al., 2015) while the present work found that increasing ignition delay decreased the total PAH concentrations. It will be interesting to experimentally confirm this correspondence on whether increasing the carbon number of hydrocarbons in diesel engine will lower exhaust PAH emissions.

The central theme of the work presented was the investigation of the influence of molecular structure on PAH formation. However, intermediate products including light gases and hydrocarbon radicals ranging from hydrogen (C_0) to ethyl benzene (C_8) are also produced during hydrocarbon pyrolysis (Sánchez et al., 2013). This work could be further extended to cover the effect of fuel molecular structure on the formation of intermediate pyrolysis products which can be useful in explaining the mechanisms involved in PAH growth.

8.4 Claims for originality

The tube reactor and diesel engine used throughout this thesis were used by other investigators, but to the best of author's knowledge, the sampling line for the particulate and gas phase PAHs was of a unique design. The novel methodology for PAH extraction and quantification by the GCMS is an improvement from that reported by the US EPA (1999). Furthermore, the systematic choice of homologous series of $C_1 – C_7$ hydrocarbon fuel molecules for PAH and soot emission analysis in tube reactor is original, producing new insights into molecular structural effects on PAH formation. Influence of ignition delay equalisation in the experiments conducted on the diesel engine and the

effects of ignition improver on PAH emissions is reported in this thesis for the first time. Furthermore, variations of total PAH emissions with premixed burnt fractions has not been previously reported in the literature.

Appendix A

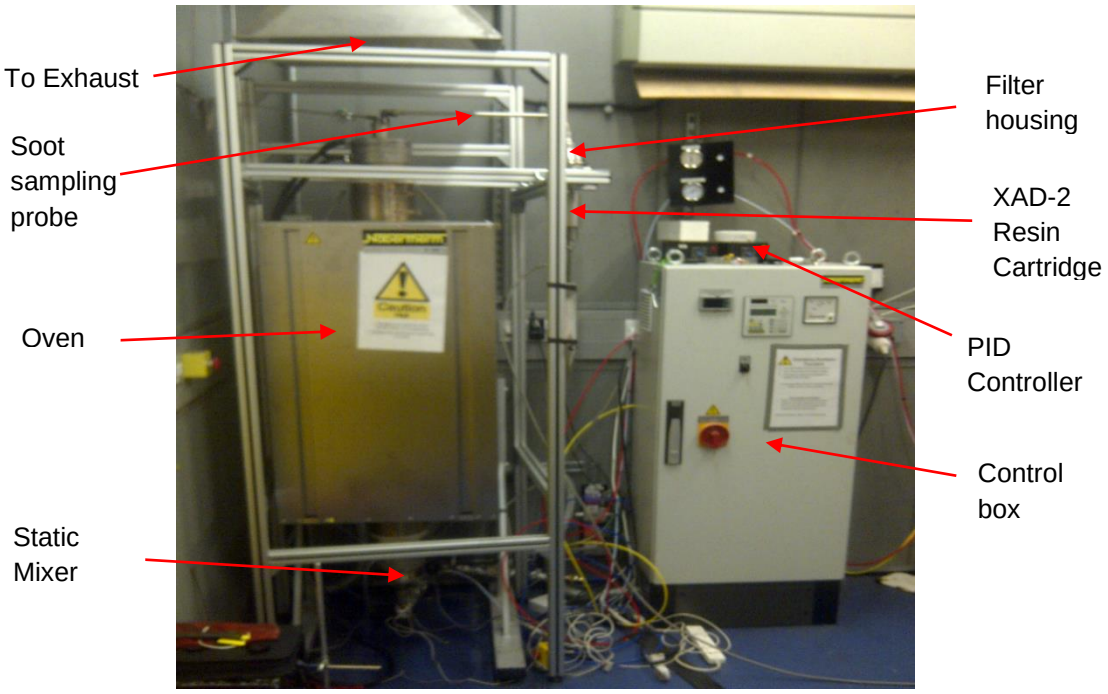

A 1: Pyrolysis tube reactor

Design of an XAD-2 resin cartridge holder

A stainless steel holder was designed in solid works 2015 to house the glass catridge containing the XAD-2 resin. The cartridge was manufactured in the UCL Mechanical Engineering work-shop. Fig.A2 shows the mechanical drawings of the manufactured resin cartridge. The top (A) and bottom (B) XAD-2 resin cartridge holders were internally and externally threaded respectively. The glass cartridge holder Fig.A2 (C) is 125 mm long, 22 mm entrance diamter and 6 mm exit diameter. The glass catridge was placed coaxially into the bottom holder which was then screwed into the top holder. A short length of plastic tube was placed between the glass catridge and the bottom holder to prevent direct contact of the glass and the stainless steel components.

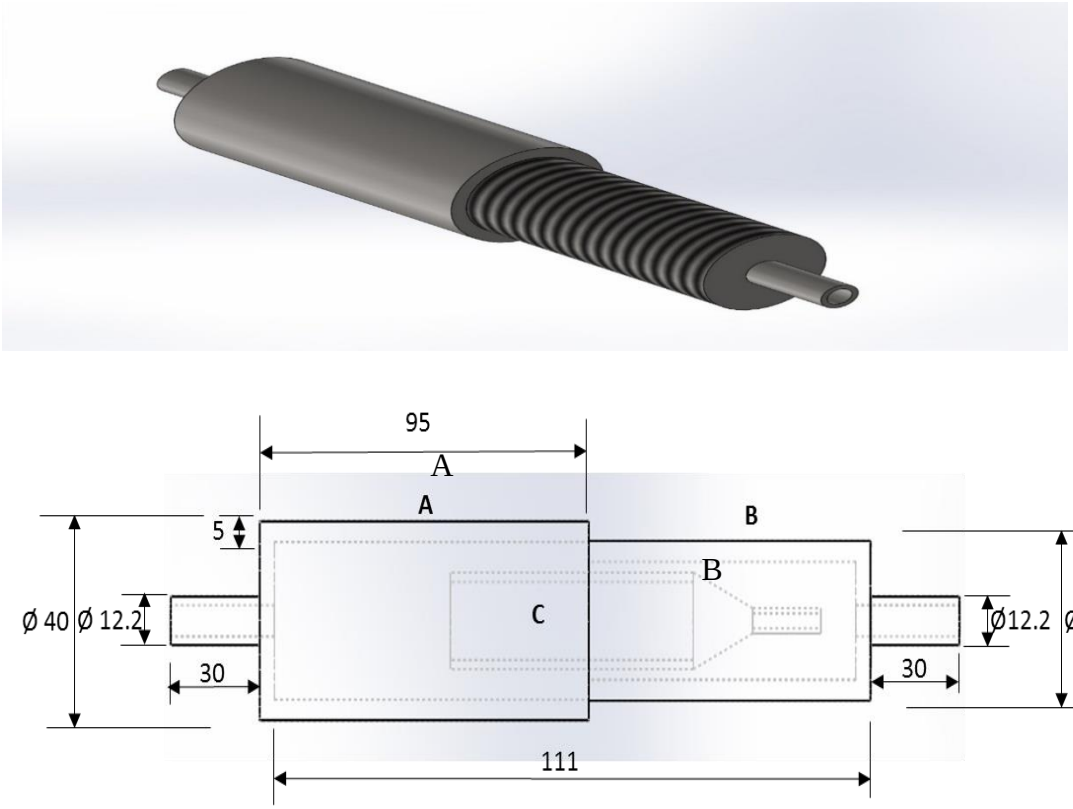

A 2: Drawings of the coupled stainless-steel cartridge holder: A denotes the top holder, B denotes the bottom holder and C denotes the glass cartridge inside which the XAD-resin is loaded. All dimensions are in mm.

A 3: Diesel Engine

A 4: Image of the DMS 500 instrument

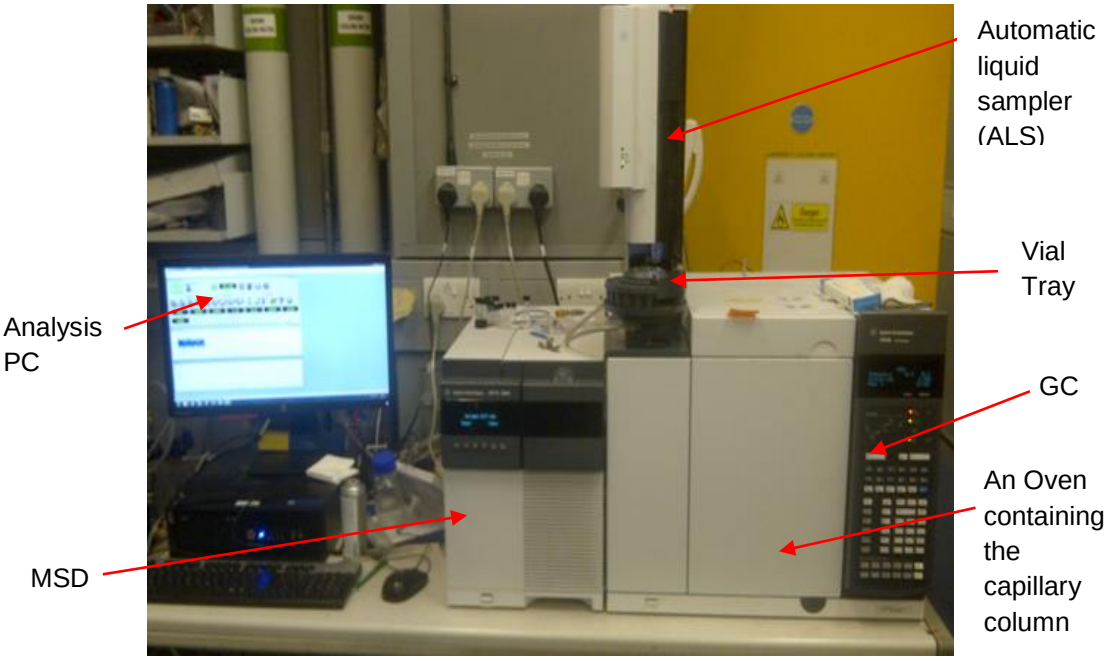

A 5: The GCMS model: 7890B GC coupled with 5977A MSD.

TraceCERT®
Traceable Certified Reference Materials

SUPELCO
Solutions within.
595 North Harrison Road · Bellefonte, PA
16823-0048 USA · Phone(814)359-3441

Certificate of Analysis

Description: TCL PAH Mix, 1x1ml, 2000µg/ml in benzene:dichloromethane

Part Number: CRM48905

Lot Number: LC06611V

Expiration Date: March 2017

Storage: Refrigerate

Analytical Method Parameters:
Column: SUPELCOSIL™ LC-PAH 25cm x 4.6mm x 5µm
WATER / ACETONITRILE;0 min. 60/40%;5 min. 60/40%;30 min. 0/100% 45 min. 0/100% 45.5 min. 60/40%
Detector: UV-254nm
Injection Volume: 2µL

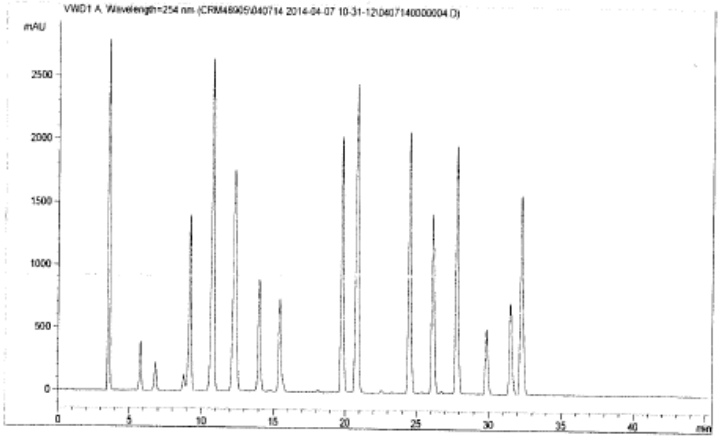

Elution	Analyte	Lot Number	CAS Number	Certified Purity %	Certified Gravimetric Conc. µg/ml	Expanded Uncertainty µg/ml	Analytical Conc. µg/ml
1.	Naphthalene, CRM	LB88072	91-20-3	99.3	1986.0	±6.6	1972.3
2.	Acenaphthylene, CRM	LB95041	208-96-8	99.2	1984.0	±10.6	2031.0
3.	Acenaphthene, CRM	LB88651	83-32-9	99.3	1986.0	±6.4	1930.3
4.	Fluorene, CRM	LB88880	86-73-7	98.2	1964.0	±10.6	1967.5
5.	Phenanthrene, CRM	LB88349	85-01-8	97.6	2034.8	±5.3	2061.9
6.	Anthracene, CRM	LB94997	120-12-7	99.0	1980.0	±9.2	2055.8
7.	Fluoranthene, CRM	LB88428	206-44-0	99.5	1990.0	±10.6	1948.5
8.	Pyrene, CRM	LB92427	129-00-0	98.9	1978.0	±6.3	1921.1
9.	Benz(a)anthracene, CRM	LB94996	56-55-3	98.5	1970.1	±7.0	1964.0
10.	Chrysene, CRM	LB95195	218-01-9	97.4	1999.9	±7.1	2055.4
11.	Benzo(b)fluoranthene, CRM	LB89946	205-99-2	97.3	1999.9	±12.7	1981.0
12.	Benzo(k)fluoranthene, CRM	LB89276	207-08-9	99.5	1990.0	±9.0	1970.5
13.	Benzo(a)pyrene, CRM	LB94317	50-32-8	95.0	1999.9	±10.9	1990.2
14.	Dibenz(a,h)anthracene, CRM	LB95201	53-70-3	99.0	1980.0	±10.6	1981.5

ACLASS ACCREDITED TESTING Cert# AT-1607

ACLASS ACCREDITED REFERENCE MATERIAL PRODUCER Cert# AR-1606

Produced in double accredited laboratory fulfulling
ISO/IEC 17025 and
ISO Guide 34

Page 1 of 3

SIGMA-ALDRICH

A 6: Certificate of analysis for the calibration standard (TCL PAH Mix, 1 x1mL in dichloromethane) (1/3).

Elution	Analyte	Lot Number	CAS Number	Certified Purity %	Certified Gravimetric Conc. µg/ml	Expanded Uncertainty µg/ml	Analytical Conc. µg/ml
15.	Benzo(ghi)perylene, CRM	LB96971	191-24-2	99.4	1988.0	±5.1	1881.6
16.	Indeno(1,2,3-C,D)pyrene, CRM	LB95042	193-39-5	99.7	1994.0	±8.9	2001.3

Cert# AT-1607 Cert# AR-1606

Produced in double accredited laboratory fulfulling ISO/IEC 17025 and ISO Guide 34

Page 2 of 3

SIGMA-ALDRICH

A6: Certificate of analysis for the calibration standard (TCL PAH Mix, 1 x1mL in dichloromethane) (2/3).

Notes:

- All starting materials are Certified Reference Materials.

- NIST traceable weights are used to verify balance calibration with the preparation of each lot. Concentration of analyte in solution is ug/ml.

- Certified value is the gravimetric concentration weighed at room temperature. Uncertainty of the gravimetric concentration in this document is expressed as Expanded Uncertainty (Ucrm) corresponding to the 95% confidence interval. Ucrm is derived from the combined standard uncertainty multiplied by the coverage factor k = 2. The components of combined standard uncertainty include the uncertainties due to characterization, homogeneity, long-term stability and short-term stability. The components due to stability are generally considered to be negligible unless otherwise indicated by stability studies.

- Homogeneity was assessed in accordance with ISO Guide 35. Completed units were sampled using a random stratified sampling protocol. The results of chemical analysis were then compared by Single Factor Analysis of Variance (ANOVA). The uncertainty due to homogeneity was derived from the ANOVA. Heterogeneity was not detected under the conditions of the ANOVA.

- Product intended for laboratory use only. Supelco warrants that its products conform to the information contained in this publication. Purchaser must determine the suitability of the product for its particular use. Please see the latest catalog or order invoice and packing slip for additional terms and conditions of sale.

Cause-Effect Diagram for Uncertainty Contributions

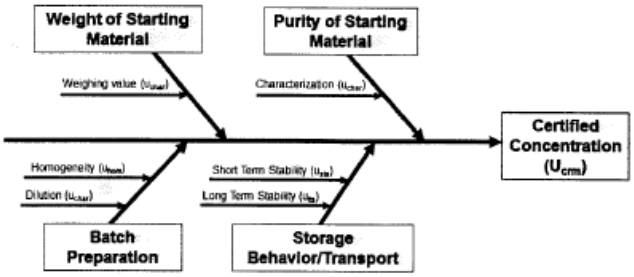

$$U_{crm} = k\sqrt{u_{char}^2 + u_{hom}^2 + u_{sts}^2 + u_{lts}^2}$$

Test Date: April 09, 2014
Form: CRM48905

Duane Funk
QC Manager

Cert# AT-1607 Cert# AR-1606

Produced in double accredited laboratory fulfulling ISO/IEC 17025 and ISO Guide 34

SIGMA-ALDRICH®

A6: Certificate of analysis for the calibration standard (TCL PAH Mix, 1 x1mL in dichloromethane) (3/3).

Haltermann Carless

Haltermann Carless UK LTD. Cedar Court Guildford Rd, Leatherhead, Surrey, KT22 9RX United Kingdom

UNIVERSITY COLLEGE LONDON
MECHANICAL ENGINEERING DEPT
TORRINGTON PLACE
LONDON
London
WC1E 7JE

Certificate 100000067345

Date: 13/09/2016
Customer PO: F45-2027445
Delivery Note: 80053075 000010
Order No.: 66057132 000010
Customer No.: 1762780

GMID: 2012360
Material: Carcal RF-06-08 B5
41.5 kg Keg
Cust. Mat.:
Batch: 0000006227
Dlvy. Qty: 83.0 KG

Revision No.: 2

Container ID:
Ship from: Harwich Pack Harwich, ES, United Kingdom

Feature	Units	Results	Limits Minimum	Maximum	Method
Density 15°C	kg/m3	834.6	833.0	837.0	ASTM D4052
I.B.Pt.	°C	187.5			ASTM D86
10% v/v Recovered at	°C	210.0			ASTM D86
50% v/v Recovered at	°C	271.0	245.0	-	ASTM D86
90% v/v Recovered at	°C	334.5			ASTM D86
95% v/v Recovered at	°C	346.5	345.0	350.0	ASTM D86
F.B.Pt.	°C	354.0	-	370.0	ASTM D86
Cetane Number		52.7	52.0	54.0	ASTM D613
Flash Point, Pensky Closed	°C	76.0	55.0	-	ASTM D93
CFPP	°C	-26	-	-5	EN 116
Cloud Point	°C	-22			ASTM D2500
Viscosity at 40°C	mm2/s	2.654	2.300	3.300	ASTM D445
Polycyclic Aromatic Hydrocarbons	%(m)	3.4	2.0	6.0	EN 12916
Total Aromatic Hydrocarbons	%(m)	22.2			EN 12916
Sulphur content	mg/kg	6.4	-	10.0	ASTM D5453
Copper Corrosion, 3hrs at 100°C	-	1B	-	-	ASTM D130
Carbon Residue (on 10% Dist. Res)	%(m)	< 0.10	-	0.20	EN ISO 10370
Ash	%(m)	< 0.001	-	0.010	ASTM D482
Water Content	mg/kg	60	-	200	EN ISO 12937
Strong Acid Number	mg KOH/g	0.00	-	0.02	ASTM D974
Oxidation Stability	mg /100ml	< 0.1	-	2.5	ASTM D2274
Lubricity (WSD 1,4) at 60°C	µm	197	-	400	ISO 12156-1
Oxidation Stability at 110°C	Hour	> 20.0	20.0	-	EN 15751
Fatty Acid Methyl Ester (FAME) Content	%(V)	5.3	4.5	5.5	EN 14078
Oxygen Content	%(m)	0.54			ELEMENTAL
ANALYSIS					
Carbon Content	%(m)	86.59			ASTM D5291
Hydrogen Content	%(m)	12.78			ASTM D5291

A 7: Certificate of analysis for the diesel fuel (1/2).

Haltermann Carless

UNIVERSITY COLLEGE LONDON
TORRINGTON PLACE
LONDON WC1E 7JE

Delivery item/date
80053075 000010 / 19/02/2016

Feature	Units	Results	Limits Minimum	Maximum	Method
Gross Heat of Combustion	MJ/kg	45.50			IP 12
Net Heat of Combustion	MJ/kg	42.77			IP 12
C/H Mass Ratio		6.73			CALCULATION
Atomic H/C Ratio		1.7711			CALCULATION
Atomic O/C Ratio		0.0047			CALCULATION
Density at 20°C	kg/m3	831.0			ASTM D4052

COA Additional Information

The certificate is electronically generated and valid without signature.

Haltermann Carless UK Ltd.

For inquiries please contact Customer Service or local Sales

A7: Certificate of analysis for the diesel fuel(2/2).

References

Ã, W. K. (2008) ‘Diesel engine development in view of reduced emission standards’, 33, pp. 264–271. doi: 10.1016/j.energy.2007.10.003.

Aakko, P. (2005) ‘PAH content of diesel fuels’, *CONCAWE Review*, 14(2), p. 18.

Abdel-Shafy, H. I. and Mansour, M. S. M. (2015) ‘A review on polycyclic aromatic hydrocarbons: Source, environmental impact, effect on human health and remediation’, *Egyptian Journal of Petroleum*. Egyptian Petroleum Research Institute, 25(1), pp. 107–123. doi: 10.1016/j.ejpe.2015.03.011.

Agency for Toxic Substances and Disease Registry, U.S. department of Health and Human services (1995) ‘Toxicological profile for Polycyclic Aromatic Hydrocarbons’, (August). Available at: http://www.atsdr.cdc.gov/toxprofiles/tp69.pdf.

Agilent (2010). Familiarisation Guide, Agilent MassHunter Workstation Software. Quatitative *Analysis.*

Alam, M. S., Delgado-saborit, J. M., Stark, C. and Harrison, R. M. (2013) ‘Using atmospheric measurements of PAH and quinone compounds at roadside and urban background sites to assess sources and reactivity’, *Atmospheric Environment*. Elsevier Ltd, 77, pp. 24–35. doi: 10.1016/j.atmosenv.2013.04.068.

Alexiou, A and Williams, A (1995) ‘A. Alexiou and A. Williams’, Soot formation in shock tube pyrolysis of tolu*ene-n-heptane and toluene-iso-octane mixtures. *Fuel,* 74(2), pp. 153–158. https://doi.org/10.1016/0016-2361(95)92648-P

Andrae, J., Johansson, D., Björnbom, P., Risberg, P. and Kalghatgi, G. (2005) ‘Co-oxidation in the auto-ignition of primary reference fuels and n-heptane/toluene blends’, *Combustion and Flame*, 140(4), pp. 267–286. doi: 10.1016/j.combustflame.2004.11.009.

Ang, K. P., Gunasingham, H. and Tay, B. T. (1985) ‘Polycyclic aromatic hydrocarbons in diesel exhaust emissions’, *International Journal of Environmental Studies*, 26(1–2), pp. 91–96. doi: 10.1080/00207238508710247.

Aracil, I., Font, R. and Conesa, J. A. (2005) 'Semivolatile and volatile compounds from the pyrolysis and combustion of polyvinyl chloride', *Journal of Analytical and Applied Pyrolysis*, 74, pp. 465–478. doi: 10.1016/j.jaap.2004.09.008.

Badger, G., Donnelly, J. and Spotswood, T. (1964) 'The formation of aromatic hydrocarbons at high temperatures. XXIII. The pyrolysis of anthracene', *Australian Journal of Chemistry*, 17(10), p. 1147. doi: 10.1071/CH9641147.

El Bakali, A., Mercier, X., Wartel, M., Acevedo, F., Burns, I., Gasnot, L., Pauwels, J. F. and Desgroux, P. (2012) 'Modeling of PAHs in low pressure sooting premixed methane flame', *Energy*. Elsevier Ltd, 43(1), pp. 73–84. doi: 10.1016/j.energy.2011.12.026.

Ballesteros, R., Guillén-Flores, J. and Barba, J. (2015) 'Environmental and health impact assessment from a heavy-duty diesel engine under different injection strategies fueled with a bioethanol-diesel blend', *Fuel*. Elsevier Ltd, 157, pp. 191–201. doi: 10.1016/j.fuel.2015.04.077.

Ballesteros, R., Hernandez, J. J. and Lyons, L. L. (2010) 'An experimental study of the influence of biofuel origin on particle-associated PAH emissions', *Atmospheric Environment*, 44(7), pp. 930–938. doi: 10.1016/j.atmosenv.2009.11.042.

Ballesteros, R., Hernández, J. J. and Lyons, L. L. (2010) 'An experimental study of the influence of biofuel origin on particle-associated PAH emissions', *Atmospheric Environment*, 44(7), pp. 930–938. doi: 10.1016/j.atmosenv.2009.11.042.

Barbella, R., Ciajolo, A. and Anna, A. D. (1989) 'Effect of Fuel Aromaticity on Diesel Emissions', *Combustion and Flames,* 77(3-4), 267–277. https://doi.org/10.1016/0010-2180(89)90134-X.

Beckerl, W. F. (1994) 'Microwave-Assisted Extraction of Organic Compounds from Standard Reference Soils and Sediments', 6(7), pp. 1097–1106.

Bittner, J. D. and Howard, J. B. (1981) 'Composition profiles and reaction mechanisms in a near-sooting premixed benzene/oxygen/argon flame', *Symposium (International) on Combustion*, 18(1), pp. 1105–1116. doi: 10.1016/S0082-0784(81)80115-4.

Blacha, T., Di Domenico, M., Gerlinger, P. and Aigner, M. (2012) 'Soot predictions in premixed and non-premixed laminar flames using a sectional approach for PAHs and soot', *Combustion and Flame*. The Combustion Institute., 159(1), pp. 181–193. doi: 10.1016/j.combustflame.2011.07.006.

Borrás, E., Tortajada-Genaro, L. A., Vázquez, M. and Zielinska, B. (2009) 'Polycyclic aromatic hydrocarbon exhaust emissions from different reformulated diesel fuels and engine operating conditions', *Atmospheric Environment*, 43(37), pp. 5944–5952. doi: 10.1016/j.atmosenv.2009.08.010.

Botero, M. L., Chen, D., González-Calera, S., Jefferson, D. and Kraft, M. (2016) 'HRTEM evaluation of soot particles produced by the non-premixed combustion of liquid fuels', *Carbon*, 96, pp. 459–473. doi: 10.1016/j.carbon.2015.09.077.

Bøwadt, S. and Hawthorne, S. B. (1995) 'Supercritical fluid extraction in environmental analysis', *Journal of Chromatography A*, 703(1), pp. 549–571. doi: 10.1016/0021-9673(95)00051-N.

Brewer, E., Li, Y., Finken, B., Quartucy, G., Muzio, L., Baez, A., Garibay, M. and Jung, H. S. (2016) 'PM2.5 and ultrafine particulate matter emissions from natural gas-fired turbine for power generation', *Atmospheric Environment*, 131, pp. 141–149. doi: 10.1016/j.atmosenv.2015.11.048.

Bruinsma, O. S. L. and Moulijn, J. A. (1988) 'The pyrolytic formation of polycyclic aromatic hydrocarbons from benzene, toluene, ethylbenze,e, styrene, phenylacetylene and n-decane in relation to fossil fuels utilization', *Fuel Processing Technology*, 18(3), pp. 213–236. doi: 10.1016/0378-3820(88)90048-3.

Calcote, H. F. and Manos, D. M. (1983) 'Effect of molecular structure on incipient soot formation', *Combustion and Flame*, 49(1–3), pp. 289–304. doi: 10.1016/0010-2180(83)90172-4.

Cambustion (2011). Manual for Fast Aerosol Mobility Size Spectrometer DMS500 MkII.

Chen, L., Zhang, Z., Lu, Y., Zhang, C., Zhang, X., Zhang, C. and Roskilly, a. P. (2017) 'Experimental study of the gaseous and particulate matter emissions from a gas turbine combustor burning butyl butyrate and ethanol blends', *Applied Energy*. Elsevier Ltd, 195, pp. 693–701. doi: 10.1016/j.apenergy.2017.03.075.

Choi, M. Y., Hamins, A., Rushmeier, H. and Kashiwagi, T. (1994) 'Simultaneous optical measurement of soot volume fraction, temperature, and CO2 in heptane pool fire', *Symposium (International) on Combustion*, 25(1), pp. 1471–1480. doi: 10.1016/S0082-0784(06)80791-5.

Cole, J. A., Bittner, J. D., Longwell, J. P. and Howard, J. B. (1984) 'Formation mechanisms of aromatic compounds in aliphatic flames', *Combustion and Flame*, 56(1), pp. 51–70. doi: 10.1016/0010-2180(84)90005-1.

Colket, M. B. and Seery, D. J. (1994) 'Reaction mechanisms for toluene pyrolysis. *Twenty fifth Symposium (International) on Combustion/ The Combustion Institute*. 883 -891. https://doi.org/10.1016/S0082-0784(06)80723-X

Collier, A. R., Rhead, M. M., Trier, C. J. and Bell, M. a. (1995) 'Polycyclic aromatic compound profiles from a light-duty direct-injection diesel engine', *Fuel*, 74(3), pp. 362–367. doi: 10.1016/0016-2361(95)93468-S.

Collins, J. F., Brown, J. P., Alexeeff, G. V and Salmon, a G. (1998) 'Potency equivalency factors for some polycyclic aromatic hydrocarbons and polycyclic aromatic hydrocarbon derivatives.', *Regulatory toxicology and pharmacology : RTP*, 28(1), pp. 45–54. doi: 10.1006/rtph.1998.1235.

Commins, B. T. (1969) 'Formation of polycyclic aromatic hydrocarbons during pyrolysis and combustion of hydrocarbons.', *Atmospheric environment (Oxford, England : 1994)*, 3(5), pp. 565–572. doi: 10.1016/0004-6981(69)90046-8.

Crittenden, B. D. and Long, R. (1973) 'Formation of polycyclic aromatics in rich premixed acetylene and ethylene flames', *Combustion and Flame*, 20(3), pp. 359–368. doi: 10.1016/0010-2180(73)90028-X.

Crossley, S. P., Alvarez, W. E. and Resasco, D. E. (2008) 'Novel Micropyrolyis Index (MPI) to Estimate the Sooting Tendency of Fuels', (6), pp. 2455–2464.

D'Anna, A., Violi, A. and D'Alessio, A. (2000) 'Modeling the rich combustion of aliphatic hydrocarbons', *Combustion and Flame*, 121(3), pp. 418–429. doi: 10.1016/S0010-2180(99)00163-7.

Dai, Q., Jiang, X., Jiang, Y., Jin, Y., Wang, F., Chi, Y. and Yan, J. (2014) 'Formation of PAHs during the pyrolysis of dry sewage sludge', *Fuel*. Elsevier Ltd, 130, pp. 92–99. doi: 10.1016/j.fuel.2014.04.017.

Dandajeh, H. A., Ladommatos, N., Hellier, P. and Eveleigh, A. (2017) 'Effects of unsaturation of C2 and C3 hydrocarbons on the formation of PAHs and on the toxicity of soot particles', *Fuel*. Elsevier Ltd, 194, pp. 306–320. doi: 10.1016/j.fuel.2017.01.015.

Dec, J. E. (2010) 'Advanced compression-ignition engines — understanding the in-cylinder processes', *Proceedings of the Combustion Institute*. The Combustion Institute, 32(2), pp. 2727–2742. doi: 10.1016/j.proci.2008.08.008.

Ding, J., He, G. and Zhang, L. (2013) 'Detailed Temperature-dependent Study of n-Heptane Pyrolysis at High Temperature', *Chinese Journal of Chemical Physics*, 26(3), p. 329. doi: 10.1063/1674-0068/26/03/329-336.

Division, D., Group, F. P., Engineering, M. and Waterloo, A. W. (2009) 'Modeling Study of the Soot Formation Process from Toluene Pyrolysis behind Reflected', pp. 2–7.

Dockery, D. W. and Pope, C. A. I. (1994) 'Acute respiratory effects of particulate air pollution', *Ann.Rev.Public Health*, 15, pp. 107–132.

Du, X. and Zeisel, S. H. (2013) 'Spectral Deconvolution for Gas Chromatography Mass Spectrometry-Based Metabolomics: Current Status and Future Perspectives', *Computational and Structural Biotechnology Journal*, 4(5), pp. 1–10. doi: 10.5936/csbj.201301013.

EFSA (2008) 'Polycyclic Aromatic Hydrocarbons in Food [1] - Scientific Opinion of the Panel on Contaminants in the Food Chain', (June), pp. 1–114. Available at: http://www.efsa.europa.eu/en/efsajournal/pub/433.

Eiceman, G. A, Viau, A C. and Karasek, F. W. (1980) 'Ultrasonic Extraction of Polychlorinated Dibenzo-p-dioxins and Other Organic Compounds from Fly Ash from Municipal Incinerators', *Analytical Chemistry*, 52(I), pp. 1492–1496.

Elghawi, U. M., Mayouf, A., Tsolakis, A. and Wyszynski, M. L. (2010) 'Vapour-phase and particulate-bound PAHs profile generated by a (SI/HCCI) engine from a winter grade commercial gasoline fuel', *Fuel*. Elsevier Ltd, 89(8), pp. 2019–2025. doi: 10.1016/j.fuel.2010.01.002.

EPA Method TO (1999) 'Method TO-13A: Compendium of Methods for the Determination of Toxic Organic Compounds in Ambient Air Second Edition

Compendium Method TO-13A Determination of Polycyclic Aromatic Hydrocarbons (PAHs) in Ambient Air Using Gas Chromatography / Mass Spectrom.

Eveleigh, A. (2015) 'The influence of fuel molecular structure on particulate emission investigated with isotope tracing', Phd Thesis submitted to the University College London.

Faccinetto, A., Focsa, C., Desgroux, P. and Ziskind, M. (2015) 'Progress toward the Quantitative Analysis of PAHs Adsorbed on Soot by Laser Desorption/Laser Ionization/Time-of-Flight Mass Spectrometry', *Environmental Science & Technology*, p. 150812140130006. doi: 10.1021/acs.est.5b02703.

Fisher, J. A., Scarlett, M. J. and Stott, A. D. (1997) 'Accelerated solvent extraction: An evaluation for screening of soils for selected U.S. EPA semivolatile organic priority pollutants', *Environmental Science and Technology*, 31(4), pp. 1120–1127. doi: 10.1021/es9606283.

Franken, C., Koppen, G., Lambrechts, N., Govarts, E., Bruckers, L., Den Hond, E., Loots, I., Nelen, V., Sioen, I., Nawrot, T. S., Baeyens, W., Van Larebeke, N., Boonen, F., Ooms, D., Wevers, M., Jacobs, G., Covaci, A., Schettgen, T. and Schoeters, G. (2017) 'Environmental exposure to human carcinogens in teenagers and the association with DNA damage', *Environmental Research*. Elsevier, 152(October 2016), pp. 165–174. doi: 10.1016/j.envres.2016.10.012.

Frenklach, M. (2000) 'Kinetic Modeling of Soot Formation with Detailed Chemistry and Physics : Laminar Premixed Flames of C 2 Hydrocarbons', *Combustion and Flame.* 136, pp. 122–136. https://doi.org/10.1016/S0010-2180(99)00135-2

Frenklach, M. (2002) 'Reaction mechanism of soot formation in flames', *Physical Chemistry Chemical Physics*, 4(11), pp. 2028–2037. doi: 10.1039/b110045a.

Frenklach, M. (2002) 'Reaction mechanism of soot formation in flames', *Physical Chemistry Chemical Physics*, 4(11), pp. 2028–2037. doi: 10.1039/b110045a.

Frenklach, M., Clary, D. W., Gardiner, W. C. and Stein, S. E. (1985) 'Detailed kinetic modeling of soot formation in shock-tube pyrolysis of acetylene', *Symposium (International) on Combustion*, 20(1), pp. 887–901. doi: 10.1016/S0082-0784(85)80578-6.

Frenklach, M., Clary, D. W., Gardiner, W. C. and Stein, S. E. (1988) 'Effect of fuel structure on pathways to soot', *Symposium (International) on Combustion*, 21(1), pp. 1067–1076. doi: 10.1016/S0082-0784(88)80337-0.

Frenklach, M., Durgaprasad, M. B., Matula, R. A. and Taki, S. (1983) 'Soot formation in pyrolysis of acetylene, allene and 1,3-butadiene', 1. doi: 10.1016/0010-2180(83)90024-X.

Frenklach, M. and Wang, H. (1991) 'Detailed modeling of soot particle nucleation and growth', *Symposium (International) on Combustion*, 23(1), pp. 1559–1566. doi: 10.1016/S0082-0784(06)80426-1.

Frenklach, M., Yuan, T. and Ramachandra, M. K. (1990) 'Soot formation in shock-tube pyrolysis and oxidation of vinylacetylene', pp. 871–878.

Furuhata, T., Kobayashi, Y., Hayashida, K. and Arai, M. (2012) 'Behavior of PAHs and PM in a diffusion flame of paraffin fuels', *Fuel*. Elsevier Ltd, 91(1), pp. 16–25. doi: 10.1016/j.fuel.2011.07.014.

Ghosh, P. (2008) 'Predicting the effect of cetane improvers on diesel fuels', *Energy and Fuels*, 22(2), pp. 1073–1079. doi: 10.1021/ef0701079.

Glarborg, P., Østberg, M., Johannessen, J. T., Livbjerg, H., Jensen, A. D. and Christensen, T. S. (2004) 'Formation of polycyclic aromatic hydrocarbons and soot in fuel-rich oxidation of methane in a laminar flow reactor', 136, pp. 91–128. doi: 10.1016/j.combustflame.2003.09.011.

Gowers, A. M., Miller, B. G. and Stedman, J. R. (2014) *Estimating Local Mortality Burdens associated with Particulate Air Pollution*, *Public Health England*. Available at: http://www.hpa.org.uk/webc/HPAwebFile/HPAweb_C/1317141074607.

Graham, S. C., Homer, J. B. and Rosenfeld, J. L. J. (1975) 'The Formation and Coagulation of Soot Aerosols Generated by the Pyrolysis of Aromatic Hydrocarbons', *Proceedings of the Royal Society A: Mathematical, Physical and Engineering Sciences*, 344(1637), pp. 259–285. doi: 10.1098/rspa.1975.0101.

Grimmer, G., Jacob, J., Naujack, K. W. and Dettbarn, G. (1981) 'Profile of the polycyclic aromatic hydrocarbons from used engine oil — inventory by GCGC/MS — PAH in environmental materials, Part 2', *Fresenius' Journal of Analytical*

Chemistry, 309(1), pp. 13–19. doi: 10.1007/BF00493445.

Guéret, C., Daroux, M. and Billaud, F. (1997) 'Methane pyrolysis: Thermodynamics', *Chemical Engineering Science*, 52(5), pp. 815–827. doi: 10.1016/S0009-2509(96)00444-7.

He, C., Ge, Y., Tan, J., You, K., Han, X. and Wang, J. (2010a) 'Characteristics of polycyclic aromatic hydrocarbons emissions of diesel engine fueled with biodiesel and diesel', *Fuel*. Elsevier Ltd, 89(8), pp. 2040–2046. doi: 10.1016/j.fuel.2010.03.014.

He, C., Ge, Y., Tan, J., You, K., Han, X. and Wang, J. (2010b) 'Characteristics of polycyclic aromatic hydrocarbons emissions of diesel engine fueled with biodiesel and diesel', *Fuel*. Elsevier Ltd, 89(8), pp. 2040–2046. doi: 10.1016/j.fuel.2010.03.014.

Hellier, P., Ladommatos, N., Allan, R. and Rogerson, J. (2013) 'Combustion and emissions characteristics of toluene/n-heptane and 1-octene/n-octane binary mixtures in a direct injection compression ignition engine', *Combustion and Flame*. The Combustion Institute., 160(10), pp. 2141–2158. doi: 10.1016/j.combustflame.2013.04.016.

Heywood, J. B. (1988). Internal combustion engine fundamentals, volume 930. Mcgraw-hill New York.

Higgins, B., Siebers, D. L., Mueller, C. J. and Aradi, A. (1998) 'Effects of an ignition-enhancing, diesel-fuel additive on diesel-spray evaporation, mixing, ignition, and combustion', *Symposium (International) on Combustion*, 27(2), pp. 1873–1880. doi: 10.1016/S0082-0784(98)80030-1.

Hollender, J., Koch, B., Lutermann, C. and Dott, W. (2003) 'Efficiency of Different Methods and Solvents for the Extraction of Polycyclic Aromatic Hydrocarbons from Soils', *International Journal of Environmental Analytical Chemistry*, 83(1), pp. 21–32. doi: 10.1080/0306731021000050723.

Ikeda, E., Tranter, R. S., Kiefer, J. H., Kern, R. D., Singh, H. J. and Zhang, Q. (2006) 'The pyrolysis of methylcyclopentadiene : isomerization and formation of aromatics', 28, pp. 1725–1732.

Jain, T., Jain, V. and Pandey, R. (2009) 'Microwave assisted extraction for

phytoconstituents-An overview', *Asian Journal of …*, 2(1), pp. 19–25. Available at: http://www.ajrconline.org/AJRC V0l2 (1) PDF Final/4RA.pdf.

Jian-guang, Y., Wu-gao, Z. and Zhen, H. (2013) 'Effect of cetane number improver on heat release rate and emissions of high speed diesel engine fueled with ethanol – diesel blend fuel', 83(2004), pp. 2013–2020. doi: 10.1016/j.fuel.2004.05.003.

Jin, T., Qu, L., Liu, S., Gao, J., Wang, J., Wang, F., Zhang, P., Bai, Z. and Xu, X. (2014) 'Chemical characteristics of particulate matter emitted from a heavy duty diesel engine and correlation among inorganic and PAH components', *Fuel*. Elsevier Ltd, 116, pp. 655–661. doi: 10.1016/j.fuel.2013.08.074.

Kaden, D. A., Hites, R. A. and Thilly, W. G. (1979) 'Mutagenicity of Soot and Associated Polycyclic Aromatic Hydrocarbons to Salmonella typhimuriumi', 39(October), pp. 4152–4160.

Kado, N. Y., Okamoto, R. a., Kuzmicky, P. A., Kobayashi, R., Ayala, A., Gebel, M. E., Rieger, P. L., Maddox, C. and Zafonte, L. (2005) 'Emissions of toxic pollutants from compressed natural gas and low sulfur diesel-fueled heavy-duty transit buses tested over multiple driving cycles', *Environmental Science and Technology*, 39(19), pp. 7638–7649. doi: 10.1021/es0491127.

Kado, N. Y., Okamoto, R. a, Kuzmicky, P. A and Haines, H. E. (1996) 'Chemical and Bioassay and Biodiesel Particulate Analyses of Diesel Matter : Pilot Study FINAL REPORT Analyses Matter : o-f Diesel Piilot Study', (November).

Karavalakis, G., Bakeas, E., Fontaras, G. and Stournas, S. (2011) 'Effect of biodiesel origin on regulated and particle-bound PAH (polycyclic aromatic hydrocarbon) emissions from a Euro 4 passenger car', *Energy*. Elsevier Ltd, 36(8), pp. 5328–5337. doi: 10.1016/j.energy.2011.06.041.

Kc, U., Beshir, M. and Farooq, A. (2015) 'Simultaneous measurements of acetylene and soot during the pyrolysis of ethylene and benzene in a shock tube', *Proceedings of the Combustion Institute*. Elsevier Inc., 36(1), pp. 833–840. doi: 10.1016/j.proci.2016.08.087.

Keller, A., Kovacs, R. and Homann, K.-H. (2000) 'Large molecules, ions, radicals and small soot particles in fuel-rich hydrocarbon flames. Part IV. Large polycyclic aromatic hydrocarbons and their radicals in a fuel-rich benzene–oxygen flame', *Physical Chemistry Chemical Physics*, 2(8), pp. 1667–1675. doi:

10.1039/a908190i.

Kidoguchi, Y., Yang, C., Kato, R. and Miwa, K. (2000) ‘Effects of fuel cetane number and aromatics on combustion process and emissions of a direct-injection diesel engine’, *JSAE review*, 21(4), pp. 469–475. doi: 10.1016/S0389-4304(00)00075-8.

Kim, K.H., Jahan, S. A., Kabir, E. and Brown, R. J. C. (2013) ‘A review of airborne polycyclic aromatic hydrocarbons (PAHs) and their human health effects.’, *Environment international*. Elsevier Ltd, 60, pp. 71–80. doi: 10.1016/j.envint.2013.07.019.

Kiss, G., Varga-Puchony, Z. and Hlavay, J. (1996) ‘Determination of polycyclic aromatic hydrocarbons in precipitation using solid-phase extraction and column liquid chromatography’, *Journal of Chromatography A*, 725, pp. 261–272. Available at: internal-pdf://kiss_g_725_261_96-3505765376/Kiss_G_725_261_96.pdf.

Kittelson, D. B. (1998) ‘Engines and nanoparticles: A review’, *Journal of Aerosol Science*, 29(5–6), pp. 575–588. doi: 10.1016/S0021-8502(97)10037-4.

Koivisto, E., Ladommatos, N. and Gold, M. (2015a) ‘Systematic study of the effect of the hydroxyl functional group in alcohol molecules on compression ignition and exhaust gas emissions’, *Fuel*. Elsevier Ltd, 153, pp. 650–663. doi: 10.1016/j.fuel.2015.03.042.

Koivisto, E., Ladommatos, N. and Gold, M. (2015b) ‘The influence of various oxygenated functional groups in carbonyl and ether compounds on compression ignition and exhaust gas emissions’, *Fuel*. Elsevier Ltd, 159, pp. 697–711. doi: 10.1016/j.fuel.2015.07.018.

Koivisto, E., Ladommatos, N. and Gold, M. (2016) ‘Compression ignition and pollutant emissions of large alkylbenzenes’, *Fuel*. Elsevier Ltd, 172, pp. 200–208. doi: 10.1016/j.fuel.2016.01.025.

Lacroix, R., Fournet, R., Ziegler-Devin, I. and Marquaire, P. M. (2010) ‘Kinetic modeling of surface reactions involved in CVI of pyrocarbon obtained by propane pyrolysis’, *Carbon*. Elsevier Ltd, 48(1), pp. 132–144. doi: 10.1016/j.carbon.2009.08.041.

Ladommatos, N., Parsi, M. and Knowles, A. (1996) 'The effect of fuel cetane improver on diesel pollutant emissions', *Fuel*, 75(1), pp. 8–14. doi: 10.1016/0016-2361(94)00223-1.

Ladommatos, N., Rubenstein, P. and Bennett, P. (1996) 'Some effects of molecular structure of single hydrocarbons on sooting tendency', *Fuel*, 75(2), pp. 114–124. doi: 10.1016/0016-2361(94)00251-7.

Lea-Langton, A. R., Ross, A. B., Bartle, K. D., Andrews, G. E., Jones, J. M., Li, H., Pourkashanian, M. and Williams, a. (2013) 'Low temperature PAH formation in diesel combustion', *Journal of Analytical and Applied Pyrolysis*, 103, pp. 119–125. doi: 10.1016/j.jaap.2012.10.009.

Ledesma, E. B., Wornat, M. J., Felton, P. G. and Sivo, J. A (2005) 'The effects of pressure on the yields of polycyclic aromatic hydrocarbons produced during the supercritical pyrolysis of toluene', *Proceedings of the Combustion Institute*. The Combustion Institute, 30(1), pp. 1371–1379. doi: 10.1016/j.proci.2004.08.086.

Levin, W., Wood, A. W., Wislocki, P. G., Kapitulnik, J., Yagi, H., Jerina, D. M. and Conney, A. H. (1977) 'Carcinogenicity on Mouse Skin of Benzo-Ring Derivatives of Benzo (a) pyrene', 37(September), pp. 3356–3361.

Li, R., Wang, Z., Ni, P., Zhao, Y., Li, M. and Li, L. (2014) 'Effects of cetane number improvers on the performance of diesel engine fuelled with methanol/biodiesel blend', *Fuel*. Elsevier Ltd, 128, pp. 180–187. doi: 10.1016/j.fuel.2014.03.011.

Lim, M. C. H., Ayoko, G. A., Morawska, L., Ristovski, Z. D. and Jayaratne, E. R. (2005) 'Effect of fuel composition and engine operating conditions on polycyclic aromatic hydrocarbon emissions from a fleet of heavy-duty diesel buses', *Atmospheric Environment*, 39(40), pp. 7836–7848. doi: 10.1016/j.atmosenv.2005.09.019.

Lin, Y. C., Lee, W. J., Wu, T. S. and Wang, C. T. (2006) 'Comparison of PAH and regulated harmful matter emissions from biodiesel blends and paraffinic fuel blends on engine accumulated mileage test', *Fuel*, 85(17–18), pp. 2516–2523. doi: 10.1016/j.fuel.2006.04.023.

Longwell, J. P. (1982) 'The formation of polycyclic aromatic hydrocarbons by com bustion. *Symposium (International) on combustion*. pp.19(1), 1339–1350. https://doi.org/10.1016/S0082-0784(82)80310-X

Luo, J., Yao, M., Liu, H. and Yang, B. (2012) 'Experimental and numerical study on suitable diesel fuel surrogates in low temperature combustion conditions', *Fuel*. Elsevier Ltd, 97, pp. 621–629. doi: 10.1016/j.fuel.2012.02.057.

Manzello, S. L., Lenhert, D. B., Yozgatligil, A., Donovan, M. T., Mulholland, G. W., Zachariah, M. R. and Tsang, W. (2007) 'Soot particle size distributions in a well-stirred reactor/plug flow reactor', *Proceedings of the Combustion Institute*, 31 I, pp. 675–683. doi: 10.1016/j.proci.2006.07.013.

Marinov, N. M., Castaldi, M. J., Melius, C. F. and Tsang, W. (1997) 'Aromatic and Polycyclic Aromatic Hydrocarbon Formation in a Premixed Propane Flame', *Combustion Science and Technology*, 128(1–6), pp. 295–342. doi: 10.1080/00102209708935714.

Marinov, N. M., Castaldi, M. J., Melius, C. F., Tsang, W., Marinov, N. M., Castaldi, M. J., Melius, C. F. and Tsang, W. (2016) 'Aromatic and Polycyclic Aromatic Hydrocarbon Formation in a Premixed Propane Flame Aromatic and Polycyclic Aromatic Hydrocarbon Formation in a Premixed Propane Flame', 2202(November). doi: 10.1080/00102209708935714.

Markatou, P., Wang, H. and Frenklach, M. (1993) 'A Computacional Study of Sooting Limits in a laminar premixed flame', *Combustion and Flame.* 482, pp. 467–482. https://doi.org/10.1016/0010-2180(93)90146-T

Marr, L. C., Kirchstetter, T. W., Harley, R. A., Miguel, A. H., Hering, S. V. and Hammond, S. K. (1999) 'Characterization of polycyclic aromatic hydrocarbons in motor vehicle fuels and exhaust emissions', *Environmental Science and Technology*, 33(18), pp. 3091–3099. doi: 10.1021/es981227l.

Marsh, N. D., Ledesma, E. B., Sandrowitz, A. K. and Wornat, M. J. (2004) 'Yields of Polycyclic Aromatic Hydrocarbons from the Pyrolysis of Catechol [o rtho - Dihydroxybenzene]: Temperature and Residence Time Effects', *Energy & Fuels*, 18(1), pp. 209–217. doi: 10.1021/ef010263u.

Martin, N., Lombard, M., Jensen, K. R., Kelley, P., Pratt, T. and Traviss, N. (2017) 'Effect of biodiesel fuel on "real-world", nonroad heavy duty diesel engine particulate matter emissions, composition and cytotoxicity', *Science of The Total Environment*. Elsevier B.V., 586, pp. 409–418. doi: 10.1016/j.scitotenv.2016.12.041.

Masih, J., Masih, A., Kulshrestha, A., Singhvi, R. and Taneja, A. (2010)

‘Characteristics of polycyclic aromatic hydrocarbons in indoor and outdoor atmosphere in the North central part of India’, *Journal of Hazardous Materials*. Elsevier B.V., 177(1–3), pp. 190–198. doi: 10.1016/j.jhazmat.2009.12.017.

Mastral, A. M., Mastral, A. M., Callén, M. S. and Callén, M. S. (2000) ‘A Review on Polycyclic Aromatic Hydrocarbon (PAH) Emissions from Energy Generation’, *Environmental Science & Technology*, 34(15), pp. 3051–3057. doi: 10.1021/es001028d.

Mathieu, O., Frache, G., Djebaïli-Chaumeix, N., Paillard, C. E., Krier, G., Muller, J. F., Douce, F. and Manuelli, P. (2007) ‘Characterization of adsorbed species on soot formed behind reflected shock waves’, *Proceedings of the Combustion Institute*, 31 I, pp. 511–519. doi: 10.1016/j.proci.2006.07.190.

Matti Maricq, M. (2007) ‘Chemical characterization of particulate emissions from diesel engines: A review’, *Journal of Aerosol Science*, 38(11), pp. 1079–1118. doi: 10.1016/j.jaerosci.2007.08.001.

McEnally, C. S. and Pfefferle, L. D. (2011) ‘Sooting tendencies of oxygenated hydrocarbons in laboratory-scale flames’, *Environmental Science and Technology*, 45(6), pp. 2498–2503. doi: 10.1021/es103733q.

McGrath, T. E., Chan, W. G. and Hajaligol, M. R. (2003) ‘Low temperature mechanism for the formation of polycyclic aromatic hydrocarbons from the pyrolysis of cellulose’, *Journal of Analytical and Applied Pyrolysis*, 66(1–2), pp. 51–70. doi: 10.1016/S0165-2370(02)00105-5.

McGrath, T. E., Wooten, J. B., Geoffrey Chan, W. and Hajaligol, M. R. (2007) ‘Formation of polycyclic aromatic hydrocarbons from tobacco: The link between low temperature residual solid (char) and PAH formation’, *Food and Chemical Toxicology*, 45(6), pp. 1039–1050. doi: 10.1016/j.fct.2006.12.010.

McGrath, T., Sharma, R. and Hajaligol, M. (2001) ‘An experimental investigation into the formation of polycyclic-aromatic hydrocarbons (PAH) from pyrolysis of biomass materials’, *Fuel*, 80(12), pp. 1787–1797. doi: 10.1016/S0016-2361(01)00062-X.

Mi, H. H., Lee, W. J., Chen, C. B., Yang, H. H. and Wu, S. J. (2000) ‘Effect of fuel aromatic content on PAH emission from a heavy-duty diesel engine’, *Chemosphere*, 41(11), pp. 1783–1790. doi: 10.1016/S0045-6535(00)00043-6.

Miguel, A. H., Kirchstetter, T. W., Harley, R. A. and Hering, S. V. (1998) 'On-road emissions of particulate polycyclic aromatic hydrocarbons and black carbon from gasoline and diesel vehicles', *Environmental Science and Technology*, 32(4), pp. 450–455. doi: 10.1021/es970566w.

Miller, J. A. and Melius, C. F. (1992) 'Kinetic and thermodynamic issues in the formation of aromatic compounds in flames of aliphatic fuels', *Combustion and Flame*, 91(1), pp. 21–39. doi: 10.1016/0010-2180(92)90124-8.

Mukherjee, J., Sarofim, A. F. and Longwell, J. P. (1994) 'Polycyclic aromatic hydrocarbons from the high-temperature pyrolysis of pyrene', *Combustion and Flame*, 96(3), pp. 191–200. doi: 10.1016/0010-2180(94)90008-6.

Murphy, D. B. (1997) 'Analysis of products of high-temperature pyrolysis of various hydrocarbons, *Carbon*, 35(12), pp. 1819–1823. https://doi.org/10.1016/S0008-6223(97)00109-7

Musculus, M., Pickett, L., Miles, P., Dec, J. and Oefelein, J. (2012) 'A Conceptual Model for Partially Premixed Low-Temperature Diesel Combustion Based on In-Cylinder Laser Diagnostics and Chemical Kinetics Modeling Sandia ' s diesel conceptual model describes mixing , combustion up to end of injection'.

Nisbet, I. C. T. and LaGoy, P. K. (1992) 'Toxic equivalency factors (TEFs) for polycyclic aromatic hydrocarbons (PAHs)', *Regulatory Toxicology and Pharmacology*, 16(3), pp. 290–300. doi: 10.1016/0273-2300(92)90009-X.

Norinaga, K. and Deutschmann, O. (2007a) 'Detailed Kinetic Modeling of Gas-Phase Reactions in the Chemical Vapor Deposition of Carbon from Light Hydrocarbons', *Industrial & Engineering Chemistry Research*, 46(11), pp. 3547–3557. doi: 10.1021/ie061207p.

Norinaga, K. and Deutschmann, O. (2007b) 'Detailed Kinetic Modeling of Gas-Phase Reactions in the Chemical Vapor Deposition of Carbon from Light Hydrocarbons', *Industrial & Engineering Chemistry Research*, 46(11), pp. 3547–3557. doi: 10.1021/ie061207p.

Norinaga, K., Deutschmann, O., Saegusa, N. and Hayashi, J. (2009) 'Analysis of pyrolysis products from light hydrocarbons and kinetic modeling for growth of polycyclic aromatic hydrocarbons with detailed chemistry', *Journal of Analytical and Applied Pyrolysis*, 86(1), pp. 148–160. doi: http://dx.doi.org/10.1016/j.jaap.2009.05.001.

Oehlschlaeger, M. a., Davidson, D. F. and Hanson, R. K. (2004) 'High-temperature thermal decomposition of isobutane and n-butane behind shock waves', *Journal of Physical Chemistry A*, 108(19), pp. 4247–4253. doi: 10.1021/jp0313627.

Olten, N. and Senkan, S. (1999) 'Formation of polycyclic aromatic hydrocarbons in an atmospheric pressure ethylene diffusion flame', *Combustion and Flame*, 118(3), pp. 500–507. doi: 10.1016/S0010-2180(99)00004-8.

Oukebdane, K., Portet-Koltalo, F., MacHour, N., Dionnet, F. and Desbèlne, P. L. (2010) 'Comparison of hot Soxhlet and accelerated solvent extractions with microwave and supercritical fluid extractions for the determination of polycyclic aromatic hydrocarbons and nitrated derivatives strongly adsorbed on soot collected inside a diesel particu', *Talanta*, 82(1), pp. 227–236. doi: 10.1016/j.talanta.2010.04.027.

Pedersen, P. S., Ingwersen, J., Nielsen, T. and Larsen, E. (1980) 'Effects of fuel, lubricant, and engine operating parameters on the emission of polycyclic aromatic hydrocarbons', *Environmental Science & Technology*, 14(1), pp. 71–79. doi: 10.1021/es60161a011.

Pies, C., Hoffmann, B., Petrowsky, J., Yang, Y., Ternes, T. A. and Hofmann, T. (2008) 'Characterization and source identification of polycyclic aromatic hydrocarbons (PAHs) in river bank soils', *Chemosphere*, 72(10), pp. 1594–1601. doi: 10.1016/j.chemosphere.2008.04.021.

Pitz, W. J. and Mueller, C. J. (2011) 'Recent progress in the development of diesel surrogate fuels', *Progress in Energy and Combustion Science*. Elsevier Ltd, 37(3), pp. 330–350. doi: 10.1016/j.pecs.2010.06.004.

Poater, J., Visser, R., Sola, M. and Bickelhaupt, F. M. (2007) 'Polycyclic benzenoid [why kinked arene is more stable than straight]', *J. Org. Chem.*, 72, pp. 1134–1142. Available at: http://pubs3.acs.org/acs/journals/doilookup?in_doi=10.1021/jo061637p.

Pope, C. J., Peters, W. A. and Howard, J. B. (2000) 'Thermodynamic driving forces for PAH isomerization and growth during thermal treatment of polluted soils', *Journal of Hazardous Materials*, 79(1–2), pp. 189–208. doi: 10.1016/S0304-3894(00)00267-3.

Popp, P., Keil, P. and Moder, M. (1997) 'Application of accelerated solvent

extraction followed by gas chromatography , high-performance liquid chromatography and gas chromatography – mass spectrometry for the determination of polycyclic aromatic hydrocarbons , chlorinated pesticides and polychl', 774, pp. 203–211.

Raquel, S. and Mesquita, S. (2016) 'Toxicity of the organic fraction of atmospheric particulate matter. PhD thesis submitted to the University of Porto'.

Ravindra, K., Wauters, E. and Van Grieken, R. (2008) 'Variation in particulate PAHs levels and their relation with the transboundary movement of the air masses', *Science of the Total Environment*, 396(2–3), pp. 100–110. doi: 10.1016/j.scitotenv.2008.02.018.

Rengarajan, T., Rajendran, P., Nandakumar, N., Lokeshkumar, B., Rajendran, P. and Nishigaki, I. (2015) 'Asian Pacific Journal of Tropical Biomedicine', *Asian Pacific Journal of Tropical Biomedicine*. Hainan Medical University, 5(3), pp. 182–189. doi: 10.1016/S2221-1691(15)30003-4.

Rhead, M. M. and Hardy, S. A. (2003) 'The sources of polycyclic aromatic compounds in diesel engine emissions☆', *Fuel*, 82(4), pp. 385–393. doi: 10.1016/S0016-2361(02)00314-9.

Rhead, M. M. and Pemberton, R. D. (1996) 'Sources of Naphthalene in Diesel Exhaust Emissions', *Energy & Fuels*, 10(3), pp. 837–843. doi: 10.1021/ef9502261.

Richter, B. E., Jones, B. A, Ezzell, J. L. and Porter, N. L. (1996) 'Accelerated Solvent Extraction : A Technique for Sample Preparation', *Anal. Chem.*, 68(6), pp. 1033–1039. doi: 10.1021/ac9508199.

Richter, H., Grieco, W. J. and Howard, J. B. (1999) 'Formation mechanism of polycyclic aromatic hydrocarbons and fullerenes in premixed benzene flames', *Combustion and Flame*, 119(1–2), pp. 1–22. doi: 10.1016/S0010-2180(99)00032-2.

Richter, H. and Howard, J. . (2000) *Formation of polycyclic aromatic hydrocarbons and their growth to soot—a review of chemical reaction pathways*, *Progress in Energy and Combustion Science*. doi: 10.1016/S0360-1285(00)00009-5.

Rodrigues, P., Franzelli, B., Vicquelin, R., Gicquel, O. and Darabiha, N. (2015) 'Unsteady dynamics of PAH and soot particles in laminar counterflow diffusion flames', *Proceedings of the Combustion Institute*. Elsevier Inc., 36(1), pp. 927–934. doi: 10.1016/j.proci.2016.07.047.

Ruiz, M. P., Callejas, A., Millera, A., Alzueta, M. U. and Bilbao, R. (2007) 'Soot formation from C2H2 and C2H4 pyrolysis at different temperatures', *Journal of Analytical and Applied Pyrolysis*, 79(1–2 SPEC. ISS.), pp. 244–251. doi: 10.1016/j.jaap.2006.10.012.

Rynö, M., Rantanen, L., Papaioannou, E., Konstandopoulos, A G., Koskentalo, T. and Savela, K. (2006) 'Comparison of pressurized fluid extraction, Soxhlet extraction and sonication for the determination of polycyclic aromatic hydrocarbons in urban air and diesel exhaust particulate matter.', *Journal of environmental monitoring : JEM*, 8(4), pp. 488–493. doi: 10.1039/b515882f.

Sánchez, N. E., Callejas, A., Millera, Á., Bilbao, R. and Alzueta, M. U. (2012) 'Polycyclic aromatic hydrocarbon (PAH) and soot formation in the pyrolysis of acetylene and ethylene: Effect of the reaction temperature', *Energy and Fuels*, 26(8), pp. 4823–4829. doi: 10.1021/ef300749q.

Sánchez, N. E., Callejas, A., Millera, A., Bilbao, R. and Alzueta, M. U. (2012) 'Formation of PAH and soot during acetylene pyrolysis at different gas residence times and reaction temperatures', *Energy*. Elsevier Ltd, 43(1), pp. 30–36. doi: 10.1016/j.energy.2011.12.009.

Sánchez, N. E., Millera, Á., Bilbao, R. and Alzueta, M. U. (2013) 'Polycyclic aromatic hydrocarbons (PAH), soot and light gases formed in the pyrolysis of acetylene at different temperatures: Effect of fuel concentration', *Journal of Analytical and Applied Pyrolysis*. Elsevier B.V., 103, pp. 126–133. doi: 10.1016/j.jaap.2012.10.027.

Di Sante, R. (2012) 'Measurements of the auto-ignition of n-heptane/toluene mixtures using a rapid compression machine', *Combustion and Flame*. The Combustion Institute., 159(1), pp. 55–63. doi: 10.1016/j.combustflame.2011.05.020.

Schenk, M., Hansen, N., Vieker, H., Beyer, A., Gölzhäuser, a. and Kohse-Höinghaus, K. (2015) 'PAH formation and soot morphology in flames of C4 fuels', *Proceedings of the Combustion Institute*, 35(2), pp. 1761–1769. doi: 10.1016/j.proci.2014.06.139.

Scientific, T. F. (2011) ‘Dionex ASE 150 Accelerated Solvent Extractor Operator Manual’, (65207).

Shokrollahi Yancheshmeh, M. S., Seifzadeh Haghighi, S., Gholipour, M. R., Dehghani, O., Rahimpour, M. R. and Raeissi, S. (2013) ‘Modeling of ethane pyrolysis process: A study on effects of steam and carbon dioxide on ethylene and hydrogen productions’, *Chemical Engineering Journal*. Elsevier B.V., 215–216, pp. 550–560. doi: 10.1016/j.cej.2012.10.078.

Shukla, B. and Koshi, M. (2011) ‘Comparative study on the growth mechanisms of PAHs’, *Combustion and Flame*. The Combustion Institute., 158(2), pp. 369–375. doi: 10.1016/j.combustflame.2010.09.012.

Shukla, B. and Koshi, M. (2012a) ‘A novel route for PAH growth in HACA based mechanisms’, *Combustion and Flame*. The Combustion Institute., 159(12), pp. 3589–3596. doi: 10.1016/j.combustflame.2012.08.007.

Shukla, B. and Koshi, M. (2012b) ‘Importance of Fundamental sp, sp 2 , and sp 3 Hydrocarbon Radicals in the Growth of Polycyclic Aromatic Hydrocarbons’.

Shukla, B., Miyoshi, A. and Koshi, M. (2010) ‘Role of Methyl Radicals in the Growth of PAHs’, *Journal of the American Society for Mass Spectrometry*. Elsevier Inc., 21(4), pp. 534–544. doi: 10.1016/j.jasms.2009.12.019.

Shukla, B., Susa, A., Miyoshi, A. and Koshi, M. (2007) ‘In Situ direct sampling mass spectrometric study on formation of polycyclic aromatic hydrocarbons in toluene pyrolysis’, *Journal of Physical Chemistry A*, 111(34), pp. 8308–8324. doi: 10.1021/jp071813d.

Shukla, B., Susa, A., Miyoshi, A. and Koshi, M. (2008) ‘Role of phenyl radicals in the growth of polycyclic aromatic hydrocarbons’, *Journal of Physical Chemistry A*, 112(11), pp. 2362–2369. doi: 10.1021/jp7098398.

Siegmann, K. and Sattler, K. (2000) ‘Formation mechanism for polycyclic aromatic hydrocarbons in methane flames’, *Journal of Chemical Physics*, 112(2), pp. 698–709. doi: 10.1063/1.480648.

Sivaramakrishnan, R., Tranter, R. S. and Brezinsky, K. (2004) ‘High-pressure, high-temperature oxidation of toluene’, *Combustion and Flame*, 139(4), pp. 340–350. doi: 10.1016/j.combustflame.2004.09.006.

Smith, O. I. (1981) ‘Fundamentals of soot formation in flames with application to diesel engine particulate emissions’, *Progress in Energy and Combustion Science*, 7(4), pp. 275–291. doi: 10.1016/0360-1285(81)90002-2.

Smith, R. (1979) ‘Formation of radicals and complex organic compounds by high-temperature pyrolysis: The pyrolysis of toluene☆’, *Combustion and Flame*, 35, pp. 179–190. doi: 10.1016/0010-2180(79)90021-X.

Smyth, K. C., Shaddix, C. R. and Everest, D. A. (1997) ‘Aspects of soot dynamics as revealed by measurements of broadband fluorescence and flame luminosity in flickering diffusion flames’, *Combustion and Flame*, 111(3), pp. 185–207. doi: 10.1016/S0010-2180(97)00017-5.

Symonds, J. P. R., Reavell, K. S. J., Olfert, J. S., Campbell, B. W. and Swift, S. J. (2007) ‘Diesel soot mass calculation in real-time with a differential mobility spectrometer’, *Journal of Aerosol Science*, 38(1), pp. 52–68. doi: 10.1016/j.jaerosci.2006.10.001.

Szewczyńska, M., Pośniak, M. and Dobrzyńska, E. (2013) ‘Study on individual PAHs content in ultrafine particles from solid fractions of diesel and biodiesel exhaust fumes’, *Journal of Chemistry*, 2013. doi: 10.1155/2013/528471.

Talibi, M. (2015) '*Co-combustion of diesel and gaseous fuels with exhaust emissions analysis and in-cylinder gas sampling'*. PhD thesis Submitted to the University College London.

Tancell, P. J. and Rhead, M. M. (1996) ‘Application of radio-chromatographic techniques to diesel emissions research’, *Journal of Chromatography A*, 737(2), pp. 181–192. doi: 10.1016/0021-9673(96)00040-4.

Tancell, P. J., Rhead, M. M., Pemberton, R. D. and Braven, J. (1995) ‘Survival of Polycyclic Aromatic Hydrocarbons during Diesel Combustion.’, *Environmental science & technology*, 29(11), pp. 2871–6. doi: 10.1021/es00011a025.

Tang, S., Frank, B. P., Lanni, T., Rideout, G., Meyer, N. and Beregszaszy, C. (2007) ‘Unregulated emissions from a heavy-duty diesel engine with various fuels and emission control systems’, *Environmental Science and Technology*, 41(14), pp. 5037–5043. doi: 10.1021/es0622249.

Tauzia, X., Maiboom, A., Chesse, P. and Thouvenel, N. (2006) 'A new phenomenological heat release model for thermodynamical simulation of modern turbocharged heavy duty Diesel engines', 26, pp. 1851–1857. doi: 10.1016/j.applthermaleng.2006.02.009.

Tobiszewski, M. and Namie, J. (2012) 'PAH diagnostic ratios for the identi fi cation of pollution emission sources', 162, pp. 110–119. doi: 10.1016/j.envpol.2011.10.025.

Toland, A. and Simmie, J. M. (2003) 'Ignition of alkyl nitrate/oxygen/argon mixtures in shock waves and comparisons with alkanes and amines', *Combustion and Flame*, 132(3), pp. 556–564. doi: 10.1016/S0010-2180(02)00504-7.

Tree, D. R. and Svensson, K. I. (2007) 'Soot processes in compression ignition engines', *Progress in Energy and Combustion Science*, 33(3), pp. 272–309. doi: 10.1016/j.pecs.2006.03.002.

Tsai, J. H., Chen, S. J., Huang, K. L., Lin, Y. C., Lee, W. J., Lin, C. C. and Lin, W. Y. (2010) 'PM, carbon, and PAH emissions from a diesel generator fuelled with soy-biodiesel blends', *Journal of Hazardous Materials*. Elsevier B.V., 179(1–3), pp. 237–243. doi: 10.1016/j.jhazmat.2010.02.085.

United State Environmental Protection Agency (US EPA) (1993) 'Provisional guidance for quantitative risk assessment of polycyclic aromatic hydrocarbons.' doi: EPA/600/R-93/089.

Valori, P., Melchiorri, C., Grella, A and Del Vecchio, V. (1970) 'Polycyclic aromatic hydrocarbons from gasoline-engine and liquefied petroleum gas engine exhausts.', *Pure and applied chemistry. Chimie pure et appliquee*, 24(4), pp. 739–748.

Vincitore, A. M. and Senkan, S. M. (1998) 'Polycyclic Aromatic Hydrocarbon Formation in Opposed Flow Diffusion Flames of Ethane', 2180(97).

Violi, A., D'Anna, A. and D'Alessio, A. (1999) 'Modeling of particulate formation in combustion and pyrolysis', *Chemical Engineering Science*, 54(15–16), pp. 3433–3442. doi: 10.1016/S0009-2509(98)00460-6.

Viteri, F., Gracia, S., Millera, Á., Bilbao, R. and Alzueta, M. U. (2017) 'Polycyclic aromatic hydrocarbons (PAH) and soot formation in the pyrolysis of butanol

isomers', *En proceso de publicación*. Elsevier Ltd, 197, pp. 348–358. doi: 10.1016/j.fuel.2017.02.026.

Vojtisek-Lom, M., Pechout, M., Dittrich, L., Bernek, V., Kotek, M., Schwarz, J., Vodi??ka, P., Milcov??, A., Rossnerov??, A., Ambro??, A. and Topinka, J. (2015) 'Polycyclic aromatic hydrocarbons (PAH) and their genotoxicity in exhaust emissions from a diesel engine during extended low-load operation on diesel and biodiesel fuels', *Atmospheric Environment*, 109, pp. 9–18. doi: 10.1016/j.atmosenv.2015.02.077.

Wang, H. and Brezinsky, K. (1998) 'Computational Study on the Thermochemistry of Cyclopentadiene Derivatives and Kinetics of Cyclopentadienone Thermal Decomposition', *The Journal of Physical Chemistry A*, 102(9), p. 1530. doi: 10.1021/jp9728262.

Wang, R. and Cadman, P. (1998) 'Soot and PAH Production from Spray Combustion of Different Hydrocarbons Behind Reflected Shock Waves', *Combustion and Flame*, 112, pp. 359–370.

Wang, X., Song, C., Lv, G., Song, J., Li, H. and Li, B. (2015) 'Evolution of in-cylinder polycyclic aromatic hydrocarbons in a diesel engine fueled with n-heptane and n-heptane/toluene', *Fuel*, 158, pp. 322–329. doi: 10.1016/j.fuel.2015.05.053.

Wang, Y. and Chung, S. H. (2014) 'Effect of strain rate on sooting limits in counterflow diffusion flames of gaseous hydrocarbon fuels: Sooting temperature index and sooting sensitivity index', *Combustion and Flame*. The Combustion Institute., 161(5), pp. 1224–1234. doi: 10.1016/j.combustflame.2013.10.031.

Wei, J., Song, C., Lv, G., Song, J., Wang, L. and Pang, H. (2014) 'A comparative study of the physical properties of in-cylinder soot generated from the combustion of n-heptane and toluene/n-heptane in a diesel engine', *Proceedings of the Combustion Institute*. The Combustion Institute, 35(2), pp. 1939–1946. doi: 10.1016/j.proci.2014.06.011.

Wen, J. Z., Thomson, M. J., Park, S. H., Rogak, S. N. and Lightstone, M. F. (2005) 'Study of soot growth in a plug flow reactor using a moving sectional model', *Proceedings of the Combustion Institute*. The Combustion Institute, 30(1), pp. 1477–1483. doi: 10.1016/j.proci.2004.08.178.

Westbrook, C. K. (2000) 'Chemical kinetics of hydrocarbon ignition in practical

combustion systems', 28(0), pp. 1563–1577.

Williams, P. T., Abbass, M. K., Andrews, G. E. and Bartle, K. D. (1989) 'Diesel particulate emissions: The role of unburned fuel', *Combustion and Flame*, 75(1), pp. 1–24. doi: 10.1016/0010-2180(89)90083-7.

Wnorowski, A. (2017) 'Characterization of the ambient air content of parent polycyclic aromatic hydrocarbons in the Fort McKay region (Canada)', *Chemosphere*. Elsevier Ltd, 174(3), pp. 371–379. doi: 10.1016/j.chemosphere.2017.01.114.

Wu, S., Lv, G. and Lou, R. (2012) 'Applications of Chromatography Hyphenated Techniques in the Field of Lignin Pyrolysis Applications of Chromatography Hyphenated Techniques in the Field of Lignin Pyrolysis'. doi: 10.5772/32446.

Xiao, Z., Ladommatos, N. and Zhao, H. (2000) 'The effect of aromatic hydrocarbons and oxygenates on diesel engine emissions', *Proceedings of the Institution of Mechanical Engineers, Part D: Journal of Automotive Engineering*, 214(3), 307–332. https://doi.org/10.1243/0954407001527448

Xu, H., Yao, C., Xu, G., Wang, Z. and Jin, H. (2013) 'Experimental and modelling studies of the effects of methanol and ethanol addition on the laminar premixed low-pressure n-heptane/toluene flames', *Combustion and Flame*. The Combustion Institute., 160(8), pp. 1333–1344. doi: 10.1016/j.combustflame.2013.02.018.

Yan, J., Wang, L., Fu, P. P. and Yu, H. (2004) 'Photomutagenicity of 16 polycyclic aromatic hydrocarbons from the US EPA priority pollutant list', *Mutation Research - Genetic Toxicology and Environmental Mutagenesis*, 557(1), pp. 99–108. doi: 10.1016/j.mrgentox.2003.10.004.

Zhang, L., Cai, J., Zhang, T. and Qi, F. (2010) 'Kinetic modeling study of toluene pyrolysis at low pressure', *Combustion and Flame*. The Combustion Institute., 157(9), pp. 1686–1697. doi: 10.1016/j.combustflame.2010.04.002.

Zhang, T., Zhang, L., Hong, X., Zhang, K., Qi, F., Law, C. K., Ye, T., Zhao, P. and Chen, Y. (2009) 'An experimental and theoretical study of toluene pyrolysis with tunable synchrotron VUV photoionization and molecular-beam mass spectrometry', *Combustion and Flame*. The Combustion Institute., 156(11), pp. 2071–2083. doi: 10.1016/j.combustflame.2009.06.001.

Zhang, Y., Yuan, W., Cai, J., Zhang, L., Qi, F. and Li, Y. (2013) 'Product Identification and Mass Spectrometric Analysis of n-Butane and i-Butane Pyrolysis at Low Pressure', *Chinese Journal of Chemical Physics*, 26(2), p. 151. doi: 10.1063/1674-0068/26/02/151-156.